Motion analysis of human cadaver knee-joints using anatomical coordinate system

Gábor Katona[1], Béla M. Csizmadia[1], István Bíró[2], Kristóf Andrónyi[3], Gábor Krakovits[3]

[1] Szent Istvan University, Faculty of Mechanical Engineering

[2] University of Szeged, Faculty of Engineering

[3] Semmelweis University, Department of Orthopaedics

katona.gabor@gek.szie.hu

Abstract

Large standard deviation can be observed during the analysis of the kinematical functions which describe the motion of the knee-joint. Screening the previous large number of published results concerning to the knee motion it seemed that they are scattered, therefore it can be regarded as unreliably. In our experiments anatomical coordinate system recommended by VAKHUM project was used in favor to reduce standard deviation. Setting up the anatomical coordinate system in its special anatomical points are very uncertain. A protocol was settled for the orientation of the anatomical points and for the anatomical coordinate system. Experiments were performed on five cadaver knees using the new protocol. The measurements were analyzed which has proved that the method offers a better accuracy.

Keywords: knee joint; rotation; flexion; anatomical coordinate-system

Introduction

The knee-joint is one of the most complex joints of the human body. The scientific interest have been focusing on the biomechanics of the knee for a long time. A lot of studies, often opposite to each other are published on this scope. One of the biggest problems is to describe the motions, because an anatomical coordinate system is needed to be defined, but there is no generally accepted standard method.

The motions of knee joint can be described more precisely by means of anatomical coordinate system, which assists to compare the results of measurements of different research teams. The results of the research can be useful for surgeons as well to prosthesis designing.

Weber brothers[16] dealt with the kinematics of walking in the XIX. century. The motions of the knee was analyzed by Braune[3] with photographs taken from two directions. It was not possible to describe the difficult three dimensional motions on the contemporary level of technology, but the effect of passive endrotation was described by him. The angular interpretation method was framed by Grood & Suntay[7] which was needed for the description of the knee motion (JCS – Joint Coordinate System). So, the possibility of uniform communication was established between engineers and doctors, but at the same time convenient recommendation was not given for the definition of axis of motion.

The fact that the knee joint has two axis of rotation was found by Hollister[8]. These are the axes of flexion-extension and axis of external-internal rotation. Abductional motion was measured only occasionally, possible due to the different sizes of the two condyles. The transepicondylar axis is traditionally used for the determination of axis of flexion-extension, which is the junction-line between the lateral and medial epicondyles. It was found by Churchill[4] that the axis of flexion-extension was approximated properly by this axis, but for nowadays it seems to fall. It is confuted by a lot of studies[5,6,8] that the two axes are the same. It is accentuated by other studies[1,9,10, 12,13,17] that the determination of the transepicondylar axis is very unsure. It can be just like 15° difference between the axes in case of different researchers.

Methods

Experiments were carried on cadaver knees for the analysis of motion of the knee using an experimental test rig built by the research team. The measurements were analyzed using a (anatomical) coordinate system in favor of comparability. It is still very important to increase the precision of determination, because Bíro et al.[2] have considered that large differences can be seen in the kinematical functions if the same measurement was analyzed in anatomical coordinate systems with minimal differences. Our measurements were determined on the basis of recommendation of VAKHUM project[15]. The anatomical coordinate system can be determined on the femur *(Figure 1)* on the basis of this recommendation, by using three typical anatomical points on it. These are the head of femur (fh), the medial (me) and lateral (le) epicondyles. The rules of the determination of the coordinate system are:

– the origin (O_t) of the anatomical coordinate system is the midpoint of the junction-line between the medial (me) and lateral (le) epicondyles
– the y_t axis of the coordinate system is the line between the origin and the fh point positive direction upwards
– the x_t axis of the coordinate system is perpendicular to the plane (quasi-coronal) defined by the three anatomical points (hf, me, le), positive direction to the anterior
– the z_t axis of the coordinate system is mutually perpendicular to the x_t and the y_t axis with positive direction to the right.

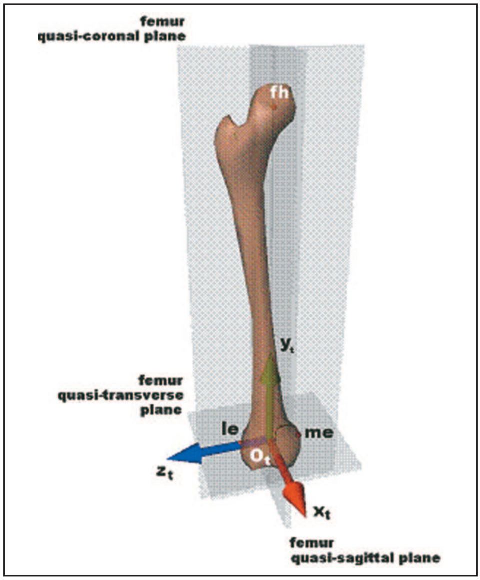

Figure 1. The anatomical coordinate system of the femur

In case of the tibia, the anatomical coordinate system can be determined by its four typical anatomical points. These anatomical points are the head of fibula (hf), tuberositas tibiae (tt), medial (mm) and lateral (lm) mallelous. The rules of the determination of the coordinate system are *(Figure 2):*

– the origin (O_s) of the coordinate system is the midpoint of the junction-line between the lateral (lm) and medial (mm) mallelous
– the y_s axis of the coordinate system is the intersection of the quasi-coronal (defined by the mm, lm hf points) and quasi-sagittal (orthogonal to the quasi-coronal plane and contains O_s and tt points both) planes with positive directions upwards

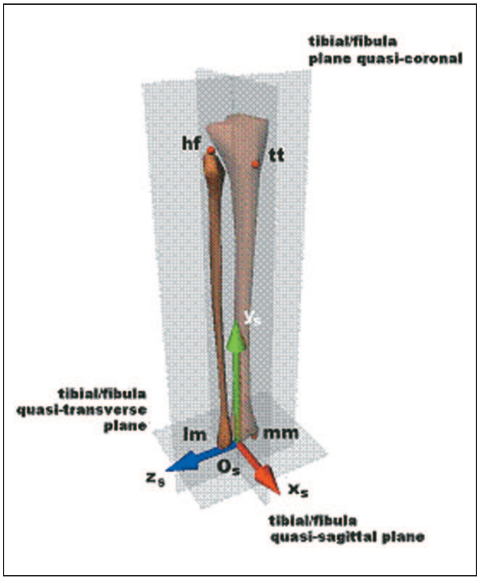

Figure 2. The anatomical coordinate system of the tibia

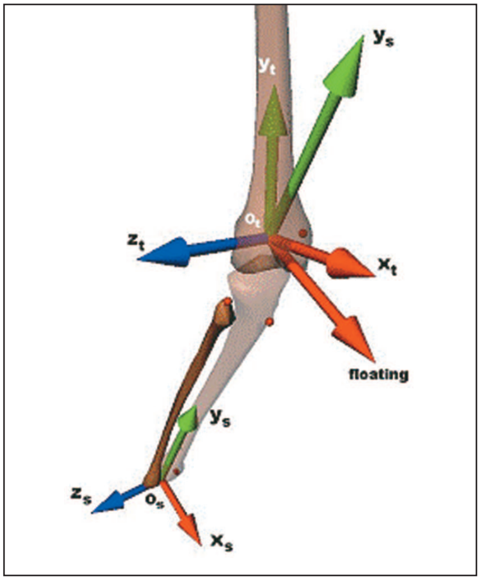

Figure 3. The joint coordinate system (JCS)

– the x_s axis of the coordinate system is perpendicular to the quasi-coronal plane with positive direction to the anterior
– the z_s axis of the coordinate system is mutually perpendicular to the x_s and y_s axis with positive direction to the right.

These anatomical points are needed to be determined during the experiments. The measurements were carried out on an experimental test rig with resected cadaver knees, so some of the anatomical points (lm, mm, fh) on the whole cadaver body had to be determined. The other points (me, le, hf, tt) can be determined on the whole cadaver body or on the fixed resection in the equipment also.

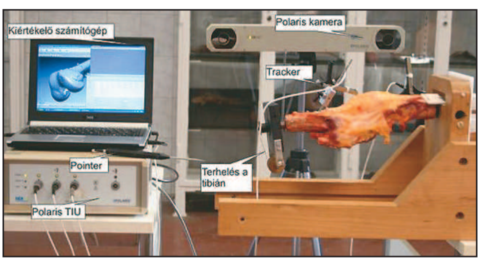

Figure 4. The experimental equipment with the Polaris system

Polaris infrared optical positioning system *(Figure 4)* was used for the determination of the position of the anatomical points during the experiments[11]. The placed trackers' positions were measured by the Polaris system in the coordinate system fixed to the still environment. The two moving trackers were attached to the femur and the tibia so they represented rigid body. The system is suitable for measuring the location of points in the coordinate system attached to the still environment which are shown by a pointer tracker. All of the anatomical points can be marked by the pointer with exception of head of femur. The location of the head of femur can be determined only with calculation.

The head of femur can be approximated with a sphere. If an orbital motion is performed by the femur then its motion is spherical motion around the center of femur head. The motion of the tracker attached to the femur also a spherical motion in this case. The center of femur head can be calculated from the measurement data.

The place of the trackers of the Polaris system was changed after the necropsy of the cadaver body and fixing the knee in the equipment. The anatomical coordinate system has to be known in the equipment also for the evaluation of the measurements performed in the equipment. So every location of the anatomical points have to be measured in the absolute coordinate system of the Polaris system. But the transformation of the location of the resected anatomical points has to be ensured to the equipment.

Six marker screws *(Figure 5)* were used for this purpose on every bone, which were screwed in the bones. The location of them was measured on the whole body and the cadaver knee fixed in the equipment also. So the connection was established by the screws between the two states. The resected anatomical points can be transformed to the equipment by the use of the coordinate system attached to the screws.

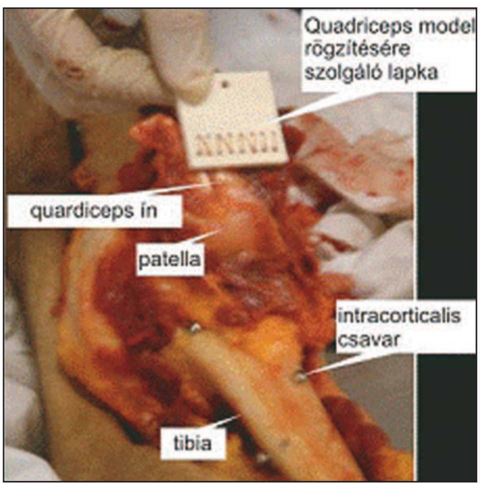

Figure 5. The prepared cadaver knee

Three marker screws are enough for the transformation, but the precision of the transformation can be increased by increasing the number of the screws.

A rubber belt which was the muscle model of the quadriceps was attached to the ligament of the quadriceps on the cadaver knee fixed in the equipment *(Figure 5)*. The load was attached to a rod fixed in the tibia by a cord *(Figure 4)*. The operation of the whole equipment was published by Szakál[14] earlier. Two types of measurements were carried out during the experiments:

– type 1.: The load was increased which caused the flexion of the knee. The load was decreased after the total flexion of the knee till the knee went to totally stretched position.
– type 2.: The force was decreased in the rubber belt which is the muscle model of the quadriceps, so the flexion of the knee was increasing. The force was increased in the rubber belt after the total flexion till the knee went to totally stretched position.

The soft tissues were removed from the bones at the end of the measurements and the location of the anatomical points was measured in the coordinate system of the Polaris.

The use of Euler angles became general for the description of the motion of the knee. The anatomical coordinate system of the femur can be rotated into the anatomical coordinate system by these angles in case of the right order of them *(Figure 3)*. The order of the Euler angles are: flexion-extension, abduction-adduction, external-internal rotation.

The angle of flexion-extension is the rotation around the z_t axis of the anatomical coordinate system of the femur (nearly transepicondylar). The external-internal rotation is the rotation around the y_s axis of the anatomical coordinate system of the tibia. The angle of abduction-adduction is rotation around the axis which is mutually perpendicular to the previous two axes (floating axis).

Results

Repetitions were done from all types of the measurements at three times, because of decreasing the errors of the measurements. Six marker screws were used instead of the needed three for the transformation of the anatomical points which could also help decrease the sum of errors. The measurements can be solidly reproduced *(Figure 6)* and the motion of the knee is independent from the type of the measurements. The functions of rotation against flexion divides in the range of the measurements between 25–70° of flexion in the range of 2° of rotation. The reason of this can be that the angular speed of flexion is increased in this range, so the reception of the signals changed. The level of the rotation compared to the abduction is quite less and the most part of the changing of rotation starts in the range of starting 35° of flexion.

The effect of the inaccuracy of determination of the anatomical coordinate system to the changing of functions of the kinematical parameters is detailed in the work of Bíró et al.[2].

The lack of accuracy can be originated to more than one reason, for example the error of the transformation of the evaluation method. The reason of this is that the marker screws are situated on a cylinder with small diameter. Thus the angular error of the coordinate system attached to the marker screws – which requires the transformation – is relatively large. Another reason of the lack of accuracy can be also the evaluation error of the center of the head of femur. The hip of the dead body cannot be fixed totally stiffly during the measurement for the determination of the center of the head of femur. So there is a little motion of the hip during the measurement. On the other hand the measurement error of the Polaris is appeared in the results during the evaluation of the location of the head of femur.

Again the reason of the accuracy of the determination can come from the fact that the ana-

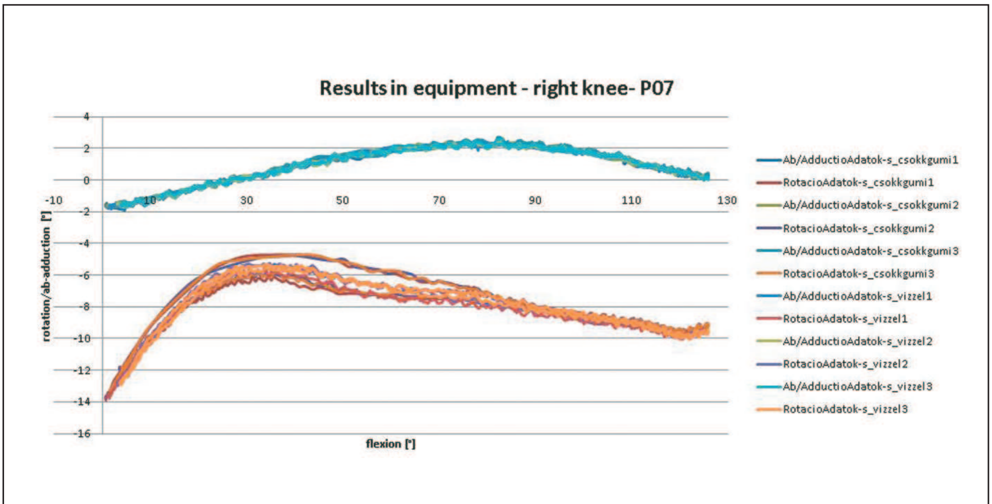

Figure 6. Rotation and ab/adduction functions against flexion in experiment no. 7.

tomical points are not exact, precisely definable points. They have to be marked on a finite size area.

It follows that different points are marked always at the repetition of the pointing (with the largest attention also). So, a lot of anatomical coordinate system can be determined close to each other. The anatomical points were marked in the equipment again in favor of estimation of these errors and the kinematical functions were also evaluated in the anatomical coordinate system determined this time.

The effect of the anatomical coordinate systems close to each other can be followed in the form of the functions of the same measurement *(Figure 7)*. It can be seen that the functions of rotation against flexion are almost parallel in the range of the starting 50° of the flexion. The characteristic of the functions totally changes after this range. The functions of ab/adduction against flexion start from nearly the same value, but their characteristic are totally different.

The measurements were carried out on five cadaver knees written down previously to predict the possibility of generalization. The external-internal rotation and abduction-adduction functions against flexion were represented during the evaluation of these measurements *(Figure 8, Figure 9)*. The functions of rotation against flexion are parallel independent from different cadaver knees and the errors of anatomical coordinate systems. The functions were represented that the starting rotation and adduction were 0° in favor of comparability. It can be seen, that the kinematical functions are in the same range in case of four from five knees. Deviation appeared in only one case. The reason of relatively little deviation between the four case can be the precariousness of the determination of anatomical coordinate system detailed previously. It was noticeable in case of the very different function (No.4) that the knee was in unusual valgus position which can be seen on its ab/adduction function *(Figure 9)*. If there is relatively large angle between the axis of flexion of the anatomical coordinate system (z_t) and the transepicondylar axis then the function of external-internal rotation changes significantly *(Figure 8)*.

It can be established that the knee starts from a lateral rotated position and ends in medial position during the flexion. The most part of

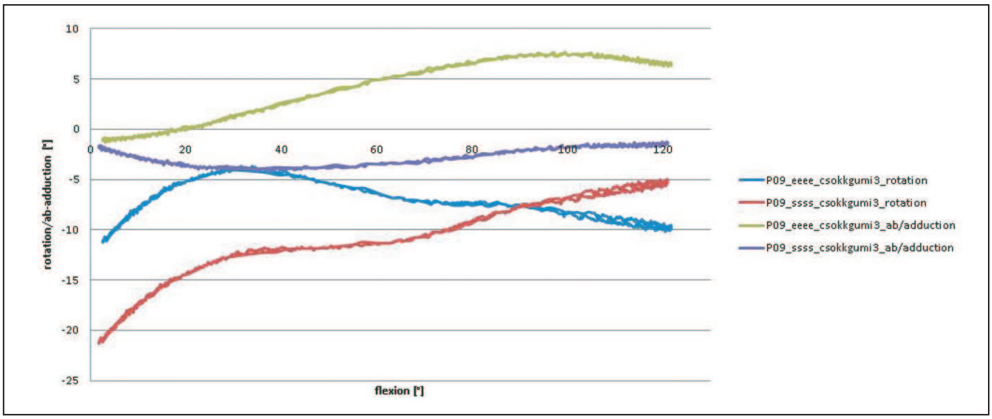

Figure 7. Rotation and ab/adduction functions against flexion of the same measurement evaluated in different anatomical coordinate system in experiment no. 9

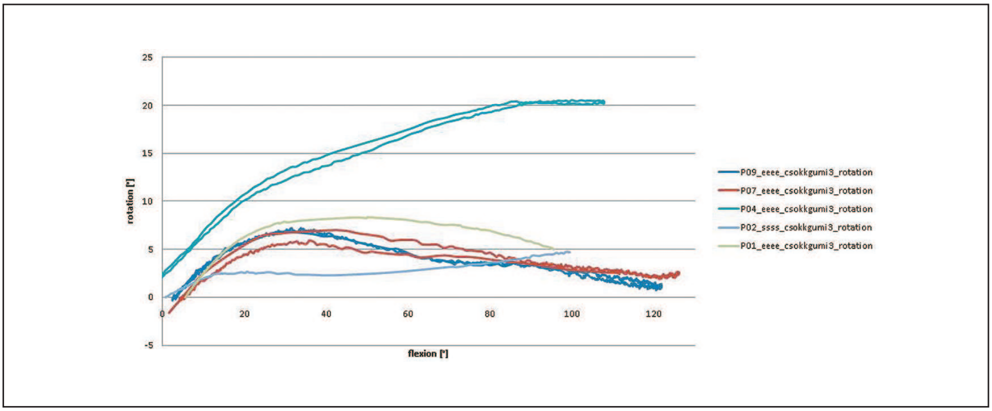

Figure 8. Rotation functions against flexion of the five experiments

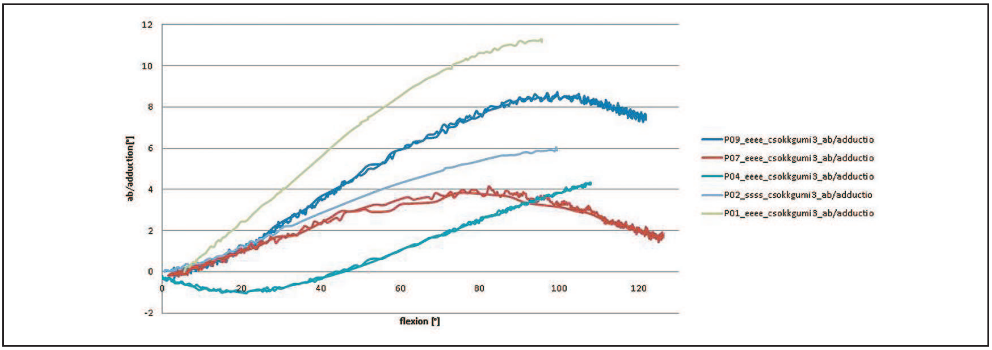

Figure 9. Ab/adduction functions against flexion of the five experiments

the changing of rotation is in the range of starting flexion around 30–35°. The value of the abduction-adduction is much less than the value of rotation.

Conclusion

The motion of the knee is described by the use of different anatomical coordinate systems and angles determined with different methods in the professional literature. Accordingly large standard deviation can be found in the kinematical parameters.

The following facts can be drawn on the basis of the published results that the use of our anatomical coordinate system based on the recommendation of VAKHUM project is well established. The protocol is suitable for the determination of the anatomical coordinate system and for the measurement. Less standard deviation can be found in the kinematical parameters with the use of our earlier presented evaluation method.

It can be established also, that it is very important to determine the location of the anatomical points more precisely and to reduce the transformation errors during the transformation of the location of anatomical points. Experiments are performed parallel with present work for minimalization of these errors and for determination of the sensitivity to inaccuracy.

References

1. *Aglietti P et al.* Rotational Position of Femoral and Tibial Components in TKA Using the Femoral Transepicondylar Axis. Clinical Orthopaedics and Related Research, 2008;466(11):2751–5.

2. *Bíró I, M. Csizmadia B,* and *Katona G.* Sensitivity investigation of three-cylinder model of human knee joint, IV. Hungarian Conference on Biomechanics, 2010.

3. *Braune W.* and *Fischer O.* Die Bewegungen des Kniegelenkes Nach Einer Neuen Methode am Lebenden Menschen Gemessen. 1891.

4. *Churchill DL et al.* The transepicondylar axis approximates the optimal flexion axis of the knee. Clinical Orthopaedics and Related Research, 1998;356:111–8.

5. *Eckhoff D et al.* Difference between the epicondylar and cylindrical axis of the knee. Clinical Orthopaedics and Related Research, 2007;461:238–44.

6. *Eckhoff DG et al.* Three-dimensional mechanics, kinematics, and morphology of the knee viewed in virtual reality. Journal of Bone & Joint Surgery – American Volume, 2005;87(Suppl 2):71.

7. *Grood ES* and *Suntay WJ.* A joint coordinate system for the clinical description of 3-dimensional motions – application to the knee. Journal of Biomechanical Engineering–Transactions of the Asme, 1983;105(2):136–44.

8. *Hollister AM et al.*, The axes of rotation of the knee. Clinical Orthopaedics and Related Research, 1993;290:259.

9. *Jenny JY* and *Boeri C.* Low reproducibility of the intra-operative measurement of the transepicondylar axis during total knee replacement. Acta Orthopaedica Scandinavica, 2004;75(1): 74–77.

10. *Jerosch J et al.* Interindividual reproducibility in perioperative rotational alignment of femoral components in knee prosthetic surgery using the transepicondylar axis. Knee Surgery Sports Traumatology Arthroscopy, 2002;10(3):194–7.

11. NDI, *http://www.ndigital.com/medical/polarisfamily-techspecs.php*

12. *Robinson M et al.* Variability of landmark identification in total knee arthroplasty. Clinical Orthopaedics and Related Research, 2006;442: 57–62.

13. *Stoeckl B, et al.* Reliability of the transepicondylar axis as an anatomical landmark in total knee arthroplasty. Journal of Arthroplasty, 2006;21 (6):878–82.

14. *Szakál Z.* Mérőberendezés térdízület mozgásvizsgálatához, GÉP 2006;LVII(1):37–40.

15. VAKHUM, *http://www.ulb.ac.be/project/vakhum*

16. *Weber WWF.* Mechanik der menschlichen Gehwerkzeuge. Göttingen, 1836.

17. *Yau WP et al.* Errors in the identification of the transepicondylar and anteroposterior axes of the distal femur in total knee replacement using minimally-invasive and conventional approaches – A cadaver study. Journal of Bone and Joint Surgery – British Volume, 2008;90B (4):520–6.

This study was carried out with the permission of the Hungarian Scientific and Research Ethical Committee (TUKEB 165-1/2002, renewed in 2007). We would like to acknowledge the help of Gábor Renner, György Szántó, and László Szobonya from the Hungarian Academy of Sciences, Computer and Automation Research Institute.

Gábor Katona
Szent Istvan University, Faculty of Mechanical Engineering
H–2100 Gödöllő, Páter Károly utca 1.

A NON-INVASIVE METHOD FOR THE EXAMINATION OF MUSCLE GEOMETRY TO THE EXPLORATION OF THE CONTEXT OF THE MUSCLE ACTIVITIES AND MUSCLE LENGTH CHANGES

Péter Katona[1], Tamás Pilissy[2], Gábor Fazekas[3], András Klauber[3], József Laczkó[1,2]

[1] Semmelweis University Faculty of Physical Education and Sport Sciences, Budapest
[2] Pázmány Péter Catholic University Faculty of Information Technology, Budapest
[3] National Institute for Medical Rehabilitation, Budapest
solg@freemail.hu

Introduction

We use functional electric stimulation (FES) in the treatment of spinal cord injured patients since 2005, in pursuance of this we use a stimulator and electrodes to make the paralyzed muscles of the lower limb drive the pedal of a stationary bicycle[1,2,3]. The stimulation pattern for this device is developed by studying muscle activity patterns of healthy subjects. The healthy muscle geometry can only be measured with expensive diagnostic devices/methods (MR, CT). Our aim is to develop a method, based on kinematic data (coordinates of ultrasonic markers) accessible by movement analyzing systems and it describes mathematically the changes of the muscle geometry during movements, in our case during cycling lower limb movement. We discern relations of geometrical changes and muscle activities.

Figure 1. A subject during the measurement (the colored points show the places where the markers were placed)

Methods

First, 3D coordinates of the markers, placed on anatomical landmarks of the left lower limb *(Figure 1.)* were measured. The measurement device was an ultrasonic movement analyzing system (CMS 70P, Zebris, Isny, Germany) that locates the place of ultrasonic speakers using three ultrasound sensitive microphones. This system applied a 3D coordinate system: the X-axis is horizontal in the frontal plane directed medial to lateral, Y-axis is horizontal in the sagittal plane directed forward, and z is perpendicular to the x-y plane directed upward. This system has widely been used in studying multijoint movements[4,5,6]. Kinematic data (marker coordinates) were assessed with sampling frequency of 50 Hz.

Then intrinsic local coordinate systems were defined (one in the ankle and one in the knee), the origo of these coordinate systems were placed into the suitable rotation center.

To localize the rotational center in the knee, the coordinates of the marker placed on the lateral epycondyle were translated along the X direction with half of the distance of the lateral and medial epycondyles. In the ankle the coordinates of the rotational center was computed from the coordinates of the marker placed on the lateral malleolus by translating it with 30 m along the X direction. This distance was a theoretical approximation of half of the distance of the lateral and medial malleoli.

The hip rotational center was localized translating the coordinates of the marker placed on the greater trochanter along the X axis with 60 mm. This distance was a theoretical approximation.

Three axes were defined in the knee (the orig is in the rotational center): the Y-axis was pointed to the rotational center of the hip, the X-axis was pointed to the lateral epycondyle (where the marker was placed), the Z-axis is the cross product of the Y- and X-axes. Then three axes were defined in the ankle: the Y-axis was pointed to the rotational center of the knee, the X-axis was pointed to the lateral malleolus (where the marker was placed), the Z-axis is the cross product of the Y- and X-axes.

The spatial coordinates of the attachment points of the muscles were determined in these coordinate systems as function of time. Data from literature[7,8] were used to compute the location of muscle attachments. The muscle length and its speed of change can be computed by trigonometric equations during the whole time of the movement. The algorithm was applied on 41 healthy subjects. The length and its change as a function of time of the subjects' Quadriceps and Biceps femoris were calculated using the received data during the movement *(Figure 2 and 3, Equation 1 and 2)*.

$$M_l = a_M + f_M + i_M \qquad a_M = \sqrt{a^2 - R^2} \qquad f_M = \sqrt{f^2 - R^2} \qquad i_M = R \cdot \beta \tag{1}$$

$$\beta = 2\Pi - (\alpha + \alpha_1 + \alpha_2) \qquad \alpha_1 = \arccos\left(\frac{R}{a}\right) \qquad \alpha_2 = a\cos\left(\frac{R}{f}\right) \tag{2}$$

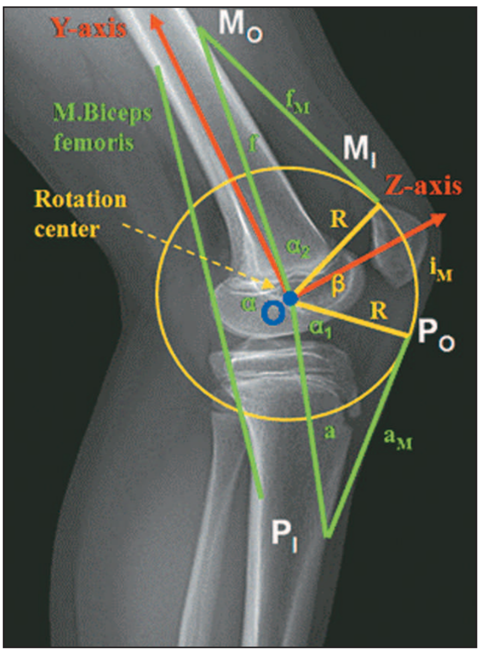

Figure 2. The schematic 3D figure of the algorithm used for the computation of the length of the Quadriceps

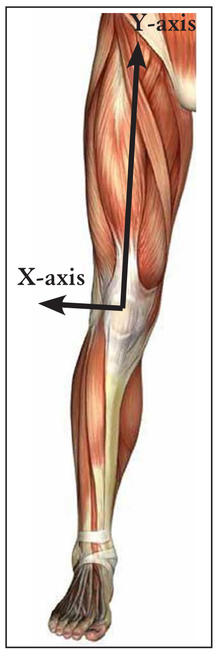

Figure 3. Two of the axes defined in the intrinsic coordinate system of the knee, the third one (Z) is visible on figure 2.

Where M_l is the muscle length, i_M is the section of the muscle that belong to the patella, f_M is the section of the muscle from its origin to the patella, a_M is the section of the muscle from its insertion to the patella (patella ligament), a is the distance between the rotation center (O) and the insertion of the patella ligament (P_I), f is the distance between the rotation center and the origin of the muscle M_O, R is the radius of the knee, P_I is the insertion and P_O is the origin of the patella ligament, α is the knee angle (spanned by a and f), α_1 is the angle spanned by the vectors OP_I and OP_O, α_2 is the angle spanned by the vectors OM_I (M_I is the insertion of the muscle) and OM_O, β is the angle belonging to the ark (i_M), all angles were used in radian.

Results

It was observed in the case of the Quadriceps *(Figure 4.),* that the largest extension of the muscle (largest length) coincides with the largest electric activity of the muscle (the maximum of the EMG curve), so the muscle activity is highest at the maximal length of the muscle.

In the case of the Biceps femoris the highest electric activity can be observed during the extension of the muscle *(Figure 5.)*. From our data, it is obvious that the maximum length of one of the observed muscle coincides with the minimal length of the other, antagonist muscle.

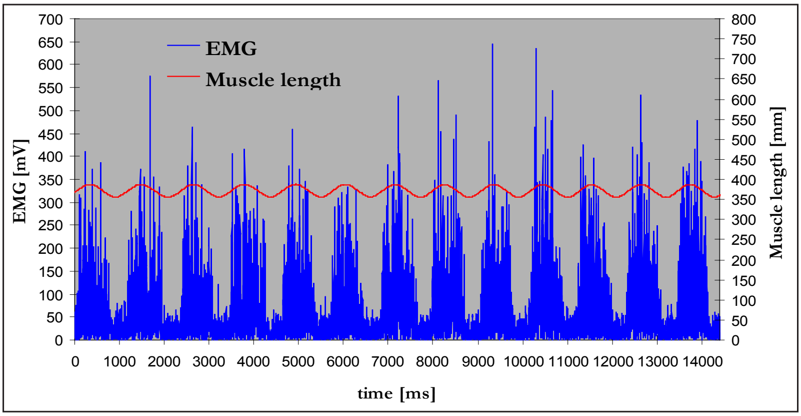

Figure 4.
The measured EMG and the computed muscle length data of subject K01's left Quadriceps muscle during the cycling movement

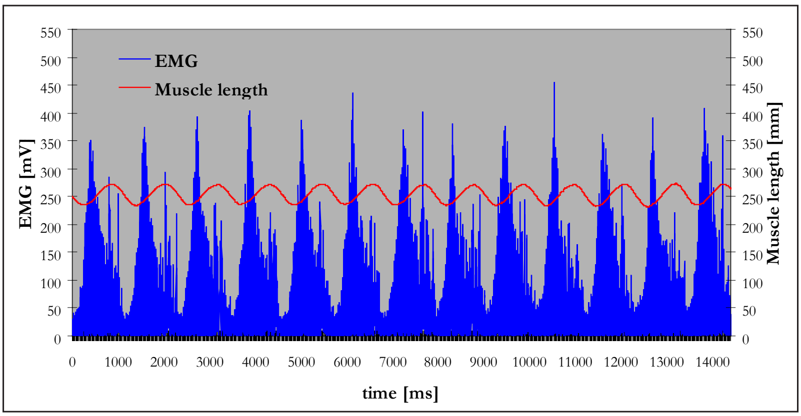

Figure 5.
The measured EMG and the computed muscle length data of subject K01's left Biceps femoris muscle during the cycling movement

Conclusion

Observing the electric activity and length of Quadriceps, the following contexts were deduced:

- When the muscle shortened maximally the length of the muscle begins to extend through the effect of the antagonist muscles (or through other force, that is in terms of the examined muscle exterior strength)

- Due to the extension, and the regulation of the motion (to increase the stability) electric signs arrive into the muscle, this leads to the deceleration of its length change

- Under the maximum electric activity of the muscle (at the maximum of the EMG curve) the extension of the muscle stops, indeed the muscle begins to contract

- Decreasing electric activity was observed during the contraction, what can be explained with the muscle force of the other lower limb. For example the Quadriceps shortening not ensues only because of his own effort but the effort of the Biceps femoris of the other lower limb. Thus, it is not necessary to produce high electric activity (force) to maintain the motion, it is more necessary during the switch between stretching and shortening, when the contraction begins in the required muscle.

The electric activity of the Biceps femoris muscle shows that this muscle plays an important role in the regulation of the motion thereby, that its activity is maximal at the time when the velocity of the stretching grows, so its activity makes the knee not to bend but it sets back the extension of it[9,10].

Discussion

Anthropometric data of individual subjects are required to define appropriate electrical activity patterns and forces of muscles rotating particular joints. Muscle synergy depends on muscle geometry. Thus the quantitative analysis of changes in muscle length is essential to define stimulation patterns for functional electrical stimulation of people with paralysed limbs. The relation between joint rotations and muscle length is studied for healthy subjects[11]. Based on this approach we proposed spatio-temporal cooperation of knee flexor and extensor muscle.

With the calculated contexts, the stimulation pattern used in the FES treatment of the spinal cord injured patients is modifiable. The therapy becomes more efficient thereby, that an artificial pattern was provided, which is biologically inspired and it takes notice of individual anatomic data. There is an infinity of different combinations of muscle activities to perform a motor task as cycling. The proper coordination and regulation of such movements may depend on geometric properties and may be enhanced by studying muscle synergies using theoretical approaches even without expensive experiments[12]. However in our knowledge no detailed quantitative analysis of muscle coordination is given for cycling lower limb movements. Our presented method is a research tool for further development of artificially designed muscle activity patterns. The next step is to establish 3D muscle forces required to execute a planned movement of a limb with given muscle geometry.

References

1. *Pilissy T, Klauber A, Fazekas G, Laczkó J, Szécsi J.* (2008): Improving functional electrical stimulation driven cycling by proper synchronization of the muscles. Clinical Neuroscience/Ideggyógy Szle 61(5-6) pp. 162–167.

2. *Szécsi J, Fincziczki Á, Laczkó J, Straube A.* (2005): Elektrostimuláció segítségével meghajtott (háromkerekű) kerékpár: Neuroprotézis harántsérült páciensek mindennapos használatára. Rehabilitáció, 15. évfolyam pp. 9–14.

3. *Laczkó J, Pilissy T, Klauber A.* (2008): Modeling of Limb Movements for Controlling Functional Electrical Stimulation of Paraplegics. Proc. of the Third Hungarian Conference on Biomechanics. ISBN 978 963 06 4307 8. pp. 151–157.

4. *Hermsdörfer J, Marquardt C, Wack S, Mai N.* (1999) Comparative analysis of diadochokinetic movements. J Elektromyogr Kinesiol 9: 283–295.

5. *Keresztényi Z, Cesari P, Fazekas G, Laczkó J.* (2008): The relation of hand and arm configuration variances while tracking geometric figures in Parkinson’s disease – “aspects for rehabilitation”. International Journal of Rehabilitation Research 2009;32:53–63.

6. *Kiss RM, Kocsis L, Knoll Zs.* Joint kinematics and spatial temporal parameters of gait measured by an ultrasound based system. Medical Engineering&Physics 2004; 26:611–620.

7. *Brand RA, Crowninshield RD, Wittstock CE, Pedersen DR, Clark CR, van Krieken FM.* (1982): A model of lower extremity muscular anatomy. Journal of Biomechanical Engineering, Vol. 104, pp. 304–310.

8. *Hoy MG, Zajac FE, Gordon ME.* (1990): A musculoskeletal model of the human lower extremity: the effect of muscle, tendon, and moment arm on the moment-angle relationship of musculotendon actuators at the hip, knee, and ankle. Journal of Biomechanics, Vol. 23, No. 2, pp. 157–169.

9. *Katona P, Pilissy T, Fazekas G, Laczkó J.* (2009): Ízületi szögsebességek, izomaktivitások és a pedálhajtás sebességének kapcsolata kerékpározó mozgáskor. VII. Országos Sporttudományi Kongresszus, In: Magyar Sporttudományi Szemle, 10. évf. 38. sz. p. 33.

10. *Katona P.* A Quadriceps és Hamstrings izmok elektromos aktivitásának vizsgálata kerékpározó mozgás során a sebesség függvényében, National Congress on Sport Sciences for Students 2009, (in Hungarian)

11. *Hawkins D & Hull ML.* (1990): A method for determininglower extremity muscle–tendon lengths during flexion/extension movements. J Biomech 23:487–494.

12. *Bernstein NA.* (1967): The co-ordination and regulation of movements. Pergamon, Oxford

Supported by ETT 363/2006, Scientific Council of Healthcare

Péter Katona
Semmelweis University Faculty of Physical Education and Sport Sciences, Budapest
H–1123 Budapest, Alkotás u. 44.

Biomechanica Hungarica III. évfolyam, 1. szám

A SÚLYFÜRDŐKEZELÉS HATÁSÁNAK VÉGESELEMES SZIMULÁCIÓJA A KEZDETI RUGALMAS SZAKASZBAN

Kurutzné Kovács Márta[1], Oroszváry László[2]
[1] Budapesti Műszaki és Gazdaságtudományi Egyetem, Budapest
[2] Knorr Bremse Hungaria Ltd, Budapest
kurutzm@eik.bme.hu

Absztrakt
A súlyfürdő a magyar reumatológia egyik legnagyobb gyakorlati jelentőségű felfedezése. Eredményeként az izmok ellazulnak, a gerinc megnyúlik, a porckorongsérv visszahúzódik, a fájdalom enyhül, a műtét megelőzhető. Ez a konzervatív kezelési mód hazánkban több mint fél évszázada széles körben elterjedt, sikeresen alkalmazzák, azonban külföldön nem ismerik, mivel korábban nem állt rendelkezésre a beavatkozás széles körű biomechanikai elemzése. A közelmúltban a kezelés biomechanikai hátterének elemzése és a keletkező megnyúlások in vivo kísérleti meghatározása, valamint a kezelés hatékonyságának klinikai kísérleti bizonyítása megtörtént. A jelen tanulmányban a kezelés numerikus szimulációjának eredményeit ismertetjük. 3D végeselemes numerikus szimulációval vizsgáljuk a kezelési folyamat mechanikai körülményeit és hatékonyságát. A súlyfürdőkezelés egy tipikus viszkoelasztikus folyamat. A jelen tanulmányban ennek a kezdeti rugalmas szakaszát vizsgáljuk. A számításainkat a lumbális L3–S1 gerincszakasz egy tipikus szegmentumának a végeselemes modellje alapján végezzük, amelynek húzási anyagállandóit a súlyfürdőben végzett in vivo kísérletek alapján állapítottuk meg, nyomási anyagállandóit a szakirodalomból vettük át. Számításaink alapján bebizonyítottuk, hogy a 40–45 év közötti korosztály lumbális szegmentumai a legsérülékenyebbek, a további idősödés során a szegmentális stabilitás erősödik. Megállapítottuk, hogy a súlyfürdőkezelés indirekt és direkt nyújtási szakaszból áll. A porckorong bilineárisan viselkedik: az indirekt szakaszban nagyobb a nyújtással szembeni ellenállása, mint a direkt szakaszban. Emiatt, annak ellenére, hogy a direkt nyújtóerő csak mintegy 6%-a az indirekt nyújtóerőnek, a direkt megnyúlások 20–80%-át teszik ki az indirekt megnyúlásoknak a szegmentum életkorától és degenerációs állapotától függően. Ugyanakkor a direkt szakaszban a porckorong feszültségi tehermentesülése csupán 2–8%-ot tesz ki. Következésképpen a többletsúlyokkal vezérelt direkt nyújtóerők elsősorban a porckorong megnyúlásaiért felelősek, előidézve az ideggyökök felszabadítását a kompressziós deformációk alól; ugyanakkor a felhajtóerő miatt lecsökkent testsúlyból és a függesztési testhelyzet miatt megszűnő izomerőkből eredő indirekt nyújtóerő a feszültségi tehermentesülésért felelős. A lumbális szegmentumok kezdeti rugalmas deformációi a súlyfürdőkezelés további viszkózus szakaszában a kúszási folyamat során mintegy megkettőződnek. A kezelés hatékonysága napi gyakoriságú többhetes kúra végére lesz optimális. Klinikai kísérletekkel azt bizonyították, hogy a súlyfürdő jótékony hatása három hónap elteltével is érzékelhető.

Kulcsszavak: súlyfürdőkezelés; lumbális szegmentum; végeselem-modell; numerikus szimuláció; direkt és indirekt nyújtás

Abstract
Weightbath hydrotraction treatment is one of the most important discoveries in the Hungarian rheumatology. Due to the treatment muscles relax, the spine stretches, the disc contracts, the pain mitigates, operation may be avoided. The weightbath treatment has been applied in Hungary successfully for more than a half century, however, it is unknown elsewhere because of the lack of experimental clinical and biomechanical analysis and proof of its efficiency. Recently, Hungarian researchers have investigated the biomechanical and experimental analysis of its stretching and clinical evidences; in this paper the numerical simulation of the treatment is presented. 3D finite element models of human lumbar functional spinal units were used for numerical analysis of weightbath hydrotraction therapy applied for treating degenerative diseases of the lumbar spine. Five grades of age-related degeneration were modeled by material properties. Tensile material parameters of discs were obtained by parameter identification based on in vivo measured elongations of lumbar segments during the regular weightbath treatment. Compressive material constants were obtained from the literature. It has been proved numerically that young adults of 40–45 years have the most deformable and vulnerable discs, while the stability of segments increases with further aging. The reasons were found by analyzing the separated contrasting effects of decreasing incompressibility and increasing hardening of nucleus, yielding non-monotonous functions of stresses and deformations in terms of aging and degeneration. The weightbath treatment consists of indirect and direct traction phases. Discs show a bilinear material behaviour with higher resistance in indirect and smaller in direct traction phase. Consequently, although the direct traction load is only 6% of the indirect one, direct traction deformations are 20–80% of the indirect ones, depending on the grade of degeneration. Moreover, the ratio of direct stress relaxation remains equally about 2–8% only. Consequently, direct traction controlled by extra lead weights influences mostly the deformations being responsible for the nerve release; while the stress relaxation is influenced mainly by the indirect traction load coming from the removal of the compressive body weight and muscle forces in the water. These initial elastic elongations of the lumbar spine are doubled during the further creep period of the treatment. The optimal efficiency of the treatment develops by the end of a 2-3 weeks long cure of daily treatments. The beneficial clinical impacts of WHT are still evident even 3 months later.

Keywords: weightbath hydrotraction treatment; lumbar segments; finite element model; numerical simulation; direct and indirect traction

---

1. Bevezetés

A súlyfürdő a magyar reumatológia egyik legnagyobb gyakorlati jelentőségű találmánya[1,2]. A száraznyújtás már nagyon régóta ismert a gyógyászatban, azonban bebizonyították[3,4,5], hogy ahelyett, hogy a kezelés alatt a porckorong tehermentesülne a nyomás alól, az izmok ellenállása miatt megnövekednek benne a feszültségek. Ezek a megfigyelések mutatják a súlyfürdőkezelés rendkívüli jelentőségét, ugyanis itt a langyos vízben kényelmesen függő betegek izomzata teljesen elernyed, semmiféle izom-összehúzódás nem történik. A betegek függőleges testhelyzetben függnek egy rugalmas nyaki galléron, vagy kétoldali hónaljtámaszon, de a kettő kombinációja is előfordulhat. Eközben ólomsúlyok függnek a betegeken, vagy a bokáikra, vagy derékszíjra akasztva, kétoldalt. Mechanikai számításokkal igazoltuk, hogy a lumbális szakasz leghatékonyabb nyújtását a nyaki felfüggesztés adja, bokasúlyokkal[6].

A jelen tanulmányban a súlyfürdőkezelés során lejátszódó mechanikai folyamatok numerikus szimulációjának legfontosabb eredményeit ismertetjük. A vizsgálat részleteiről a nemzetközi kutatás számára a Kurutz és Oroszváry[14] tanulmányban számoltunk be.

A numerikus szimulációval azt kívántuk kimutatni, hogy hogyan tehermentesülnek a lumbális szegmentumok a súlyfürdő kezdeti rugalmas fázisában a káros kompressziós hatások, a feszültségek és összenyomódások alól. A szerzők ismerete szerint tiszta centrikus húzásra vonatkozó numerikus szegmentummodellek nem léteznek a szakirodalomban, mivel a húzás nem tipikus igénybevétele a gerincnek. Húzás említésére csupán mint az egyéb fiziológiai igénybevételek, az előre- és hátrahajlás, vagy az oldalra hajlás vizsgálatakor fellépő járulékos hatásra kerül sor[4,7,8,9], nem fordul elő, hogy a húzást mint domináns igénybevételi formát kezelnék.

A jelen tanulmányban a lumbális L3–S1 szakaszra kidolgozott numerikus szegmentummodellt domináns húzási igénybevételre dolgoztuk ki, az L3–4, L4–5 és L5–S1 szegmentumokon a súlyfürdőben végzett in vivo nyúlásméréseink alapján[10,11], amelyeket egy speciális, az adott célra kifejlesztett víz alatti ultrahangos mérési módszer segítségével végeztük[12,13].

A súlyfürdőkezelés általában 20 percig tart, ezalatt egy tipikus viszkoelasztikus folyamat játszódik le a gerincben. A vízben történő felfüggesztés után azonnal lejátszódik a pillanatnyi rugalmas szakasz, azután indul a kúszás, változatlan teher mellett. E helyt csak a kezelés első, rugalmas fázisával foglalkozunk, a második, viszkoelasztikus kúszási folyamat elemzéséről később számolunk be.

2. Módszerek

2.1. Terhek és megnyúlások a súlyfürdőben

Biomechanikai elemzés szerint[6] nyaki felfüggesztésnél három teherhatás okoz megnyúlást a gerincoszlop mentén: (1) a *dekompressziós erő,* amely a vízben megszűnő testsúly és az elernyedt izomerők összegéből áll, (2) az *aktív nyújtóerő,* amely a testsúly és a felhajtóerő különbségének felel meg; (3) az alkalmazott *ólomsúlyokból* származó nyújtóerő. Az első teher az *indirekt nyújtóerő,* a második és harmadik együtt a *direkt nyújtóerő*[30].

A jelen numerikus analízis során az átlagos, 700 N testsúlyból indulunk ki. Ennek alapján 840 N direkt és 50 N indirekt nyújtóerőt vettünk figyelembe[6,12,14].

Mivel senki nem ismeri a porckorong vagy a szegmentum intakt, tehermentes állapotát, definiálnunk kellett a megnyúlásra vonatkozó viszonyítási rendszert. A lumbális szegmentum és porckorong megnyúlását a kezelés előtti egyenesen álló testhelyzetben fennálló összenyomott állapothoz viszonyítottuk, vagyis ezt az állapotot tekintettük zérus megnyúlású állapotnak.

2.2 A szegmentum végeselemes modellje

Az L3–S1 szegmentum 3D geometriai modelljét egy tipikus lumbális szegmentum méretei alapján vettük fel *(1. a ábra)*. A csigolyatestnél megkülönböztettük a corticalis és trabecularis részt, és a nyúlványokhoz tartozó elemeket. A csigolyafal vastagsága 0,35 mm, a véglemezek vastagsága 0,5 mm volt. A porckorong nucleusát és annulusát külön kezeltük, az annulus mátrixát két gyűrűre osztottuk, amelyeket egymástól és a nucleustól szálrétegek választanak el[15,16]. A szálak keresztmetszeti területe 0,1 mm^2 volt. A kisízületek iránya és

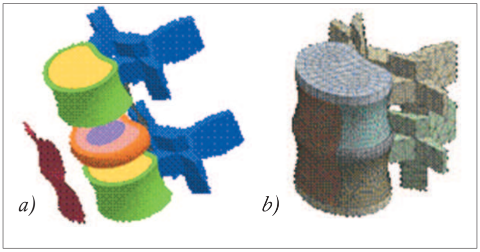

Figure 1. The geometrical model and FE mesh of FSU

geometriája a szakirodalmi adatokat követte[17]. Mind a hét lumbális gerincszalagot beillesztettük a modellbe.

A végeselemes hálózatot három lépésben alakítottuk ki: (1) geometriai modell felvétele Pro/Engineer, (2) a végeselemes hálózat felvétele ANSYS Workbench, és (3) a szegmentum különböző alkotórészeinek integrálása a modellbe ANSYS Classic programmal *(1. b ábra)*. Az annulusmátrixot, a nucleust és a szivacsos csontot, a nyúlványokat és a kisízületeket, továbbá bizonyos kapcsolatokat térfogatelemekből, a csontos véglemezeket és a csigolya corticalis részét, valamint a szalagokat héjelemekből, végül az annulus szálait rúdelemekből építettük fel.

2.3 A szegmentum-modell anyagállandói

A súlyfürdőkezelés kezdeti pillanatnyi fázisában a szegmentum minden alkotórésze rugalmasan viselkedik. A csontelemekre húzásra és nyomásra azonosan viselkedő rugalmas, izotrop anyagot feltételeztünk a szakirodalom alapján[15,16,18-25] *(1. táblázat)*. A porckorong nucleusát és annulusának mátrixát lineárisan rugalmasnak feltételeztük nyomásra, és bilineárisan rugalmasnak húzásra. Nyomáshoz és dekompressziós nyújtáshoz a szakirodalmi nyomási adatokat használtuk, de aktív nyújtáshoz a rugalmassági modulust a nyúlásmérési adataink alapján végzett paraméter-identifiká-

A szegmentum alkotórészei	Rugalmassági modulus [MPa]	Poisson-tényező
Corticalis héj	12000	0,3
Szivacsos csont	150	0,3
Csigolyanyúlványok	3500	0,3
Véglemezek	100	0,4
Annulusmátrix	4/0,4*	0,45
Annulusszálak	500/400/300**	–
Nucleus	1/0,4*	0,499
Elülső hosszanti szalag	8*	0,35
Hátulsó hosszanti szalag	10*	0,35
A többi szalag	5*	0,35

*húzás, **külső/közbenső/belső szálak, húzás

1. táblázat. Az egészséges szegmentum anyagállandói

ciós módszerrel[14] határoztuk meg. A nucleus collagen szálait csak húzásra dolgozó lineárisan rugalmas anyagúnak feltételeztük[26,18,27,21], a kollagéntartalom radiális változását kifelé növekvő merevséggel szimuláltuk[28,15,16]. A gerincszalagokat lineárisan rugalmas, csak húzásra dolgozó anyaggal modelleztük[18,29,24].

Mivel a súlyfürdőkezelés degenerált szegmentumokon történik, figyelembe vettük az életkori degeneráció egyes stádiumait. Öt degenerációs fokozatot dolgoztunk ki *(2. táblázat)*, amelyben a nucleus folyadékszerű állapotának megszűnését a Poisson-tényező csökkenésével, a nucleus fokozatos keményedését pedig a rugalmassági modulusa növekedésével modelleztük[33,8,9]. Az annulus és a véglemezek károsodását is követtük[28,34,35,36].

Az egészséges és a degenerált végeselemes modell validálását húzásra és nyomásra egyaránt elvégeztük. 2000 N centrikus nyomás esetén a porckorong szagittális középsíkjában keletkező függőleges nyomófeszültségek számításból kapott nagyságát és eloszlását hasonlítottuk össze Nachemson[37], Adams és munkatársai[32,33], Dolan és Adams[8], Adams és Dolan[9] ún. stress-profilometriával nyert kísérleti eredményeivel. Az eredmények meggyőző egyezést

Degenerációs fokozatok	1. fokozat egészséges		2. fokozat		3. fokozat		4. fokozat		5. fokozat teljes deg.	
	E (MPa)	ν	E (MPa)	ν	E (MPa)	ν	E (MPa)	ν	E (MPa)	ν
Nyomás										
nucleus	1	0.499	3	0.45	9	0.4	27	0.35	81	0.3
annulusmátrix	4	0.45	4.5	0.45	5	0.45	5.5	0.45	6	0.45
szivacsos csont	150	0.3	125	0.3	100	0.3	75	0.3	50	0.3
véglemezek	100	0.4	80	0.4	60	0.4	40	0.4	20	0.4
Húzás										
nucleus	0.4	0.499	1.0	0.45	1.6	0.4	2.2	0.35	2.8	0.3
annulusmátrix	0.4	0.45	1.0	0.45	1.6	0.45	2.2	0.45	2.8	0.45

2. táblázat. A degenerált szegmentum anyagállandói

mutattak. Húzás esetén az L3–S1 lumbális szakaszhoz tartozó szegmentumra 1000 N indirekt és 50 N direkt nyújtóerővel számított megnyúlási eredményeinket hasonlítottuk össze Kurutz[12] és munkatársai[11] a súlyfürdőben in vivo mért kísérleti eredményeivel. Nemcsak a megnyúlási értékek, hanem azok életkori megoszlását mutató függvények is nagy hasonlóságot mutattak. Ennek alapján a fenti táblázatok szerint felvett anyagállandók elfogadható alapot képeztek a súlyfürdő mechanikai jelenségeinek numerikus szimulációjához.

3. Eredmények

A *2. a ábrán* a porckorong megnyúlását, azaz a kezelés előtti összenyomódásának csökkenését látjuk a degeneráció függvényében az indirekt és a direkt nyújtóerők külön-külön és együttes hatására. A *2. b ábrán* a posterolaterális annulus szálaiban keletkező maximális húzóerő csökkenését ábrázoltuk a kezelés első fázisában a degeneráció függvényében, ugyancsak elkülönítve az indirekt és direkt nyújtóhatást. A megnyúlások két komponensét szemügyre véve látható, hogy az egészséges porckorongnál (1. fokozat) a direkt nyúlások az indirekt nyúlásoknak mintegy a 46%-át teszik ki, a közepesen degenerált porckorongnál (3. fokozat) a 26%-át, míg a degeneráció utolsó fázisában (5. fokozat) a 83%-át. A szálerőknél e három degenerációs fázisban a direkt hatásra keletkezők az indirekt nyújtóerőből keletkező szálerők 37, 21 és 17%-át teszik ki.

A *3. ábrán* a porckorong kihasasodásának csökkenését látjuk, azaz az elülső, hátulsó és ol-

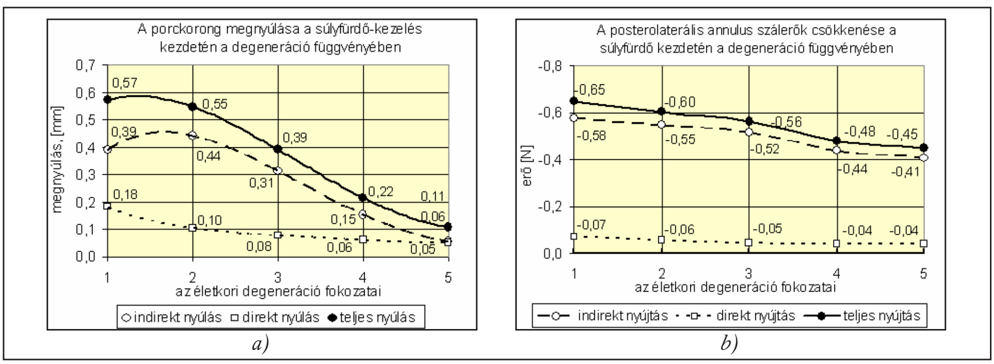

2. ábra. a) A porckorong megnyúlása és *b)* az annulus szálaiban lévő húzóerő csökkenése a súlyfürdőkezelés kezdetén az életkori degeneráció függvényében

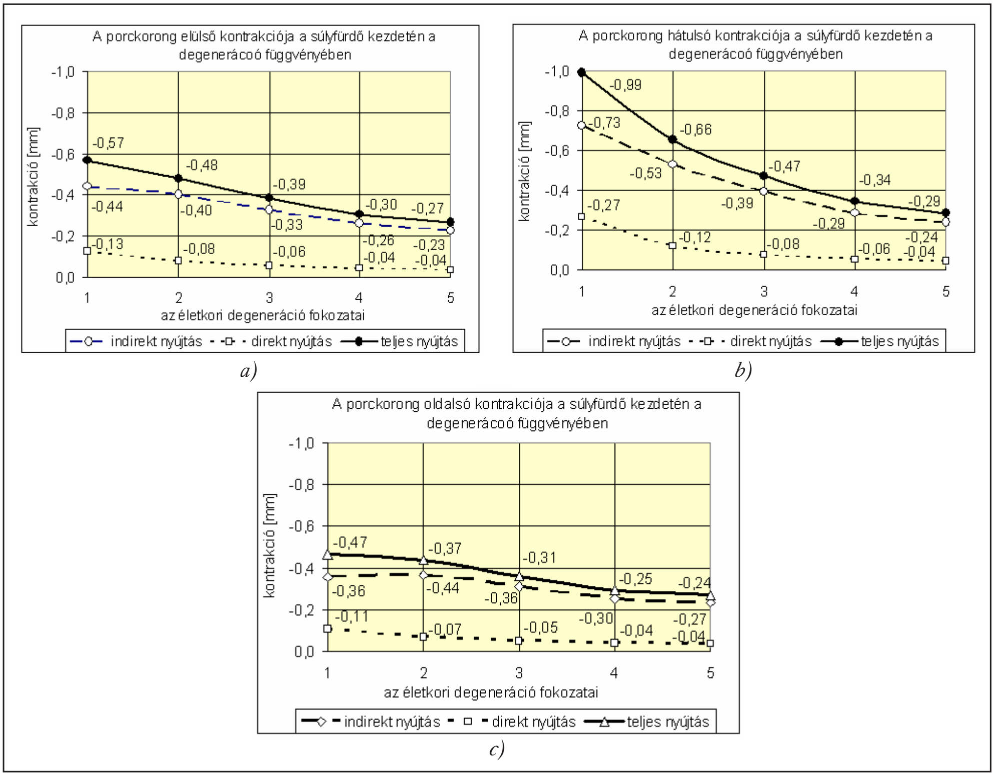

3. ábra. A porckorong *a)* elülső, *b)* hátulsó és *c)* oldalsó kontrakciójának növekedése, vagyis kihasasodásának csökkenése a súlyfürdőkezelés kezdetén az életkori degeneráció függvényében

dalsó kontrakció növekedését a súlyfürdőkezelés kezdeti pillanataiban, az indirekt és a direkt nyújtóerő hatására a degeneráció függvényében. A porckorong megnyúlásához hasonlóan, amelyet az összenyomódás csökkenéseként definiáltunk, a kontrakciót is a kezelés előtti egyenesen álló testhelyzetben fennálló kihasasodás csökkenéseként értelmeztük. Az elülső direkt kontrakció *(3. a ábra)* az egészséges, közepesen és súlyosan degenerált esetben (1., 3. és 5. fokozat) az indirekt kontrakció 30, 18 és 17%-át teszi ki, ugyanez a hátulsó kontrakció *(3. b ábra)* esetén 37, 21 és 17%, míg oldalsó kontrakciónál *(3. c ábra)* 31, 14 és 15%.

A *4. ábra* a porckorong nucleusában lezajló feszültségi tehermentesülés eseteit mutatja. A nucleus közepén fellépő függőleges és vízszintes nyomófeszültségek kezelés hatására bekövetkező csökkenését *4. a* és *4. b ábrán* ábrázoltuk, a degeneráció függvényében. A *4. c* és a *4. d ábrákon* ugyanezt láthatjuk a nucleus szélén, az annulussal határos szakaszokon. Látható, hogy a feszültségek esetén a direkt nyújtás hatása csekélyebb, mint a deformációknál: a függőleges és vízszintes feszültségek csökkenése a direkt nyújtás hatására egészséges, közepesen és súlyosan degenerált esetben (1., 3. és 5. fokozat) egyaránt csupán mintegy 6–8, 4–5 és 2–3%-át teszi ki az indirekt nyújtásból keletkezett feszültségcsökkenésnek.

Az *5. ábra* a külső annulusban fellépő függőleges nyomófeszültségek csökkenését mutatja a súlyfürdőkezelés kezdetén a degeneráció függvényében. Itt a direkt nyújtás hatására létrejövő

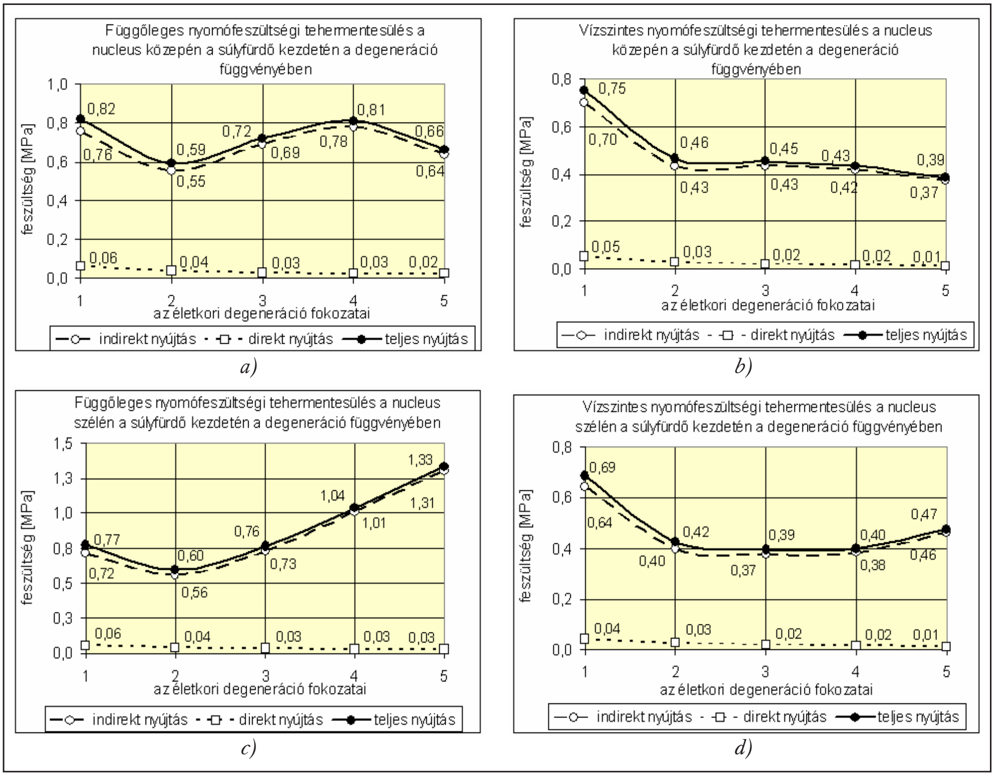

4. ábra. Nyomófeszültségek csökkenése a porckorong nucleusában a súlyfürdőkezelés kezdetén a degeneráció függvényében
a) függőleges és *b)* vízszintes nyomófeszültségek a porckorong közepén, *c)* függőleges és *d)* vízszintes nyomófeszültségek a nucleus szélén, az annulus határán

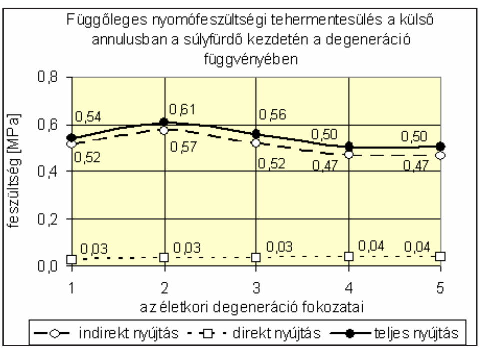

5. ábra. Függőleges nyomófeszültségek csökkenése a porckorong külső annulusában a súlyfürdőkezelés kezdetén a degeneráció függvényében

feszültégcsökkenés ugyancsak csupán 6, 6 és 9%-a az indirekt nyújtásból keletkezőnek egészséges, közepesen és súlyosan degenerált esetben.

4. Megbeszélés

A súlyfürdőkezelés elsősorban a különféle porckorong-bántalomban szenvedő betegek számára javasolt[30]. Hatására a kompressziós teher miatt összenyomódott porckorongokban jótékony tehermentesülési folyamat játszódik le, a szegmentumok flexibilitása megnő, a fájdalom csökken, megszűnik. A napi mintegy 20 perces kezelést két-négy héten át ismételve, a kedvező klinikai hatások még három hónap múlva is megfigyelhetők, amint azt Oláh és munkatársai[43] klinikai kísérleteikkel kimutatták.

A porckorong degenerációs változásának fő megnyilvánulása a folyadékszerű viselkedés megszűnése az egyidejű szilárdulással. Ennek modellezése a nucleus Poisson-tényezőjének csökkentésével és a rugalmassági modulusának egyidejű növelésével történt[40,41], a porckorong egyéb tulajdonságainak a változtatásával együtt[22,42].

A súlyfürdőkezelés első, rugalmas szakaszában a terhelés és az ennek következtében fellépő deformációk és feszültségek indirekt és direkt fázisra bonthatók. Centrikus húzásra ugyanis a porckorong nucleusa és annulusának mátrixa bilineárisan rugalmas anyagúnak tekinthető: az indirekt nyújtási fázisban nagyobb, a direkt fázisban kisebb ellenállással. Acaraglou és munkatársai[38], valamint Ebara és munkatársai[39] szerint a húzási tulajdonságok a porckorongon belül a hely függvényei. Valóban, centrikus nyomásnál az egészséges porckorongban hidrosztatikus nyomás uralkodik, amely erős támaszt ad az annulus lamelláinak belülről, és a csaknem vízszintes, abroncsszerűen elhelyezkedő szálakban levő húzóerők pedig kívülről. Hasonló ellenhatást gyakorol az annulus a nucleusra. Centrikus húzásnál azonban ennek ellentéte történik. A szálak húzóereje csökken, ugyanakkor a szálak iránya egyre meredekebbé válik[33], és egyidejűleg a nucleusban lecsökken a hidrosztatikus nyomás, és mintegy szívássá válik, következésképpen, a dekompresszió végeztével, az aktív nyújtási szakaszban indokolt a kisebb ellenállás figyelembevétele.

Az extra súlyokkal végzett direkt nyújtás elsősorban a deformációkért, tehát az ideggyökök felszabadításáért, míg az indirekt nyújtás a feszültségek tehermentesítő hatásáért felelős. Annak ellenére, hogy a direkt nyújtóerő csak mintegy 6%-a az indirekt nyújtóerőnek, a porckorong megnyúlásában a direkt nyújtás hatása 20–80%-a az indirekt nyújtásénak. Különösen érvényes ez idős embereknél, a degenerációs folyamat végén, ahol ez a direkt/indirekt arány a legmagasabb. A porckorong kontrakciójában a direkt hatás 15–35%-az indirektnek. Ugyanakkor a feszültségeknél a direkt nyújtóerőből származó feszültségcsökkenés mindössze 2–8%-a volt az indirekt nyújtóerőből keletkezőnek. Éppen ez, a direkt nyújtóerőknek, az alkalmazott extra ólomsúlyoknak a jelentős nyújtóhatása adja a súlyfürdőkezelés nagy jelentőségét. Amint a fenti eredményekből kiderül, a súlyfürdőkezelés során az extra súlyok alkalmazásának nagy fontossága van, különösen idős embereknél, ahol a direkt nyújtóerőnek domináns hatása van. Ez egyben óvatosságra kell, hogy intse a kezelést előíró orvost az alkalmazandó súlyok nagyságának mérlegelésénél.

Az extra súlyok hatásának fontossága vezette Moll Károlyt a jelenleg használtaknál nagyobb súlyok alkalmazásához, anélkül, hogy ezek komolyabb sérüléssel jártak volna. Valóban, előfordulhat, hogy a súlyfürdőkezelésnél a megszokott 2-szer 2-3 kg-os súlyoknál nagyobb súlyt kell alkalmazni a kívánt nyújtóhatás eléréséhez. Végh[44] in vivo kísérleteivel igazolta, hogy extra súly nélkül csupán a test felhajtóerejéből számított direkt nyújtóerő negatív is lehet, ha a beteg fajsúlya kisebb, mint a vízé. Ekkor a beteget a víz a felszínre dobja, és a kezelés extra súlyok nélkül nem is hajtható végre. Ez előfordulhat, ha a beteg kövér, vagy a víz olyan gyógyvíz, amelynek magas az ásványianyag-tartalma.

A lumbális gerinc centrikus nyújtására vonatkozóan sem kísérleti, sem numerikus eredmények nem találhatók a nemzetközi szakirodalomban. Kurutz és munkatársai voltak az elsők, akik a porckorong centrikus húzásából keletkező megnyúlásokat in vivo megmérték[10–13], és numerikusan szimulálták[14]. A kísérleti és numerikus eredményeiket összehasonlítva megnyugtató egyezést találtak[14]. A gyengén degenerált porckorong a súlyfürdőben 0,1–0,15 mm direkt, 0,4–0,45 mm indirekt és mintegy 0,6 mm teljes azonnali rugalmas megnyúlást szenvedett, miközben 0,1–0,3 mm direkt, 0,5–0,7 mm indirekt és mintegy 0,7–1,0 mm teljes hátulsó kontrakciója keletkezett. A súlyosan degenerált porckorong mintegy 0,05 mm direkt, 0,06 mm indirekt és 0,11 mm teljes megnyúlást, továbbá 0,05 mm direkt, 0,25 mm indirekt és 0,3 mm teljes hátulsó kontrakciót mutatott a kezdeti, rugalmas szakaszban.

Összefoglalva: elvégeztük a súlyfürdőkezelés kezdeti rugalmas szakaszában a szegmentum gyógyítóhatású nyúlásának és tehermentesülésének numerikus szimulációját. Megállapítottuk, hogy a porckorong alakváltozás-képessége az öregedéssel és a degenerációval csökken, azonban fiatal felnőtt korban, 40–45 év körül a legmozgékonyabb, egyben a legsérülékenyebb. Bender[45] szerint a hazai gyógyfürdőkben és reumatológiai osztályokon a porckorong-bántalmakkal kezelt betegek zöme a 40–55 év közöttiek közül kerül ki. Ennek okát kizárólag numerikus szimulációval tudtuk kimutatni: az öregedés kezdetén a nucleusban megszűnő hidrosztatikus nyomásnak, később a nucleus keményedésének van domináns hatása[14]. A direkt és indirekt trakciós fázisban az annulusmátrix eltérően viselkedik: jóval merevebb az indirekt, és hajlékonyabb a direkt fázisban, ezért jóval nagyobb deformációk keletkeznek az alkalmazott extra súlyoknál. Ez a tény a kezelő orvost a súlyok alkalmazásakor megfontolásra figyelmezteti. A súlyfürdőkezelés indirekt fázisában keletkezik a feszültségrelaxáció, azaz a feszültségi tehermentesülés, míg a direkt fázisában keletkezik az alakváltozási tehermentesülés, a porckorong kontrakciója, az ideggyökök felszabadulása a környezeti káros deformációk alól. Oláh és munkatársai[43] bebizonyították, hogy a súlyfürdőkezelés előnyös klinikai hatása még három hónap múltán is kimutatható.

IRODALOM

1. *Moll K,* 1956. Die Behandlung der Discushernien mit den sogenannten “Gewichtsbadern”. Contempl. Rheum., 97:326–329.
2. *Moll K.* 1963. The role of traction therapy in the rehabilitation of discopathy. Rheum. Balneol. Allerg., 3:174–177.
3. *Andersson GB, Schultz AB, Nachemson AL.* 1983. Intervertebral disc pressures during traction. Scand. J. Rehabil. Med. Suppl. 9:88–91.
4. *White AA, Panjabi MM.* 1990. Clinical Biomechanics of the Spine, Lippincott Williams and Wilkins, Philadelphia, etc.
5. *Ramos G, Martin W.* 1994. Effects of vertebral axial decompression on intradiscal pressure. Journal of Neurosurgery, 81(3):350–353.
6. *Bene É, Kurutz M.* 1993. Weight-bath and its biomechanics (in Hungarian). Orvosi Hetilap, 134. 21:1123–1129.
7. *Bader DL, Bouten C.* 2000. Biomechanics of soft tissues. In: Dvir, Z. (Ed.), Clinical Biomechanics. Churchill Livingstone, New York, Edinburgh, London, Philadelphia, pp. 35–64.
8. *Dolan P, Adams MA.* 2001. Recent advances in lumbar spinal mechanics and their significance for l. Clinical Biomecanics., 16, Suppl.(1):S8–S16.
9. *Adams MA, Dolan P.* 2005. Spine biomechanics. Journal of Biomechanics, 38(10):1972–1983.
10. *Kurutz M, Bene É, Lovas A, Molnár P, Monori E.* 2002a. In vivo biomechanical experiments for measuring traction deformations of human

lumbar spine during weightbath therapy. (In Hung.). Orvosi Hetilap, 143 (13):673–684.

11. *Kurutz M, Bene É, Lovas A.* 2003. In vivo deformability of human lumbar spine segments in pure centric tension, measured during traction bath therapy. Acta of Bioengineering and Biomechanics, 5(1):67–92.

12. *Kurutz M.* 2006a. Age-sensitivity of time-related in vivo deformability of human lumbar motion segments and discs in pure centric tension. Journal of Biomechanics, 39(1):147–157.

13. *Kurutz M.* 2006b. In vivo age- and sex-related creep of human lumbar motion segments and discs in pure centric tension. Journal of Biomechanics, 39(7):1180–9.

14. *Kurutz M, Oroszváry L.* 2010. Finite element analysis of weightbath hydrotraction treatment of degenerated lumbar segments in elastic phase. Journal of Biomechanics, 43(3):433–441.

15. *Denoziere G.* 2004. Numerical modeling of ligamentous lumbar motion segment. Master thesis. Georgia Institute of Technology, 2004.

16. *Denoziere G, Ku DN.* 2006. Biomechanical comparison between fusion of two vertebrae and implantation of an artificial intervertebral disc, Journal of Biomechanics, 39:766–775.

17. *Panjabi MM, Oxland T, Takata K, Goel V, Duranceau J, Krag M.* 1993. Articular facets of the human spine, quantitative three dimensional anatomy. Spine, 18:1298–1310.

18. *Goel VK, Monroe BT, Gilbertson LG, Brinckmann P.* 1995. Interlaminar shear stresses and laminae separation in the disc. Finite element analysis of the L3–L4 motion segment subjected to axial compressive loads. Spine, 20(6);689–698.

19. *Ciach M, Awrejcewicz J.* 2000. Finite element analysis and experimental investigations of the intervertebral discs in the human lumbar and cervical spine and porcine lumbar spinal segment. Computer Assisted Mechanics and Engineering Sciences, 7:91–101.

20. *Antosik T, Awrejcewicz J.* 1999. Numerical and experimental analysis of biomechanics of three lumbar vertebrae. Journal of Theoretical and Applied Mechanics, 3:37.

21. *Cheung JTM, Zhang M, Chow DHK.* 2003. Biomechanical responses of the intervertebral joints to static and vibrational loading: a finite element study. Clinical Biomechnaics, 18:790–799.

22. *Rohlmann A, Zander T, Schmidt H, Wilke HJ, Bergmenn G.* 2006a. Analysis of the influence of disc degeneration on the mechanical behaviour of a lumbar motion segment using the finite element method. Journal of Biomechanics, 39: 2484–2490.

23. *Rohlmann A, Bauer L, Zander T, Bergmann G, Wilke HJ.* 2006b. Determination of trunk muscle forces for flexion and extension by using a validated finite element model of the lumbar spine and measured in vivo data. Journal of Biomechanics, 39:981–989.

24. *Noailly J, Wilke HJ, Planell JA, Lacroix D.* 2007. How does the geometry affect the internal biomechanics of a lumbar spine bi-segment finite element model? Consequences on the validation process, Journal of Biomechanics, 40:2414–2425.

25. *Williams JR, Natarajan RN, Andersson GBJ.* 2007. Inclusion of regional poroelastic material properties better predicts biomechanical behaviour of lumbar discs subjected to dynamic loading. Journal of Biomechanics, 40:1981–1987.

26. *Fagan MJ, Julian S, Siddall DJ, Mohsen AM.* 2002b. Patient specific spine models. Part 1: finite element analysis of the lumbar intervertebral disc – a material sensitivity study, Proceedings of the Institution of Mechanical Engineers. Part H: 216(5):299–314.

27. *Lavaste F, Skalli W, Robin S, Roy-Camille R, Mazel C.* 1992. Three-dimensional geometrical and mechanical modelling of lumbar spine. Journal of Biomechanics, 25(10):1153–116.

28. *Little JP, Adam CJ, Evans JH, Pettet GJ, Pearcy MJ.* 2007. Nonlinear finite element analysis of

anular lesions in the L4/5 intervertebral disc. Journal of Biomechanics, 40:2744–2751.

29. *Zander T, Rohlmann A, Bergmann G.* 2004. Influence of ligament stiffness on the mechanical behaviour of a functional spinal unit. Journal of Biomechanics, 37:1107–1111.

30. *Kurutz M, Bender T.* 2010. Weightbath hydrotraction treatment – application, biomechanics and clinical effects. Journal of Multidisciplinary Healthcare (in press).

31. *McNally DS, Adams MA.* 1992. Internal intervertebral disc mechanics as revealed by stress profilometry. Spine, 17:66–73.

32. *Adams MA, McNally DS, Dolan P.* 1996. Stress distributions inside intervertebral discs. The effects of age and degeneration. J. Bone Joint Surg. Br. 78(6):965–972.

33. *Adams MA, Bogduk N, Burton K, Dolan P.* 2002. The Biomechanics of Back Pain. Churchill Livingstone, Edinburgh, London, New York, Oxford, Philadelphia, St Louis, Sydney, Toronto, 238 p.

34. *Natarajan RN, Williams JR, Andersson GB.* 2004. Recent advances in analytical modelling of lumbar disc degeneration. Spine, 29:2733–2741.

35. *Natarajan RN, Williams JR, Andersson GB.* 2006. Modeling changes in intervertebral disc mechanics with degeneration. Journal of Bone and Joint Surgery Am. 88(4), Suppl. 2:36–40.

36. *Acaroglu ER, Iatridis JC, Setton LA, Foster RJ, Mow VC, Weidenbaum M.* 1995. Degeneration and aging affect the tensile behaviour of human lumbar anulus fibrosus. Spine, 20(24):2690–2701.

37. *Nachemson AL.* 1981. Disc pressure measurements. Spine, 6(1):93–97.

38. *Acaroglu ER, Iatridis JC, Setton LA, Foster RJ, Mow VC, Weidenbaum M.* 1995. Degeneration and aging affect the tensile behaviour of human lumbar anulus fibrosus. Spine, 20(24):2690–2701.

39. *Ebara S, Iatridis JC, Setton LA, Foster RJ, Mow VC, Weidenbaum M.* 1996. Tensile properties of nondegenerate human lumbar anulus fibrosus. Spine, 21, 4:452–461.

40. *Kim YE, Goel VK, Weinstein JN, Lim TH.* 1991. Effect of disc degeneration at one level on the adjacent level in axial mode. Spine, 16:331–335.

41. *Kurowski P, Kubo A.* 1986. The relationship of degeneration of the intervertebral disc to mechanical loading conditions on lumbar vertebrae. Spine, 11:726–731.

42. *Polikeit A, Nolte LP, Ferguson SJ.* 2004. Simulated influence of osteoporosis and disc degeneration on the load transfer in a lumbar functional spinal unit. Journal of Biomechanics, 37: 1061–1069.

43. *Oláh M, Molnár L, Dobai J, Oláh C, Fehér J, Bender T.* 2008. The effects of weightbath traction hydrotherapy as a component of complex physical therapy in disorders of the cervical and lumbar spine: a controlled pilot study with follow-up. Rheumatology International, 28(8): 749–756.

44. *Vegh G.* 2007. Cervical traction forces in weightbath therapy (In Hungarian). Conference of Hungarian Society of Balneology, Esztergom, Hungary, November 16–18, 2007.

45. *Bender T, Karagülle Z, Bálint GP, Gutenbrunner C, Bálint PV, Sukenik S.* (2005). Hydro-therapy, balneotherapy, and spa treatment in pain management. Rheumatology International, 25(3): 220–224.

A szerzők köszönik az OTKA K-075018 projektbeli támogatását, továbbá Kutrik Attila végeselemes modellezésben nyújtott segítségét.

Kurutzné Kovács Márta
Budapesti Műszaki és Gazdaságtudományi Egyetem, Budapest
H–1111 Budapest, Műegyetem rkp. 3.

Biomechanica Hungarica III. évfolyam, 1. szám

LUMBÁLISGERINC-SZEGMENTUMOK DEGENERÁCIÓJÁNAK NUMERIKUS SZIMULÁCIÓJA: II. A HIRTELEN FELLÉPŐ DEGENERÁCIÓ

Kurutzné Kovács Márta[1], Oroszváry László[2]
[1] Budapesti Műszaki és Gazdaságtudományi Egyetem, Budapest
[2] Knorr Bremse Hungaria Ltd, Budapest
kurutzm@eik.bme.hu

Absztrakt
A lumbális gerinc degenerációja nemcsak az életkor előrehaladásával léphet fel, hanem hirtelen mechanikai hatásokra is, például túlterhelésre vagy rossz mozdulatra is bekövetkezhet. 3D végeselemes szimuláció segítségével vizsgáljuk a centrikusan nyomott lumbálisgerinc-szegmentum túlterhelésből származó, hirtelen bekövetkező degenerációs folyamatait. Mivel hirtelen degeneráció bármely életkorban bekövetkezhet, figyelembe kell venni a gerinc aktuális életkori degenerációs állapotát is. Az életkori degenerációhoz hasonlóan a hirtelen degenerációt is a szegmentum anyagállandóival modelleztük. Figyelembe vettük a hirtelen lecsökkenő hidrosztatikus nyomást a nucleusban, az annulus felrepedését, szálszakadását, a véglemez és a szivacsos csigolyacsont károsodását. Megkülönböztettük a fiatal, életkorilag gyengén károsodott szegmentumok, és az idős, előrehaladott életkori degenerációval rendelkező szegmentumok hirtelen degenerációját. Az életkori degenerációval ellentétben, ahol a porckorong merevsége 5-6-szorosára is megnőhet a degenerációs folyamat végére, a hirtelen károsodásnál a merevség 60–80%-kal csökken, ami a szegmentum instabilitásához vezet, különösen fiatal korban, életkorilag gyengén károsodott szegmentumnál, mivel ott a hirtelen merevségcsökkenés a legalacsonyabb szintről indul. Fiatalabb korban a hirtelen degeneráció mintegy 2100 N/mm életkori merevségi szintről 75–80%-kal, mintegy 400–500 N/mm szintre csökken; míg idősebb korban mintegy 3600 N/mm életkori merevségről 60–65%-kal, mintegy 1300 N/mm merevségi szintre csökken. Következésképpen, az életkori károsodáshoz hasonlóan a hirtelen károsodás is a fiatal felnőtt korosztályt sújtja leginkább. Az életkori károsodással ellentétben, ahol a porckorong alakváltozási képessége, összenyomódása, kihasasodása a degenerációs folyamat végére mintegy 30–85%-kal csökken, a hirtelen károsodásnál ez szignifikánsan megnő mintegy 2-3-szorosára, amely a szegmentum instabilitásához és fájdalomhoz vezet, ugyancsak leginkább fiatal felnőtt korban.

Kulcsszavak: emberi lumbális mozgás-szegmentum; hirtelen degeneráció; porckorong; végeselem-modell; numerikus szimuláció; nyomási merevség

Abstract
Lumbar degeneration can be caused by aging and by other environmental effects like sudden mechanical overload. 3D finite element simulation of accidental degeneration processes of lumbar functional spinal units is presented for axial compression overload. Since sudden accidental degeneration can happen at any state of long-term age-related degeneration, consequently, it was modeled by considering the actual grade of aging degeneration of segments. Accidental degeneration was modeled by the material properties of components of segments and by overloading.

Systematic analysis of the effect of several components of accidental degeneration was investigated: the sudden loss of fluid like characteristics of nucleus; the buckling, tears or fiber break of annulus; endplate damage or cancellous bone collapse. In contrast to the age-related degeneration where the stiffness of discs increased by 500–600% during the aging process, in accidental degeneration processes the stiffness of discs decreased by 60–80%, leading to segmental instability and injury. Accidental degeneration may be more dangerous in young age since in this case the sudden stiffness loss starts at a smaller stiffness level, namely, lightly degenerated young discs have the smallest stiffness reported by many studies. Accidental degeneration in young age in this study started equally at 2100 N/mm stiffness that suddenly decreased by 75–80% to 400–500 N/mm; while in old age it started at about 3600 N/mm and decreased by 60–65% to 1300 N/mm. These effects explain that low back pain problems insult so frequently the young adults. The most important factor both in age-related and accidental change of disc stiffness is the stiffness change of nucleus. In contrast to the age-related degeneration where the disc deformability and bulging decrease during aging by 30–85%, in accidental degeneration processes they increase significantly by 200–300% that may lead to segmental instability and injury again.

Keywords: human lumbar functional spinal unit; sudden accidental degeneration; intervertebral disc; finite element model; numerical simulation; compressive stiffness

1. Bevezetés

A gerincdegeneráción annak felépítésében, szerkezetében és működésében beálló káros elváltozásokat értjük, A degeneráció általános fogalom, a gerinc degenerációi két alapvető osztályba sorolhatók: (1) a hosszú idejű, *életkorral járó degenerációk,* és (2) a külső hatásra kialakuló rövidebb idejű ún. *környezeti degenerációk*. Ilyen környezeti hatások elsősorban a mechanikai hatások, a különféle terhek, a fiziológiai, a sportolási vagy munkavégzési terhek, vagy éppen a balesetből eredő traumatikus terhek. További környezeti degenerációt okozhat a fagyás, égés, vegyi vagy sugárkárosodás stb. A mechanikai eredetű degenerációk a környezeti degeneráció külön osztályát képezik, ezek a rövid idő alatt, rendszerint váratlanul fellépő mechanikai túlterhelésből adódó ún. *hirtelen degenerációk*. Ilyen lehet például az elesés, vagy éppen egy rossz mozdulat[1]. Ebben a tanulmányban csak a hirtelen mechanikai károsodásokkal foglakozunk; az életkori károsodást a tanulmány első részében elemezzük[2].

A porckorong a szegmentum legkritikusabb alkotórésze, amelynek bármilyen károsodása jelentősen befolyásolhatja a szegmentum teherbírását és stabilitását[3]. Az öregedéssel járó károsodás a porckorong nucleusában jelentkezik először, amely fokozatosan elveszti folyadékszerű tulajdonságait, és egyidejűleg keményedik, merevsége növekszik[4,5,1]. Eközben a porckorongban egyéb károsodási formák is megjelenhetnek, például annulusfelhasadás, a belső annulus kihajlása, a véglemez-károsodás, vagy a csontritkulásos csigolyák megroppanása[6,7]. Az utóbbi idők kutatásai, valamint a porckorong-bántalommal orvoshoz forduló betegek életkori statisztikái kimutatták, hogy a fiatal, kevéssé degenerált szegmentumokat fenyegeti inkább a stabilitásvesztés, míg az idősödés során a stabilitás egyre inkább biztosított[1,8,9]. Ennek okait numerikus szimulációval kimutattuk a tanulmány első részében[2], a jelen cikkben a hirtelen degenerációs folyamatok numerikus elemzésének eredményeiről számolunk be.

Az utóbbi időben számos tanulmány foglalkozik a lumbális gerinc degenerációjának végeselemes modellezésével, de ezek nem foglalkoznak a hirtelen degeneráció kérdésével. Iatridis és munkatársai[10,11] a folyadékból szilárd anyaggá válás halmazállapotát vizsgálták. Többen[6,12] poro elasztikus végeselem-modellt alkalmaztak, mások[8,13-16] több degenerációs fokozatot definiáltak a porckorong anyagállandóinak és geometriájának változtatásával. E tanulmányok legtöbbje leszögezi, hogy az instabilitás leginkább a gyengén degenerált fiatalabb szegmentumokat veszélyezteti.

A jelen tanulmány célja a különböző életkori degenerációs állapotban fellépő hirtelen kompressziós túlterhelésből származó degenerációs folyamatok numerikus követése, a vonatkozó következtetések levonása.

2. Módszerek

A hirtelen károsodás szimulációjánál az életkori degenerációs vizsgálathoz kidolgozott geometriai és hálózati modellt alkalmaztuk[2]. A hirtelen károsodást az anyagi tulajdonságoknál vettük figyelembe.

2.1. A lumbális szegmentum végeselemes modellje

A 3D geometriai modellt egy tipikus lumbális szegmentum méretei alapján vettük fel. A végeselemes hálózatot Pro/Engineer, ANSYS Workbench és ANSYS Classic programok segítségével vettük fel. A csontok rugalmas anyagállandóinak felvételénél a szakirodalomra támaszkodtunk[17-23], a nucleus collagen szálainak anyagállandóinál is az irodalmi adatokra támaszkodtunk[17-20,24-30], akárcsak a szalagok esetében[18,31,32]. A geometriai és a végeselemmodell kialakítása szempontjait a vonatkozó anyagállandókkal a tanulmány első részében[2] ismertettük.

2.2. A lumbális szegmentum hirtelen degenerációs modellje

Az életkori degeneráció modellezése során a nucleus összenyomhatatlanságának megszűnését a Poisson-tényező csökkenésével, a nucleus fokozatos keményedését pedig a rugalmassági modulusa növekedésével modelleztük[33,34]. Öt degenerációs fokozatot állítottunk fel az egészségestől a teljesen degenerált állapotig. A modellben a szivacsos csont és a véglemezek korral járó gyengülését is figyelembe vettük. Az életkori degenerációs fokozatok modelljét a vonatkozó anyagállandókkal a tanulmány első részében[2] ismertettük.

A hirtelen degenerációnál azt feltételeztük, hogy a nucleus mintegy kipukkad, és hirtelen elveszti a folyadékszerű viselkedését, vagyis összenyomhatatlanságát anélkül, hogy az anyagának a szilárdsága megváltozna. Ezt a jelenséget a nucleus Poisson-tényezőjének hirtelen csökkenésével modelleztük keményedés nélkül. A jelenséget a szegmentumot alkotó többi szerv hirtelen károsodása kísérheti, mint az annulus felrepedése, kihajlása, a véglemez repedése, a csigolyák szivacsos csontjának összeroppanása. Mindez azonban a szegmentum hirtelen károsodáskori aktuális életkori degenerációjának az állapotától is függ.

Az életkori degenerációs modellhez kapcsolódva öt hirtelen degenerációs fázist állítottunk fel, az egészségestől a teljesen degenerált állapotig. A modellezéshez az életkori degeneráció vizsgálatához használt adatokat felhasználva[2] egy futtatási táblázatot készítettünk. Ennek soraiban a nucleus keményedéséhez tartozó életkori degenerációs adatok vannak a nucleus adott Poisson tényezője mellett. A táblázat oszlopaiban a Poisson tényező csökkenésével jellemzett hirtelen degeneráció adatai foglalnak helyet, adott nucleus rugalmassági modulus mellett. Ugyanakkor a táblázat főátlójában az öregedési degeneráció modelljének a tanulmány első részében[2] ismertetett adatai szerepelnek. Mivel a hirtelen degeneráció bármely életkorban és életkori degenerációs stádiumban bekövetkezhet, a táblázat segítségével a különféle életkorban bekövetkező hirtelen degenerációs esetek modellezhetők.

A jelen tanulmányban a hirtelen degeneráció alábbi eseteit vizsgáltuk: (1) fiatal felnőtt korban belső annulus kihajlással, továbbá (2) annulus károsodással és szálszakadással, valamint (3) idősebb korban véglemez- és szivacsoscsont-károsodással. Ezekhez az esetekhez tartozó anyagállandókat az *1. táblázat* mutatja.

A hirtelen degeneráció numerikus szimulációját a fiziológiai nyomóteher hirtelen megkettőződésére, vagyis 2000 N nyomóteherre végeztük[37]. Itt figyelembe vettük, hogy a lumbális fiziológiai nyomóerőt egyrészt a felsőtest súlya (a testsúly mintegy 60%-a[35,36]) másrészt a gerincet egyensúlyban tartó izomerők alkotják.

2.3. A lumbális szegmentum végeselemes modelljének validálása

Az egészséges és a degenerált végeselemes modell validálását húzásra és nyomásra egyaránt elvégeztük[38]. Nyomás esetén a porckorong szagittális középsíkjában keletkező függőleges nyomófeszültségek számításból kapott nagyságát és eloszlását hasonlítottuk össze Nachemson[35], Adams és munkatársai[1,5], Dolan és Adams[39], Adams és Dolan[40] stress-profilometriás vizsgálattal kapott kísérleti eredményeivel. Az eredmények meggyőző egyezést mutattak. Húzás esetén a számított lumbális megnyúlá-

Hirtelen degenerációs fokozatok	1	2	3	4	5
Fiatalon, belső annulus kihajlással					
nucleus	3/0.499	3/0.45	3/0.4	3/0.35	3/0.3
belső annulus	4/0.45	3/0.45	2/0.45	1/0.45	0.5/0.45
külső annulus	4.5/0.45	4.5/0.45	4.5/0.45	4.5/0.45	4.5/0.45
annulusszálak	500/400/300	500/400/300	500/400/300	500/400/300	500/400/300
véglemez	80/0.4	80/0.4	80/0.4	80/0.4	80/0.4
szivacsos csont	125/0.3	125/0.3	125/0.3	125/0.3	125/0.3
Fiatalon, annulushasadással és szálszakadással					
nucleus	3/0.499	3/0.45	3/0.4	3/0.35	3/0.3
belső annulus	4/0.45	3.5/0.45	3/0.45	2.5/0.45	2/0.45
külső annulus	4/0.45	3.5/0.45	3/0.45	2.5/0.45	2/0.45
annulusszálak	500/400/300	375/300/225	250/200/150	125/100/75	5/4/3
véglemez	80/0.4	80/0.4	80/0.4	80/0.4	80/0.4
szivacsos csont	125/0.3	125/0.3	125/0.3	125/0.3	125/0.3
Idősebb korban, véglemez- és szivacsoscsont-károsodással					
nucleus	9/0.499	9/0.45	9/0.4	9/0.35	9/0.3
belső annulus	4/0.45	4/0.45	4/0.45	4/0.45	4/0.45
külső annulus	4/0.45	4/0.45	4/0.45	4/0.45	4/0.45
annulusszálak	500/400/300	500/400/300	500/400/300	500/400/300	500/400/300
véglemez	60/0.4	45/0.4	30/0.4	15/0.4	1/0.4
szivacsos csont	100/0.3	75/0.3	50/0.3	25/0.3	5/0.3

1. táblázat. A hirtelen degeneráció modellezése sokat hasonlítottuk össze Kurutz[41] és munkatársai[42] in vivo mért kísérleti eredményeivel. Az eredmények alapján a modell alkalmasnak látszott az öregedési és hirtelen degenerációs folyamatok numerikus szimulációjához.

3. Eredmények

Az *1. ábra* a fiatalon bekövetkező, a belső annulus kihajlásával járó hirtelen degenerációs folyamat *(1. táblázat)* numerikus szimulációjának eredményeit foglalja össze.

Az *1. a ábrán* a függőleges nyomófeszültségek megoszlását látjuk a porckorong szagittális középsíkjában az öt degenerációs fázisra vonatkozóan. Látható, hogy a függőleges nyomófeszültségek a nucleusban és a belső annulusban mintegy a harmadára csökkentek, ugyanakkor a külső annulusban mintegy a kétszeresére növekedtek a hirtelen lejátszódó folyamat végéig. Az *1. b ábra* a porckorong radikális összenyomódását mutatja: középen 287%, elöl 222%, hátul 191% volt az összenyomódás növekedése a hirtelen degenerációs folyamat során. Az *1. c ábra* a porckorong összetevőiben keletkező legnagyobb nyomófeszültségek átlagának a változását mutatja a degenerációs folyamat során. A nucleusban a csökkenés azonnal lejátszódott a hidrosztatikus nyomás megszűnésével (67%); a belső annulusban a csökkenés egyenletes (70%) volt. A külső annulusban jelentős, 138%-os volt a növekedés. Hasonló tendencia volt megfigyelhető az átlagos nyomófeszültségekben is: 66% csökkenés a nucleusban és 61% a belső annulusban, míg 150% növekedés a külső annulusban *(1. d ábra)*. Az annulus szálaiban keletkező maximális húzóerők, amelyek a hátulsó-oldalsó szakaszon keletkeztek, 1.38 N értékről 2.28 N értékre növekedtek (66%) a degenerációs folyamat során. Ezzel összhangban a porckorong kihasasodásának növekedése a hátulsó szakaszon nem-monoton nőtt (33%), az elülső és oldalsó szakaszon monoton növekedett (104% és 112%).

Az *1. f ábra* mutatja a porckorong összetevőinek függőleges nyomómerevség-csökkenését a hirtelen degenerációs folyamat során. A nucleusban hirtelen megszűnő hidrosztatikus nyomásnak köszönhetően az annulus belső támasza megszűnt, így a belső annulus lamellák kihajlottak befelé. Következésképpen, a nucleus és a belső annulus radikálisan elvesztette függőleges nyomómerevségét 91%, illetve 88%-kal, és vele együtt a teherbíró-képességét, ezért a terhelés a külső annulusra tevődött át, amelynek a merevsége csak kissé csökkent (21%). A teljes porckorong merevségcsökkenése a hirtelen degenerációs folyamat során 79% volt. Látható, hogy a degenerációs folyamat első fázisaiban a belső annulus, míg utolsó fázisaiban a külső annulus a fő teherviselő elem.

A *2. ábra* a fiatalon, az annulus károsodásával és szálszakadással járó hirtelen degenerációs folyamat *(1. táblázat)* numerikus szimulációjának eredményeit foglalja össze.

A *2. a ábrán* az öt degenerációs fázisra vonatkozóan a függőleges nyomófeszültségek megoszlását látjuk a porckorong szagittális középsíkjában. Látható, hogy a függőleges nyomófeszültségek a nucleusban és a belső annulusban mintegy a negyedére csökkentek, ugyanakkor a külső annulusban a károsodás miatt alig növekedtek. A *2. b ábra* a porckorong szignifikáns összenyomódását mutatja: amelynek növekedése középen 257%, elöl 230%, hátul 165% volt a hirtelen degenerációs folyamat során. A *2. c ábra* a porckorong összetevőiben keletkező nyomófeszültségek átlagos csúcsértékeinek a változását mutatja a degenerációs folyamat során. A nucleusban ismét hirtelen és erős csökkenés történt, összességében 69%-ban, a belső annulusban csupán 26% volt a feszültségcsökkenés, míg a külső annulusban a szálszakadás miatt nem volt jelentős növekedés, csupán 7%. Hasonló tendencia volt megfigyelhető az átlagos nyomófeszültségekben is: erős, 67% csökkenés a nucleusban és gyenge,

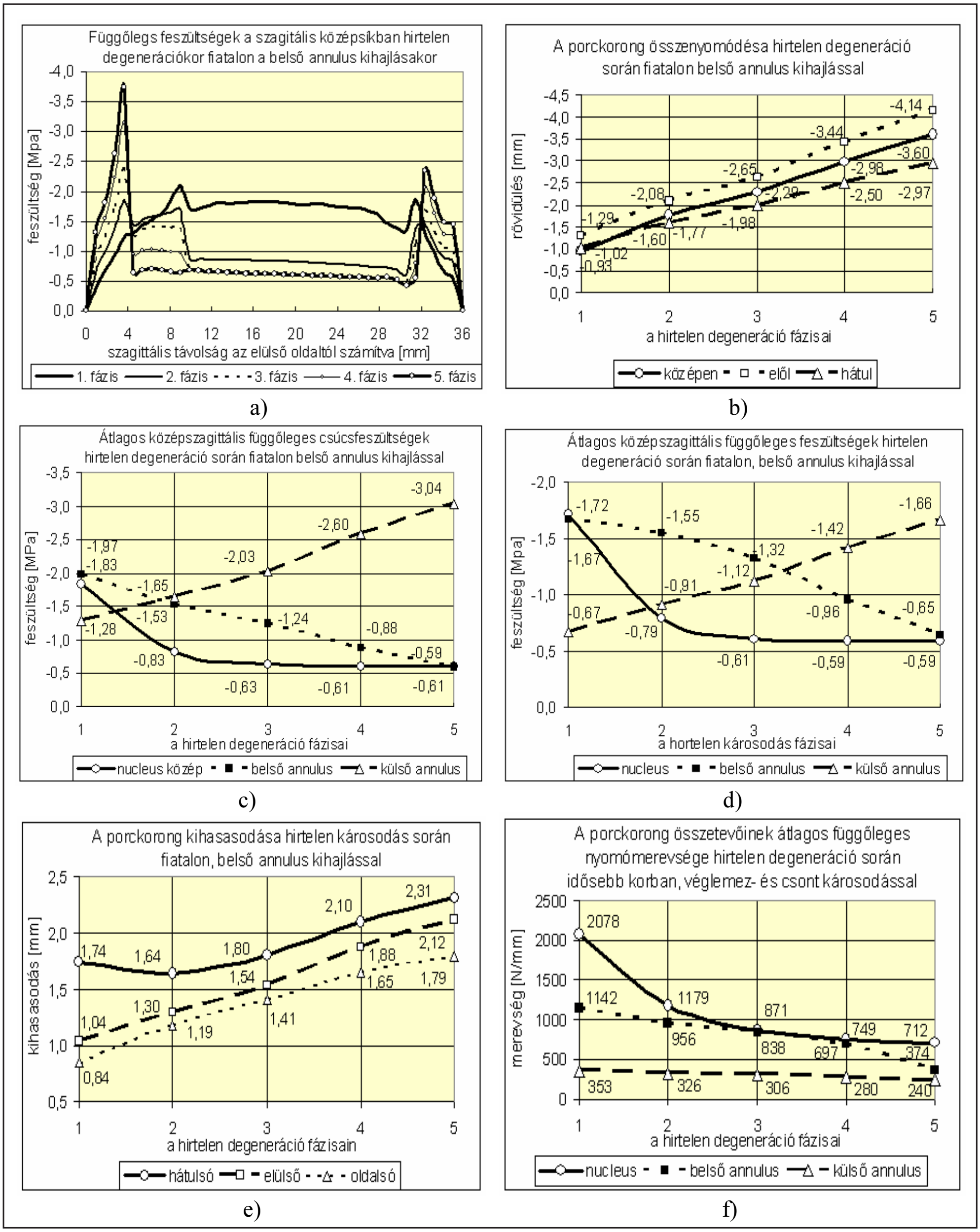

1. ábra. Hirtelen degeneráció numerikus szimulációja: fiatalon, belső annulus kihajlással. Változások a hirtelen degeneráció során
a) a függőleges nyomófeszültségekben a porckorong szagittális középsíkjában, *b)* a porckorong középső, elülső és hátulsó összenyomódásában, *c)* a porckorong összetevőiben keletkező átlagos függőleges csúcsfeszültségekben, *d)* a porckorong összetevőiben keletkező átlagos függőleges feszültségekben, *e)* a porckorong hátulsó, elülső és oldalsó kihasasodásában, *f)* a porckorong összetevőinak átlagos függőleges nyomómerevségében

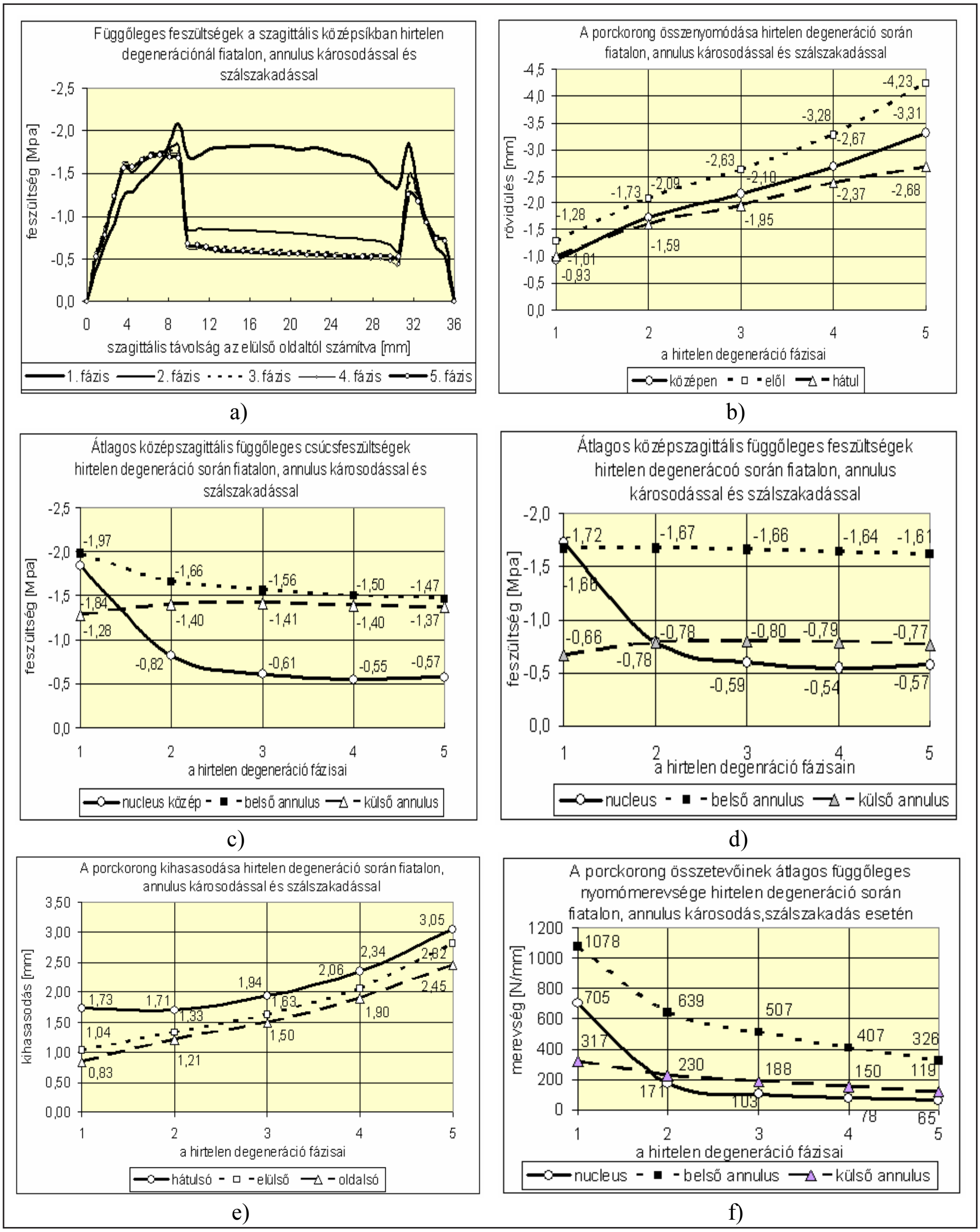

2. ábra. Hirtelen degeneráció numerikus szimulálása: fiatalon, annuluskárosodással és szálszakadással. Változások a hirtelen degeneráció során
a) a függőleges nyomófeszültségekben a porckorong szagittális középsíkjában, *b)* a porckorong középső, elülső és hátulsó összenyomódásában, *c)* a porckorong összetevőiben keletkező átlagos függőleges csúcsfeszültségekben, *d)* a porckorong összetevőiben keletkező átlagos függőleges feszültségekben, *e)* a porckorong hátulsó, elülső és oldalsó kihasasodásában, *f)* a porckorong összetevőinak átlagos függőleges nyomómerevségében

csupán 3% a belső annulusban, míg a növekedés a külső annulusban annak gyengülése miatt csupán 16% volt a *2. d ábra* szerint. Az annulus szálaiban bekövetkezett szakadás miatt bennük a maximális húzóerők gyakorlatilag eltűntek, 1,38 N-ról 0,06 N-ra csökkentek (98%) a hirtelen degenerációs folyamat során. A szálszakadás miatt a porckorong kihasasodása is radikálisan megnőtt: a *2. e ábrán* a hátsó kihasasodás nem-monoton növekedése 76%, az elülső és oldalsó kihasasodás monoton növekedése 172% és 195% volt.

A *2. f ábra* mutatja a porckorong összetevőinek függőleges nyomómerevség-csökkenését a hirtelen degenerációs folyamat során. A nucleusban hirtelen megszűnő hidrosztatikus nyomásnak köszönhetően az annulus belső támasza megszűnt, így a belső annulus lamellák most is kihajlanak befelé, következésképpen, a nucleus radikálisan elvesztette függőleges nyomómerevségét 91%-kal, a belső annulus most 70%-kal, és most a külső annulus a szálszakadás miatt ugyancsak nagy merevségcsökkenést szenvedett, 62%-ban. A teljes porckorong merevségcsökkenése a hirtelen degenerációs folyamat során 76% volt. Látható, hogy a degenerációs folyamat során végig a belső annulus a fő teherviselő elem.

A *3. ábra* az idősebb korban bekövetkező, a véglemez és a többé-kevésbé osteoporotikus csigolyák szivacsos csontjának a károsodásával járó hirtelen degenerációs folyamat *(1. táblázat)* numerikus szimulációjának eredményeit foglalja össze.

A *3. a ábrán* az öt degenerációs fázisra vonatkozóan a függőleges nyomófeszültségek megoszlását látjuk a porckorong szagittális középsíkjában. Látható, hogy a függőleges nyomófeszültségek a nucleusban az ötödére csökkentek, a belső annulusban alig változtak, a külső mintegy kétszeresre növekedtek. A *3. b ábrán* látható, hogy a már idősebb, ezért keményebb porckorong benyomódott a már idősebb, ezért lágyabb véglemezbe és trabekuláris csontállományba, ezért középen lényegében nem is nyomódott össze, a szélein pedig a nagyszilárdságú kortikális csigolyahéj gyakorolt rá nagy nyomást, főleg a hirtelen degenerációs folyamat végére. Így a porckorong párnaszerű alakot vett fel, középen először mintegy 50%-ot nőtt az összenyomódása, majd 56%-ot csökkent, míg a széleken többszörösére növekedett az összenyomódása (elöl 234%, hátul 228%).

A *3. c ábra* a porckorong összetevőiben keletkező nyomófeszültségek átlagos csúcsértékeinek a változását mutatja a degenerációs folyamat során. Az idősebb és merevebb nucleusban az eredetileg nagyobb nyomófeszültségek most is erősen, mintegy lineárisan csökkentek összességében 82%-kal, miközben a teher a külső annulusra tevődött át, ahol a nyomófeszültségek 54%-os növekedést mutattak. Eközben a belső annulusban szinte nem történt változás. Hasonló tendencia volt megfigyelhető az átlagos feszültségekben is: szignifikáns, 77%-os csökkenés a nucleusban, jelentős, 115%-os növekedés a külső annulusban, jelentéktelen változás a belső annulusban *(3. d ábra)*. A hátulsó-oldalsó annulus szálaiban fellépő maximális húzóerők 23%-os növekedést mutattak, 1,07 N-ról 1,32 N értékre. Az összenyomódáshoz hasonlóan a porckorong kihasasodására ugyancsak hatással volt, hogy az eleve keményebb porckorong kisebb ellenállásra talált a véglemezben és a szivacsos csontban, ezért a *3. e ábrán* látható mindhárom irányú kihasasodás is kezdetben csekély, majd az utolsó fázisban erőteljesebb növekedést mutatott (hátul 62%, elöl 63% és oldalt 53%).

A *3. f ábra* mutatja a porckorong összetevőinek függőleges nyomómerevség-csökkenését a hirtelen degenerációs folyamat során. Az eleve keményebb és nagyobb merevségű nucleusban 66%, a sokkal kevésbé merev belső annulusban 67%, míg a kis merevségű külső annulusban

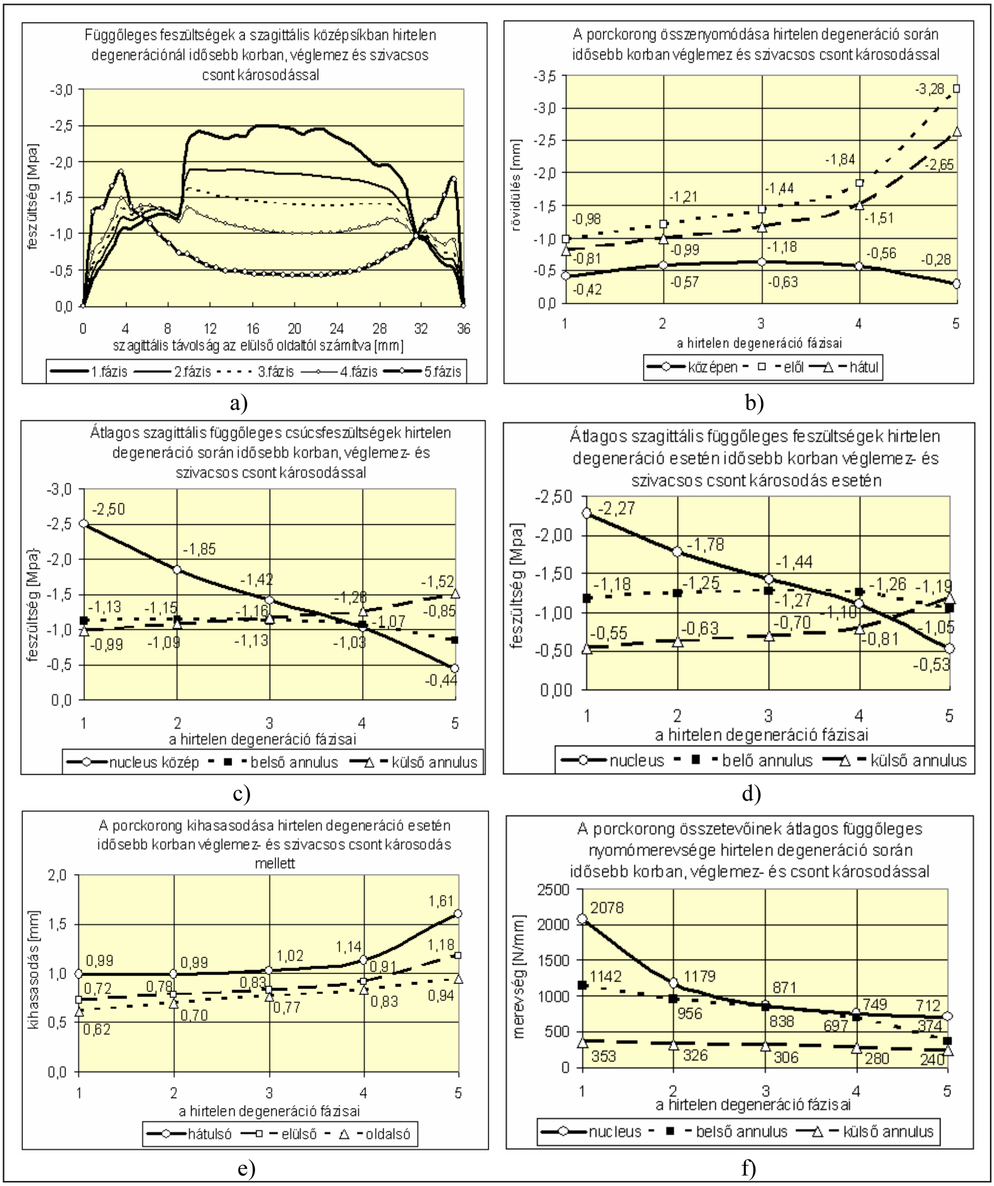

3. ábra. Hirtelen degeneráció numerikus szimulációja: idősebb korban, véglemez- és szivacsoscsont-károsodással. Változások a hirtelen degeneráció során *a)* a függőleges nyomófeszültségekben a porckorong szagittális középsíkjában, *b)* a porckorong középső, elülső és hátulsó összenyomódásában, *c)* a porckorong összetevőiben keletkező átlagos függőleges csúcsfeszültségekben, *d)* a porckorong összetevőiben keletkező átlagos függőleges feszültségekben, *e)* a porckorong hátulsó, elülső és oldalsó kihasasodásában, *f)* a porckorong összetevőinak átlagos függőleges nyomómerevségében

Merevségcsökkenés %-ban	Fiatalon, belső annulus kihajlással	Fiatalon, nucleuskárosodással és szálszakadással	Idősebb korban, a véglemezek és a szivacsos csont károsodásával
nucleus	91	91	66
belső annulus	88	70	67
külső annulus	21	62	32
a teljes porckorong	79	76	63

2. táblázat. A porckorong és alkotórészeinek merevségcsökkenése a hirtelen degenerációs folyamatok során

32% mervségcsökkenés játszódott le. A teljes porckorong merevségcsökkenése a hirtelen degenerációs folyamat során 63% volt. Látható, hogy a degenerációs folyamat során végig a nucleus a fő teherviselő elem.

A *2.* összehasonlító *táblázatban* a porckorong és alkotórészeinek merevségcsökkenését foglaltuk össze a különböző hirtelen degenerációs folyamatok során.

4. Megbeszélés

Hasonlóan a gerinc életkori degenerációs folyamataihoz, a hirtelen degenerációs folyamatokat befolyásoló tényezők hatása numerikus szimulációval elemezhető.

Az életkori degenerációs folyamattal ellentétben, amelynek során a szegmentum és a porckorong alakváltozó képessége csökken, a hirtelen degenerációs folyamat során szignifikánsan nő, ami a szegmentum instabilitásához és fájdalom kialakulásához vezethet, kiváltképp fiatal korban, gyenge életkori degenerációs stádiumban. Míg a porckorong deformációképessége az életkori degenerációs folyamat végére 85–87%-kal csökkent[2], a hirtelen degeneráció során 200–300%-kal növekedett a fiataloknál, és kisebb mértékben, de növekedett az idősebbeknél is. Míg a porckorong kihasasodása 30–70%-kal csökkent az életkori degeneráció során, a hirtelen degenerációnál 100–250%-kal nőtt a fiataloknál, és 60%-kal az idősebbeknél.

A szakirodalomban csak a kezdeti degenerációs fokozathoz tartozó összenyomódások és kihasasodási értékek állnak rendelkezésre, Fagan és munkatársai[29] 0,5 mm összenyomódást kaptak 0,8 mm hátulsó és 0,55 mm elülső kihasasodással 1000 N nyomóerőre az egészséges porckorongon. Heuer és munkatársai[44,45] 500 N nyomóerőre 0,7 mm kihasasodást kaptak intakt porckorongon. Little és kutatótársai[7] 0,45 mm hátulsó és 0,2 mm oldalsó, Li és Wang[46] 0,38 mm hátsó-oldalsó és 0,23 mm oldalsó kihasasodást számítottak. Ezek az eredmények a 100 N és 2000 N centrikus nyomóerőre számított értékeinkkel összhangban vannak[2,38].

Az életkori degenerációs folyamattal ellentétben, amelynek során a nucleusban a függőleges nyomófeszültségek nagysága nagy különbségeket mutat (a közepén nagy a feszültségcsökkenés, a szélén inkább növekedés van), viszont a hirtelen degeneráció során a feszültségek megoszlása a nucleusban egyenletes. Ennek oka az, hogy a nucleus szilárdulása először a szélein kezdődik, legutoljára a közepén, így a széleken a feszültségek nagyobbak. Hirtelen degenerációnál nincs anyagi változás, ezért a feszültségek egyenletesek.

Míg fiatal korban a hirtelen degeneráció a külső annulus megterhelésével jár, idősebb korban a hirtelen degeneráció során a belső annulus is viseli a terheket. Ennek oka, hogy az idősebb korban már szilárdabb nucleus belső támaszt nyújt az annulusnak, és így a kihajlását megakadályozza, ami a teherbírása megmaradásával jár.

Az életkori degenerációs folyamattal ellentétben, amelynek során a porckorong függőleges nyomási merevsége és teherbírása a folyamat során növekszik, a hirtelen degenerációs folyamatban szignifikánsan lecsökken, ami szegmentális instabilitáshoz és sérüléshez, fájdalomhoz vezethet. Kurutz és Oroszváry[2,38] ugyanezen numerikus modell alapján kimutatta, hogy a gyenge életkori degenerációs fokozathoz tartozó leggyengébb merevséghez viszonyítva a porckorong merevsége 580%-kal nő a folyamat végére. Ugyanakkor a hirtelen degenerációs folyamatban a porckorng merevsége a fiataloknál 60–80%-kal, az időseknél 60%-kal csökken, a degeneráció típusától és kísérő jelenségeitől függően *(2. táblázat)*.

Az életkori degenerációs folyamatokhoz hasonlóan a hirtelen degenerációs folyamatokat is a nucleus állapota befolyásolja leginkább. A porckorong merevségváltozásban is a legfontosabb faktor a nucleus merevsége. Akár életkori, akár hirtelen degenerációs folyamatról van szó, a legélénkebb merevségváltozást a nucleus mutatja, élénken változik a belső annulus merevsége is, míg a külső annulus merevségében általában csekélyebb a változás. Kimondhatjuk tehát, hogy a porckorong „merevségérzékenysége” a nucleus közepétől kifelé radiálisan csökken. Életkori degeneráció végére a nucleus merevsége 1100%-kal, a külső és belső annulus merevsége 350–600%-kal növekedett (Kurutz és Oroszváry[2,38]). Hirtelen degenerációnál a nucleus merevségcsökkenése fiatalon 90%, idősebben 60–70%; a belső annulusé fiatalon 70–90%, idősebben 70%; a külső annulusé fiatalon 20–60%, idősebben 30%, a degenerációtól és kísérő jelenségeitől függően *(2. táblázat)*. Valóban, Iatridis és munkatársai[43] bizonyították, hogy a szálas és réteges szerkezetű annulus, amelynek domináns anizotrop szerepe van húzás esetén, nem játszik domináns szerepet a porckorong nyomómerevségében.

Az életkori degenerációhoz hasonlóan a hirtelen degeneráció is a fiatal, alig degenerált szegmentumokat veszélyezteti leginkább. Ezt a korosztályt ugyanis a hirtelen degenerációnál fellépő radikális merevségcsökkenés éppen akkor éri, amikor a porckorngok merevsége az életkori degenerációs skálán a legkisebb[2,38]. Számos publikációban leszögezték, hogy fiatal korban a gyenge degeneráció instabilitáshoz vezet, míg idősebb korban az előrehaladott degeneráció a stabilitási esélyt javítja, mivel a gyengén degenerált szegmentumnak a legkisebb az ellenállása[1,8,9,14,15,38]. Valóban, a fiatal, gyengén degenerált porckorongnál a hirtelen degenerációs merevségcsökkenés mintegy 2100 N/mm szintről indul, és hirtelen lecsökken mintegy 75–80%-kal 400–500 N/mm szintre. Ugyanakkor idősebb korban a merevségcsökkenés magasabb szintről, 3600 N/mm-ről indul, és mintegy 60%-kal, 1440 N/mm-re csökken. A fiatalabb korban nagyobb deformáció-képesség is abban az irányban hat, hogy a hirtelen degenerációnál keletkező nagy alakváltozások ebben a korban a legveszélyesebbek a lumbális szakaszon fellépő sérülések és fájdalom szempontjából.

Számításainkkal igazoltuk a fiatal felnőtt korosztály veszélyeztetettségét a lumbális porckorongbántalom szempontjából. Valóban, a magyar balneológusok és hidroterapeuták tapasztalata szerint[47] a porckorongbántalom miatt kezelt betegek legnagyobb százaléka a 40–55 éves korosztályból kerül ki. Ez a korosztály nemcsak az életkori, hanem a hirtelen degeneráció szempontjából is a legsérülékenyebb. A végeselemes modell és szimuláció alapján ennek mechanikai összetevőit és okait mutattuk ki, segítve ezzel a degenerációs folyamatok minél jobb megértését és a kezelési módok hatékonyabbá tételét.

IRODALOM

1. *Adams MA, Bogduk N, Burton K, Dolan P.* 2002. The Biomechanics of Back Pain. Churchill Livingstone, Edinburgh, London, New York, Oxford, 238 p.

2. *Kurutz M, Oroszváry L.* 2010. Lumbális gerincszegmentumok degenerációjának numerikus szimulációja: I. Az életkorral járó degeneráció. A IV. Magyar Biomechanikai Konferencia kiadványa, Pécs, 2010. május 8–9.

3. *Ferguson SJ, Steffen T.* 2003. Biomechanics of the aging spine, Eur. Spine J. 12(Suppl 2):S97–S103.

4. *McNally DS, Adams MA.* 1992. Internal intervertebral disc mechanics as revealed by stress profilometry. Spine, 17, 66–73.

5. *Adams MA, McNally DS, Dolan P.* 1996. Stress distributions inside intervertebral discs. The effects of age and degeneration. J. Bone Joint Surg. Br. 78(6):965–972.

6. *Natarajan RN, Williams JR, Andersson GB.* 2004. Recent advances in analytical modelling of lumbar disc degeneration. Spine, 29, 2733–2741.

7. *Little JP, Adam CJ, Evans JH, Pettet GJ, Pearcy MJ.* 2007. Nonlinear finite element analysis of anular lesions in the L4/5 intervertebral disc. Journal of Biomechanics, 40, 2744–2751.

8. *Rohlmann A, Zander T, Schmidt H, Wilke HJ, Bergmenn G.* 2006a. Analysis of the influence of disc degeneration on the mechanical behaviour of a lumbar motion segment using the finite element method. Journal of Biomechanics, 39, 2484–2490.

9. *Schmidt H, Heuer F, Simon U, Kettler A, Rohlmann A, Claes L, Wilke HJ.* 2006. Application of a new calibration method for a three-dimensional finite element model of a human lumbar annulus fibrosus. Clinical Biomechanics, 21, 337–344.

10. *Iatridis JC, Wedenbaum M, Setton LA, Mow VC.* 1996. Is the nucleus pulposus a solid or a fluid? Mechanical behaviours of the nucleus pulposus of the human intervertebral disc. Spine, 21(10): 1174–1184.

11. *Iatridis JC, Setton LA, Wedenbaum M, Mow VC.* 1997. Alterations in the mechanical behavior of the human lumbar nucleus pulposus with degeneration and aging. Journal of Orthopaedic Research, 15(2):318–322.

12. *Natarajan RN, Williams JR, Andersson GB.* 2006. Modeling changes in intervertebral disc mechanics with degeneration. Journal of Bone and Joint Surgery Am. 88(4), Suppl. 2:36–40.

13. *Polikeit A, Nolte LP, Ferguson SJ.* 2004. Simulated influence of osteoporosis and disc degeneration on the load transfer in a lumbar functional spinal unit. Journal of Biomechanics, 37, 1061–1069.

14. *Tang XJ, Chen QX, Liu YS, Li FC.* 2008. Analysis of lumbar disc degeneration using three-dimensional nonlinear finite element method, (Article in Chinese), Zhonghua Yi Xue Za Zhi, 88(23):1634–1638.

15. *Schmidt H, Kettler A, Rohlmann A, Claes L, Wilke HJ.* 2007. The risk of disc prolapses with complex loading in different degrees of disc degeneration – a finite element analysis. Clinical Biomechanics, 22(9):988–998.

16. *Schmidt H, Heuer F, Wilke HJ.* 2009. Dependency of disc degeneration on shear and tensile strains between annular fiber layers for complex loads. Med. Eng. Physics, 31(6), 642–649.

17. *Shirazi-Adl SA, Shrivastava SC, Ahmed AM.* 1984. Stress analysis of the lumbar disc-body unit in compression. A three-dimensional nonlinear finite element study. Spine, 9(2):120–34.

18. *Goel VK, Monroe BT, Gilbertson LG, Brinckmann P.* 1995. Interlaminar shear stresses and laminae separation in the disc. Finite element analysis of the L3-L4 motion segment subjected to axial compressive loads. Spine, 20(6):689–698.

19. *Cheung JTM, Zhang M, Chow DHK.* 2003. Biomechanical responses of the intervertebral joints to static and vibrational loading: a finite element study. Clinical Biomechnaics, 18, 790–799.

20. *Denoziere G, Ku DN.* 2006. Biomechanical comparison between fusion of two vertebrae and implantation of an artificial intervertebral disc. Journal of Biomechanics, 39, 766–775.

21. *Rohlmann A, Bauer L, Zander T, Bergmann G, Wilke HJ.* 2006b. Determination of trunk muscle forces for flexion and extension by using a validated finite element model of the lumbar spine and measured in vivo data. Journal of Biomechanics, 39, 981–989.

22. *Noailly J, Wilke HJ, Planell JA, Lacroix D.* 2007. How does the geometry affect the internal biomechanics of a lumbar spine bi-segment finite element model? Consequences on the validation process. Journal of Biomechanics, 40, 2414–2425.

23. *Williams JR, Natarajan RN, Andersson GBJ.* 2007. Inclusion of regional poroelastic material properties better predicts biomechanical behaviour of lumbar discs subjected to dynamic loading. Journal of Biomechanics, 40, 1981–1987.

24. *Shirazi-Adl A, Ahmed AM, Shrivastava SC.* 1986. A finite element study of a lumbar motion segment subjected to pure sagittal plane moments. Journal of Biomechanics, 19(4), 331–350.

25. *Spilker RL, Jakobs DM, Schultz AB.* 1986. Material constants for a finite element model of the intervertebral disc with a fibre composite annulus. J. of Biomechanical Engineering, 108, 1–11.

26. *Shirazi-Adl A.* 1989a. On the fibre composite material models of the annulus – comparison of predicted stresses. Journal of Biomechanics, 22, 357–365.

27. *Shirazi-Adl A.* 1989b. Strain in fibers of a lumbar disc. Analysis of the role of lifting in producing disc prolapse. Spine, 14(1):96–103.

28. *Rao AA, Dumas GA.* 1991. Influence of material properties on the mechanical behaviour of the L5-S1 intervertebral disc in compression: a nonlinear finite element study. Journal of Biomedical Engineering, 13(2):139–151.

29. *Fagan MJ, Julian S, Siddall DJ, Mohsen AM.* 2002b. Patient specific spine models. Part 1: finite element analysis of the lumbar intervertebral disc – a material sensitivity study, Proceedings of the Institution of Mechanical Engineers. Part H: 216(5):299–314.

30. *Lavaste F, Skalli W, Robin S, Roy-Camille R, Mazel C.* 1992. Three-dimensional geometrical and mechanical modelling of lumbar spine. J. of Biomechanics, 25(10):1153–1164.

31. *Zander T, Rohlmann A, Bergmann G.* 2004. Influence of ligament stiffness on the mechanical behaviour of a functional spinal unit. Journal of Biomechanics, 37, 1107–1111.

32. *Noailly J, Lacroix D, Planell JA.* 2005, Finite element study of a novel intervertebral disc substitute. Spine, 30(20):2257–2264.

33. *Kim YE, Goel VK, Weinstein JN, Lim TH.* 1991. Effect of disc degeneration at one level on the adjacent level in axial mode. Spine, 16, 331–335.

34. *Kurowski P, Kubo A.* 1986. The relationship of degeneration of the intervertebral disc to mechanical loading conditions on lumbar vertebrae. Spine, 11, 726–731.

35. *Nachemson AL.* 1981. Disc pressure measurements. Spine, 6(1):93–97.

36. *Sato K, Kikuchi S, Yonezawa T.* 1999. In vivo intradiscal pressure measurement in healthy individuals and in patients with ongoing back problems. Spine, 24(23):2468–2474.

37. *Acaroglu ER, Iatridis JC, Setton LA, Foster RJ, Mow VC, Weidenbaum M.* 1995. Degeneration and aging affect the tensile behaviour of human lumbar anulus fibrosus. Spine, 20(24):2690–2701.

38. *Kurutz M, Oroszváry L.* 2010. Finite element analysis of weightbath hydrotraction treatment

of degenerated lumbar spine segments in elastic phase. Journal of Biomechanics, 43(3):433–441.

39. *Dolan P, Adams MA.* 2001. Recent advances in lumbar spinal mechanics and their significance for l. Clinical Biomechanics, 16, Suppl.(1):S8–S16.

40. *Adams MA, Dolan P.* 2005. Spine biomechanics. Journal of Biomechanics, 38(10):1972–1983.

41. *Kurutz M.* 2006. Age-sensitivity of time-related in vivo deformability of human lumbar motion segments and discs in pure centric tension. Journal of Biomechanics, 39(1):147–157.

42. *Kurutz M, Bene É, Lovas A.* 2003. In vivo deformability of human lumbar spine segments in pure centric tension, measured during traction bath therapy. Acta of Bioengineering and Biomechanics, 5(1):67–92.

43. *Iatridis JC, Setton LA, Foster RJ, Rawlins BA, Weidenbaum M, Mow VC.* 1998. Degeneration affects the anisotropic and nonlinear behaviours of human anulus fibrosus in compression. Journal of Biomechanics, 31(6):535–544.

44. *Heuer F, Schmidt H, Wilke HJ.* 2008a. The relation between intervertebral disc bulging and annular fiber associated strains for simple and complex loading. Journal of Biomechanics, 41(2008):1086–1094.

45. *Heuer F, Schmidt H, Wilke HJ.* 2008b. Stepwise reduction of functional spinal structures increase disc bulge and surface strains. Journal of Biomechanics, 41(2008):1953–1960.

46. *Li H, Wang Z.* 2006. Intervertebral disc biomechanical analysis using the finite element modell-ing based on medical images, Computerized Medical Imaging and Graphics, 30, 363–370.

47. *Bender T, Karagülle Z, Bálint GP, Gutenbrunner C, Bálint PV, Sukenik S.* 2005. Hydro-therapy, balneotherapy, and spa treatment in pain management. Rheumatology International, 25(3): 220–224.

A szerzők köszönik az OTKA K-075018 projektbeli támogatását, továbbá Kutrik Attila végeselemes modellezésben nyújtott segítségét.

Kurutzné Kovács Márta
Budapesti Műszaki és Gazdaságtudományi Egyetem, Budapest
H–1111 Budapest, Műegyetem rkp. 3.

Microstructural simulations of the bone surrounding dental implants by means of a stochastically generated frame model

Éva Lakatos, Imre Bojtár
Department of Structural Mechanics, Budapest University of Technology and Economics
lakatoseva@mail.bme.hu

Abstract
The biomechanical behaviour of a dental implant plays an important role in its functional longevity inside the bone. Occlusal forces affect the bone surrounding an oral implant. To avoid fracture and bone resorption – by achieving the most even stress distribution in the bone – implants should be applied that transfer occlusal forces to the bone within physiologic limits with geometry capable to enhance bone formation. The following study deals with the trabecular bone substance especially surrounding dental implants considering the microscopic conformation of the bone. The dental surgical use of a formerly developed stochastically generated frame model of the trabecular bone is introduced, which is created by interlinking a stochastically generated set of nodes in a certain domain, according to a previously defined linking-rule. The finite element model possesses the geometrical and mechanical microstructural properties – obtained from literature – of the trabecular bone substance of an average man from the edentulous mandibular region. The finite element beam model was submitted to compression, shear and torsion tests, and the macro-structural elastic properties were computed from the result data obtained by means of finite element analysis. The thus received frame model was combined with the finite element model of the cortical bone layer in the mandible (lower jaw bone) and a dental implant, where the incompleteness of the bone-implant interface was taken into account.

Keywords: dental implants; trabecular bone; finite element analysis; bone mechanics

1. Introduction

Application of dental implants is currently the most general and physiologically the most favourable procedure for tooth replacement in dental surgery. Implants can have either advantageous or destructive effect on the surrounding bone, depending on several physiological, material and mechanical factors. The most general method for estimating the biomechanical behaviour of the bone is finite element analysis, which has become indispensable in determining the mechanical behaviour – stress and strain distributions under a certain load – of the cortical and cancellous bone surrounding dental implants, since being applicable in vivo. These numerical experiments have their importance in making the implantation the possibly most secure, reliable and efficient, and the lifetime of the implant the longest conceivable, by finding the most favourable thread formation, surface, material, etc. In finite element analysis of the bone several assumptions need to be made, that influence the accuracy of the results. Recently, in most of the reported works the geometry of the implant can be modelled accurately, the assumptions are made in the aspect of the bone and bone-implant interface – where optimal osseointegration is assumed, which is acceptable after the bone healing period only at some parts of the implant surface – and the boundary conditions. Materials are mostly treated as continuum, with material properties usually set homogenous and linear with elastic material properties characterized by two material constants: Young's modulus and Poisson's ratio. This assumption approaches the behaviour of the metal alloys quite well, the properties of the bone are still intensively investigated.

The macromechanical properties of the bone are influenced by its microstructure. For this reason, microstructural information needs to be included in the analysis to predict individual mechanical bone properties[1]. Microstructural modelling of trabecular bone has become an extensively investigated field of biomechanical researches nowadays. The most commonly used tool for characterizing the complex architecture and material properties of bony organs is the conversion of micro-computed tomography images into micro-FE models[2]. The micro-computed tomography images (3D high resolution images) can be transformed into finite element models by means of different methods. The 3D reconstruction can be directly transformed into an equally shaped micro finite element model by simply converting all voxels to equally sized 8-node brick elements (identical hexahedral elements). This results in finite element models with a very large number of elements, which means the need of high computational capacity and time[3]. Representing each trabecula with just one beam element reduces computational time and leads to the reduction in computational efforts as well[4]. These methods have been developed for simulating the mechanical behaviour of several types of bones of the human skeleton, usually for simulating the effect of bone diseases – such as osteoporosis – on the mechanical properties of the bone. In the majority of cases the models are from the vertebral or the femoral bone substance and not from the mandible or maxilla and include no implants in or cortical layer around the examined trabecular bone. The use of CT-imaging means a serious restriction in the everyday applicability of the afore-mentioned bone models applying either volume- or beam-elements. In micro-computed tomography imaging cadaveric samples are examined. In conventional CT-imaging or in Cone Beam Computed Tomography (CBCT) or Dental Volume Tomography (DVT) scanners, which are the latest generations of CT imaging in dentistry the – often otherwise healthy – patients are exposed to radiation exposure. On the contrary densitometry is accompanied by negligible radiation dose. Furthermore these kinds of examinations are patient specific and only suitable for describing the small, previously scanned fragment of the bone. In the initial phase of the researches the objective was to create a program that generates a stochastic beam structure, which has the format identical with the input data of program system ANSYS and has parameters, which are revisable according to the bone that is simulated (in the aspect of density, porosity, elastic properties etc.). A finite element bone model was produced, which – on the microstructural level – possesses the properties of the trabecular bone substance of an average man from the edentulous mandibular region, such as the geometry (average length and diameter) and the material attributes of a single trabecula or the porosity (or density) of the bone substance.

The received finite element frame model was submitted to compression, shear and torsion tests, and the macro-structural elastic properties were computed. The results were compared with the mechanical properties of the real bone tissue – drawn from literature – and the parameters of the model were set according to them[5]. In the following study the finite element model of the trabecular bone is combined with the models of the cortical layer of the mandible and of a screw type dental implant.

2. Methods and results

2.1. Modelling the bone

In building the finite element models of biological systems assumptions need to be made. In most reported studies – where the bone around dental implants is examined by means of finite element analysis – the macroscopic geometry of the bone is modelled and the assumption is made, that the materials are homogeneous and linear and that they have elastic material behaviour. In most models simulating the mechanical behaviour of bone surrounding dental implants the cortical and trabecular bone substances are treated as continuums – except for some early works, where sometimes only the compact bone is taken into account and the cancellous substance is neglected – with no local failures, discontinuities, cracks or inhomogeneities.

In case of the present study the porous structure of the trabecular bone was taken into account by using its previously published microstructural model, while the solid, compact material of the cortical bone was considered as a homogeneous, linearly elastic continuum.

The finite element beam model of the cancellous bone *(Figure 1)* was created by interlinking a stochastically generated set of nodes in a certain domain (Representative Volume Element), according to a previously defined linking-rule[5]. The extent of the Representative Volume is characteristic of the mechanical properties of the modelled material volume and has to be selected to be convenient to the aims of the planned investigations. In the present case the desired number of nodes was set in a 5 mm×5 mm×5 mm sized cubical shaped domain, which represents the identical sized bone substance. The stability of the model is provided by the appropriate number of linkings between the nodes and by the rigidity of the connections. Each node was connected with a beam to the closest at least three nodes, but considering the geometry of the trabecular bone of the human mandible this number had to be set from 5 to 7. To achieve the required approximately 70% porosity (percentage value of voids volume of bone material in proportion to the volume of the whole cube) – according to literary data[6,7,8,9] – the number of the nodes and the applied linkings were changed, with the length and diameter kept on the values achieved from microscopic images. In the thus received finite element model each trabecula was represented by one beam element. From the assortment of program system ANSYS the so-called BEAM188 element was applied, which is a three dimensional linear finite strain beam based on Timoshenko beam theory, in which shear deformation effects are included[10]. The consideration of the shear deformations are justified because of the beams being slightly stubby and possessing porous contexture.

The material properties of the trabeculae, and the macrostructural properties of the trabecular and the cortical bone were set according to the data achieved from the literature. Several techniques can be found for determining the Young's modulus of the single trabeculae[6,11]: direct mechanical testing of a single trabecula in tension (Ryan and Williams, 1989), 3-point bending (Kuhn et al., 1987 and Choi et al., 1990) or buckling (Townsend et al., 1975 and Runkle and Pugh, 1975); ultrasonic wave propagation and scanning acoustic microscopy in trabecular bone specimens (Ashman and Rho, 1988[12]; Turner et al., 1999[13]; and Nomura et al, 2007[14]); finite element analysis (Pugh et al., 1973; Williams and Lewis, 1982; Mente and Lewis, 1987; van Rietbergen et al., 1995 and Kabel et al., 1999[15]) and nanoidentation (Rho et al., 1997[16]; Zysset et al., 1999[17]). The macro structural Young's modulus value of cancellous bone was estimated by means of three different methods: using Hodgkinson and Currey's (1992) empirical equations relating modulus and density[6], by the means of finite element analysis[15] or compression tests[18,19].

The finite element model of the cortical bone *(Figure 1)* was meshed with tetrahedral volume elements because of the complex geometry at the surface where the bone meets the implant.

2.2. Modelling the implant

Dental implants are artificial tooth root replacements. They are implanted in the jaw bones during small surgical operations to hold the prosthesis and to fasten it to the bone. In dental surgery the most commonly used implant types are the screw type endosteal – that are imbedded in the bone – implants, for this reason the most of the related studies – so do the present research of ours – examine the mechanical behaviour of these or of the bone surrounding them, considering various geometry, thread formation, length and diameter. Material properties of dental implants can be approached quite accurately – since being metal alloys – as homogeneous and linear with elastic material behaviour characterized by two material constants, Young's modulus and Poisson's ratio. Nowadays the application of metallic materials in dental implantology is limited to commercially pure titanium and its (Ti-6Al-4V) alloy[20].

In this stage of the research a method was developed for describing the geometry of the screw type implants by means of mathematical functions and several modifiable or revisable parameters to make the procedure of finite element modelling faster and easier. The parameters, which can be altered according to the sizes and shapes of the implants chosen by the dental surgeon, are the following: the length of the implant, the inner and outer diameter of the implant, the thread formation and thread pitch, all of which can change along the length according to a function or differ in certain segments and the shape of the implant apex. In *Figure 2.* the models of two different dental implant types can be seen.

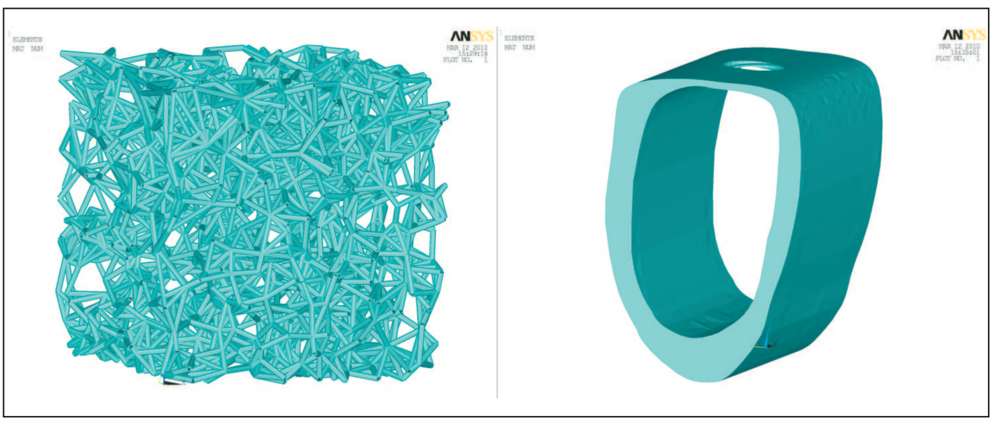

Figure 1. Finite element models of the trabecular (left) and the cortical (right) bone

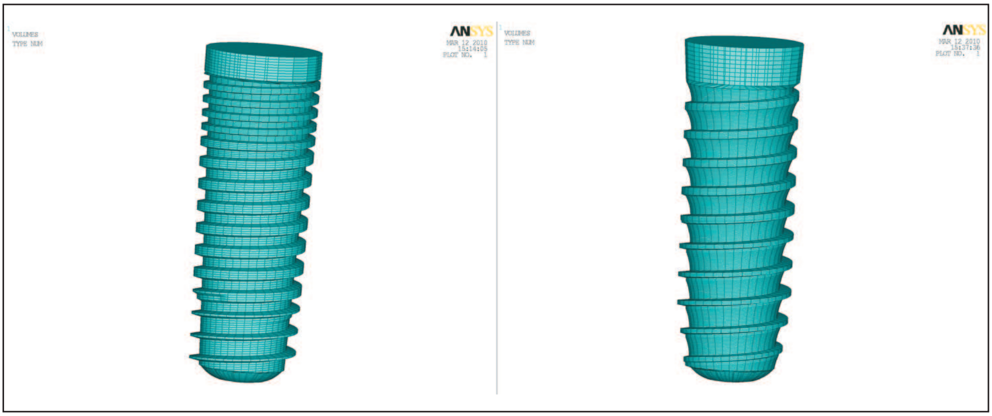

Figure 2. Finite element models of two different screw type dental implants

Since especially the behaviour of the bone is in the centre of our interest, and since being titanium alloy the material of the implants was assumed to be much stiffer than the bone, and only the surface of the screw was taken into account and meshed with triangular shell elements with high stiffness value.

2.3. Modelling the bone-implant interface

At the bone-implant interface most of the finite element models assume optimal osseointegration, which means, that the bone is perfectly bonded to the whole surface of the implant, which cannot be assumed during the healing period and arguable after the complete healing, because of the presence of an intermediary layer between the two materials, which can be connected to the implant surface in different degrees. The degree of the osseointegration can be characterized by the BIC (bone-implant contact) value, which means the percentage of the implant area connected to the bone and the area of the whole implant surface[21].

The imperfection of the osseointegration could be taken into account by modelling the aforementioned intermediary layer as a mem-

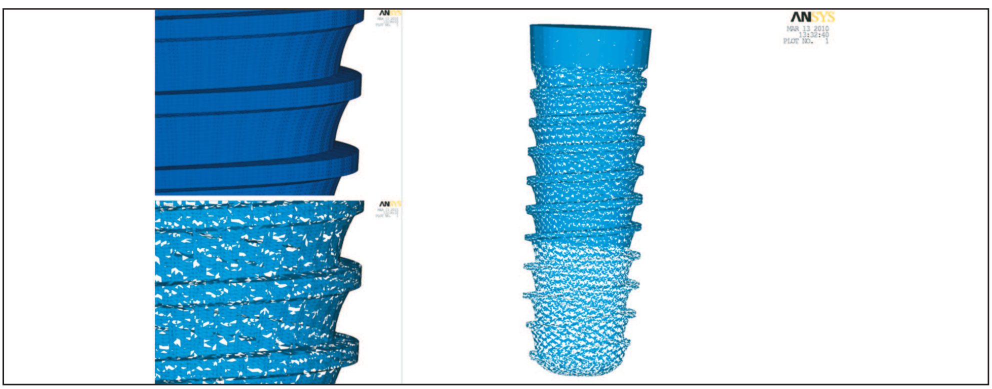

Figure 3. Finite element mesh of intermediary membrane between the bone and the implant with the finite element mesh of the implant

brane covering different percents of the surface of the implant (30% at the apex, 60% in the middle, where it meets the trabecular bone, and 90% at the upper region of the implant, where the mambrane meets the cortical bone) by using an additional layer also meshed with triangular shell elements *(Figure 3)*. The elements forming the cortical and trabecular bone are attached to these elements instead of the implant.

2.4. Compiling the model

While compiling the complex finite element model from the aforementioned four parts (implant, trabecular bone, cortical bone, intermediary layer) especially while intersecting the beams with the volume or shell elements we faced several difficulties. The problem of connecting the different element types had to be solved. The beams cut by the surfaces of the implant or the cortical bone had to be connected to the nodes of the surface mesh *(Figure 4)*, so an algorithm had to be developed, which changes the end points of the cut beams from the original connection points to the closest nodes of the surfaces. The second problem, which came up when the beams were cut, was the appearance of too short elements, and beams that were not connected to any other beams. These elements had to be found and erased.

3. Conclusions

In this study a numerical modelling method of the trabecular bone microstructure was introduced, which was developed for the examination of the mandibular or maxillar cancellous bone especially around dental implants in the framework of a former research. The mechanical behaviour of biological materials – such as cancellous bone – are most commonly examined by the means of direct mechanical testing or finite element analysis, the latter of which is the in vivo applicable method in humans. In the aspect of oral implantation in the upper- and lower-jawbones the finite element models reported so far consider the trabecular bone substance as a continuum. The fact, that microstructural properties have remarkable effect on the overall behaviour of the bone, indicates the need of micromechanical simulations. The most commonly used method for modelling

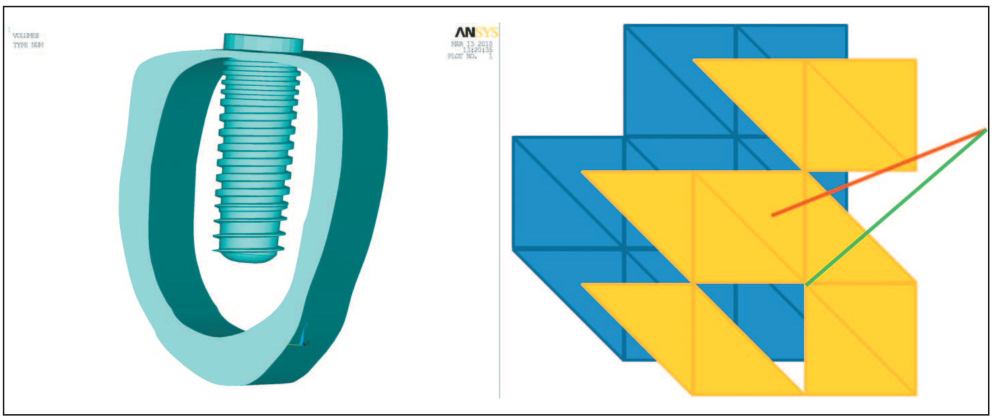

Figure 4. The combined finite element model of the implant and cortical bone (left) and the connection of the beams to the intermediary membrane (right), the original beam (red) changed to a properly connecting one (green)

the cancellous bone's microstructure is the conversion of CT images into finite element meshes using either volume or beam elements, the latter of which overcomes the difficulties resulting from the high computational time and effort demand. The application of CT imaging can be avoided by creating a stochastically generated, porosity (or density) dependent finite element frame model, in which each trabecula is simulated by one beam element. The received model was combined with the finite element models of the mandibular cortical bone and the dental implant. The incomplete contact between the cancellous or cortical bone and the implant was taken into account by using an intermediary layer between the two surfaces, which covers the implant according to the value of the bone-implant contact area and connects it to the bone.

References

1. *Stauber M* and *Müller R*. Volumetric spatial decomposition of trabecular bone into rods and plates – a new method for local bone morphometry. Bone, 2006;38:475–484.

2. *Hellmich C, Kober C* and *Erdmann B*. Micromechanics-Based Conversion of CT Data into Anisotropic Elasticity Tensors, Applied to FE Simulations of a Mandible. Annals of Biomedical Engineering. 2008;36(1):108–122.

3. *Rudnyi EB, Van Rietbergen B* and *Korvik JG*. Efficient harmonic simulation of a trabecular bone finite element model by the means of model reduction, *Proceedings of 12th Workshop „The Finite Element Method in Biomedical Engineering, Biomechanics and Related Fields"*. University of Ulm, July 2005., Proceedings of the 12th FEM Workshop, 61–68.

4. *Van Lenthe GH, Stauber M* and *Müller R*. Specimen-specific beam models for fast and accurate prediction of human trabecular bone mechanical properties. Bone, 2006;39:1182–1189.

5. *Lakatos É, Bojtár I*. Stochastically generated finite element beam model for dental research. Periodica Polytechnica Ser Civ Eng 2009;53(1):3–8.

6. *Gibson LJ* and *Ashby MF*. Cellular solids – Structure and properties. University Press, Cambridge, second ed., 1997.

7. *Renders GAP, Mulder L, Van Ruijven LJ* and *Van Eijden TMGJ*. Porosity of human mandibular condylar bone. J. Anat., 2007;210(3):239–248.

8. *Hogskinson R, Njehz CF, Whitehead MA* and *Langton CM*. The non-linear relationship between BUA and porosity in cancellous bone. Phis. Med. Biol., 1996;40:2411–2420.

9. *Moon HS, Won YY, Kim KD, Ruprecht A, Kim HJ, Kook HK* and *Chung MK*. The three-dimensional microstructure of the trabecular bone in the mandible. Surg. Radiol. Anat., 2004; 26;466–473.

10. ANSYS 11.0 User's Manual

11. *Rho JY, Kuhn-Spearing L* and *Zioupos P*. Mechanical properties and the hierarchical structure of bone. Medical Engineering & Physics, 1998;20:92–102.

12. *Ashman RB* and *Rho JY*. Elastic modulus of trabecular bone material. Journal of Biomechanics, 1988;21(3):177–181.

13. *Turner CH, Rho JY, Takano Y, Tsui TY* and *Pharr GM*. The elastic properties of trabecular and cortical bone tissues are similar: results from two microscopic measurement techniques. Journal of Biomechanics, 1999;32:437–441.

14. *Nomura T, Katz JL, Powers MP* and *Saito C*. A micromechanical elastic property study of trabecular bone in the human mandible. J. Mater. Sci.: Mater. Med. 2007;18:629–633.

15. *Kabel J, Van Rietbergen B, Dalstra M, Odgaard A* and *Huiskes R*. The role of an effective isotropic

tissue modulus in the elastic properties of cancellous bone. Journal of Biomechanics, 1999; 32:673–680.

16. *Rho JY, Tsui TY* and *Pharr GM.* Elastic properties of human cortical and trabecular lamellar bone measured by nanoindentation. Biomaterials, 1997;18(20):1325–1330.

17. *Zysset PK, Guo XE, Hoffler CE, Moore KE* and *Goldstein SA.* Elastic modulus and hardness of cortical and trabecular bone lamellae measured by nanoindentation in the human femur. Journal of Biomechanics, 1999;32:1005–1012.

18. *Kang Q, An YH* and *Friedman RF.* Mechanical properties and bone densities of canine trabecular bone. Journal of Materials Science: Materials in Medicine, 1998;9:263–267.

19. *O'Mahony AM, Williams JL, Katz JO* and *Spencer P.* Anisotropic elastic properties of cancellous bone from a human edentulous mandible. Clinical Oral Implants Research, 2000; 11(5):415–421.

20. *Divinyi T.* Dental implantology (in Hungarian – Fogászati implantológia). Springer Hungarica Kiadó Kft., 1998.

21. *Misch CE.* Contemporary Implant Dentistry, Mosby Inc., 3rd ed., 2007.

We thank Prof. Tamás Divinyi and Dr. Attila Szűcs from the Faculty of Dentistry, Semmelweis University, Budapest for providing the medical background for the research.

Éva Lakatos
Department of Structural Mechanics, Budapest University of Technology and Economics
H–1111 Budapest, Műegyetem rkp. 3.

Mesoporous silica-calcium phosphate composites for experimental bone substitution

István Lázár[1], Sándor Manó[2], Zoltán Jónás[2], László Kiss[2], István Fábián[1], Zoltán Csernátony[2]
[1] University of Debrecen, Department of Inorganic and Analytical Chemistry
[2] University of Debrecen, Department of Orthopaedic Surgery
lazar@delfin.unideb.hu

Introduction

Artificial materials of controled strength, chemical composition and pore structure have gained significant attention in the medical practice in the last two decades. Synthetic materials used for bone substitution are of either inorganic or organic origin. Inorganic materials like tricalcium phosphate[1,2] and hydroxylapatite[3] are preferred nowadays, but other materials such as ceramics and bioceramics[4], bioglass[5,6], metals with bioactive ceramic surface coating[7,8] or calcium sulfate[9,10] are also in active duty. Organic substances, ie. polylactic acid[5], PMMA[11], collagen or chitosan[12,13] are also widely used, most frequently in combination with one or more of the beforementioned inorganic fillers.

Most recently the role of silica in living organisms has been revised and now is considered essential for the development of bone tissues[14]. Silica containing calcium phosphate have shown osteoinductivity in human osteoblast cultures in vitro[15] and preparations with various silica and calcium phosphate compositions are under clinical studies[16].

Pore size distribution of bones and artificial bone substitute materials are of critical importance. Natural pores in the 100–1000 μm region are required for bone tissue ingrowth, while smaller pores in the 10–100 μm range conduct only the unmineralized fibrous tissue[17] and contribute to materials transport. Most recently ordered structure silicas like MCM-41 are under investigation in combination with polilactic acid or other biopolymers as new, high porosity bone substitutes[5].

Sol-gel technology opened the way to the synthesis of mesoporous silicas that can be used as extremely high porosity matrix and excellent drug delivery materials. In combination with calcium ions containing inorganic materials they may represent the third generation of bone substituent bioceramics[18]. Based upon our earlier experiences in aerogel synthesis and supercritical drying technology we have decided to synthesize potentially bioresorbable composite materials containing calcium phosphate powder and mesoporous silica of controlled pore size.

Methods

Materials

Tetramethoxysilane (TMOS, 98%) was purchased from Fluka, microgranular cellulose from Sigma, methanol (purum), acetone (purum) and ammonia solution (analytical grade, 25%) from Acidum-2 Kft. (Debrecen, Hungary), tricalcium phosphate (Ph Eur) from a local pharmacy. Triple deionized, membrane and carbon filtered water was prepared with a water station, which was constructed of a high capacity double ion exchange battery connected to a high purity MilliQ instrument. Carbon dioxide cylinders were purchased from Linde.

Methods and instrumentation

Plastic molds (approx. 70 mm tall) were machined from a regular pvc waterwork pipe of 28/32 mm id/od. The inner walls of the molds were covered with thin teflon foil. The bottom of the molds were sealed with multiple layers of parafilm. Supercritical carbon dioxide drying was performed in a custom made 1.5 L volume stainless steel SCO_2 dryer at 70–80 °C. Heating and sintering of the samples was carried out in a 14 L volume WiseTherm rectangular furnace, the temperature accuracy was better than –1/+3 °C at 1150 °C.

Compresive stress of the samples were determined with a INSTRON 8874 Servohydraulic Biaxial Material Testing Machine. Thermogravimetric and thermoanalytical measurement was carried out with a MOM Derivatograph-C instrument in the 100–1200 °C range. Scanning electron microscopic images were recoreded on a Hitachi S-4300 CFE instrument.

Cellulose-tricalcium phosphate alcogel

To a vigorously stirred solution of 21.00 mL (21.48 g, 0.1411 mol) of tetramethoxy silane (TMOS), 154 mL (121 g, 3.80 mol) of methanol (MeOH), 14,0 mL (14.0 g, 0.77 mol) of water was added 7.00 g of microgranular cellulose and 7.00 g of very finely powdered tricalcium phosphate. The mixture was sonicated in a common laboratory ultrasonic bath for 1-2 minutes to evenly disperese the solids, then stirred vigorously meanwhile 35 mL of ammonium hydroxyde (25 m/m%, 0.47 mol NH_3) was added in one portion. The homogenous mixture was poured rapidly into the plastic molds, sealed and let to stand at room temperature for several days. Setting occured within a few ten seconds to a few minutes, depending on the actual temperature and the length of ultrasound treatment. The longer was the sonication, the shorter was the setting time. (Note that changing of the molar ratios or particle size of the solid components may lead to too short or too long setting times or to sedimentation of tricalcium phosphate. Some experimentation might be necessary to find the optimal conditions.)

Preparation of X1-700 and X1-900 xerogels

Cellulose-tricalcium phosphate alcogel monoliths were pushed out of the molds with a machined plunger and placed into a Petri dish lined with five layers of round filter paper. To avoid cracking and ensure uniform drying the monoliths were surrounded and covered nearly airtight with cylinders made of several layers of regular filter paper and let to stand and dry under a hood for several days. In this period significant linear shrinking occured, but cracks did not appear. The resulted gels were dried in an oven at 100–110 °C for at least one day, then heated in a furnace at 700 °C for 5 hours to burn out cellulose and reach the final structure and dimensions (shrinking from 28.0 mm od. to 14.5 mm od. occured). Those xerogels were still fairly fragile and sensitive pieces, which could be broken easily by bare hands (Sample X1-700).

A X1-700 xerogel monolith was sintered at 900 °C for 12–24 hours to reach the required mechanical strength. It shrinked further to a final diameter of 10.5 mm, and its strength increased so much that it could not be broken by bare hands any more (Sample X1-900).

Preparation of A1-SC aerogel

Water and alcohol content of the alcogel monoliths were replaced with acetone in the following manner. The alcogels were pushed out of the plastic molds and soaked first in pure methanol, then in methanol-acetone mixtures (acetone content was increased gradually in 25% steps) and in acetone, for one day in each solvent mixtures. Acetone gels were then transfered into the SCO_2 dryer under acetone. After sealing the reactor body, acetone was drained and flushed with liquid carbon dioxide. Remaining acetone entrapped in the the gel bodies was expelled by liquid carbon dioxide and formed an immiscible secondary liquid phase in the bottom of the reactor. This was drained in several portions in a 4–12 hours period of time. The system was considered acetone-free when dry ice collected from the flushing carbon dioxide gave no liquid residue evaporated on a horizontal steel surface. The temperature was then increased to and kept at approximately 60–70 °C for at least one hour, then the pressure was released in 3–4 hours through a needle valve and a capillary made of a 100 mm long 1/16” od. 0.005” id. HPLC steel tubing. The aerogel samples were removed from the reactor and stored either in a heated cabinet at 110 °C or in sealed vials (Sample A1-SC).

Preparation of A1-1000 aerogel

Aerogel sample A1-SC was sintered in a furnace at 1000 °C for 6 hours resulting in a significantly shrinked aerogel monolith.

Tricalcium phosphate alcogel

To a vigorously stirred solution of 12.60 mL (12.89 g, 0.085 mol) of TMOS, 92 mL (73 g, 2.27 mol) of MeOH, 8,4 mL (8.4 g, 0.47 mol) of water was added 7.00 g of very finely powdered tricalcium phosphate. The mixture was sonicated for a short while to evenly disperese the solids, then stirred very vigorously meanwhile 21 mL of ammonium hydroxyde (25 m/m%, 0.28 mol NH_3) was added in one portion. The homogenous mixture was vigorously stirred until the viscosity had increased significantly, then poured rapidly into plastic molds. Bamboo sticks (soaked in methanol before, dimensions: 3 mm×3 mm×70 mm) were inserted into one of the monoliths before setting occured to make a hexagonally ordered template. The molds were then sealed and let to age at room temperature for several days. (Note that it is quite difficult to catch the right moment for casting to prevent rapid sedimentation of tricalcium phosphate granules, therefore preliminary experimentation is recommended. Moderate increase or decrease of the volume of ammonium hydroxyde may also be necessary, as the concentration depends on the brand, the temperature and the age of the solution.)

Preparation of tricalcium-phosphate aerogels A2-SC

These samples were prepared by the same supercritical drying method as given for A1-SC aerogel. From the templated aerogel the bamboo sticks could have been pulled out without cracking of the monolith and left rectangular channels behind.

Preparation of A2-1000 aerogel

A2-SC aerogel samples were sintered at 1000 °C for 6 hours in a furnace.

Results and discussion

Effect of drying technique on gel structures

The alcogel samples were dried by two different ways. The first one was ambient drying at room temperature, followed by heating in a furnace, which gave higher density, significanly shrinked xerogels X1-700 and X1-900. The second one was supercritical carbon dioxide drying resulted in aerogel samples A1-SC and A2-SC, from which samples A1-1000 and A2-1000 were prepared by heating at 1000 °C. Xerogels showed increased pore sizes and loss of mesoporosity compared to the corresponding aerogel analogs, which was the consequence of shrinking and deterioration of the aerogel structure due to the presence of capillary forces in the atmospheric drying phase.

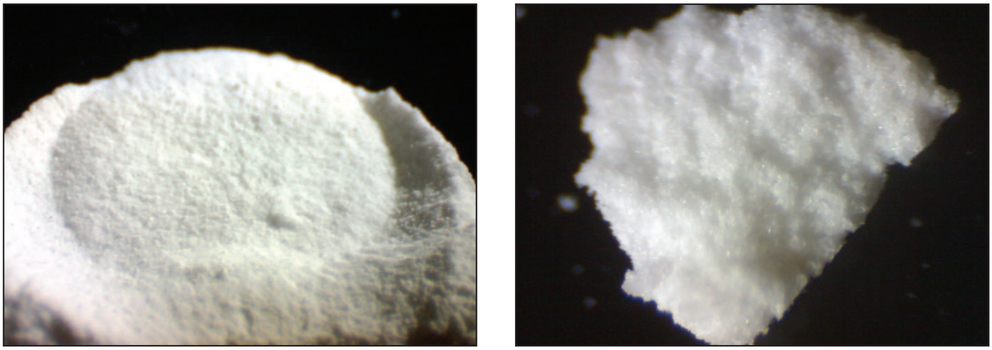

Figure 1. Optical microscopy images of silica-tricalcium phosphate xerogel monolith X1-900 in 16× and 120× magnification, respectively

Figure 1 shows optical microscopic picture of the X1-900 monolith. The grainy structure proved to be characteristic to all calcium-phosphate powder containing silica composites.

Structure of aerogel composites

Chemical composition of the aerogel and xerogel samples were identical for all of the samples as follows (calculated, expressed as oxides): SiO_2 54.3 %, CaO 24.8 %, P_2O_5 20.9%. Cellulose was used as a disposable template material for the creation of pores in the submicron and microne range and can be burned out at 500 °C. *Figure 2* shows the SEM pictures of A1-1000 and A2-1000 aerogels. It can be seen quite well that burnt cellulose left large pores behind in the matrix, the pore diameters are in the range of approx. 100–7000 μm, which belongs to the macropore region. A2-1000 shows a normal aerogel structure characterized by evenly distributed mesopores in the 10–100 μm range.

Optical microscopic images show the difference between the macrostructures of A1-SC and A2-SC aerogel composites in *Figure 3.* In sample A1-SC the optical transparency is much lower and the gel structure seems to be more homogeneous then in A2-SC. The difference is most likely due to the presence of cellulose in A1 alcogel in the setting phase. Cellulose and calcium phosphate together

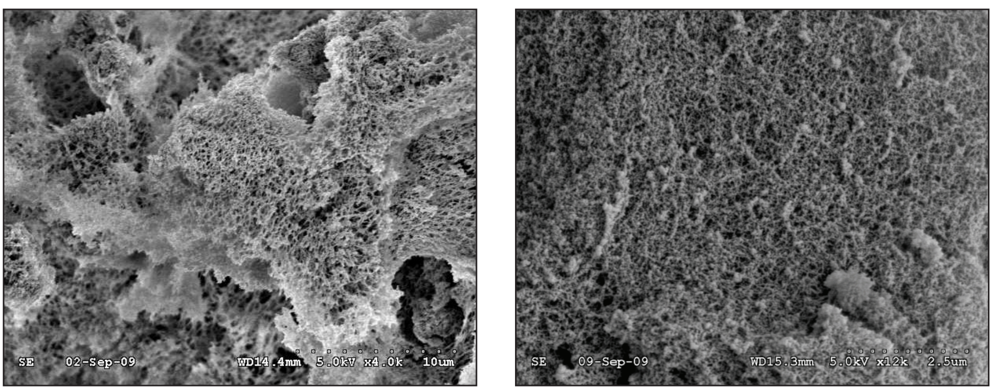

Figure 2. SEM pictures of composite aerogel samples A1-1000 and A2-1000. Magnification of the left and right pictures are 4k and 12k, respectively

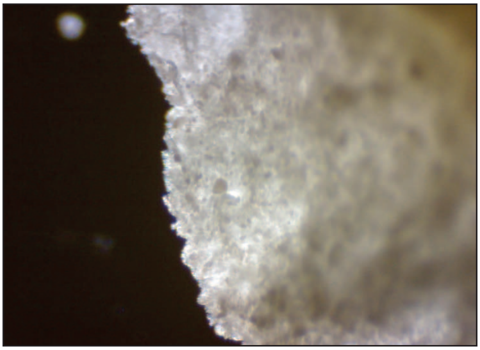

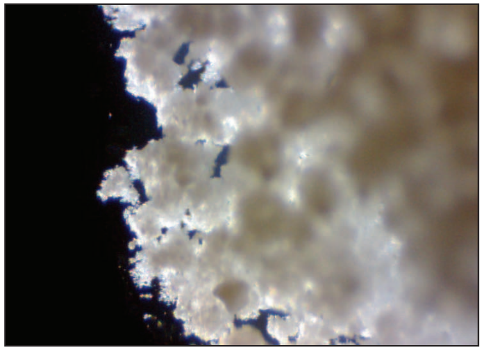

Figure 3. Microscopic images of aerogels A1-SC (left) and A2-SC (right) in 120× magnification. Aerogel matrix is transparent and almost completely invisible in the right picture (some blueish tint can be observed between the seeds)

provided a much higher number of seeds for crystal forming, while in the A2 alcogel the relatively large particles of tricalcium phosphate were present in much less number resulting in formation of large condensed particles, which were embedded in and connected by a nearly transparent silica aerogel matrix.

Sintering, shrinking

Changes of density and length of the aerogel sample A1-SC on heating was studied and the results are represented in *Figure 4*. The sample was heated for 24 hours at each temperature given, except for 1000 °C and 1050 °C, which were kept for 3 and 1 hours, respectively. As it can be seen in *Figure 4* the linear shrinking was moderate until 700 °C (1073 K) and became very significant above 800 °C. The virtual density of the sample decreased a bit at low temperature due to desorption of adsorbed solvents and water, then remained nearly unchanged (0,09 g/cm^3) between 500 °C and 600 °C and then increased significantly over 800 °C to reach 0.49 g/cm^3 value at 1000 °C.

Extended heating of the sample at 12 h/ 1000 °C and then 3h/1050 °C resulted in even higher densities of 0.75 g/cm^3 and 1.04 g/cm^3, respectively. The sample shrinked to 38% of the original length by reaching 1050 °C.

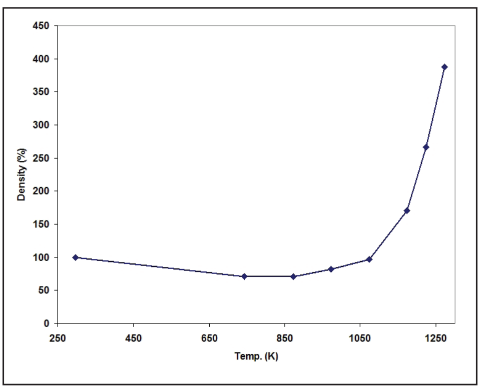

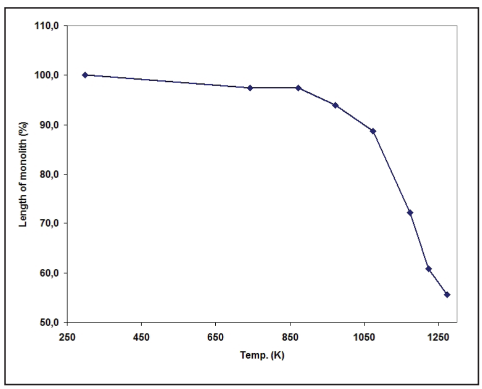

Figure 4. Change of relative density and length of aerogel monolith A1-SC versus the sintering temperature

Thermogravimetry analysis

Thermic behaviour of sample A1-700 was studied by thermogravimetry/differential thermoanalysis technique. 69 mg amount of aerogel was tested and the change of weight and inner temperature was recorded as a function of time. TG-DTG-DTA curves of sample A1-700 can be seen in *Figure 5*.

At the first part of the DTA curve an endothermic change can be observed, which is in accordance with the loss of weight in the TG curve. Both end by approx. 240 °C and the phenomenon corresponds to the desorption of water. From 240 °C to 975 °C no thermic process occured in the gel. At 975 °C an exothermic coalescence of the fine silica matrix has started and finished by 1150 °C. This process can be attributed in minor part to the condensation of silanol grups and in major part to the reduction of surface (by melting and slow viscous flow) in the aerogel and led to the formation of large grains in the micron range.

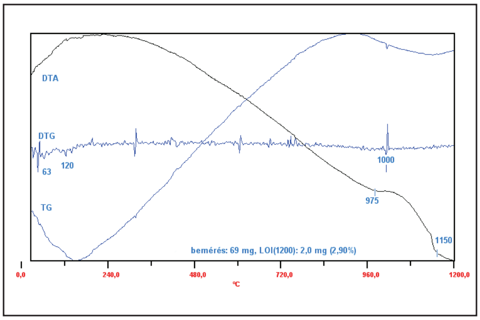

Figure 5. TG-DTG-DTA curves of sample A1-700

Mechanical testing

Cylindrical specimens of X1-900 and A2-1000 with known geometry were placed in the servohydraulic tester between 2 mm thick hard polypropylene plates. Compressive load vs. compressive extension curves *(Figure 6)* were recorded by using the 10 kN probe and compressive stress values were calculated. Compressive stress of aerogel sample A1-900 has also been determined, but its value was very low (0.28 MPa). This weakening of the aerogel composite structure was most likely the consequence of the presence of large pores and thin walls that were formed on baking out cellulose from the gel.

The calculated compressive stress values of X1-900 and A2-1000 samples were 18.2 MPa and 35.1 MPa, respectively. These values can be considered fairly promising in the point of view of potential bone substitution, as they reached or exceeded the average strength of natural cancellous bones.

Conclusions

Two drying techniques have been developed for the preparation of tricalcium phosphate containing high porosity materials based

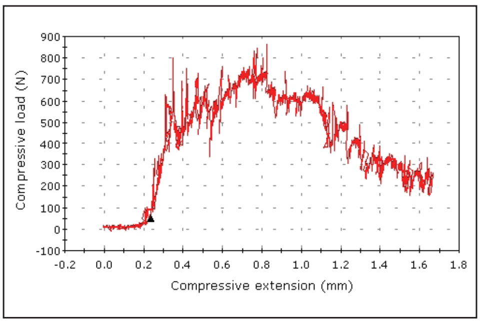

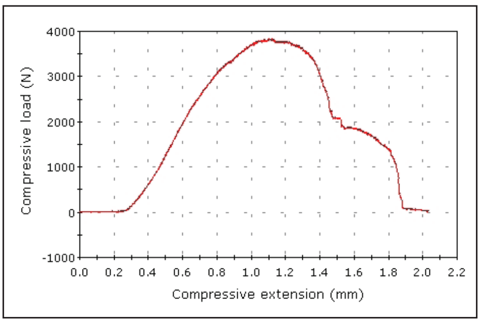

Figure 6. Compressive load vs. compressive extension curves of X1-900 (left) and A2-1000 (right) samples

on silica aerogels or xerogels for artificial bone substitution. Xerogel sample X1-900 was more simple to make by ambient drying but showed somewhat less mechanical strength. Silica aerogel A2-1000, which contained evenly distributed tricalcium phosphate particles embedded and chemically bonded in silica aerogel showed the highest compressive strength and reached the strength of cancellous bones. Based upon our experimental data, this tricalcium phosphate-silica aerogel composite prepared by the sol-gel technology and supercritical drying have the potential to be used as an artificial bone substitute. In addition, the characteristic aerogel pore structure offers an extra possibility to be used not just as bone substitute but also as a slow release drug carrier, which might be used for simultaneous treatment of bone infections or other diseases.

References

1. *Kamitakahara M, Ohtsuki C, Oishi M, Ogata S, Miyazaki T, Tanihara M.* Preparation of porous biphasic tricalcium phosphate and its in vivo behavior. Key Engineering Materials 2005;284–286, 281–284.

2. *Li P, Zhang K, Colwell CW Jr.* Experimental Study on the Osteoinduction of Calcium Phosphate Biomaterials In Vivo and the Capability of Supporting Osteoblast Proliferation In Vitro. Key Engineering Materials 2005;284–286, 293–296.

3. *Gerber T.* Production of highly porous ceramics for artificial bone. DE 19825419, 19991209, 1999.

4. *Chevalier J, Gremillard L.* Ceramics for medical applications: A picture for the next 20 years. Journal of the European Ceramic Society 2009;29: 1245–1255.

5. *Korventausta J, Rosling A, Andersson J, Lind A, Linden M, Jokinen M, Yli-Urpo A.* Bioactive glass (S53P4) and mesoporous MCM-41-type SiO2 adjusting in vitro bioactivity of porous PDLLA. Key Engineering Materials 2004;254–256, 557–560.

6. *Ohtsuki C, Kamitakahara M, Miyazaki T.* Bioactive ceramic-based materials with designed reactivity for bone tissue regeneration. Journal of the Royal Society Interface 2009;6:S349–S360.

7. *Liu X, Morra M, Carpi A, Li B.* Bioactive calcium silicate ceramics and coatings. Biomedicine & Pharmacotherapy 2008;62:526–529.

8. *Meretoja VV, De Ruijter AE, Peltola TO, Jansen JA, Naerhi TO.* Osteoblast Differentiation with Titania and Titania-Silica-Coated Titanium Fiber Meshes. Tissue Engineering 2005;11:1489–1497.

9. *Gisep A, Rahn B.* Calcium-Phosphate – Calcium-Sulphate Bone Cements. Structure and Compression Strength after Setting. European Cells and Materials 2004;7(Suppl. 2):34–35.

10. *Guo H, Wei J, Liu CS.* Development of a degradable cement of calcium phosphate and calcium sulfate composite for bone reconstruction. Biomedical Materials 2006;1:193–197.

11. *Shinzato S, Kobayashi M, Mousa WF, Kamimura M, Neo M, Kitamura Y, Kokubo T, Nakamura T.* Bioactive polymethyl methacrylate-based bone cement: comparison of glass beads, apatite- and wollastonite containing glass-ceramic, and hydroxyapatite fillers on mechanical and biological properties. Journal of Biomedical Materials Research 2000;51:258–272.

12. *Lee E-J, Shin D-S, Kim H-E, Kim H-W, Koh Y-H, Jang J-H.* Membrane of hybrid chitosan-silica xerogel for guided bone regeneration. Biomaterials 2009;30(5):743–750.

13. *Muzzarelli RAA.* Chitins and chitosans for the repair of wounded skin, nerve, cartilage and bone. Carbohydrate Polymers 2009;76:167–182.

14. *Martin KR.* The chemistry of silica and its potential health benefits. Journal of Nutrition, Health & Aging 2007;11(2):94–98.

15. *Phan PV, Grzanna M, Chu J, Polotsky A, El-ghannam A, Van Heerden D, Hungerford DS, Frondoza CG.* The effect of silica-containing calcium-phosphate particles on human osteoblasts in vitro. Journal of Biomedical Materials Research, Part A 2003;67A(3):1001–1008.

16. *Bienengraeber V, Gerber T, Trykova T, Kundt G, Henkel K-O.* A new high porous silica-sol-gel-ceramics for bone grafting – in-vivo long-time investigations. Materialwissenschaft und Werkstofftechnik 2004;35(4):234–239.

17. *Karageorgiou V, Kaplan D.* Porosity of 3D biomaterial scaffolds and osteogenesis. Biomaterials 2005;26:5474–5491.

18. *Izquierdo-Barba I, Colilla M, Vallet-Regi M.* Nanostructured Mesoporous Silicas for Bone Tissue Regeneration. Journal of Nanomaterials 2008, 2008, Article ID 106970.

Financial support from the Hungarian Research Fund (OTKA 76834) is gratefuly acknowledged. The authors would like to express their thank to Lajos Daróczi (Department of Solid State Physics) and István Papp (Department of Mineralogy and Geology) for their kind help in electron microscopy and thermogravimetric examinations.

István Lázár
University of Debrecen, Department of Inorganic and Analytical Chemistry
H–4032 Debrecen, Egyetem tér 1.

FUSION OF VIDEO AND MOTION DATA: ENGINEERING TASKS AND CLINICAL APPLICABILITY

Ferenc Pongrácz
NKTH, Budapest
pongraczf@t-online.hu

Abstract

Status of a new project – focusing on technical aspects of fusion of live video and data from optical motion tracking – is summarized. Also, the significance of development in two areas is marked out: (1) in clinical field of endoscopic surgeries as demonstrating and training tool; (2) in biomechanical research for accurate detection of human motion curves.

Keywords: video tracking, motion data fusion, endoscope, movement analysis

Introduction

The idea of representing video image and captured motion data in a common reference frame is not new[1,2,3,6] but, because of many application areas and latest achievements in technology, it's worth to give attention to related technical and clinical aspects.

As an important application, this article gives an introduction of tools for training and demonstrations in endoscopic surgery. These goals can be reached by integrating endoscopic video into surgical navigation environment and performing motion tracking of surgical devices and endoscope. In future extension, for internet-based training and demonstrations, a special network transfer can be developed for transmitting live video with surgical planning and motion data. The education of surgical skills is a common problem in endoscopic surgery[7] that supports the proposed project plan[8]. Personal communications with head physicians in local hospitals confirm that, inexperienced intervention frequently rearranges the anatomical structures during ENT (Ear Nose and Throat) surgeries that can cause large obstacles in acute cases. In case of surgical planning with imaging data (CT, MR), the client observers follow in real-time the trajectory of endoscope and identify the critical anatomical parts.

Another important area of fused (conventional) video and motion data is closely related to biomechanical research. Reconstruction of 3D human movement is difficult if predefined graphical models are supposed to match bone movements during gait analysis or study of any pathologic motion[4,5,9]. Correction of geometrical axes or use of constraints in modeling after experiments makes the interpretation of motion diagrams almost impossible[12]. Introduction of 3D registered video and fused motion data from bone sensors helps a lot in testing kinematical models. The misalignment of graphical models can be visualized and compared to real anatomy on video screen using different camera positions. On screen editing is possible in live and playback modes. After involving and registering diagnostic volume (CT, MR volumetric models or planar X-Rays) to tracker's space, the accuracy of kinematical models – during video screen editing – can be easily tested even on static diagnostic data.

Methods

Video calibration

Positioning of video frame into 3D navigation environment is performed by registration of camera space to the space of motion tracking device. This is possible between 3D orthogonal coordinate spaces; therefore it has to be preceded by conversion of visible (usually distorted) image plane into an undistorted image plane. This step is named as calibration procedure which means calculation of transform between the distorted and undistorted image planes. Distortion parameters are given by[11]:

$$j' = a_0 + a_1u + a_2v + a_3u^2 + a_4uv + a_5v^2 \quad (1)$$

$$k' = b_0 + b_1u + b_2v + b_3u^2 + b_4uv + b_5v^2 \quad (2)$$

where u, v are the coordinates on undistorted (ideal) image plane and) are the calculated values. Undistorted image plane is a calibration grid containing large number of markers. Error function between observed *(j',k')* and calculated coordinate

$$E = (j - j')^2 + (k - k')^2 \quad (3)$$

in vector form:

$$E = \|\boldsymbol{j} - \boldsymbol{Pa}\|^2 + \|\boldsymbol{k} - \boldsymbol{Pb}\|^2 \quad (4)$$

where $\boldsymbol{j}, \boldsymbol{k}$ are the vectors which are from distorted image plane. $\boldsymbol{P}$ represents the matrix which is set from values of ideal undistorted image plane (calibration grid):

$$\boldsymbol{P} = \begin{bmatrix} 1 & u_1 & v_1 & u_1^2 & u_1v_1 & v_1^2 \\ 1 & u_2 & v_2 & u_2^2 & u_2v_2 & v_2^2 \\ \cdots & \cdots & \cdots & \cdots & \cdots & \cdots \\ 1 & u_{m-1} & v_{m-1} & u_{m-1}^2 & u_{m-1}v_{m-1} & v_{m-1}^2 \\ 1 & u_m & v_m & u_m^2 & u_mv_m & v_m^2 \end{bmatrix} \quad (5)$$

Distortion parameters if both coordinates are involved:

$$\boldsymbol{a} = [a_0 \quad a_1 \quad a_2 \quad a_3 \quad a_4 \quad a_5] \quad (6)$$

$$\boldsymbol{b} = [b_0 \quad b_1 \quad b_2 \quad b_3 \quad b_4 \quad b_5] \quad (7)$$

In case of ideal radial distortion (for many endoscopes) distortion equations (1, 2) can be modified:

$$r' = c_0 + c_1u + c_2u^2 + c_3u^3 \quad (8)$$

where u is the radial distance on undistorted plane and r' is the estimated distance after distortion. In this case the error between the observed *(r)* and calculated *(r')* values:

$$E = \|\boldsymbol{r} - \boldsymbol{Pc}\|^2 \quad (9)$$

where *P* contains the ideal image coordinates:

$$\boldsymbol{P} = \begin{bmatrix} 1 & u_1 & u_1^2 & u_1^3 \\ 1 & u_2 & u_2^2 & u_2^3 \\ \cdots & \cdots & \cdots & \cdots \\ 1 & u_{m-1} & u_{m-1}^2 & u_{m-1}^3 \\ 1 & u_m & u_m^2 & u_m^3 \end{bmatrix} \quad (10)$$

$$\boldsymbol{c} = [c_0 \quad c_1 \quad c_2 \quad c_3] \quad (11)$$

(4) and (9) can be optimized by statistical methods. Vectors (6, 7) and (11) can be calculated by SVD[11] (singular value decomposition) which accurately estimates video distortions for both conventional and endoscopic cameras:

$$\boldsymbol{a} = (\boldsymbol{P^TP})^{-1}\boldsymbol{P^Tj} \quad (12)$$

$$\boldsymbol{b} = (\boldsymbol{P^TP})^{-1}\boldsymbol{P^Tk} \quad (13)$$

$$\boldsymbol{c} = (\boldsymbol{P^TP})^{-1}\boldsymbol{P^Tr} \quad (14)$$

Target positions marked out on video image should be also transformed back to the tracker's reference space or diagnostic volume. It's possible if the inverse of distorting equations (1)(2)(8) are known. This calculation is difficult from the results of first, "distorter" step and only numerically possible. Therefore another approach is proposed. According to it, the inverted parameters are calculated in the same way as the forward values but with different assignments. The input coordinates or distances *(u, v)*, used in the first step, are replaced by values located on the distorted image *(j, k, r)*. Afterwards, the parameters *P* depend on the distorted coordinates and the error functions are used to approximate the ideal, undistorted values ("undistorter" step). Finally, the optimization can be the same as it was during the forward calculation.

In practical implementation the endoscopes with oblique lens axis should be also calibrated *(Figure 1)*. Best approach is to use ready-made, special calibration modules (clamps). These contain the calibration grid and are able to hold endoscopes in a predefined position.

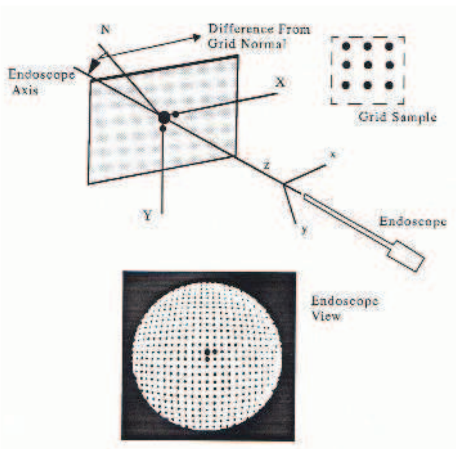

Figure 1. Endoscope camera calibration

Registration tasks

Two registration problems should be solved: (1) registration between the spaces of motion tracking device and diagnostic volume (CT, MR image sequence); (2) registration of video image to 3D space of motion tracking device. Next the procedure for video image registration is described.

Video frame registration

The registration matrix between the motion tracking device and the coordinate system of undistorted video *($\boldsymbol{T}_{W,C}$)* can be given as

$$[X_{C,i} \quad Y_{C,i} \quad Z_{C,i} \quad P_{C,i}] = [X_{W,i} \quad Y_{W,i} \quad Z_{W,i} \quad 1] \times \boldsymbol{T}_{W,C} \tag{15}$$

where $[X_{C,i} \quad Y_{C,i} \quad Z_{C,i} \quad P_{C,i}]$ represents the coordinates within the perspective camera space and $[X_{W,i} \quad Y_{W,i} \quad Z_{W,i} \quad 1]$ is the position in the tracker's space. The matrix elements with nonzero last column values according to perspective projection:

$$\boldsymbol{T}_{W,C} = \begin{bmatrix} T_{1,1} & T_{1,2} & T_{1,3} & T_{1,4} \\ T_{2,1} & T_{2,2} & T_{2,3} & T_{2,4} \\ T_{3,1} & T_{3,2} & T_{3,3} & T_{3,4} \\ T_{4,1} & T_{4,2} & T_{4,3} & T_{4,4} \end{bmatrix} \tag{16}$$

The perspective division should be present in calculation of real image coordinates:

$$[X^*_{C,i} \quad Y^*_{C,i} \quad Z^*_{C,i} \quad 1] = [X_{C,i}/P_{C,i} \quad Y_{C,i}/P_{C,i} \quad Z_{C,i}/P_{C,i} \quad 1] \tag{17}$$

These equations can be rearranged if :

$$X^*_{C,i} \frac{(X_{W,i}T_{1,4}+Y_{W,i}T_{2,4}+Z_{W,i}T_{3,4}+1)}{X_{W,i}T_{1,1}+Y_{W,i}T_{2,1}+Z_{W,i}T_{3,1}+T_{4,1}} = 1 \tag{18}$$

$$Y^*_{C,i} \frac{(X_{W,i}T_{1,4}+Y_{W,i}T_{2,4}+Z_{W,i}T_{3,4}+1)}{X_{W,i}T_{1,2}+Y_{W,i}T_{2,2}+Z_{W,i}T_{3,2}+T_{4,2}} = 1 \tag{19}$$

from

$$X^*_{C,i} = X_{W,i}T_{1,1} + Y_{W,i}T_{2,1} + Z_{W,i}T_{3,1} + T_{4,1} - \\ - \left(X^*_{C,i}X_{W,i}T_{1,4} + X^*_{C,i}Y_{W,i}T_{2,4} + X^*_{C,i}Z_{W,i}T_{3,4}\right) \tag{20}$$

$$Y^*_{C,i} = X_{W,i}T_{1,2} + Y_{W,i}T_{2,2} + Z_{W,i}T_{3,2} + T_{4,2} - \\ - \left(Y^*_{C,i}X_{W,i}T_{1,4} + Y^*_{C,i}Y_{W,i}T_{2,4} + Y^*_{C,i}Z_{W,i}T_{3,4}\right) \tag{21}$$

this can be written into matrix equation with 11 unknowns $\boldsymbol{A} \times \boldsymbol{x} = \boldsymbol{b}$ $(T_{4,4} = 1)$:

$$
\boldsymbol{A}=\begin{bmatrix}
X_{W,1} & 0 & -X^*_{C,1}X_{W,1} & Y_{W,1} & 0 & -X^*_{C,1}Y_{W,1} & Z_{W,1} & 0 & -X^*_{C,1}Z_{W,1} & 1 & 0\\
0 & X_{W,1} & -Y^*_{C,1}X_{W,1} & 0 & Y_{W,1} & -Y^*_{C,1}Y_{W,1} & 0 & Z_{W,1} & -Y^*_{C,1}Z_{W,1} & 0 & 1\\
X_{W,2} & 0 & -X^*_{C,2}X_{W,2} & Y_{W,2} & 0 & -X^*_{C,2}Y_{W,2} & Z_{W,2} & 0 & -X^*_{C,2}Z_{W,2} & 1 & 0\\
0 & X_{W,2} & -Y^*_{C,2}X_{W,2} & 0 & Y_{W,2} & -Y^*_{C,2}Y_{W,2} & 0 & Z_{W,2} & -Y^*_{C,2}Z_{W,2} & 0 & 1\\
X_{W,3} & 0 & -X^*_{C,3}X_{W,3} & Y_{W,3} & 0 & -X^*_{C,3}Y_{W,3} & Z_{W,3} & 0 & -X^*_{C,3}Z_{W,3} & 1 & 0\\
0 & X_{W,3} & -Y^*_{C,3}X_{W,3} & 0 & Y_{W,3} & -Y^*_{C,3}Y_{W,3} & 0 & Z_{W,3} & -Y^*_{C,3}Z_{W,3} & 0 & 1\\
X_{W,4} & 0 & -X^*_{C,4}X_{W,4} & Y_{W,4} & 0 & -X^*_{C,4}Y_{W,4} & Z_{W,4} & 0 & -X^*_{C,4}Z_{W,4} & 1 & 0\\
0 & X_{W,4} & -Y^*_{C,4}X_{W,4} & 0 & Y_{W,4} & -Y^*_{C,4}Y_{W,4} & 0 & Z_{W,4} & -Y^*_{C,4}Z_{W,4} & 0 & 1\\
X_{W,5} & 0 & -X^*_{C,5}X_{W,5} & Y_{W,5} & 0 & -X^*_{C,5}Y_{W,5} & Z_{W,5} & 0 & -X^*_{C,5}Z_{W,5} & 1 & 0\\
0 & X_{W,5} & -Y^*_{C,5}X_{W,5} & 0 & Y_{W,5} & -Y^*_{C,5}Y_{W,5} & 0 & Z_{W,5} & -Y^*_{C,5}Z_{W,5} & 0 & 1\\
X_{W,6} & 0 & -X^*_{C,6}X_{W,6} & Y_{W,6} & 0 & -X^*_{C,6}Y_{W,6} & Z_{W,6} & 0 & -X^*_{C,6}Z_{W,6} & 1 & 0
\end{bmatrix} \tag{22}
$$

$$
\boldsymbol{x}=\begin{bmatrix} T_{1,1}\\ T_{1,2}\\ T_{1,4}\\ T_{2,1}\\ T_{2,2}\\ T_{2,4}\\ T_{3,1}\\ T_{3,2}\\ T_{3,4}\\ T_{4,1}\\ T_{4,2}\end{bmatrix}
\qquad
\boldsymbol{b}=\begin{bmatrix} X^*_{C,1}\\ Y^*_{C,1}\\ X^*_{C,2}\\ Y^*_{C,2}\\ X^*_{C,3}\\ Y^*_{C,3}\\ X^*_{C,4}\\ Y^*_{C,4}\\ X^*_{C,5}\\ Y^*_{C,5}\\ X^*_{C,6}\end{bmatrix} \tag{23}
$$

The solution vector *(x)* can be calculated (for quadratic matrix in (22)) by simple matrix inversion (originally DLT method[13], for X-Ray processing see[14]). Unfortunately, this doesn't work in practice (especially in video image registration) because of marker localization errors. Statistical approach (with SVD algorithm[11]) was found much more promising[1,2] which is applicable for over-determined equations of more than 6 markers (acceptable accuracy is possible with 7-8 markers). Marker localization is possible by detecting the tip of the probe of tracking device in "frame-freezing" mode. In case of endoscopes, the "undistorter" step (see Video calibration section) provides for linearized camera position which is suitable for 3D registration.

Results

For this kind of complex project, establishing application concepts and suitable architecture of system elements (hardware, software) appear as major tasks. The results at this time are technical and highly depend on resources available for development. Important elements of clinical application[8], which have been made

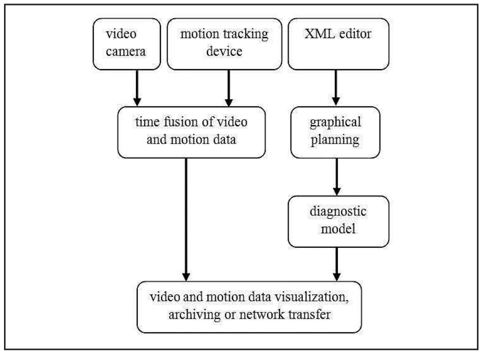

Figure 2. Simplified system architecture

already available or developed by own resources, are: (1) video digitalization with DT3131 frame-grabber board (Data Translation Inc., USA) *(http://www.datatranslation.com/products/imaging/pci/)*; (2) integrating GPU (graphical processing unit) *(http://www.nvidia.com)* with GLSL programming („Open GL Shading Language" *http://www.opengl.org/documentation/glsl/*); (3) use of modern 6 DOF mouse in surgical planning *(http://www.3Dconnexion.com)*; (4) software control of optical motion tracking for different Northern Digital cameras (Polaris Standard and Vicra, http://www.ndigital.com); (5) use of XML (Extensible Markup Language, *http://www.w3.org/XML/)* compressed files for archiving, editing and transmitting information on surgical plan, registration and camera distortion parameters, tool calibration, diagnostic data, etc. XML files guarantee the easy communication through internet and are important parts of telemedicine applications.

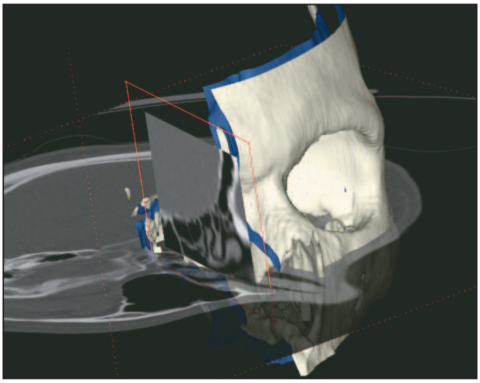

Figure 3. Use of modern GPU in modeling diagnostic data. The calculation of arbitrarily oriented cutting planes from a skull CT and comparison to surface graphics occurs in real-time according to actual state of the 6 DOF mouse

Figure 2 represents the core elements of the system which is under investigation. *Figure 3* illustrates the practical advantage of GPU programming with GLSL language.

Discussion

This article gives an introduction to a new project which can be considered as the author's personal initiative based on earlier experience. Hopefully, in the future, it can gain more institutional support especially for software development. In this case there is a chance to move faster with new applications of real clinical value and usability. Procedure, similar to the presented one in this paper, for tracking the location of endoscopic image relative to CT volume is described in[16] but without time-synchronized archiving of video and motion data. Interesting new approach is already known to integrate endoscopic video with CT diagnostic data[15] without motion sensor attached to endoscope. However, this direct (based on image feature detection) approach is not suitable for clinical use yet.

Valuable survey has been given about human motion tracking systems[3]. The classification distinguishes vision based (without using motion tracking device) and non-vision based (with motion tracking device) applications. The fusion of video and tracking data, as proposed in this article, usually is available in expensive, commercial systems (Elite Biomech, Vicon) but without clear information on technology behind. The need for subsequent, repeated analysis or network transfer of motion data certainly demands fused, compressed representation of results with video sequence and kinematical models. This paper outlines also the involvement of preoperative diagnostic images in motion analysis and an effective control of the complex environment through XML file representation.

Conclusions

Overview and mathematical description of most critical parts of fusing video and motion data have been given. The results can be used in two areas: (1) for training and reliability improvement of endoscopic surgeries of high risk (like in ENT); (2) in kinematical modeling of human movement by representing video image and graphical models in a common reference space.

In Endoscopic Paranasal Sinus surgeries[7,8] and other fields of endoscopic intervention the real fusion (in time and 3D space) of video sequence and tools' position makes archiving or transmitting information on actual state of surgery possible. This can be used for evaluating problematic results or educating risky interventions.

In biomechanical research, the proposed approach solves the critical problem of human motion analysis if soft tissue markers can't be used for bone axis definition or diagnostic images (X-Ray, CT or MR) are not available. However, if valid registration between body parts and diagnostic images is available, the video-based representation of bone axis can be projected back and compared to the static diagnostic volume during motion.

References

1. *Truppe M, Pongracz F, Ploder O, Wagner A* and *Ewers R.* Interventional Video Tomography. In Proceedings of Lasers in Surgery, vol. 2395. San Jose, CA: SPIE 1995:150–152.

2. *Freysinger W, Truppe M, Gunkel AR, Thumfart WL, Pongracz F,* and *Maierbaeuerl J.* Interactive telepresence and augmented reality in ENT surgery : Interventional Video Tomography. In: Proceedings of CVRmed – MRCAS 97, Grenoble, 1997;1205:817–820.

3. *Zhou H, Hu H.* Human motion tracking for rehabilitation–A survey. Biomedical Signal Processing and Control 2008 Jan;3(1):1–18.

4. *Amaya K, Hara Y, Aoki S.* Reconstruction of 3D human movement using inverse analysis. Inverse Problems in Engineering Mechanics. In: Proceedings of International Symposium on Inverse Problems in Engineering Mechanics (ISIP'98) 1998; Nagano, Japan, 1998:583–592.

5. *Luo Y, Lopez FJP* and *Pipaon JJV.* An automatic rotoscopy system for human motion based on a biomechanic graphical model. Computers & Graphics 1992;16(4):355–362.

6. *Berkelman P, Cinquin P, Boidard E, Troccaz J, Létoublon C, Ayoubi JM.* Design, control and testing of a novel compact laparoscopic endoscope manipulator. Proceedings of the Institution of Mechanical Engineers, Part I: Journal of Systems and Control Engineering 2003;217(4): 329–341.

7. *Kumagai T. et al.* Distance Education System for Teaching Manual Skills in Endoscopic Paranasal Sinus Surgery Using "HyperMirror" Telecommunication Interface. In: Proceedings of IEEE Virtual Reality, 2008, March 8–12, Reno, Nevada: 233–236.

8. *Pongrácz F.* Use of video motion tracking and telepresence for training and reliability improvement of endonasal surgery. Supported project by National Office for Research and Technology (NKTH), Budapest 2009 under OMFB-01134/ 2009.

9. *Marin F, Mannel H, Claes L* and *Dürselen L.* Correction of axis misalignment in the analysis of knee rotations. Human Movement Science 2003 Aug;22(3):285–296.

10. *Bowman ME* and *Forrest AK.* Transformation calibration of a camera mounted on a robot. Image and Vision Computing 1987;5(4):261–266.

11. *Press WH, Teukolsky SA, Vetterling WT, Flannery BP.* Numerical Recipes in C. The Art of Scientific Computing. Cambridge: Cambridge University Press; 1992.

12. *Andrónyi K* and *Szobonya L.* The importance of axis alignment in the human knee examination. In: Proceedings of Third Hungarian Conference on Biomechanics, 2008, July 4–5, Budapest: 13–22.

13. *Abdel-Aziz YI* and *Karara HM.* Direct linear transformation into object space coordinates in close-range photogrammetry. In: Proceedings of the Symposium on Close-Range Photogrammetry, 1971, Jan. University of Illinois, 1971:1–8.

14. *Fekete K et al.* X-Ray image processing by direct linear transformation. In: Proceedings of Third Hungarian Conference on Biomechanics, 2008, July 4–5, Budapest; 75–81.

15. *Mirota D et al.* Toward video-based navigation for endoscopic endonasal skull base surgery. In: Proceedings of MICCAI 2009, Lecture Notes in Computer Science, Springer Berlin/Heidelberg, Vol. 5761/2009:91–99.

16. *Shahidi et al.* Implementation, calibration and accuracy testing of an image-enhanced endoscopy system. IEEE Trans Med Imaging 2002; 21(12):1524–35.

The author thanks to Zoltán Bárdosi (ELTE ITK) and Balázs D. Tóth (SZTAKI, Budapest) for help in software development. This work was supported by the Bureau of National Research and Development in Hungary (NKTH) under contract OMFB-01134/2009.

Ferenc Pongrácz
Project Employment Supported by 5LET 2008 Contract with
Bureau of National Research and Development in Hungary (NKTH)
Phone: (+36) 1 275-8615
Mobile: (+36) 30 562-1806

Neck posture measurement amongst schoolchildren

Gábor Ormos[1], Rita Kiss[2]

[1] National Institute for Rheumatology and Physiotherapy, Budapest

[2] Budapest University of Technology and Economics, Department of Structures, Research Center for Biomechanics

ormosdr@gmail.com

Abstract

Background: There is a paucity in basic data concerning neck posture in childhood. Our aim was to gain preliminary data on the head/neck/shoulder posture, and to document their evolution with growth in schoolchildren.

Methods: For measuring posture *digital photographs* were taken of the children seated in a straight-high-backed chair. The camera (Agfa 5Ti, 5.2 megapixels) was located perpendicularly to each subject's height, positioned from the left side, the focus was on the tragus with a standard distance of 150 cm. The first photo was taken in the "neutral head posture" and a second photo in "resting" posture). The digital photos were then evaluated by a computer software program (distributed as Marker Angels). The angles analyzed were as follows: the craniovertebral angle (CVA), the head tilt angle (HTA), the shoulder angle (SHA). **Subjects** were hundred and forty-seven 9-year old, and hundred and fourtythree 16-year old schoolchildren, who were attending public school in different districts of Budapest.

Results: In the 16-year old's group the CVA values have been found reduced significantly (by an average of 8 degrees in neutral position and 6 degrees in resting position) compared to the 9 year olds. The HTA elevated by an average of 1.6 degrees (NS) in neutral position and reduced significantly (by 4.2 degrees) in resting position. The values of the SHA elevated significantly (by an average of 13.33 degrees in neutral position and 13.32 degrees in resting) between the 9–16 year olds, which referred to more protracted shoulder posture.

Discussion: The CVA characterizes the neck posture, the less it's value, the more the forward position. The neck posture is in strong correlation to the head and the shoulder positions. That means forward bent neck position is in correlation to the so called "rounded" shoulder or the shoulder protraction. Although the position of the was found not consequent in neutral position, however was in correlation in resting position.

Conclusion: Measuring head/neck/shoulder posture by means of digital photos and evaulated by computer program proved easy, useful method. We obtained preliminary descriptive data on neck posture in degrees of two age groups of schoolchildren. The comparison of the results proved the tendency of progression in "poor posture" during 7 schoolyears, between in the age of 9–16.

Keywords: neck posture; schoolchildren's posture; method for measurement

Introduction

Our investigation on neck posture has been indicated by the observation that in everyday life more and more schoolchildren look like they have their head held forward and neck postural abnormalities have been found in association with chronic neck pain in adults[2,8,16]. There is a paucity in the literature concerning neck posture measurement in children, we have found studies on schoolchildren's posture in standing[3,6,9,12], but only one in sitting[14]. To evaluate the "physiological posture", the term "natural head position" was suggested in cephalometry, measured by x-ray pictures[4,5,13], Fiebert[7] determinated "neutral head posture", which differed from the "resting head posture", definied by Hunten[10]. In most studies posture has been measured by the distance from the vertical line, Braun and Amundson established measuring angles by means of photos, first the craniovertebral angle (CVA)[1], than Braun measured the shoulder position by the shoulder angle (SHA)[2]. Szeto evaluated the head posture by videorecording, and defined it by the head tilt angle (HTA)[16]. Measuring posture by means of making photos on surface was doupted by Johnson[11], but later has been validated by two studies[14,15], and digital camera was used in the largest investigation with children[12].

Our aim was to gain preliminary data on the head/neck/shoulder posture amongst schoolchildren, the study was designated to determine their neck posture in sitting by measuring the angles mentioned and comparing the two group's data to evaluate the change in the children's posture by aging.

Methods

Subjects were hundred and fortyseven 9-year old, hundred and thirtyeigth 12 year old and hundred and fourtythree 16-year old schoolchildren who attended a public school, from different districts of the City Budapest. Informed consent was obtained from each child as well as their parents, and approval was also obtained from the institution's ethics committee.

Digital photos were taken seated in a straight-high-backed chair, with the children touching their scapulae to the back of the chair, thus the effect of the thoracic spine could be excluded. The following anatomical landmarks were identified by small colored adhesive markers: the tragus of the ear, C7 spinous process, and the base of the nose. The subject's position was at right angles, with left side facing the camera (Agfa 5Ti, 5.2 megapixels), the focus was on the tragus with a standard distance of 150 cm *(Figure 1)*. The first photo was taken in the "neutral head position" *(Figure 2. a)*, which meant that the head is centered over the midline of the body when viewed from either the antero-postero or lateral plane, or with a slight (5°) forward lean[7]. The second photo was taken in a relaxed, "resting" posture[7,10], shown on *Figure 2. b*. The digital photos were evaluated by a computer software program (distributed as Marker Angels), which enabled the use of standard protocols for digitizing the angles from the photographs. The angles analyzed were as follows: CVA= between the line con-

Figure 1. Taking digital photo for measuring neck posture

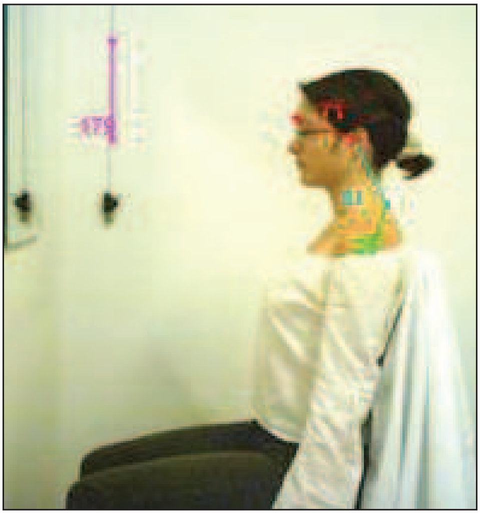

Figure 2. a Neutral head position

Figure 2. b Resting head position

necting the tragus and C7 spinous process and the x-axis, the HTA= between the line connecting the tragus and the base of the nose and the y-axis, shoulder angle (SHA)= between the line connecting the acromion and C7 spinous process and the x-axis *(Figure 3)*.

Statistical analysis was made by Student t-test and Spearmen correlation test.

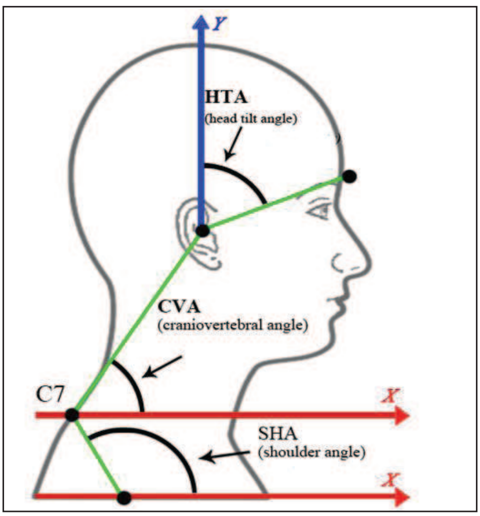

Figure 3. Angles characterising neck posture

Results

The data concerning neck posture angles are shown on *Table 1.*

The comparison of the data amongst the groups demonstrated that in the 16-year olds CVA values have been found reduced significantly, by an average of 8 degrees ($p=0.0028$) and 6 degrees ($p=0.0016$) in resting position compared to the 9 year olds. That meant, neck posture changed into more forward position. The values of the SHA elevated significantly ($p<0.0001$), by an average of 13.33 degrees in neutral position and 13.32 degrees in resting between the 9–16 year olds, which referred to more protracted shoulder posture. The HTA was found elevated not significant ($p=0.9145$) by an average of 1.6 degrees in neutral position and became reduced significantly (0.0022), by 4.2 degrees in resting position. That meant, neck posture changed into forward flexed position, but the head's position was not consequent.

Correlations amongst angles are shown on *Table 2.* The CVA values measured in neutral

ANGLES	AGE 9 n=147 AGE 16 n=143	MINIMUM (degree)	MAXIMUM (degree)	MEAN (degree)	SD
CVA neutral	AGE 9	40.00	84.00	**60.30**	1,88
	AGE 16	41.00	63.00	**52.35**	1.35
CVA „resting”	AGE 9	34.00	72.00	**52.98**	1,87
	AGE 16	31.00	60.00	**48.47**	1.53
HTA neutral	AGE 9	42.00	87.00	**68.26**	1,27
	AGE 16	55.00	80.00	**69.56**	1.88
HTA „resting”	AGE 9	54.00	93.00	**73.74**	1,72
	AGE 16	57.00	83.00	**69.88**	1.98
SHA neutral	AGE 9	91.00	123.00	**106.41**	2,74
	AGE 16	90.00	149.00	**119.74**	2.74
SHA „resting”	AGE 9	91.00	124.00	**107.32**	2,47
	AGE 16	95.00	153.00	**120.64**	2.54

Table 1. CVA, HTA and SHA values (in degrees)

n=147+143			**CVA neutral**
	HTA neutral	Correlation Coefficient	-,278(*)
		Sig. (2-tailed)	0,018
	SHA neutral	Correlation Coefficient	-,415(*)
		Sig. (2-tailed)	0,018
	CVA resting	Correlation Coefficient	,722(**)
		Sig. (2-tailed)	0,000
** Correlation is significant at the 0.01 level (2-tailed).			
* Correlation is significant at the 0.05 level (2-tailed).			

Table 2. Correlations amongst neck angles (by Spearman test)

and resting position were in strong correlation. The CVA neutral values were in negative correlation to HTA and SHA neutral values.

Discussion

Our results on posture correlate with the relevant literature with children[3,6,9,12], and also the data published with adults[1,2,16]. The CVA values of age-matched children previously published were slightly lower[9], but the difference is due to that they were measured in standing. The CVA angle mean value has been found 51,97° in adults[1], which roughly equal to our mean data with the 16 year olds. The SHA values measured by us correlated to the data published in adults[2]. The HTA characterizes the head position to the neck, the position of C 0/1 joint. The less its degree is, the more extended the head should be. HTA was found (by video recording in adults 57°[16], that was lower than our mean data with children. The HTA neutral mean value of the 16 year olds became slightly higher, but not significantly, compared to the 9 year olds. This is in contradiction to the observations with adults, i.e. the lesser CVA is associated to lesser HTA, which means the head posture changes to an extended position. Our different results with children could be explained by the flexibility of the cranio-cervical segment in young age, or that might be due to individual head posture stereotype. In resting position the HTA was in negative correlation to the CVA, as expected. That means with forward bent neck an extended head posture is needed.

The angles measured in neutral and in resting posture were characteristic to what can be seen in real life. The higher degree of SHA referred to the clinical symptom, which should be called "rounded shoulder".

The comparison of the data found in the two age groups (9–16), during 7 years, spent at school, might demonstrate a tendency to "poorer posture" with aging. That correlates to the results published by Lafond, who has also found statistically significant associations with age for „forward head translation" and „forward shoulder translation"[12], which are similar the entities to „forward head/neck position".

Conclusions

Measuring head/neck/shoulder posture by means of digital photos and the evaulation by computer program proved easy, useful method. That method should be used for further studies. Descriptive data have been obtained on neck posture in groups of 9 and 16 years old schoolchildren, and we have found a significant tendency to poorer posture with aging.

References

1. *Braun BL, Amundson LR.* Quantitative assessment of head and shoulder posture. Arch Phys Med Rehabil 1989;70:322–329.

2. *Braun BL.* Postural differences between asymptomatic men and women and craniofacial pain patients. Arch Phys Med Rehabil 1991;72:653–656.

3. *Chansirinukor W, Wilson D, Grimmer K, Dansie B.* Effects of backpacks on students: measurement of cervical and shoulder posture. Aust. J. Physiother. 2001;47:110–116.

4. *Gore DR, Sepic SB, Gardner GM.* Roentgenographic findings of the cervical spine in asymptomatic people. Spine 1986;6:521–4.

5. *Harrison DD, Janik TJ, Troyanovich SJ, Holland B.* Comparisons of lordotic cervical spine curvatures to a theoretical ideal model of the static sagittal cervical spine. Spine 1996;21:667–75.

6. *Cil A, Yazici M, Uzumcugil A, Kandemir U, Alanay A, Alanay Y, Acaroglu RE, Surat A.* The evolution of sagittal segmental alignment of the spine during childhood. Spine 2005;30(1): 93–100.

7. *Fiebert I, Roach K, Yang S, Dierking L, Hart F.* Cervical range of motion and strength during resting and neutral head postures in healthy young adults. J. Back Musculosceletal. Rehabilitation 1999;12:165–178.

8. *Griegel-Morris P, Larson K, Mueller-Klaus K, Oatis CA.* Incidence of common postural abnormalities in the cervical, shoulder, and thoracic regions and their association with pain in two age groups of healthy subjects. Phys Ther 1992;(72):425–431.

9. *Grimmer KA, Williams MT, Gill TK.* The associations between adolescent head-on-neck posture, backpack weight, and anthropometric features. Spine. 1999;24:2262–2267.

10. *Hanten WP, Lucio RM, Russell JL, Brunt D.* Assessment of total head excursion and resting

head posture. Arch. Phys. Med. Rehabil. 1991; 72:877–880.

11. *Johnson GM.* The correlation between surface measurement of head and neck posture and the anatomic position of the upper cervical vertebrae. Spine. 1998;23:921–927.

12. *Lafond D, Descarreaux M, Normand MC, Harrison DE.* Postural development in school children: a cross-sectional study. Chiropr Osteopat. 2007 Jan 4;15:1.

13. *Lundstrom A, Lundstrom F, Lebret LM, Moorrees CF.* Natural head position and natural head orientation: basic considerations in cephalometric analysis and research. Eur. J. Orthod. 1995;17:111–120.

14. *van Niekerk SM, Louw Q,Vaughan C, Grimmer-Somers K, Schreve K.* Photographic measurement of upper-body sitting posture of high school students: a reliability and validity study. BMC Musculoskelet Disord. 2008 Aug 20;9: 113.

15. *Refshauge KM, Goodsell M, Lee M.* The relationship between surface contour and vertebral body measures of upper spine curvature. Spine. 1994;19:2180–2185.

16. *Szeto GP, Straker L, Raine S.* A field comparison of neck and shoulder postures in symptomatic and asymptomatic office workers. Appl. Ergon. 2002;33:75–84.

Gábor Ormos
National Institute for Rheumatology and Physiotherapy, Budapest

Biomechanica Hungarica III. évfolyam, 1. szám

The effects of infrared laser therapy and weightbath traction hydrotherapy in disorders of the lumbar spine: a controlled pilot study with follow-up

Csaba Oláh[1], Mihály Oláh[4], Béla Demeter[1], Zoltán Jancsó[3], Valéria Páll[1], Tamás Bender[2]

[1] Borsod-Abaúj-Zemplén County Hospital and University Teaching Hospital, Miskolc, Hungary
[2] Hungarospa Health Resort, Hajdúszoboszló, Hungary
[3] University of Debrecen Medical and Health Science Center, Hungary
[4] Polyclinic of the Hospitaller Brothers of St. John of God Hospitalin Buda, Hungary
olahcs@gmail.com

Abstract

Introduction: The therapeutic modalities available for the conservative management of chronic lumbar pain included infrared laser therapy and underwater traction, which usefulness is not universally acknowledged. This study was intended to ascertain any beneficial impact of infrared laser therapy and weightbath treatment on the clinical apramesters and quality of life of patients with lumbar discopathy.

Material and methods: The study population comprised 54 randomised subjects. I. group of 18 patents received only infrared laser therapy to lumbar region and painful Valley points. II. Group of 18 subjects each received underwater traction therapy of lumbar spine with add-on McKenzie exercise and iontophoresis. The remaining III. Group treated with exercise and iontophoresis, served as control.

VAS, Oswestry index, SF36 scores, range of motion, neurological findings and thermography were monitored to appraise therapeutic afficacy in lumbar discopathy. A CT or MRI scan was done at baseline and after 3 months follow-up.

Result: infrared laser therapy and underwater traction for discopathy achieved significant improvement of all study parameters, which was evident 3 months later. Among the controls, significant improvement of only a single parameter was seen in patients with lumbar discopathy.

Conclusions: infrared laser therapy and underwater traction treatment effectively mitigate pain, muscle spasms, enhance joint flexibility, and improve the quality of life of patients with lumbar discopathy.

Introduction

Low back pain and sciatica comprise the second most frequent reason for seeking medical advice. The chance for contracting lumbosacral complaints is between 60 to 90 per cent during a lifetime; annual incidence is 5 percent. In 90 per cent of cases, symptoms resolve over 2 to 4 weeks, but recur within a year in 70 per cent[1,2,3,4]. The predominant underlying causes of these symptoms are the protrusion or the herniation of intervertebral discs. The management options of lumbar and radicular pain include conservative treatment, surgical therapy, and invasive neurointervention procedures. When herniation causes paresis through the compression of nerve roots or results in myelopathic symptoms, fecal or urinary incontinence, or the cauda equina syndrome, prompt surgical intervention – i.e. open or minimally invasive discectomy – is recommended[4]. In absence of these symptoms, various nucleoplasty techniques are performed; however, the long-term outcome of these is still questionable and the strength of supporting evidence remains below Level I. The alternative is conservative management, usually consisting of pharmacotherapy (including infusion therapy), physical therapy, and various forms of remedial gymnastics[5,6]. In Hungary and in Hungarian rheumatology institutions, the range of conservative treatment modalities also includes weightbath traction, along with soft laser therapy.

Notwithstanding its long tradition, recent review articles evaluating non-immersion (motorized, auto-, or gravitational) traction therapy have disapproved the use of this modality for the management of spinal complaints, in view of its potential hazards[7,8,9].

Underwater traction hydrotherapy was invented by the Hungarian rheumatologist, Károly Moll, who has been developing this treatment since the fifties of the last century into a therapeutic option widely used in many rheumatology and balneology centers in Hungary[10]. Among the latter, Hajdúszoboszló spa resort is one of the institutions that have accumulated the widest experience with this treatment modality. In contrast to non-immersion traction, weightbath traction hydrotherapy in tepid to warm water affords improving the patient's condition without any risk. Previous biophysical studies have measured (taking into account the patient's body weight, hydrostatical forces and buoyancy effect) the traction forces exerted on individual spinal segments. Additionally, Hungarian bioengineers have determined optimum loading, as well as the load-bearing capacity and deformability of various spinal compartments[11,12].

Weightbath hydrotherapy in warm water relaxes muscles and ligaments, whereas moderate and sparing traction – aided by the protective effect of hydrostatical pressure – accomplishes retraction of intervertebral disc protrusions and herniations; relieves the tension of nerve root canals; as well as mitigates axial and radicular pain.

Since years, we have been using soft laser therapy on cervical, thoracic, and lumbar segments of the spine to relieve pain, to relax muscles and to control inflammation. A number of Hungarian academic researchers have contributed to the development of soft laser treatments.

The term 'biostimulation' has been coined by Prof. Endre Mester 25 years ago to describe specific phenomena underlying the healing processes observed during soft laser therapy. The phenomenon of biostimulation is implemented by reversible cell physiological processes, activated – among others – by the laser beam. The effect of repetitive biostimulation is cumulative. As shown by the results of experiments, laser stimulation elicits repair processes in specific or multiple levels of deranged cellular metabolism. Soft laser facilitates the restoration of original – physiological – reparative functions. The initiation of such processes is believed to occur at the level of terminal oxidation, in the mitochondria. Healing is not restricted to topical only processes – it is influenced by a variety of systemic factors. In addition to biostimulation, soft laser therapy exerts anti-inflammatory action, it relieves muscle spasm, and it has a direct analgesic effect.

Patients & methods

We have conducted a pilot study with follow-up on rheumatology outpatients. Weightbath traction hydrotherapy was performed at the Hajdúszoboszló spa resort, whereas the control and laser therapy groups were treated at the Borsod County University Teaching Hospital in Miskolc. The study protocol was approved by the regional ethics board.

Patients over 18 years of age, with lumbar pain radiating to the lower extremities – demonstrated by MRI to result from lumbar discopathy – were enrolled into the study. Patients with any acute condition considered an indication for surgery, those with spondylolisthesis, oseteoporosis causing vertebral compression, spondylitis, malignancies or other severe systemic disorders were not included. Patients who had undergone previous surgery of the spine were not enrolled either.

Eligible patients were randomized into three groups of 18 subjects each:

1. Standard control group: patients in this group were treated with McKenzie remedial gymnastics (20-minute sessions) and iontophoresis for 3 weeks.
2. Weightbath traction hydrotherapy group: in addition to the remedial gymnastics and iontophoresis described above, these patients underwent underwater traction on 15 occasions.
3. Soft laser group: these patients were treated exclusively with infrared laser illumination of the lumbar region and Valleix's points.

Paracetamol was allowed for use as a rescue analgesic in all three groups. The first session of weightbath traction hydrotherapy was implemented with single (cervical) suspension, without extra weights, whereas during subsequent sessions, triple suspension (cervical plus armpit support) was used with 2×3 kg weight affixed to the waist belt. The duration of the initial session was 15 minutes – this was extended to 20 minutes for subsequent sessions. The temperature of the water bath was 34 °C. Laser treatment for 15 days was performed using a 600 mW KLS equipment (Fajro), delivering 30 J infrared illumination to the lumbar region (with a laser shower head containing 6 laser diodes) and 2 J/point to painful Valleix's points (with a single-point laser head).

The neurological status of patients was checked daily, as well as their complete medical and neurological status was recorded before and after each treatment session. Additionally, the subjects completed the SF-36 questionnaire and the Oswestry disability index before treatment. VAS scores, finger-floor distance, the range of lateral flexion (shifting of the patient's hand placed on the thigh in centimeters) were recorded. The physicians' rating of the condition of their patients, as well as the subjective opinion of the latter on their own well-being was obtained through interviews. In the standard control and in the weightbath hydrotherapy groups, these parameters were recorded again 3 months after treatment and follow-up MRI was performed. In the laser group, thermographic images were recorded at baseline as well as after treatment.

Statistical analysis

The normality of study parameters was checked with the one-tailed Kolmogorov–Smirnoff test. The Mann–Whitney or the t-test was used for the comparison of baseline values. Changes were analyzed with the paired Student's t-test or Wilcoxon's signed rank test.

Results

In the control group the beneficial effect was significant on just a single parameter (floor-finger distance), and significant improvement of only two parameters (Oswestry index and SF-VT) was ascertained 3 months later *(Table 1)*. All parameters improved significantly after weightbath therapy, the improvement proved lasting after 3 months and increased further in the case of two parameters *(Table 2)*. All clinical parameters improved after infrared laser therapy, 9 parameters significantly *(Table 3)*.

Parameter	At baseline (mean±SD)	After treatment (mean±SD)	After 3-month follow-up (mean±SD)	p-value		
				After treatment vs. baseline	After 3-month follow-up vs. baseline	After 3-month follow-up vs. post-treatment
VAS	5.28±1.87	5.72±1.87	5.39±2.20	NS	NS	NS
Floor-finger distance	42.22±14.07	37.06±14.29	39.39±16.20	0.029	NS	NS
Lateral flexion LEFT	15.17±4.84	16.78±3.67	15.78±4.26	NS	NS	NS
Lateral flexion RIGHT	15.67±4.34	17.11±4.09	17.22±4.01	NS	NS	NS
Oswestry Index	67.11±12.60	66.67±17.78	72.33±13.83	NS	0.022	0.041
SF-PF: physical functioning	48.61±18.93	51.67±20.93	53.33±21.83	NS	NS	NS
SF-RP: role limitations – physical	27.50±34.22	20.83±32.37	31.94±35.15	NS	NS	NS
SF-RE: role limitations – emotional	31.33±36.96	25.83±38.81	27.72±41.61	NS	NS	NS
SF-VT: vitality	32.11±20.97	37.50±26.58	41.39±25.19	NS	0.008	NS
SF-MH: mental health	51.50±31.98	46.67±31.11	53.00±30.39	NS	NS	NS
SF-SF: social functioning	49.78±32.13	48.39±32.16	56.33±30.25	NS	NS	NS
SF-BP: bodily pain	40.28±18.19	40.94±16.71	48.11±16.50	NS	NS	NS
SF-GH:general medical health	31.56±18.47	31.78±17.91	35.44±21.32	NS	NS	NS

Table 1. Control group with lumbar discopathy

Parameter	At baseline (mean±SD)	After treatment (mean±SD)	After 3-month follow-up (mean±SD)	p-value		
				After treatment vs. baseline	After 3-month follow-up vs. baseline	After 3-month follow-up vs. post-treatment
VAS	7.94±1.47	3.06±2.67	2.41±2.48	0.000	0.000	NS
Floor-finger distance	32.50±16.40	14.06±12.68	11.29±12.46	0.000	0.000	NS
Lateral flexion LEFT	12.22±4.01	18.11±5.09	21.59±5.20	0.000	0.000	0,005
Lateral flexion RIGHT	12.94±4.68	18.50±4.88	21.65±5.28	0.001	0.000	0,017
Oswestry Index	52.17±24.91	79.33±16.12	81.59±15.55	0.001	0.001	NS
SF-PF: physical functioning	33.06±20.08	68.89±20.97	68.24±27.27	0.005	0.000	NS
SF-RP: role limitations – physical	15.28±28.62	44.44±43.35	58.82±42.34	0.011	0.003	NS
SF-RE: role limitations – emotional	27.67±39.94	62.83±44.12	64.59±43.28	0.007	0.007	NS
SF-VT: vitality	41.39±22.41	62.78±26.80	62.06±28.56	0.007	0.009	NS
SF-MH: mental health	47.56±24.46	74.44±22.72	73.65±26.00	0.001	0.000	NS
SF-SF: social functioning	51.22±27.43	73.44±23.10	74.88±24.97	0.005	0.024	NS
SF-BP: bodily pain	35.06±18.10	66.17±21.65	64.18±20.50	0.000	0.000	NS
SF-GH:general medical health	42.50±21.23	55.00±23.83	57.35±24.76	0.022	0.006	NS

Table 2. Weightbath therapy for lumbar discopathy

Parameter	At baseline (mean±SD)	After treatment (mean±SD)	p-value
			After treatment vs. baseline
VAS	6,93±2,37	3,93±2,46	0,000
Floor-finger distance	32,93±10,15	18,00±9,51	0,000
Lateral flexion LEFT	13,00±3,04	18,93±5,96	0,000
Lateral flexion RIGHT	14,27±4,62	19,33±6,30	0,000
Oswestry Index	64,93±16,01	80,13±16,67	0,002
SF-PF: physical functioning	45,00±26,11	60,33±24,16	0,008
SF-RP: role limitations – physical	16,67±34,75	51,67±48,51	0,027
SF-RE: role limitations – emotional	22,22±41,00	42,22±46,23	NS
SF-VT: vitality	41,33±19,50	49,33±49,32	NS
SF-MH: mental health	47,73±23,20	58,13±18,61	NS
SF-SF: social functioning	50,90±26,50	70,83±24,85	0,008
SF-BP: bodily pain	36,00±17,33	55,33±23,73	0,015
SF-GH: general medical health	35,33±17,16	41,00±21,88	NS

Table 3. Laser therapy for lumbar discopathy

Discussion

As shown by a previous biophysical study performed with a special ultrasound device for underwater use, moderate loading (with 4 kg weight) accomplished a 0.9 to 1.6 mm increase of disc height in 75 per cent of patients. The deformation of the disc peaked after approx. 20 minutes. In view of the foregoing, it is expedient to implement loading with smaller weight, but over a prolonged period[11,12].

Underwater traction affords both symptomatic relief and causal therapy simultaneously; it is particularly suitable for the alleviation of axial pain. The retraction of protruding intervertebral discs slightly eases the pressure on nerve roots and accordingly, radicular pain is relieved along with local vertebral pain, as well as with muscle spasm, and the pressure in spinal compartments.

Laser therapy alleviates muscle spasm; it exerts a direct analgesic action as well as anti-inflammatory and neuroregenerative effects[13,14,15,16,17]. These properties we found useful in reducing both vertebral and radicular pain. There have been a number of mechanisms investigated in attempts to determine how disc herniations heal. Histological investigations have shown the presence of granulation tissue with abundant vascularization surrounding the fibrocartilaginous fragments. Within the granulation tissue, the prevailing cell types are macrophages with fibroblasts endothelial cells. These cell types have been demonstrated to be positively affected by laser therapy. The stimulation of marophages and fibroblasts could be the primary mechanism by which laser therapy heals disc herniations[18]. Inflammatory markers such as IL-1, IL-6 and TNF are also present at the site of disc herniations, laeding to higher prostaglandin E2 concentrations. Two studies have demonstrated that laser therapy effective in reducing prostaglandin E2 concentrations[19,20].

Both treatment modalities were superior to the therapy administered in the standard control group. Both the patients and their physicians agreed that weightbath traction and laser therapy improved the patients' condition more rapidly and intensely. Compared to the controls, patients in the laser therapy and weightbath hydrotherapy groups used much less rescue medication, which did not cause any gastric complaints or ulcer symptoms in these subjects. In the standard control group by contrast, paracetamol-induced gastric complaints were observed in two patients. The favorable outcome of therapy persisted longer in the weightbath hydrotherapy group – the significantly improved subjective and objective status was maintained even 3 months after treatment. In the majority of cases, the follow-up MRI repeated 3 months after treatment did not depict any substantial difference compared to baseline – the reduction of disc protrusion/herniation was seen in a few cases only. According to the literature, an increase in the distance between individual vertebrae was verified using a special, underwater US equipment and furthermore, MRI performed immediately after treatment depicted reduced disc protrusion/herniation. However, this radiologically evident improvement was no longer evident 3 months later.

In the laser group, improvement and the relief of pain was confirmed by thermography, which showed attenuation in higher temperature ranges in the paralumbar segment and in regions corresponding to nerve roots.

Both weightbath traction hydrotherapy and laser therapy accomplished a statistically significant reduction of lumbar and radicular pain, as well as mitigated paresthesia. The range of motion of the lumbar segment increased simultaneously. SF-36 scores and Oswestry indexes both improved. The relief of symptoms was associated with improved qual-

Thermographic pictures (4 patients)

Before treatment | After treatment

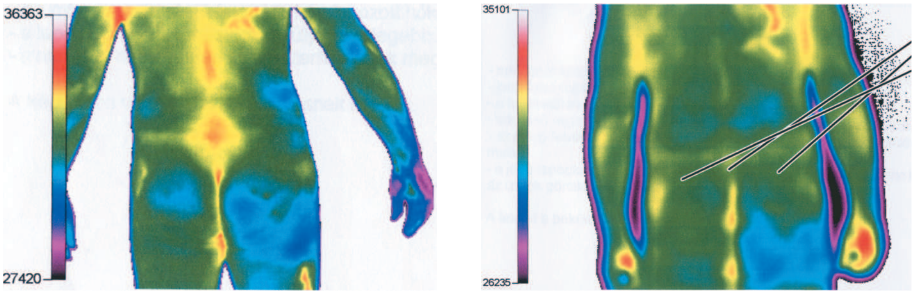

Patient No. 1.

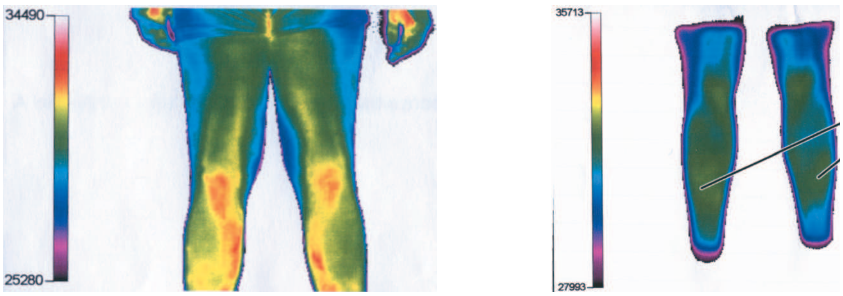

Patient No. 2.

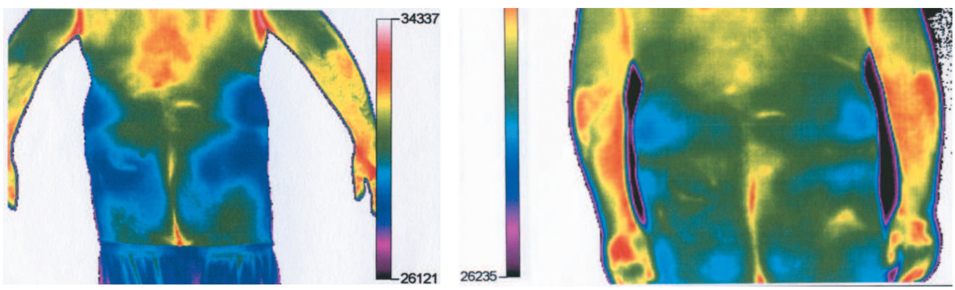

Patient No. 3.

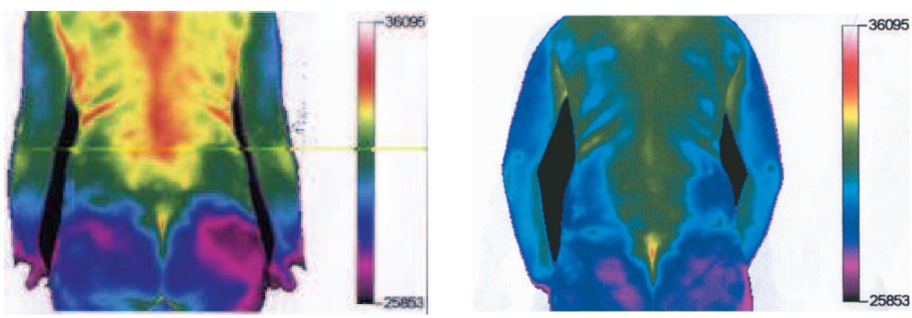

Patient No. 4.

ity of life and enabled the patients to resume their everyday activities, as well as reduced their absenteeism from work.

Conclusion

Both soft laser illumination and underwater traction hydrotherapy exert their beneficial action promptly. These are easy to implement, low-cost, and non-invasive treatment modalities devoid of any relevant hazard. Considering that both relieve pain and increase articular range of motion, we recommended integrating these treatments into the algorithm of conservative management. Additionally, we suggest conducting additional studies to confirm the beneficial effect of these treatments – with special emphasis on the combined use of underwater traction and soft laser therapy.

References

1. *Koes BW, Van Tulder MW, Thomas S.* Diagnosis and treatment of low back pain. BMJ 2006; 332:1430–1434.

2. *Van Tulder M.* Low back pain. Best Practice & Research in Clinical Rheumatology 2002;16:761.

3. *Hicks GS, Duddleston DN, Russell LD, Holman HE, Shepherd JM, Brown CA.* Low back pain. AmJ Med Sci 2002;324:207–211.

4. *Greeenberg MS.* Handbook of Neurosurgery. 5th edition. Thieme 2001.

5. *Li LC* & *Bombardier C.* Physical therapy management of low back pain: an exploratory survey of therapist approaches. Phys Ther 2001;81:1018–1027.

6. *Van Tulder MW, Koes B, Malmivaara A.* Outcome of non-invasive treatment modalities on back pain: an evidence-based review. Eur Spine J. 2006;15(Suppl)1:64–81.

7. *Harte AA, Baxter GD, Gracey JH.* The efficacy of traction for back pain: a systematic review of randomized controlled trials. Arch Phys Med Rehabil 2003;84:1542–53.

8. *Beurskens AJ, de Vet HC, Koke AJ et al.* Efficacy of traction for non-specific low back pain: a randomised clinical trial. Lancet 1995;346:1596–1600.

9. *Clarke JA, van Tulder MW, Blomberg SEI, de Vet HCW, van der Heijden GJMG, Bronfort G.* Traction for low-back pain with or without sciatica. COCHRANE DATABASE OF SYSTEMATIC REVIEWS (4): Art. No. CD003010 2005.

10. *Moll K.* Treatment of discushernia with so-called “weightbath” therapy. Orvosi Hetilap 1953; 94:292–296 (in Hungarian).

11. *Kurutz M, Bene E, Lovas A.* In vivo deformability of human lumbar spine segments in pure centric tension, measured during traction bath therapy. Acta of Bioengineering and Biomechanics 2003;5:67–92.

12. *Kurutz M.* Age-sensitivity of time-related in vivo deformability of human lumbar motion segments and discs in pure centric tension. Journal of Biomechanics 2006;39:147–157.

13. *Soriano F, Rios R.* Gallium Arsenide laser treatment of chronic low back pain: a prospective, randomized and double blind study. Laser Therapy, 1998;l0:175–180.

14. *Basford JR, Sheffield CG, Harmsen WS.* Laser therapy: a randomized, controlled trial of the effects of low-intensity Nd: YAG laser irradiation on musculoskeletal back pain. Arch Phys Med Rehabil, 1999;80(6):647–52.

15. *Toya S., Motegi M, Inomata K, Ohshiro T, Maeda T.* Report on a computer randomized double blind trial todetermine the effectiveness of the GaA1As (830 nm) diode laser for attenuation in selectedpain groups. Laser Therapy, 1994;6:43–148.

16. *Djavid GE, Mehrdad R, Ghasemi M, Hasan-Zadeh H, Sotoodeh-Manesh A, Pouryaghoub G.* In chronic low black pain, low level laser therapy combined with exercise is more beneficial than exercise alone in the long term: a randomized trial. Aust J Physiother, 2007;53(39): 155–60.

17. *Gur A, Krakoc M, Cevik R, Nas K, Sarac AJ, Karakoc M.* Efficacy of low power laser therapy and exercise on pain and functions in chronic low back pain. Lasers Surg Med, 2003;32(39): 233–38.

18. *Young S, Bolton P, Dyson M, Harvey WDiamantopoulos C.* Macrophage responsiveness to light therapy. Lasers Surg Med,1989;9(5):497–505.

19. *Lim W, Lee S, Kim I, Chung M, Kim M, Lim H, Park J, Kim O, Choi H.* The inflammatory mechanismof 635 nm light-emmiting-diode irradiation compared with existing COX inhibitors. Lasers Surg Med, 2007;39(7):614–21.

20. *Bjordal JM, Lopes-Martins RA, Iversen VV.* A randomized, placebo controlled trial of low level laser therapy for activated Achilles tendonitis with microdialysis measurement of peritendinous prostaglandin E2 concentration. Br J Sports Med, 2006;40(1):76–80.

Dr. Oláh Csaba
Borsod-Abaúj-Zemplén County Hospital & University Teaching Hospital, Miskolc, Hungary
H–3526 Miskolc, Szentpéteri kapu 72–76.

Minimal invasive surgical techniques for the treatment of pathologic lesions, situated in the midline of the spinal canal

Zoltán Papp[1], János Vajda[1], Róbert Veres[2], Péter Banczerowski[1]
[1] National Institute of Neurosurgery, Budapest, Hungary
[2] Department of Neurosurgery ÁEK, Budapest, Hungary
zolpapp@oiti.hu

Abstract

Objective: Multilevel laminectomy for exposing the spinal canal to remove spinal cord lesions has been widely used in spine surgery. Destruction of the dorsal structures of the spinal column, detachment of the longitudinal musculature, resection of the vertebral arches, and injury of the joint capsules and ligaments are responsible most of short and late-time complications. Spinal deformities, instability, subluxation, invasion of haematoma and scar tissue into the spinal canal are the most often mentioned complications in the literature. The author main objective was to develop and summarize the novel minimally invasive techniques suitable for exploring and treating different pathologies, located in the midline of the spinal canal with preservation of the stability of the spine.

Methods: 38 patients were operated on with intramedullary laesions located from CIII to LI level of the spine with the newly developed multilevel spinous process splitting and distracting laminotomy technique. The dorsal, paraspinal musculature was not detached from the vertebras. With splitting and distracting the spinous processes and the vertebral arches, the vertebral joints, the joint capsules and the ligaments were not injured, these structures remained mostly intact. To achieve a moderate enlargement and decompression of the spinal canal, complementary intervertebral spacer insertion was performed in some cases. The patients were followed with regular MRI, CT scans and neurological examinations.

Results: Adequate surgery of the lesions located intramedullary was achieved in all patients using our new procedures. Moderate enlargement and permanent decompression of the spinal canal was achieved with the insertion of homologues tricortical iliac crest bone graft or heterologous PEEK spacer. The numbers of split laminae were 3 to 6. The split spinous processes were closed directly to each other in 24 patients. In 9 cases a tricortical bone graft and in 5 cases a heterologous PEEK spacer was inserted between the facing bony parts.

The incidence of postoperative local pain was lower, within acceptable limits, and early mobilization was allowed. The average length of hospital stay was shorter too. The postoperative follow-up CT scans demonstrated bony healing, with the inserted graft or cage between the osteotomized faces. No compression or dislocation of the spacer was seen. Instability was not detected in any of the patients by flexion or extension lateral radiographs.

Conclusion: The split laminotomy surgical procedure with or without complementary auto- or heterologous grafting method fulfills the requirements of other laminotomy techniques. This technique is suitable for removing intramedullary tumors, and the posterior stabilizing structures of the spine, as the vertebral laminae and the longitudinal musculature are completely preserved, nearly anatomical situation can be maintained. Leaving the longitudinal paraspinal musculature innervations intact, and with the preservation of the bone-muscle attachments and ligaments, the dynamic stability of the spine remains unchanged. Retaining the bony structures (vertebral arches) and the vertebral joints the static stability of the spinal column remain intact, the chance of developing the long-term spinal deformation is minimal. The grafts, inserted between the osteotomized faces, provided permanent decompression of the spinal canal, and bony healing – throughout the graft or spacer – of the split vertebral laminae. With the use of the PEEK spacer the short and long time complications of the autologous bone graft harvesting procedure can be avoided.

This newly developed surgical procedure and its modifications can be used at any age of the patients, any level of the spine, theoretically on unlimited number of spinous processes.

Keywords: laminotomy; splitting laminotomy; intramedullary tumor; intervertebral spacer

Introduction

Multilevel laminectomy for exposing the spinal canal to remove spinal cord lesions has been widely used in spine surgery[4,7]. Many of short and late-time complications of this surgical procedure have been reported. Spinal deformities, instability, subluxation, invasion of haematoma and scar tissue into the spinal canal are the most often mentioned complications in the literature[6,8,20]. Several surgical procedures have been reported to preserve the posterior structures. Various kinds of laminoplasty techniques have been described with osteoplastic posterior spinal arch reconstruction, in tumor removal and in degenerative cases as well[7,11]. The conventional posterior surgical approaches invariably separate the muscle attachments from the spinous processes and laminae. Damage to these muscles and bony connections can lead to persistent axial pain, cervical malalignment and spinal instability[10]. Postlaminectomy kyphotic deformation is one of the most known long-term complications of the classic dorsal surgical procedures. The operative treatment of this deformation is very difficult and less effective.

To preserve the dynamic and static stabilizing structures of the spinal column new minimally invasive ways to explore the spinal canal have been developed. To follow the principle of less invasiveness the split laminotomy technique for surgery of multilevel lesions located in the spinal canal was introduced[1,9]. This surgical procedure is suitable for exploring and removing different pathologies located in the spinal canal. It has been proven, that the split laminotomy approach is suitable to remove intramedullary tumors located in the midline.

If total resection of an intramedullary tumor was not possible due to the infiltration to the surrounding spinal cord or re-growing of the malignant tumor is expectable, an enlargement of the spinal canal is needed. To achieve the permanent enlargement of the spinal canal and decompression of the spinal cord, a bone graft or PEEK cage implantation was performed between the split laminas. The bone grafting procedure is a well developed and widely used method in spine surgery. The tricortical iliac bone graft is most commonly used at ventral cervical discectomy or cervical corpectomy procedures[2,3,5,13]. To avoid the short and long-term bone harvesting area complications, and to shorten the time of the surgical procedure, the use of different interbody spacers is widely accepted at spinal surgical procedures. With the cage implantation all of the donor site complications, and the possibility of late-time bone graft resorption or compression is avoidable[12,14,15,16]. The bony healing throughout the spacer is similar to the iliac crest bone graft procedure[17,18]. Solid fusion between the osteotomized parts can be shown about 12 months after the implantation.

Clinical Materials and Methods

The authors used the multilevel spinous process splitting and distracting laminotomy technique with or without complementary auto,- or allograft insertion in 38 adult patients with intramedullary lesions, located in various level of the spinal cord. The split spinous processes were closed directly to each other in 24 patients (Group I). In 9 cases a tricortical iliac crest bone graft (Group II/A) and in 5 cases a heterlogous Poly-Ether-Ether-Ketone (PEEK) intervertebral spacer (Group II/B) was inserted between the facing bony parts *(Table 1)*.

Patient no.	Age (yr)/ sex	Histology	Resection (MRI)	No. of split laminae	Group	Preoperative functional assessment	Postoperative functional assessment
1	44/M	Astrocytoma Gr III	partial	3	II/A	II	II
2	59/M	Ependymoma	complete	4	I	II	I
3	47/F	Ependymoma	complete	4	I	I	I
4	55/F	Astrocytoma Gr II	subtotal	5	I	III	III
5	61/F	Astrocytoma Gr III	partial	3	II/A	I	II
6	44/F	Ependymoma	partial	3	II/A	I	I
7	52/M	Astrocytoma Gr II	partial	5	II/A	II	II
8	61/M	Astrocytoma Gr I	complete	6	I	II	II
9	46/M	Ependymoma	partial	3	II/A	I	II
10	55/F	Cavernoma	complete	3	I	II	I
11	49/F	Ependymoma	complete	4	I	I	I
12	58/M	Astrocytoma Gr II	subtotal	3	I	II	III
13	38/M	Astrocytoma Gr I	complete	4	I	I	I
14	57/M	Ependymoma	partial	5	II/A	II	II
15	56/F	DAVF	closed	3	II/A	II	I
16	48/F	Ependymoma	complete	4	I	I	I
17	43/F	Ependymoma	complete	4	I	I	I
18	60/F	Astrocytoma Gr III	partial	3	II/A	II	II
19	55/M	Cavernoma	complete	5	I	I	I
20	47/F	Cavernoma	complete	3	I	I	I
21	52/M	Ependymoma	complete	3	I	I	I
22	59/M	Astrocytoma Gr II	complete	3	I	II	II
23	52/F	Ependymoma	complete	5	I	I	I
24	43/M	Astrocytoma Gr III	partial	6	II/A	II	II
25	46/F	AVM	closed	3	II/B	I	I
26	57/M	Ependymoma	complete	4	I	I	I
27	54/M	Haemangioblastoma	complete	3	I	II	II
28	47/F	Astrocytoma Gr II	complete	5	I	II	III
29	59/F	Astrocytoma Gr III	partial	3	II/B	II	II
30	56/M	Ependymoma	complete	3	I	I	I
31	47/F	Ependymoma	complete	4	I	I	I
32	41/M	Astrocytoma Gr II	subtotal	5	I	II	III
33	50/F	Astrocytoma Gr II	partial	4	II/B	II	III
34	57/M	DAVF	closed	3	II/B	I	I
35	52/M	Astrocytoma Gr III	partial	5	II/B	II	III
36	45/M	Ependymoma	complete	6	I	I	I
37	61/F	Ependymoma	complete	6	I	I	I
38	44/M	Ependymoma	complete	4	I	I	I

Table 1. Characteristics of the patients

There were 18 women and 20 men with an average age of 51.6 years (range 38–63 years) at the time of surgery. *(Table 1)* Functional assessment (McCormic) was performed preoperatively and postoperatively every 6 months at the time of the MRI follow-up visits. To confirm the extension of resection and to check for recurrence or to follow the growing patterns of the tumor, all patients underwent postoperative MRI evaluations at 3 and 6 months postoperatively, thereafter every 6 months or as needed by the patient's condition. To check the bony changes, all patients had postoperative CT imaging as well immediately after the operation and repeatedly thereafter (at 2, 6, and 12 months).

The patients were positioned sitting or prone for cervical and prone for thoracic and thoracolumbar surgeries. A special midline posterior approach was used. The skin, fascia, and nuchal in the cervical region and the supraspinous ligament in the midline were incised. The interspinous ligaments and muscles were dissected longitudinally between the spinous processes without injuring the attachments of the interspinous muscles. All muscle attachments on the spinous processes and laminas, as well as the laminas themselves, were completely preserved. The innervations of the longitudional paravertebral musculature left completely intact. The vertebral joints, and the capsules were also not injured. The ligamentum flavum was removed at the middle part to expose the midline epidural space above and below the intended levels. In some cases involving the upper and midthoracic region of the spine, it was necessary to remove the cephalad small bony part of the angle of the vertebral arcuses in the midline as a result of the oblique location of the spinous processes. The spinous processes were split in the midline with an oscillating saw or craniotome. The spinous processes and the laminae were separated and distracted with Cloward-type retractors *(Figure 1)*. It is important to accurately fit

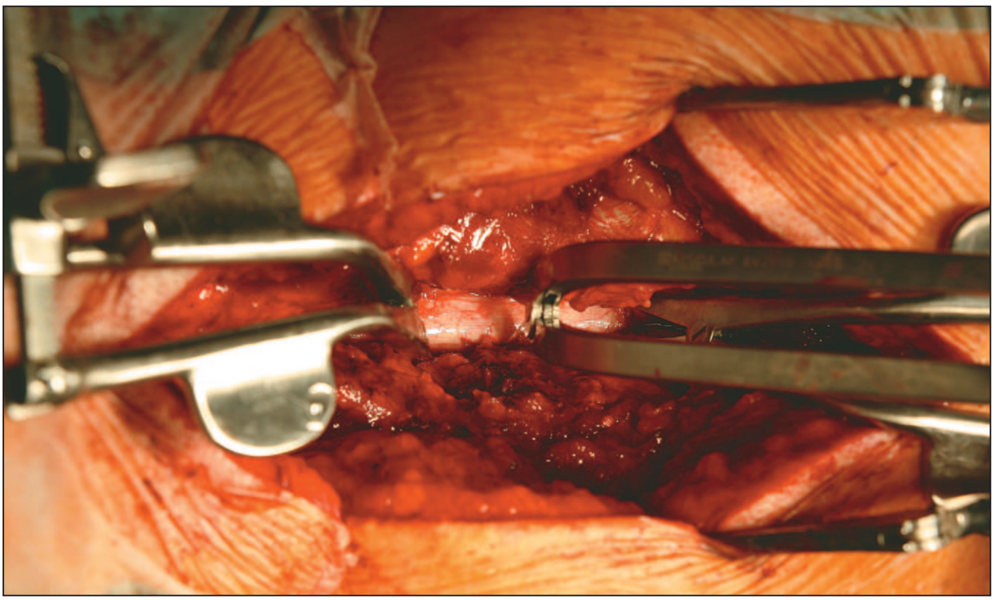

Figure 1. Intraoperative photograph showing the step-by-step distraction of spinous processes and laminas by Cloward-type retractors. The separated and distracted laminae open the operating field and the dura becomes visible

the end of the retractors to the inner cortex of the vertebral arcus immediately above the dura in the epidural space and to open the retractor with gentle force to prevent the fracture of the spinous process during distraction. Two retractors were applied for each laminae to aid step-by-step distraction of the bone and to prevent its fracture. In the case of intramedullary lesions, the dura was opened and the pathology was removed. If the lesion is visible on the dorsal surface of the cord, a longitudinal posterior midline surgical approach was used with one exception. If the lesion was seen on the posterior surface of the cord, it was approached directly. If the lesion was entirely intraspinal, surgery was performed through a midline exposure. Following removal of space occupying lesions, the dura was partialy closed with or without the use of duraplasty. The narrow operative field and the limited lateral view by the operating microscope make the duraplasty very difficult and time-consuming procedure. In our limited series we left the dural flaps opened in a few cases, and covered the surface with heterologous dural patch and fibrin glue.

In case of the total resection of the intramedullary tumor was not possible due to the lack of recognizable cleavage (diffusely infiltrative tumors) and thus intraspinal space occupation was considered to be solved only temporarily, a bony decompression was indicated to create extra intraspinal space. To avoid the laminae returning to their original position – with the aim of moderate enlargement of the spinal canal – a spacer was placed between the bony parts facing each other *(Figure 2 A* and *B)*. The space between the distracted laminae was first measured then the appropriate sized tricortical iliac crest bone graft was harvested and inserted between the osteotomized parts of the spinous processes. To avoid the donor site complications we slightly modified the surgical procedure and in 5 cases haemostatic gelatin sponge filled PEEK cages were inserted. We used the

Figure 2. Sagittal T1-weighted magnetic resonance imaging scans showing an intramedullary tumor in the thoracic region before (A) and 12 months after the surgery (B). On the postoperative MRI scan the inserted spacers are also shown

SOLIS Cervical Cage (Stryker Spine SAS, Z.I Marticot – 33610 Cestas France). This cage has a D shape design, with 4° wedge configuration. It has serrations on the top and the bottom face, and incorporates titanium spikes for fixation as well. The cage is available in two footprints, and a variety of heights ranging from 4 mm to 12 mm. We inserted the cage between the laminae as the plane side of the D shaped cage facing toward the spinal cord, and the convex side of the cage facing outward. The wedge shape of the cage preventing it to sliding out whiles the serrations on the top and bottom side preventing it to sliding into the spinal canal. The strong grasping power of the retracted laminate – returning to their original position – and the two pairs of titanium spikes – located both sides of the cage – fixed it firmly in place. Precise insertion and continuous control of the inner edge of the spacer under the insertion process was necessary to avoid penetration of the graft into the spinal canal, and to avoid compression of the spinal cord.

The bony parts were sutured with Vycril (Ethicon, Inc., Sommerville, NJ) by passing the sutures through the spacer (bone graft or cage) and the holes of the halves created with a small burr. Finally, the fascia and the skin were closed.

Results

We performed the split laminotomy procedure with or without spacer insertion at various levels of the spine from the level of CIII to the level of LI. The number of split laminae was 3 to 6. (mean:4) The split spinous processes were closed directly to each other in 24 cases. In 9 cases tricortical bone graft, while in 5 cases PEEK cage insertion was performed.

The average follow-up was 18.7 months, with a range from 7 to 19 months.

Histological results were as follows: 15 intramedullary astrocytomas (Grade I [pilocytic astrocytoma], n:2; Grade II, n:7; Grade III, n:6), 16 ependymomas, 3 cavernous hemangiomas, 2 dural arteriovenous malformations, one intramedullary arteriovenous malformation, and one hemangioblastoma. The resection of the intramedullary tumor was continued only until that layer where the tumor could clearly be differentiated from the surrounding spinal cord. The completeness of surgical removal depended only on the cleavage plane and not on the approach.

The use of PEEK cages between the osteotomized bony faces requires shorter operative time compared to the classic iliac crest bone grafting method. In our cases the mean duration of the complete surgical procedure was 118 minutes with the range of 91 to 145 minutes. The unnecessary preparation and isolation of the bone graft harvesting area also spare about 12 to 25 minutes.

The mean blood loss was only 110 ml (range, 79–194), as extensive detachment of the muscles, and the second skin incision and iliac bone harvesting was avoided. None of the patients required blood transfusion. No dural tear occurred in our short series. Injury to nervous structures was never observed. No wound infections occurred.

The patients were not braced due to the minimally disturbed anatomy.

The incidence of postoperative local pain was lower, within acceptable limits. (VAS: 2 to 5) Furthermore, the patients needed smaller doses of analgesic medications, and early mobilization was allowed. In Group II/B lack of the iliac bone harvesting procedure, no iliac crest pain was detected. The average length of hospital stay was 6 days (ranged 5 to 7).

Results of the preoperative neurological functional assessment in the astrocytoma group were as follow: Grade I, two of all patients, Grade II, twelve of all patients, and Grade III one of the patients. In nine of all patients (60%) the initial neurological state was unchanged after the surgery, while in six cases (40%) we detected the worsening of the neurological functions. The ependymoma group patients the initial neurological assessment was: Grade I, fourteen of all patients, Grade II, two of all patients, and Grade III none of the patients. After the surgery we detected improvements of the neurological function in one case (6.25%). The neurological functions were unchanged in fourteen cases (87.5%), and worsening of the symptoms have seen in one patient (6.25%). The other patients, operated on different lesions had good (Grade I or II) initial neurological functions, and this mostly remained or improved after the surgical procedure *(Table 1)*. The progression of the neurological deficits are due to the malignant (diffusely infiltrative) behavior of the tumor, not the way of the surgical exploration.

To confirm the extension of resection, all patients underwent postoperative MRI evaluations. Neither the inserted homologous bone graft, nor the PEEK cage with the incorporated titanium spikes disturbs the evaluation of the spinal cord on MRI images. Of the 15 astrocytomas, four were removed completely, three were removed subtotally, and eight were partially removed. Of the 16 ependymomas, 13 were removed completely and 3 were partially removed, as confirmed by postoperative MRI scans at 2 months. Cavernous hemangiomas and hemangioblastomas were all completely removed, but the AVM-s were only closed and decompressed. To check bony changes, all patients had postoperative CT imaging. Early postoperative CT scans and 3D reconstructions showing the split halves of the spinous processes facing each other when no graft was inserted (Group I) *(Figure 3 A* and *B)* or the distracted spinous processes and the grafts in-between with the planned slight enlargement of the spinal canal (Group II/A and B) *(Figure 4 A* and *B)*. Later partial bony healing was seen, mostly in Group I and Group

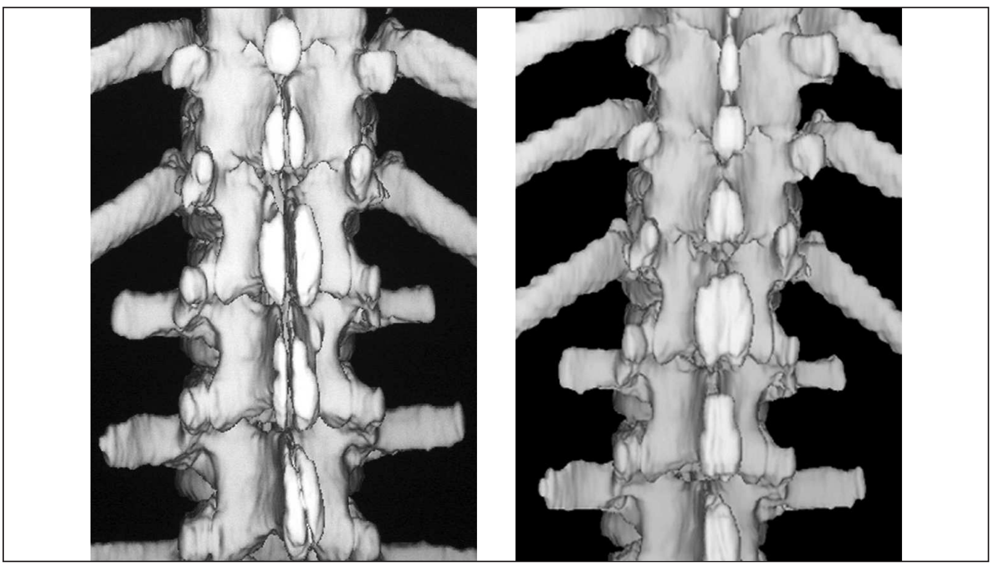

Figure 3. Three-dimensional reconstructed computer tomographic images showing the directly closed spinous processes just after the surgery (A) and bony healing 1 year later (B)

II/A patients. In Group II (A and B) the permanent distraction of the laminar arches has been followed on CT scans *(Figure 5 A* and *B)*. Neither graft dislocation nor compression was shown. Some partial fracture of the spinous process was shown on postoperative CT scans in all groups, without clinical significance. Instability was not detected in any of the patients by flexion or extension lateral radiographs.

Discussion

The surgical approach for treatment of intramedullary tumors has been laminotomy until the last decades. With the aim of preventing the frequently reported postoperative complications various types of surgical techniques have been developed. The main objective of these developments to preserve and reconstruct the posterior spinal structures. The lit-

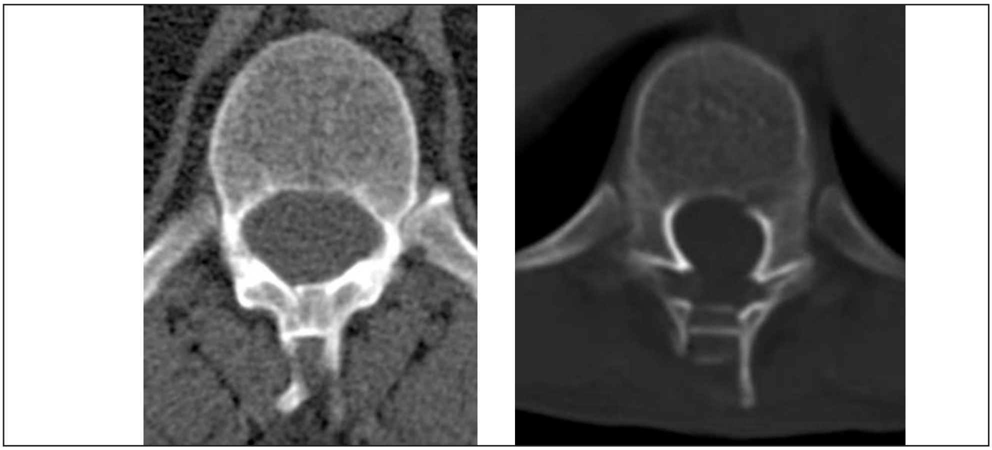

Figure 4. The postoperative axial computed tomographic scans showing the distracted spinal processes, and the position of the bone graft (A), and the PEEK cage (B)

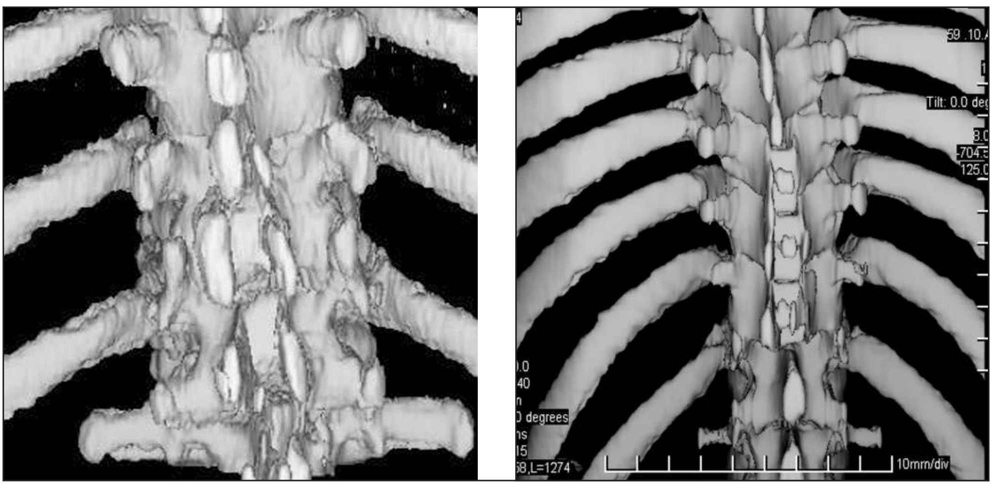

Figure 5. Three-dimensional reconstructed computer tomographic images showing the distracted spinous processes and the positions of tricortical iliac crest bone grafts (A) and PEEK cages (B) after surgery

erature emphasizes the important role of the deep extensor muscles, the semispinalis, and the multifidus group, especially in the neck. The multifidus and the semispinalis cervicis muscles act as dynamic stabilizers of the cervical spine together with the important static stabilizer structures, including the intervertebral discs, the vertebral arches, ligaments and intervertebral joint capsules. Once these muscles have been detached, it is impossible to reconstruct the complicated anatomy[8,10]. The integrity of the nerves is also important because if they are injured (branches ramified from the dorsal ramus), preservation of the muscles becomes meaningless[19]. The spinous process splitting and distracting laminotomy technique fulfills the requirements of other minimal invasive laminotomy techniques and helps to preserve the attachments of the posterior spinal musculature.

With this method the operative field is restricted compared to laminectomy, but according to the keyhole principle, it is still enough under the operating microscope for the surgery of lesions located within the spinal canal, especially of intramedullary lesions in the midline. Intraoperative identification of the cleavage plane makes removal of intramedullary tumors possible. If there is no recognizable plane in cases of infiltrative or malignant intramedullary tumors (or if intraoperative appearance suggests an infiltrating tumor), tumor removal is not continued at any cost, as this could be dangerous and unnecessary for the patient. If partial tumor removal is performed, or gradually growing residual tumor is expected, bony decompression of the spinal canal is indicated to provide more space. The complementary use of iliac bone graft provide moderate enlargement of the spinal canal at the expense of the postoperative donor site complications. The surgical procedure was modified to achieve the enlargement of the spinal canal by placing heterologous spacer between the facing split bony parts of the spinous process in a way similar to the cervical anterior iliac bone grafting technique. The degree of enlargement of the spinal canal depends on the elasticity of the arches, the force of distraction and the size of the inserted spacer. The press force between the closing laminae and the wedge shape and the serrated face of the cage with the titanium spikes does not allow the spacer to penetrate into the spinal canal or slipping out from the split laminae after its placement. The precise insertion of the bone graft or PEEK cage between the laminae is important, as spacer penetration during the insertion process is a very rare, but possible complication. With this modification of the split laminotomy process, no iliac crest bone graft needed, and all complications of the graft harvesting procedure avoided.

Lack of the most frequent short time postoperative donor site complications, as local pain and hematoma, early recovery and discharge of the patients were possible. The time of the surgical procedure was significantly shorter than the iliac bone grafting procedure. The blood loss during the surgical procedure was also less, compared to the classic iliac bone grafting procedure. Fusion – through the bone grafts or PEEK cages – of the split bony faces of the spinous process was seen in most cases during follow up. There was no patient in whom osseous bridging was missing in all segments.

The bony healing between the osteotomy sites was in agreement with findings of the literature in connection with posterior arch reconstructions of the cervical canal in spondylotic myelopathy cases, and with reconstructions of the laminar roof for a posterior approach. Through our sort follow-up period neither compression, nor displacement of the implanted spacers have been detected. Developing of specially shaped cages for better positioning and distraction of the split laminae need further evaluation.

It is more difficult to perform a complete distraction of the spinous process and the lamina in adults than in pediatric cases because the spinal arch is less elastic and more fragile. In children, elasticity of the spinal arch is much more pronounced, which allows a wider field for manipulation relative to the diameter of the spinal canal. In the elderly, elasticity is reduced, and fractures are more frequent in patients with osteoporosis. It is easier to distract the relatively thinner and more elastic arches in the cervical region than in the thoracic or lumbar part of the spine. Traumatic bony changes can rarely be observed in the body of the vertebra, mainly in the midline, and fracture of the spinous process can also occur. This had no clinical significance and later showed complete healing. Spinous process distraction may separate the facet joints, but no morphological signs of the destruction or damage of the facet joints or its capsules were observed on CT or MRI scans during the follow-up period, the static stabilizing structures of the spine does not injured. Theoretically, the compliance and elasticity of the spinal arches, facet joints, capsules, and ligaments together allow enough movement under the distraction process to prevent irreversible damage to these structures. In the case of rarely observed overload distraction, these structures moved together, and traumatic bony changes occurred in the midline of the body of the vertebra without clinical significance; they were only seen on CT scan.

The rates of spinal deformities after intraspinal surgery reported in the literature vary considerably. The development of a spinal deformity is a multifactorial process. In our series, no newly developed instability, subluxation, or kyphotic deformity was observed. Open laminectomy produced much greater changes in extension, flexion, and axial rotation than the split laminotomy from the intact. Lateral bending was similarly unaffected for both exposures[10]. Although the clinical and radiological results are very promising, the limited follow-up period precludes conclusions regarding the long-term results of the procedure, especially with respect to kyphotic deformity. The bony protection of the spinal canal and the function of the paraspinal muscles were restored, and we observed better cosmetic results compared with the laminectomy technique. The minimally invasive splitting laminotomy technique allows the incision to be limited to the immediate region of exploration of the spinal canal because, with this method, tissue retraction is minimal and there is excellent access to the affected area. The preservation of the spinous processes and the restoration of the inter- and supraspinosus ligamentous complex maintains the normal posterior median furrow, which is often lost with other, more destructive techniques. Nevertheless, this is a newly developed approach with relatively few cases for each spinal region, and the technique needs further evaluation concerning its limitations. Based on our limited experience, it seems to be safe on all spinal segments (the cervical, thoracic, and lumbar spine) with an acceptable complication rate. Furthermore, it proved to be suitable for removing different, mainly intramedullary spinal pathologies located in the midline. Our novel, modified, minimally invasive technique enables surgeons to obtain a sufficient field for exploring different spinal pathologies that do or do not require spinal canal decompression with preservation of the posterior structures of the spine and the attachments of the muscles.

Conclusions

The minimally invasive multilevel spinous process splitting and distracting laminotomy approach with or without auto- or allograft (spacer) insertion is a safe and effective surgical management, suitable for removing intramedullary tumors located in the midline of the spinal canal, and ensuring permanent decompression of the spinal cord when necessary. The posterior dynamic and static stabilizing structures of the spine, as the vertebral laminae, the joint capsules, ligaments, and the longitudinal musculature are completely prevented. Preservation of these structures helps to avoid the short and long term complications of the widely used laminectomy.

References

1. *Banczerowski P, Vajda J, Veres R.* Exploration an decompression of the spinal canal using split laminotomy and its modification, the "Archbone" technique. Neurosurgery 2008;62:(5 suppl 2): ONS 432–440.

2. *Bartels RH, Donk R, van Azn RD.* Height of cervical foramina after anterior discectomy and implantation of a carbon fiber cage. J Neurosurg 2001;95:1 Suppl 40–42.

3. *Brooke NS, Rorke AW, King AT, Gullan RW.* Preliminary experience of carbon fiber cage prostheses for treatment of cervical spine disorders. Br J Neurosurg 1997;11:221–227.

4. *Brotchi J:* Intrinsic spinal cord tumor removal. Neurosurg 2002;50:1059–1063.

5. *Celik SE, Kara A, Celik S.* A comparison of changes over time in cervical foraminal height after tricortical iliac graft or polyetheretherketone cage placement following anterior discectomy. J Neurosurg: Spine 2007;6:10–16.

6. *Hosono N, Yonenobu K, Ono K.* Neck and shoulder pain after laminoplasty. A noticeable complication. Spine 1996;21:1969–1973.

7. *Hukuda S, Ogata M, Mochizuki T, Shichikawa K.* Laminectomy versus laminoplasty for cervical myelopathy: brief report. J Bone Joint Surg (Br) 1988;70:325–326.

8. *Katsumi Y, Honma T, Nakamura T.* Analysis of cervical instability resulting from laminectomies for removal of spinal cord tumour. Spine 1989; 14:1171–1176.

9. *Kurokawa T, Tsuyama N, Tanaka H.* Enlargement of spinal canal by the sagittal splitting of the spinous process (Jpn). Bessatu Seikeigeka 1982;2:234–240.

10. *Ogdena AT, Bresnahanb L, Smith JS, Natarajand R, Fesslerb RG.* Biomechanical comparisons of traditional and minimally invasive intradural tumor exposures using finite element analysis. Clinical Biomechanics 2009;24:143–147

11. *Raimondi AJ, Guiterrez FA, Di Rocco C.* Laminotomy and total reconstruction of the posterior arch for spinal canal surgery in childhood. J Neurosurg 1976;45:550–560.

12. *Rawlinson JN.* Morbidity after anterior cervical decompression and fusion. The influence of the donor site on recovery, and the results of a trial of surgibone compared to autologous bone. Acta Neurochir (Wien) 1994;131(1–2):106–118.

13. *Ryu SI, Mitchell M, Kim DH.* A prospective randomized study comparing a cervical carbon fiber cage to the Smith–Robinson technique with allograft and plating: up to 24 months follow-up. Eur Spine J 2006;15:157–164.

14. *Sawin PD, Traynelis VC, Menezes AH.* A comparative analysis of fusion rates and donor-site morbidity for autogenic rib and iliac crest bone grafts in posterior cervical fusions. J Neurosurg 1998;88:255–265.

15. *Schnee CL, Freese A, Weil RJ, Marcotte PJ.* Analysis of harvest morbidity and radiographic outcome using autograft for anterior cervical fusion. Spine 1997;22:2222–2227.

16. *Shad A, Leach JC, Teddy PJ, Cadoux-Hudson TA.* Use of the Solis cage and local autologous bone graft for anterior cervical discectomy and fusion: early technical experience. J Neurosurg Spine 2005;2:116–122.

17. *Shono Y, McAfee P, Cunningham BW, Brantigan JW.* A biomechanical analysis of decompression and reconstruction methods in the cervical spine. Emphasis on a carbon-fiber-composite cage. J Bone Joint Surg Am 1993;75:1674–1684.

18. *Wilke HJ, Kettler A, Claes L.* Primary stabilizing effect of inter-body fusion devices for the cervical spine: an in vitro comparison between three different cage types and bone cement. Eur Spine J 2000;9:410–416.

19. *Zhang J, Tsuzuki N, Hirabayashi S, Saiki K. Fujita K.* Surgical anatomy of the nerves and muscles in the posterior cervical spine: Aguide for avoiding inadvertent nerve injuries during the posterior approach. Spine 2003;28:1379–1384.

20. *Yasuoka S, Peterson HA, MacCarthy CS.* Incidence of spinal column deformity after multilevel laminectomy in children and adults. J Neurosurg 1982;57:441–445.

Zoltán Papp
National Institute of Neurosurgery
H–1145 Budapest, Amerikai út 57.
Tel: (+36) 1 251-2999
Fax: (+36) 1 251-5678

INVESTIGATION AND APPLICATION OF PNEUMATIC ARTIFICIAL MUSCLES

József Sárosi, Gábor Szabó, János Gyeviki
Department of Technical and Process Engineering, Faculty of Engineering
University of Szeged
sarosi@mk.u-szeged.hu

Abstract
The movement of pneumatic artificial muscle (PAM) is soft that similar to the human muscle therefore it can be used as the actuator for rehabilitation devices and prostheses. In this paper a Fluid Muscle manufactured by Festo is tested, and some experimental results, rehabilitation devices and prostheses are shown. Our goal is to construct an intelligent prosthetic arm using PAMs.

Keywords: pneumatic artificial muscle; test-bed; experimental results; therapy devices; prosthetic arms

Introduction

The pneumatic artificial muscle is a pneumatic actuator with a comprehensive history of applications in the biomechanical field. The most promising pneumatic actuator is evidently the McKibben pneumatic muscle actuator. The McKibben muscle was invented in the 1950's by physician Joseph L. McKibben to help the movement of polio patients and to motorize pneumatic arm orthotics. There exists several types of artificial muscles that are based on the use of rubber or some similar elastic materials, such as the McKibben muscle, the Rubbertuator made by Bridgestone company, Air Muscle made by Shadow Robot company, Fluid Muscle made by Festo company, Pleated PAM developed by Vrije University of Brussel, ROMAC (RObotic Muscle ACtuator), Yarlott and Kukolj PAM and some others. There are a lot of advantages of artificial muscles like the high strength, good power-weight ratio, low price, little maintenance needed, great compliance, compactness, inherent safety and usage in rough environments. Disadvantages are connected with the accuracy of control and nonlinearities of pneumatic systems[1,2].

Pneumatic muscle actuators consist of a rubber bladder enclosed within a helical braid that is clamped on both ends. As the bladder is pressurized, its volume increases and the braid and clamps act to shorten the overall length of the actuator. The general behaviour of PAM with regard to shape, contraction and tensile force when inflated depends on the geometry of the inner elastic part and of the braid at rest and on the materials used *(Figure 1)*. Typical materials used for the membrane construction are latex and silicone rubber, while nylon is normally used in the fibres[3].

Pneumatic artificial muscles show similarity to biological muscles. The PAMs are one-way acting, we need two ones to generate bidirectional motion: one of them moves the load, the other one will act as a brake to stop the load at its desired position and the muscles have to change function to move the load in the oppo-

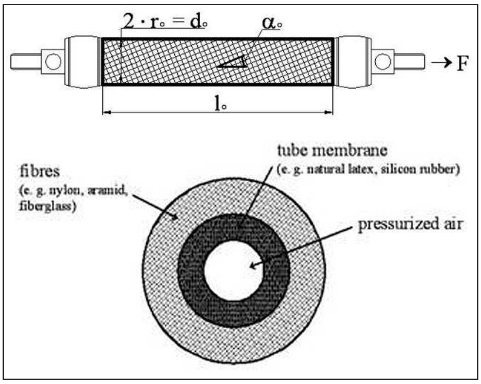

Figure 1. Geometry parameters of PAM and its orthotropic material layers

site direction. This specific connection of the muscles to the load is generally named as an antagonistic set-up[2,4,5].

The Fluid Muscle DMSP-20-200N-RM-RM (with inner diameter of 20 mm and initial length of 200 mm) produced by Festo company is selected for our newest study. *Figure 2* shows different Fluid Muscles.

The layout of this paper is as follows. Section 2 (Materials and Methods) is devoted to display our test-bed for investigation of pneumatic muscles. In section 3 (Results and Discussion), we present some experimental results, our new approximation algorithm of force as a function of pressure and length (contraction) and several devices for rehabilitation and prostheses using PAMs. Finally, section 4 (Conclusions and Future Work) gives the future work we plan.

Figure 2. Fluid Muscles made by Festo

Materials and Methods

Good description of our experimental results can be found in[6].

The experimental set-up *(Figure 3)* consists of a slider mechanism. One side of the muscle is fixed to a load cell, while the other side is attached to the movable frame. The load cell (7923 type from MOM) is a 4 bridge element of strain gauges. It is mounted inline to the PAM on the fixed surface. The load cell measures the force exerted by the PAM. The tests are performed by changing the displacement of this slider. The linear displacement of the actuator is measured using a LINIMIK MSA 320 type linear incremental encoder with 0.01 mm resolution. During each test, frame position, muscle force and applied gauge pressure are recorded.

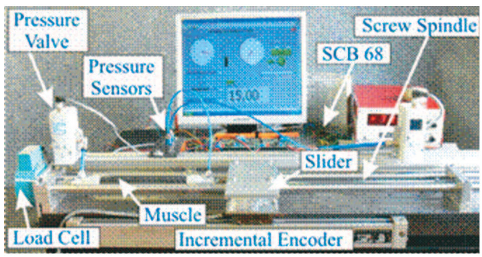

Figure 3. Experimental setup for investigations of PAMs

In the test-bed two fluidic muscles can be mounted. Instead of second PAM a bias spring or an external load can be attached with a flexible steel cable, producing the necessary counter force to pull the actuator back when it is not activated.

The air pressure applied to the actuators can be regulated with two adjustable regulators type Festo VPPM-6L-L-1-G1/8-0L6H-V1N-S1C1. The proportional pressure regulators (PPRs) are controlled by voltage inputs. The main purpose of the PPR is to regulate the

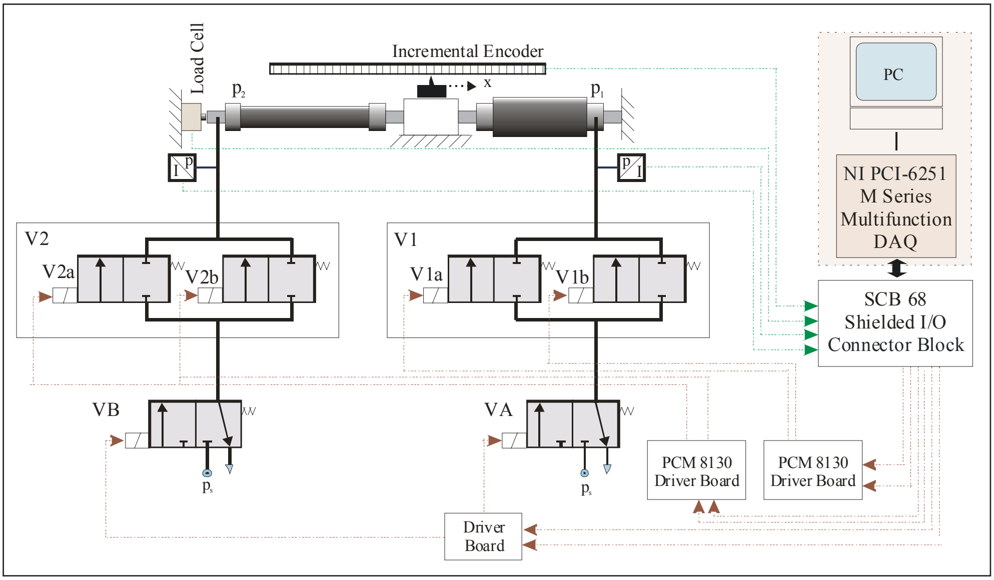

Figure 4. Configuration of pneumatic positioning system with ON/OFF valves

pressure entering the PAM. To measure the air pressure, two Motorola MPX5999D pressure sensors were plumbed into the pneumatic circuit. A National Instruments Multi-I/O card (NI 6251) reads the signal of force, pressure sensors and incremental encoder into the PC.

National Instruments LabVIEW is a typical example for high level software, capable of connecting various kinds of DAQ boards with a PC. We used this program to monitor and collect the data imported through the DAQ card. It also dispatches the control profiles for the PPRs.

For positioning, in the test-bed, two Fluidic Muscles can be controlled by tree-way and two-way solenoid valves (MATRIX HX 751.102 C 324 3/2 NC and PX 861.9E4C2KK fast switching types) *(Figure 4)*.

Results and discussion

Tensile force of artificial muscle under different constant pressures is a function of muscle length (contraction) and of air pressure. The force always drops from its highest value at full muscle length to zero at full inflation and position *(Figure 5)*.

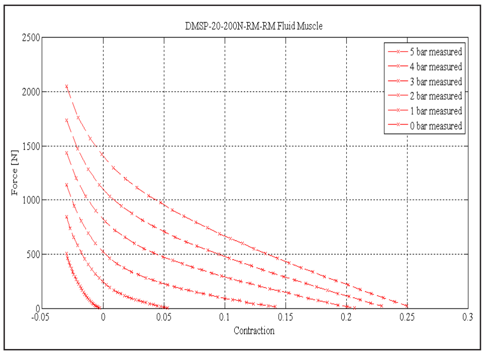

Figure 5. Isobaric force-contraction diagram of Fluid Muscle

Many researchers have investigated the behaviour of PAM and some of them have introduced different mathematical models for this actuator. However, we have noticed significant differences between the theoretical and experimental results. Therefore, we have worked out a better approximation algorithm for the equation of force. Under fixed pressure the contraction to force function can be approximated by an exponential function:

$$F(\kappa) = a \cdot e^{(b \cdot \kappa + c)} + d \cdot \kappa + e \qquad (1)$$

To make our *equation 1* universal meaning usable under various pressures we need to make the algorithm vary from pressure:

$$F(p, \kappa) = (a \cdot p + b) \cdot e^{(c \cdot \kappa + d)} + (e \cdot p + f) \cdot \kappa + \\ + g \cdot p + h \qquad (2)$$

The unknown *a, b, c, d, e, f, g* and *h* parameters were found using least squares method in Matlab.

Comparison and consistent fitting of measured data and force model using *equation 2* is shown in *Figure 6.*

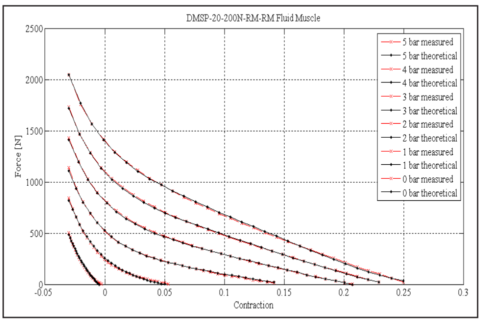

Figure 6. Comparison of measured data and our force model

Numbers have investigated the precise position control of pneumatic muscles during the past several years, too[2,4,7,8,9]. Most of them dealt with the control of single or antagonistic pneumatic muscles. The positioning of PAMs requires accurate determination of the dynamic model of pneumatic actuators. With the help our test-bed the hysteresis can be accurately predicted. Chou and Hannaford in[4] report hysteresis to be substantially due to Coulomb friction, which is caused by the contact between the bladder and the shell, between the braided threads and each other, and the shape changing of the bladder. An experiment was made to illustrate the hysteresis *(Figure 7)*.

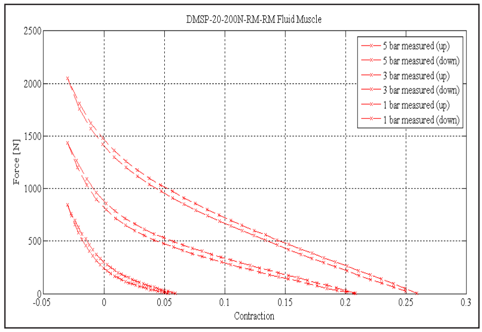

Figure 7. Hysteresis in the tension-length (contraction) cycle

To prove versatility of *equation 2,* another comparison was done between the measured data and force model. The accurate fitting is demonstrated in *Figure 8.*

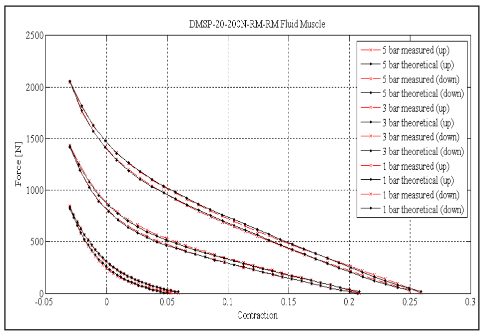

Figure 8. Approximation of hysteresis loop

Beside the traditional linear controllers several modern control methods with adaptive controller, fuzzy controller, neural network controller, sliding-mode controller among others have been developed. On the basis of sliding-mode control, the next probe was a positioning with high-speed ON/OFF solenoid valves. The time functions of the position and control signal are shown in *Figure 9.*

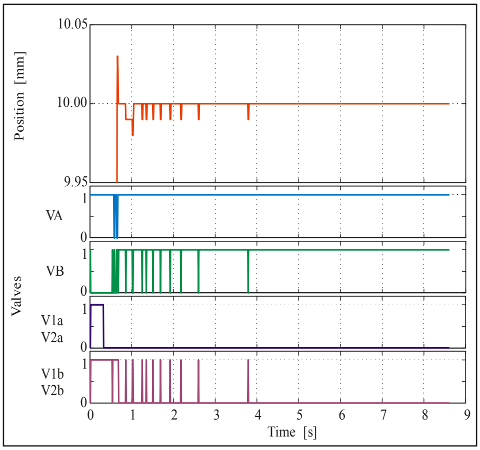

Figure 9. The time functions of the position and control signal (in LabVIEW environment)

We repeated the previous experiment with PLC type Allen-Bradley CompactLogix L23E. *Figure 10* and *Figure 11* show the results.

Several therapy devices have been developed, but the typical robotic systems tend to be expensive and complex for clinical use and impossible for home use. Even, generally, these devices are built with electric motors and the movements are far from natural. The pneumatic artificial muscles are possible to be the actuators for these devices because of its soft motion and cheap and these devices can be used by patients at their own homes. Therapeutic devices provide training of reaching and feeding motions *(Figure 12, 13)*.

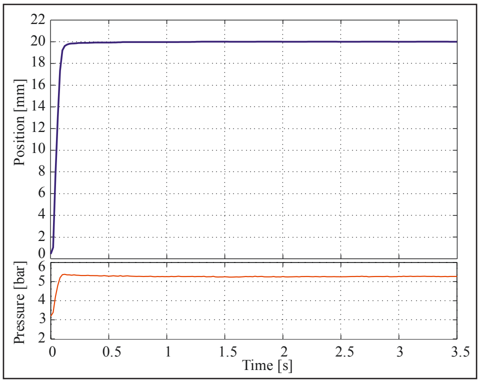

Figure 10. The time functions of the position and pressure (with PLC)

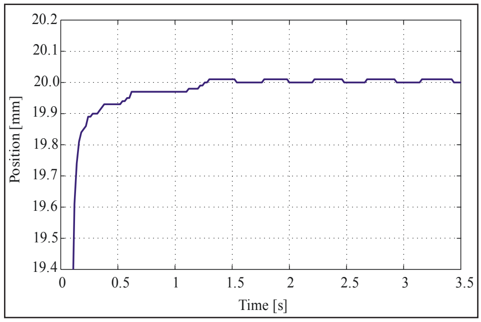

Figure 11. The time function of the position (with PLC, enlarged)


Figure 12. Mentor™ hand therapy device (left[10]) and RUPERT IV upper extremity therapeutic device (right[11])

Figure 13. Muscle Suit[12]

Different prosthetic arms actuated by PAMs are shown in *Figure 14.* These were inspired by the human arm muscular system.

Conclusions and future work

The pneumatic artificial muscle is a pneumatic device characterized by its high level of functional analogy with human skeletal muscle. In this paper we have presented our testbed. With the help of it several static and dynamic investigations and control methods can be carried out. Some experimental results and rehabilitation devices and prosthetic arms using pneumatic artificial muscles have been shown, too. Our goal and future work is to construct a prosthetic arm with PAMs, because these muscles seem a better choice than present day electric or other drives.

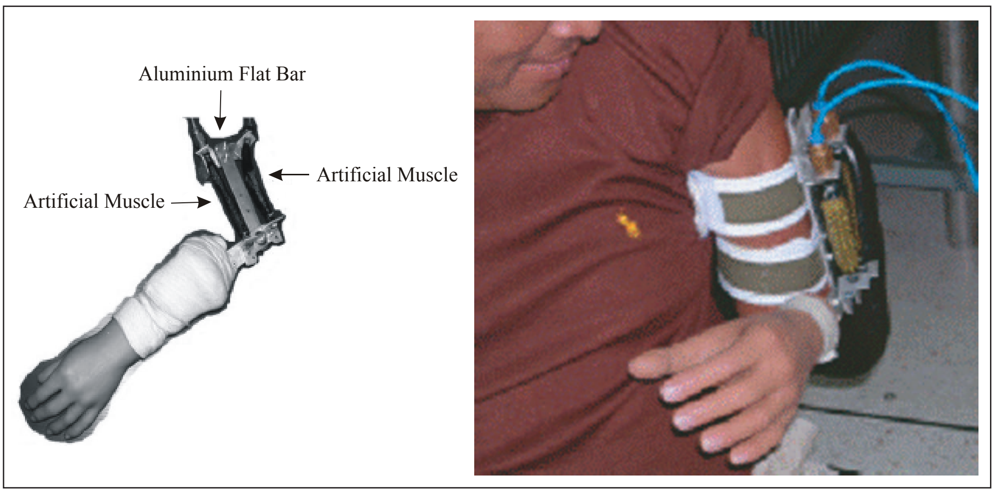

Figure 14. Artificial limbs with PAMs[13,14]

References

1. *Daerden F, Lefeber D.* Pneumatic artificial muscles: actuator for robotics and automation. European Journal of Mechanical and Environmental Engineering 2002;47:10–21.

2. *Situm Z, Herceg Z.* Design and control of a manipulator arm driven by pneumatic muscle actuators. 16th Mediterranean Conference on Control and Automation; 2008 Jun 25–27; Ajaccio, 2008;926–31.

3. *Daerden F.* Conception and realization of pleated artificial muscles and their use as compliant actuation elements. PhD Dissertation, Vrije Universiteit Brussel, Faculteit Toegepaste Wetenschappen Vakgroep Werktuigkunde 1999;9.

4. *Chou CP, Hannaford B.* Measurement and modelling of McKibben pneumatic artificial muscles. IEEE Transactions on Robotics and Automation 1996;12(1):90–102.

5. *Versluys R, Naudet J, Vanderborght B, Lenaerts G, Lefeber D.* Intelligent prosthesis actuated by pleated pneumatic artificial muscles. Proceeding on the 9th International Conference on Climbing and Walking Robots 2006 Sept 12–14, Brussels; 2006;1–9.

6. *Sárosi J, Gyeviki J, Szabó G, Szendrő P.* Laboratory investigations of fluid muscles. Annals of Faculty of Engineering Hunedoara, International Journal of Engineering 2010;8(1):137–42.

7. *Tondu B, Lopez P.* Modelling and control of McKibben artificial muscle robot actuator. IEEE Control System Magazine 2000;20:15–38.

8. *Caldwell DG, Medrano-Cerda GA, Goodwin M.* Control of Pneumatic Muscle Actuator. IEEE Control Systems Magazine 1995 Feb: 40–8.

9. *Lilly JH, Yang L.* Sliding-mode tracking for pneumatic muscle actuators in opposing pair configuration. IEEE Transaction on Control System Technology 2005;13(4).

10. *Koeneman EJ, Schultz RS, Wolf SL, Herring DE, Koeneman JB.* A pneumatic muscle hand therapy device. Proceedings of the 26th Annual International Conference of the IEEE EMBS; 2004 Sept 14; San Francisco, 2004:2711–13.

11. *Balasubramanian S, Wei R, Perez M, Shepard B, Koeneman E, Koeneman J, He J.* RUPERT. An exoskeleton robot for assisting rehabilitation of arm functions. Virtual Rehabilitation 2008; 2008 Aug 25–27, Vancouver, 2008;163–7.

12. *Kobayashi H, Hiramatsu K.* Development of muscle suit for upper limb. Proceedings of the 2004 IEEE, International Conference on Robotics and Automation 2004 Apr 26–May 1; Tokyo, 2004:2480–5.

13. *Wongsiri S, Laksanacharoen S.* Design and construction of an artificial limb driven by artificial muscles for amputees. International Conference on Energy and the Environment; 2003 Dec 11–12; Songkla, 2003;4.

14. *Laksanacharoen S.* Artificial muscle contsruction using natural rubber latex in Thailand. The 3rd Thailand and Material Science and Technology Conference; 2004 Aug 10–11; Bangkok, 2004;3.

József Sárosi
Department of Technical and Process Engineering
Faculty of Engineering
University of Szeged
H–6724 Szeged, Mars tér 7.
Tel.: (+36) 62 546-021

STUDY AND EXAMINATION OF THE IMPLEMENTS USED FOR SECURING PELVIS BONE

János Simonovics[1], Tamás Bodzay[2], Károly Váradi[1]
[1] Budapest University of Technology and Economics, Faculty of Mechanical Engineering Department of Machine and Product Design, Budapest
[2] National Institute of Traumatology and Emergency Medicine, Budapest
janos@simonovics.hu

Abstract
Our goal was to compare the direct plate known as the "gold standard" technology in case of a pelvis fracture with the H-plate technology reinforced with iliolumbar fusion and the pelvis screwing technology reinforced with iliolumbar fusion, especially focusing on the matter of stability.

In our work we studied and examined the securing possibilities and stability of the transforaminal pelvis fracture using the finite element analysis. My colleauges and I created the anatomically correct model (including the 4th and 5th lumbars and cartilages under the lumbars). To create the model we used a previous geometric model used for older preceding analyses. During the modeling we perfected the geometry; we separated the different bone regions and paid close attention to create the scale model of the implements. The placements of the implements are appropriate and in accordance with real surgery procedures. We examined three different cases: standing on the healthy leg, standing on both legs and standing on the injured leg. The boundary conditions for the finite element analysis: the femur is fixed and in case of standing on one leg the opposing side of the hip bone is fixed on both the X and Z axes directions. Furthermore both hip bones are fixed on the Y axis direction, and this applies when standing on both legs as well. We added the load to the 4th lumbar on the model. The value of the load is 500 N and the direction is –Z. We defined surface to surface connection between the femur and acetabulum and also between the side of the symphysis pubica and the fracture ends. We defined bonded connection between all the other components. In our analyses and evaluation we examined the arising stress values and also the displacements in the cortical and spongiosa regions and in the implements. We examined the elongation of the ligaments in the pelvis and measured the maximal distance between the fracture ends under load.

Considering the results of the stress states, the iliolumbar fusion technologies provide more stability. Therefore it is recommended to use these technologies, not mentioning the fact that the dorsal exposure puts the patient through considerably less trauma.

Considering the results of the fracture ends displacements it can be declared that the reason for the existence of the H-plate technology reinforced with iliolumbar fusion cannot be questioned. Therefore continuing the research can be justified by further analyzing and examining dynamic loads on models extracted from CT images.

Keywords: sacrum; fracture; transforaminal

Introduction

According to the data, in 1995 there were 64,000 registered bone fractures as hospitalized patients, and this number reaches 85,000 if we count in the outpatients (patients, who are able to walk with walking cast) as well. Among the outpatients there were 1572 registered pelvis fractures.

The pelvis usually gets injured by a high impact force, and this is mostly a part of a polytrauma. These injuries heal with high functionality damage, therefore the surgery of the rotationally and vertically instable pelvis ring injures obviously is needed. The direct plate technology, known as the "gold standard" of the fractured sacrum raises the question, if it is possible to use a fixing technology, which during the trauma of the surgery is smaller, but the stability remains the same. During the comparison, the direct plate technology will be examined against the H-plate technology reinforced with iliolumbar fusion and the pelvis screwing technology reinforced with iliolumbar fusion, and the transsacral plate technology reinforced with iliolumbar fusion. There is a limited amount of results deduced from the comparison of the biomechanical analysis due to ethical, technical and hygiene reasons. The limited number of results calls for a new method, which is the finite element method (FEA).

My colleauges and I created a new improved model from a previous geometric one, which corresponds with the transforaminal fractures. During the development of the model, we tried to simulate real conditions of a surgery. We added the 4th and 5th lumbars with the cartilages to the model, and also divided the different bone members. Furthermore we paid close attention to create the exact sized model of the implements used in clinical surgeries, and the punctual placements of these parts to the pelvis. We examined the above mentioned fixing technologies in case of standing on one leg and also on two legs, using the anatomically correct boundary conditions. We compared and evaluated the different technologies according to the arising stresses, displacement of the fracture ends and elastic states.

Methods

There are different ways to extract information needed to use the finite element analysis, such as the dense based model extracted from CT or the point cloud based model extracted from CT, which is a simplified model using surfaces stretched onto the point cloud. In order to speed up the calculation, the most likely model to use is the simplified one, which is anatomically correct, but there is some negligence about the model. There was an existing model at our disposal to use in the biomechanical analysis, on which we made the necessary modifications. In addition to the pelvic ring, the 4th and 5th lumbars were added to the model with the cartilages below. We had to modify the sacrum in order to implement the 5th lumbar to the pelvis. We used a plastic medical pelvis and a spinal cord to measure and create the exact model of the additional parts. During the modeling we paid attention to the curve of the spinal cord and the fitting of the two lumbars. My colleauges and I used the ProEngineer Wildfire 4 M60 engineering program to create the modified model. Obviously the fracture is secured with implements that are fixed with screws to the bone; therefore part of the load will be projected to these screws. It was necessary to examine the nature and structure of the bone in the vicinity of these screws. The material properties cannot be neglected, thus these give the mechanical properties of the bone. For example, in the cortical region, which is a sponge like region, the material property numbers are considerably smaller. For this particular reason we divided the hard and spongy regions in the model. The cortical part is about 3 mm thick, and the spongiosa is located within. During the analysis we examined the sacrum fracture, more closely the transforaminal fracture, which causes rotational and vertical instability. Usually, when these high impact traumas occur, the ligamentum sacrospinale and ligamentum sacrotuerale, and also the symphysis pubica are torn on the side of the fracture. We took these effects in account in the model. The geometric model of the transforaminal fracture is shown on the *Figure 1.*

The sacrum fracture line is directly secured with a reconstructional plate, which is fixed with spongiosa screws. This surgery is carried out with ventral exposure technology. The plate is 3 mm thick, 10 mm wide, and the gap between the drill holes is 8 mm. The symphysis tear is secured with a longer bridging reconstructional plate, which is fixed with two cortical screws to the pubic bone. The diameter of the cortical bone is 3.5 mm, core diameter is 2.4 mm, head diameter is 6 mm, and the length is 10–110 mm. The direct plate technology is carried out with a high trauma surgery, which takes a longer recovery process, but the remaining fracture parts have smaller amplitude of movements. The x-ray picture of the direct plate technology can be seen on the *Figure 3,* and the geometric model on the *Figure 2.*

The H-plate technology requires dorsal surgery, which is performed by the incision over the butt cheeks. The sacrum is reached by putting aside the muscles. The fracture is secured with H-plates, which are fixed with cortical screws. The symphysis tear is similar to the direct plate technology and is secured with reconstructional plates, which are fixed with two-two cortical screws to the two sides of the pubic bone. The H plate is 25 mm long, 1 mm thick, and the hole diameter is 3.5 mm. The hole distance in between is 18 mm. The parameters of the cortical screws for fixing the H-plate are exactly the same to the direct plate technology. During the examination of the H-plate technology we used iliolumbar fusion reinforcement. At this reinforcement method, dorsal exposure is used, that way giving access to the lumbars and the hip bone. Two-two screws are placed through the pedunculus of the lumbar extension to the lumbar body itself. Through these, one-one connecting lengthwise rods are extended until the screws fixed in the hip bone. With the help of these rods part of the load is transferred to the hip bone. This securing method puts a smaller load on the

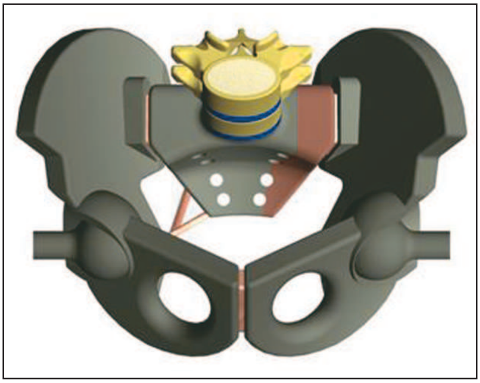

Figure 1. Geometric model of the transforaminal fracture

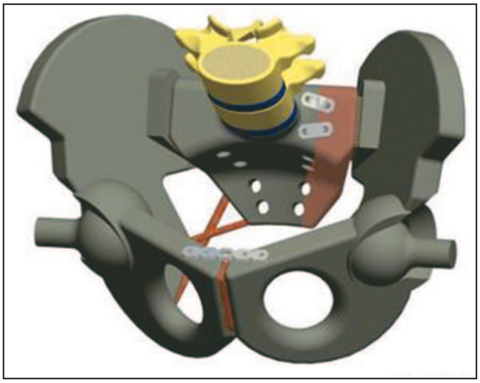

Figure 2. Geometric model of the direct plate securing technology

sacrum, which results in a smaller displacement, thus the fixation is more secure. The lengthwise connecting rods under the lumbar are reinforced by a transversal stabilizing rod. The purpose is to reduce the movements of the bridging parts, and to compensate the stresses. The x-ray picture of the H-plate technology can be seen on the *Figure 3,* and the reinforced with iliolumbar fusion is on the *Figure 4.*

The H-plate iliolumbar fusion technology was constructed in light of the above mentioned facts and can be seen on the *Figure 5.*

Figure 3. X-ray picture of the H-plate and direct plate technology

Figure 4. X-ray picture of the iliolumbar fusion technology

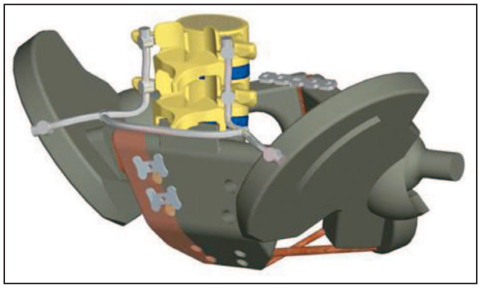

Figure 5. Geometric model of the H-plate technology reinforced with iliolumbar fusion

The pelvis screwing technology does not bear the necessity of exposure. The screws are placed with the help of an x-ray amplifying machine, which gives a real time picture of the surgery. After the anatomical reposition, the iliosacralis screws are inserted from lateral position. The drilling and placement of the screws are monitored from inlet and outlet views as well. The selection of the appropriate screws is important. These screws need to go further than the fracture line, so the length is a factor. The long thread is vital in the stability, without this the screws are not reliable. The thread length is usually 16, 32, 48 and 64 mm and the screw length is about 65–125 mm. The pelvis screwing technology is shown on the *Figure 6.* Similarly to the H-plate technology, we used iliolumbar fusion reinforcement for the examination.

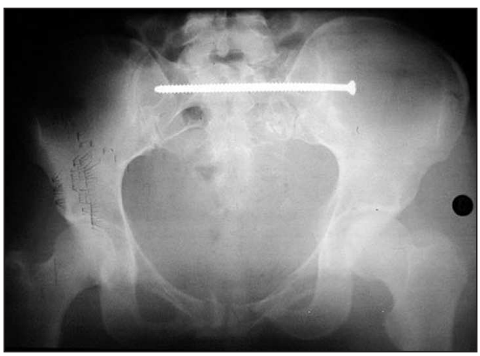

Figure 6. X-ray picture of the pelvis screwing technology

As it was mentioned before, we considered the different material properties of the cortical and spongiosa regions before using the finite element analysis. My colleauges and I separated these regions in the sacrum, lumbars, hip bone and pubic bone. For those regions that were not separated we defined homogeneous material properties. Using 90% spongiosa and 10% cortical region in the homogeneous parts

the elasticity modulus:
$0.9 \cdot 400\ \text{MPa} + 0{,}1 \cdot 17{,}000\ \text{MPa} = 2{,}060\ \text{MPa}$,

the Poisson factor:
$0.9 \cdot 0.2 + 0.1 \cdot 0.3 = 0.21$.

The material properties of the bones, ligaments, joints, cartilages, implements and screws are shown in the table below. Each component is considered to be isotropic and linearly elastic.

We used brick and tetrahedral elements for meshing the model in the finite element analysis. During the meshing we also considered and separated the cortical and spongiosa regions. The examination consists of the three main conditions; standing on two legs, standing on the healthy leg, and standing on the injured leg. As defining the boundary conditions, the hip bone is fixed on the Y-axis direction, corresponding to the muscles responsible to keep the pelvis in a standing fixed position. In case of standing on one leg the musculus gluteus medius (part of the hip muscles) prevents the pelvis to topple to the moving side, keeping the hip bone in a straight position. In light of this, I fixed the X and Z axis directions on both standing on the healthy and injured leg cases as well. The boundary conditions defined for the femur in case of standing on both legs are fixed, while standing on one leg logically the appropriate side femur is fixed. In

Material properties		Elasticity modulus [MPa]	Poisson factor
Screws and plates used for implements	H-plate	200,000	0.28
	Direct plate	200,000	0.28
	Reconstructional plate	200,000	0.28
	Screws	200,000	0.28
	Elements of the iliolumbar fusion	200,000	0.28
Bones	Corticalis region	17,000	0.3
	Spongiosa region	400	0.2
	Homogeneous region	2,060	0.21
Cartilages	Cartilages under the lumbars	50	0.2
Joints	Symphysis	50	0.2
	Pelvis joint	68	0.2
Ligaments	Ligamentum sacrotuberale	355	0.2
	Ligamentum sacrospinale	355	0.2

Table 1. Material properties

every case the 4th lumbar transfers the load. This load is about 500 N for an average adult calculated from the weight of the upper body part. The direction of the load is (–Z). In the geometric model between the femur and the acetabulum, and between fracture surfaces on the sacrum (both cortical and spongiosa regions), and between the side of the symphysis and corresponding pubic bone, surface to surface connection was defined. Every other part is connected to each other with the bonded function. The examination determines the amount of the arising stresses and displacement. With the defined boundary conditions the gap between the fractured sides are measurable. Based on these results the stability of each technology can be determined and evaluated. We used the Algor v19 SP1 program for the finite element analysis. The direct plate technology while standing on the healthy leg is shown on the *Figure 7.*

Results

The *Figure 8* and *9* shows the result of stress and displacement while standing on both legs using the H-plate technology reinforced with iliolumbar fusion. The *Figure 10* and *11* show the results of stress and displacement while standing on the healthy leg using the Pelvis screwing technology reinforced with iliolumbar fusion.

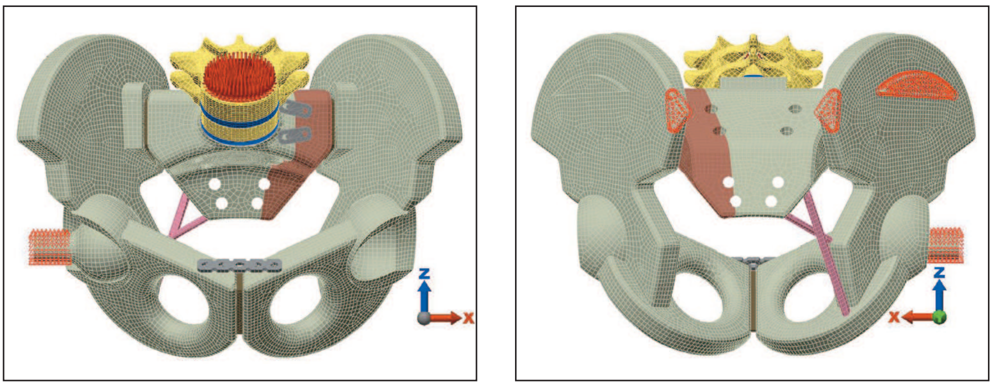

Figure 7. Boundary conditions and meshing of the direct plate technology

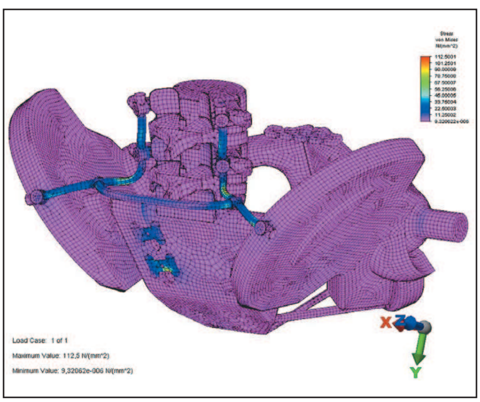

Figure 8. Stress states of the H-plate technology reinforced with iliolumbar fusion

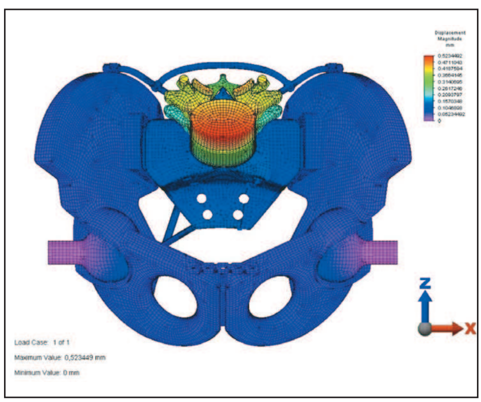

Figure 9. Displacement of the H-plate technology reinforced with iliolumbar fusion

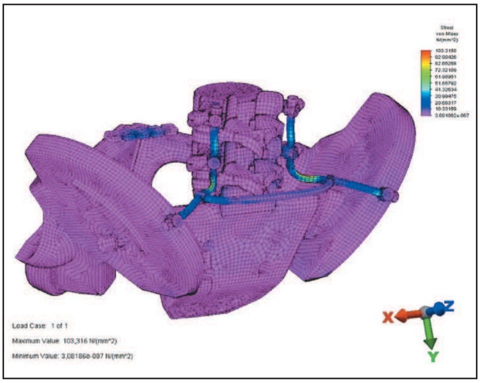

Figure 10. Stress states of the Pelvis screwing technology reinforced with iliolumbar fusion

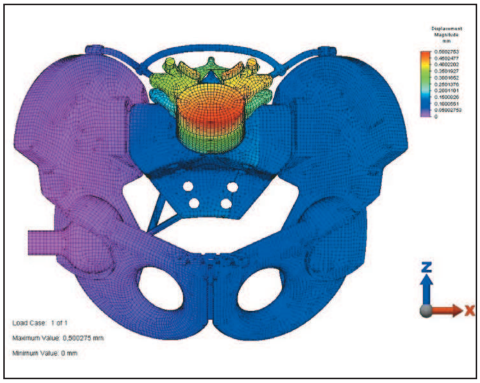

Figure 11. Displacement of the Pelvis screwing technology reinforced with iliolumbar fusion

For the sake of simplicity and better understanding, we summarized the results in the table shown below.

In the cortical bone region, the highest amount of stress arises in case of a transforaminal fracture secured with direct plate technology. It is notable that during the iliolumbar fusion the maximal arising stress isn't located in the near vicinity of the fracture on the sacrum, but rather in the lumbars, where the fixing screws for the lengthwise rods are placed. The most preferable securing method in the cortical bone region considering the arising stresses is the H-plate technology. The highest stress values are shown in the *Table 2.*

In the spongiosa bone regions the direct plate technology somehow is not as good as the other ones. Considering the results the best securing method for the spongiosa bone region is the H-plate technology with iliolumbar fusion as well. The highest stress values can be seen in the *Table 3.* The arising stresses in the implement parts are below of the allowable 800 MPa by a considerable amount. This means that the arising stresses in the implements are not affecting any of the three technologies. Therefore each method is usable and appropriate.

During the analysis of the elongation of the ligaments, my colleauges and I examined the elongation of both the ligamentum sacrospinal and the ligamentum sacrotuberal. It is noticeable from the results that the ligamentum sacrospinal has the higher value of elongation.

Arising maximal stress in the cortical bone regions [MPa] Allowed stress: 70 MPa	Examined cases		
	Standing on the healthy leg	Standing on both legs	Standing on the injured leg
Direct plate technology	66.495 – smaller part of the sacrum	27.4976 – smaller part of the sacrum	38.1396 – smaller part of the sacrum
H-plate + iliolumbar fusion	31.9222 – bigger part of the sacrum	23.0433 – 5th lumbar	35.5964 – bigger part of the sacrum
Pelvis screwing + iliolumbar fusion	26.4753 – 4th lumbar	30.2540 – 4th lumbar	30.7423 – 4th lumbar

Table 2. Maximal arising stresses in the cortical bone region

Arising maximal stress in the cortical bone regions [MPa] Allowed stress: 15 MPa	Examined cases		
	Standing on the healthy leg	Standing on both legs	Standing on the injured leg
Direct plate technology	14.7519 – bigger part of the sacrum	9.5197 – bigger part of the sacrum	9.2406 – bigger part of the sacrum
H-plate + iliolumbar fusion	0.799 – 5^{th} lumbar	0.9106 – 5^{th} lumbar	0.8791 – 5^{th} lumbar
Pelvis screwing + iliolumbar fusion	3.5758 – bigger part of the sacrum	3.5758 – bigger part of the sacrum	3.5139 – bigger part of the sacrum

Table 3. Maximal arising stresses in the spongiosa bone region

Maximal elongation of the ligaments [%] Allowed elongation: 5%	Examined cases		
	Standing on the healthy leg	Standing on both legs	Standing on the injured leg
Direct plate technology	0.0084 – in the ligamentum sacrospinal	0.0085 – in the ligamentum sacrospinal	0.0107 – in the ligamentum sacrospinal
H-plate + iliolumbar fusion	0.0019 – in the ligamentum sacrospinal	0.0034 – in the ligamentum sacrospinal	0.0033 – in the ligamentum sacrospinal
Pelvis screwing + iliolumbar fusion	0.0024 – in the ligamentum sacrospinal	0.0029 – in the ligamentum sacrospinal	0.0038 – in the ligamentum sacrospinal

Table 4. Highest elongation values of the ligaments

Maximal diplacement between the fracture ends [mm]	Examined cases		
	Standing on the healthy leg	Standing on both legs	Standing on the injured leg
Direct plate technology	0.3123	0.1719	0.1965
H-plate + iliolumbar fusion	0.0718	0.0739	0.0801
Pelvis screwing + iliolumbar fusion	0.1318	0.1410	0.1191

Table 5. Maximal displacement between the fracture ends

This is true to each examined case. In each case the elongation is considerable below the allowable threshold value. The highest value of elongation was measured during the direct plate technology, while during the H-plate and pelvis screwing technologies the amount of elongation is more than half of the previously mentioned. The highest elongations values are shown in the *Table 4.*

It is noticeable that during those methods using the iliolumbar fusion the displacement between the fracture ends is considerable lower than the direct plate technology. Furthermore the H-plate technology with iliolumbar fusion is even better than the pelvis screwing technology. The values of the displacement of the fracture ends are shown in the *Table 5.*

It can be stated that the use of the direct plate technology with ventral position exposure can be avoided and justified. The H-plate technology using dorsal exposure is achieved with a considerably lower trauma. This technology results in smaller amount of stresses and provides higher stability.

References

1. *Abé H, Hayashi K, Sato M.* Data Book on Mechanical Properties of Living Cells, Tissues, and Organs. Springer Verlag. Tokyo. 1996.
2. *El-Asfoury MS, El-Hadek MA.* Static and Dynamic Three-Dimensional Finite Element Analysis of Pelvic Bone. International Journal of Mathematical, Physical and Engineering Sciences 2009;3:1. p. 35–41.
3. *Szentágothai J, Réthelyi M.* Funkcionális anatómia I.. Bp.: Medicina Könyvkiadó Rt., 2002.
4. *Burján T.* A töréskezelés végeselemes modellezése medencegyűrű-sérülés esetén – Thesis. Bp.: BME GSZI 2003.
5. *Dr. Varga E.* A medencegyűrű sérülései. Available: *http://www.vitalitas.hu/?ctype=3&todo=bet&id=18&showbet=2792.* Last accessed 2009. 08.20.
6. (2009). Finite element study of trochanteric gamma nail for trochanteric fracture. Available: *http://www.materialise.com/materialise/view/en/393575-Finite+element+study+of+trochanteric+gamma+nail+for+trochanteric+fracture.html?cat=2414683.* Last accessed 2009.08.29.
7. *Cilingir AC, Ucar V, Kazan R.* (2007). Three-Dimensional Anatomic Finite Element Modelling of Hemi-Arthroplasty of Human Hip Joint. Available: *http://www.sbaoi.org/pdf/vol-21%281%29/2116372.pdf.* Last accessed 2009.09.16.

I would like to express my gratitude towards my two consultants Dr. Károly Váradi and Dr. Tamás Bodzay for helping and guiding my work. Furthermore I would like to say a special thanks to Tamás Burján, Cecília Bagdi and László Asbóth for letting me use their geometric model, which I developed further for my examinations and analysis. And last but not least I would like to thank Péter Mészáros for his help and support.

János Simonovics
Budapest University of Technology and Economics, Faculty of Mechanical Engineering Department of Machine and Product Design, Budapest
H–1111 Budapest, Műegyetem rkp. 3.

Biomechanica Hungarica III. évfolyam, 1. szám

Aktív koronáriasztentek bevonatainak összehasonlítása gyógyszerfelvevő és -leadó képességük alapján

Szabadíts Péter[1], Dobránszky János[2]
[1] Budapesti Műszaki és Gazdaságtudományi Egyetem, Anyagtudomány és Technológia Tanszék
[2] Magyar Tudományos Akadémia–Budapesti Műszaki és Gazdaságtudományi Egyetem Fémtechnológiai Kutatócsoport
szabadits@freemail.hu

Absztrakt
Az aktív, gyógyszer-hatóanyagot kibocsátó sztentek folyamatosan bővülő családjának fejlődése jellemzi az elmúlt évek orvoslását. Az orvoslás eredményei igazolták az aktív és passzív sztentek használatának létjogosultságát. Egy jelenleg már használt passzív sztentnek, a gyártóval együttműködve, aktív bevonattal való ellátása a kitűzött célunk. A bevonatnak kétféle célja is van, egyrészt a sztent biokompatibilitását fokozza, másrészt mint aktív bevonat, a sztent felhasználásának körét bővítse.

Kísérleteink során a megfelelően előkészített, sztentek felületével megegyező felületű lapkákra felvitt PUR bevonatok (Carbothane®, Tecothane®, ChronoFlex®) gyógyszermegkötő és időben elhúzódó -leadási képességeit vizsgáltuk.

A PUR bevonatok jól használhatóak a sztentek bevonására, és gyógyszert is képesek tárolni. A PUR bevonatok alaptulajdonságaik szerint – mint hidrofil vagy hidrofób – több vagy kevesebb hatóanyagot tudtak megkötni a felületükön és a mélyebb rétegeikben. A több rétegben felvitt bevonatok nagyobb mennyiségű hatóanyagot tudtak megkötni, mint az egyrétegű bevonatok. A leadási görbék alapján értelmezhető egy, a PUR bevonatok felületről és az anyag belsejéből leadott hatóanyag mennyiség, ez a PUR alaptulajdonságától függően változó az idő függvényében. A legtöbb hatóanyagot a hidrofil tulajdonságú ChronoFlex® bevonat tudta felvenni, míg a legkevesebbet a hidrofób Tecothane®.

A PUR bevonatok megfelelő kiválasztásával a felhasználási területük bővíthető, kombinálásukkal szélesíthető az indikációs területük. Az eredmények alapján a többrétegű bevonatok előnyösebb gyógyszermegkötő képessége látszik az egyrétegűvel szemben, és ezzel bizonyítható a híg oldatok használatának javaslatát a bevonási eljárásban a töménnyel szemben. A kapott eredmények alapján tervezhető a bevonatok gyógyszermegkötő kapacitása, és a bevonatok szendvicsszerkezetű elrendezésével az időbeli leadás szabályozható lehet. A hidrofil PUR bevonatok nagyobb hatóanyag-felvétele az anyag duzzadásával magyarázható, és ez alapján tervezhető a bevonat által bejuttatható hatóanyag mennyisége.

Kulcsszavak: sztent; polimer bevonat; heparin; gyógyszerleadó képesség

Investigation of the polymer coatings of drug eluting coronary stents from the aspect of drug absorbing and eluting

Abstract
Coronary stents are the most important materials in our day's cardiology. The rate of restenosis can be decreased by the usage of drug eluting stents compared to bare metal stents. The aim of this work was to optimize polymer coatings for medical applications and the examination of drug absorbing and releasing properties of these coatings. The examined medical grade polymers were Chronoflex®, Carbothane® and Tecothane®. Control groups were bare metal stent models (316 LVM type austenitic stainless steel tube slices). The three medical grade polyurethane granules were applied onto the stent surface. In this paper different techniques were used to cover the samples by polyurethanes then topcoated with heparin. The heparin was injected into the coatings by soaking. The polyurethane coating is an appropriate passive coating. It is expedient to add pharmaceutical agent as a topcoating to prevent the inflammatory reactions and to obtain other pharmaceutical effects. All of the applied polyurethanes were able to bind the heparin, but in different ways depending on their properties. The most bound heparin was found at the three-layer Chronoflex® coating, by 48-hour soaking. Tecothane® coating bound the least heparin, but this coating had the longest elution time. Based on these results it can be concluded that the applied coatings were swelling and it is possible to set an optimum recovery time and concentration of the solution where the maximum amount of heparin can be dissolved in the coatings.

Keywords: Stent, polymer coating, heparin, drug eluting

Bevezetés

A '90-es évektől folyamatosan elterjedő percutan coronaria intervenció (PCI) fő problémája a relatíve gyakori érlumen-visszaszűkülés, a restenosis, amely a coronaria-angioplastica és a sztentimplantáció után kialakuló neointima-hyperplasia és érsimaizomsejt-proliferáció következtében jön létre[1]. A sztentek olyan különleges felépítésű szövetbarát fémhálók, amelyeket a különböző okok miatt beszűkült érszakaszba helyezve, az erek falát megtámasztva az érlumen átjárhatóságát biztosítják. A bevonat nélküli sztentek (BMS) bevezetése, az egyszerű ballondilatációhoz képest közel felére, 20–30%-ra csökkentette ennek az ismételt érelzáródások szövődménynek a gyakoriságát[2]. A restenosis számos klinikai formában jelenhet meg, az ezt okozó túlzott sejtproliferáció kivédésére fejlesztették ki a gyógyszerkibocsátó sztenteket (drug eluting stent – DES)[3]. A sztentek anyagukat tekintve készülhetnek rozsdamentes acélból, nitinolból, tantálból, Co-ötvözetekből, Mg-ötvözetekből, polimerekből, ezek az anyagok mechanikai szempontból megfelelőek. Bizonyos anyagok kiváló mechanikai tulajdonságokat birtokolnak, de a biokompatibilitásuk nem megfelelő, míg más anyagok biokompatibilitása kiváló, de nem alkalmasak sztentek alapanyagának. Ezen ellentmondás feloldására egy alkalmas megoldás a különböző anyagok kombinálása és szendvicsszerkezetű anyagok létrehozása[4,5]. Ennek a gondolatnak a következő eleme az, amikor a bevonat nem csak passzív módon fedi el az alapanyagot, hanem biológiai szempontból aktív anyagokat juttat a környezetébe, és ezáltal segíti a beültetett sztent beépülését a szervezetbe[6].

Az Amerikai Egyesült Államokban az FDA (Food and Drug Administration) gyorsított eljárással két ilyen típusú sztentet engedélyezett, a Cordis sirolimust kibocsátó Cypher sztentjét 2003-ban és a Boston Scientific paclitaxelt leadó Taxus sztentjét 2004-ben[7]. Ezt követően ugrásszerűen megnőtt a költséges gyógyszerkibocsátó sztentek felhasználása, 2004 végére a percutan coronaria intervenciók során 80%-ban ezek kerültek beültetésre az Egyesült Államokban; három év alatt világszerte több millió ilyen típusú sztentet implantáltak[8]. Az utóbbi években számos új hatóanyaggal rendelkező sztent jelent meg, így a zotarolimus bevonatú Endeavor és az everolimus bevonatú Xience V és Promus. A Cypher és Taxus sztentek FDA általi engedélyezése randomizált, kontrollált vizsgálatok alapján történt. A relatíve rövid, kilenc hónapos utánkövetés során lényegesen kevesebbszer észleltek restenosist, sztent okozta trombózist, valamint az érintett ér működészavarát, és kisebb számban volt szükség revascularisatióra, mint a hagyományos sztentek esetében[9,10]. Patológiai vizsgálatok azonban kimutatták, hogy a kedvező neointima-proliferációt gátló hatás mellett a gyógyszerkibocsátó sztent felületének endothelisatiója is késedelmet szenved, illetve tökéletlen, amely a sztent thrombogenitásának fokozódásával jár. A sztentek tökéletlen endothelisatiója következtében kialakuló nagyon késői, egy éven túli sztentthrombosis a DES-ekre jellemző[11,12].

A DES-ekkel elért jobb eredményeket annak köszönhetik, hogy hatóanyagaik helyileg fejtik ki hatásukat, így agresszív hatóanyagokat is tartalmazhatnak, hiszen a helyi leadás és a kismértékű teljes szervezeti hatás miatt kevesebb a mellékhatásuk, mint per os adagolva az azonos hatóanyagokat[4].

Jelen fejlesztések során a különböző típusú poliuretán bevonatok összehasonlítása volt a cél többféle szempontból. Előzetes vizsgálatok alapján egyértelműen látható, hogy minél több réteget viszünk fel a felületre, vagy minél töményebb poliuretán oldatot alkalmazunk, annál egyenletesebb bevonatot kapunk, de a túl vastag vagy tömény bevonatok már hártyákat képezhetnek a sztentek bordái között[6]. A bevonatok felületi egyenletessége segíti a sztentek biokompatibilitását, ezért a vastagabb bevonatok elméletileg jobbak. A DES-ek esetében viszont kérdéses, hogy az egyrétegű vagy a többrétegű bevonat az előnyösebb. Ezt a poliuretán bevonatok hatóanyag-megkötő és -leadó képessége határozza meg.

Módszerek

A vizsgálatokhoz a sztenteknél meghatározott, úgynevezett fémmel fedett felülettel (MSA) megegyező felületű, 316L alapanyagú csőszeleteket használtunk. A csőszeletek előkészítését maratással, majd elektorpolírozással végeztük. A minták maratását minden minta esetében kereskedelmi forgalomban kapható maratópáccal és ultrahangos tisztító készülék segítségével végeztük. A maratópác hidrogénfluorid (HF) és salétromsav (HNO_3) elegye, amelyet 1 : 3 arányban hígítva, 50 ml maratópác és 150 ml desztillált víz keverékeként alkalmaztunk. A maratási folyamat egyenként 5 percig tartott, minden minta esetében. A maratás hatására egyenletes felületi minőség jött létre, megszüntetve a lézeres vágás okozta nagyon kiálló csúcsokat és a jelentősebb felületi érdességbeli különbségeket, valamint az éleket is finomabbá tette.

A maratást követően a mintákat víz és alkohol segítségével megtisztítottuk, majd a száradást követően egyenként elektropolíroztunk (H_2O [desztillált víz] + 88%-os H_3PO_4 [foszforsav] + 96%-os H_2SO_4 [kénsav]).

A három, különböző típusú poliuretán granulátumot (Carbothane®, Tecothane®, Chronoflex®) tetrahidrofuránban oldottuk fel 24 óra alatt. Az elkészített oldatok mind a három anyag esetében 1 tömegszázalékosak voltak. A rétegeket egyenként vittük fel a lapkákra és az egyes felvitelek között szárítottuk. A bevonatokat egy vagy három rétegben alkalmaztuk. A bevonatok felvitele után 24 órán keresztül szárítottuk szobahőmérsékleten a mintákat. A heparint a bevonatokba áztatással juttattuk be. A heparinoldatot kétféle koncentrációban használtuk. Ehhez 10 és 3 mg/ml koncentrációjú heparin HEPES oldatát használtuk. A bevonatokat tartalmazó lapkák 24 vagy 48 órán keresztül áztak az oldatban, majd szobahőmérsékleten 24 órán keresztül száradtak.

Az elkészített mintákat bevonatainak és heparinfelvitelének adatait az *1. táblázat* részletezi.

Minta jelölése	Bevonat		Áztatás	
	típusa	rétegszám	ideje (óra)	heparin/ HEPES
Chr1	Chronoflex	1	24	10 mg/ml
Chr3	Chronoflex	3	24	10 mg/ml
Chr48	Chronoflex	3	48	10 mg/ml
Chr0,3	Chronoflex	3	24	3 mg/ml
Tec1	Tecothane	1	24	10 mg/ml
Tec3	Tecothane	3	24	10 mg/ml
Tec48	Tecothane	3	48	10 mg/ml
Tec0,3	Tecothane	3	24	3 mg/ml
Car1	Carbothane	1	24	10 mg/ml
Car3	Carbothane	3	24	10 mg/ml
Car48	Carbothane	3	48	10 mg/ml
Car0,3	Carbothane	3	24	3 mg/ml

1. táblázat. Az elkészített minták jelölése és előkészítési paraméterei

A hatóanyag-leadási meghatározásához SPECORD UV VIS kétcsatornás spektrofotométert használtunk 333,3 nm és 186,4 nm hullámhossztartományban ahol az abszorbanciát mértük (1).

$$A = -\lg\frac{I}{I_0} = \lg\frac{I_0}{I} \qquad (1)$$

A koncentrációt a Lambert–Beer összefüggés (2) alapján határoztuk meg:

$$\lg\frac{I_0}{I} = \varepsilon \cdot c \cdot d \qquad (2)$$

ahol I_0 a megvilágító, I a d vastagságú rétegen áthaladt fény intenzitása, ε az adott anyagra jellemző állandó (extinkció), c a koncentráció.

A mérést 3 ml térfogatú HEPES oldatban végeztük, amely a spektroszkóppal mérhető minimális térfogat. Az oldatok koncentrációját 0', 5', 15' perceknél, valamint 1, 2, 24 óra elteltével határoztuk meg.

Kontrollcsoportnak a három rétegben felvitt poliuretán bevonatú, de heparint nem tartalmazó HEPES-oldatokban áztatott lapkákat használtunk.

Eredmények

A vizsgálatok során a hidrofil és a hidrofób tulajdonságú bevonatok hatóanyag-megkötő képessége jól elkülönült. A 217 nm elnyelési maximumon mért értékek alapján számított oldatok koncentrációját a különböző típusú bevonatok esetében és az oldatok időegységenkénti koncentrációváltozását az *1–6. ábrák* mutatják.

Az *1. ábrán* a hidrofil tulajdonságú Chronoflex® bevonatok heparinleadása látható, az idő függvényében. A bevonat esetében mindegyik bevonási eljárás esetén megfigyelhető a teljes vizsgálati idő alatt a folyamatos hatóanyag-leadás, a vizsgált HEPES oldat töményedése. A legtöbb heparint a háromrétegű bevonat adta le (15,6 ng), amely 48 órán keresztül volt a heparin 10 mg/ml oldatában. A *2. ábrán* az oldatok időegységenkénti koncentrációváltozása látható a Chronoflex® bevonatok esetén.

A *3. ábrán* a hidrofób tulajdonságú Carbothane® bevonatok heparinleadása látható, az

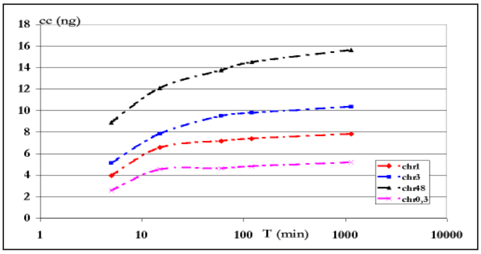

1. ábra. A Chronoflex® bevonatú csőszelet heparinleadása az idő függvényében, az oldat összkoncentrációját tekintve

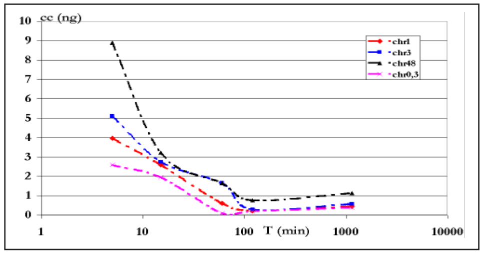

2. ábra. A Chronoflex® bevonat mérési időpontok közötti heparinleadása

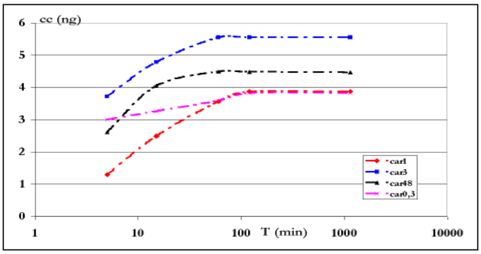

3. ábra. A Carbothane® bevonatú lapka heparinleadása az idő függvényében, az oldat összkoncentrációját tekintve

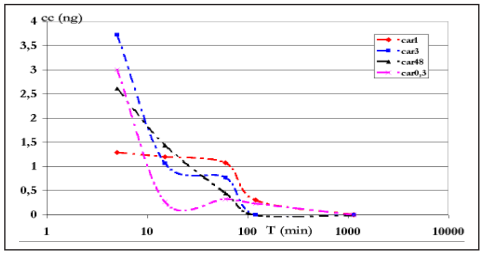

4. ábra. A Carbothane® bevonat mérési időpontok közötti heparinleadása

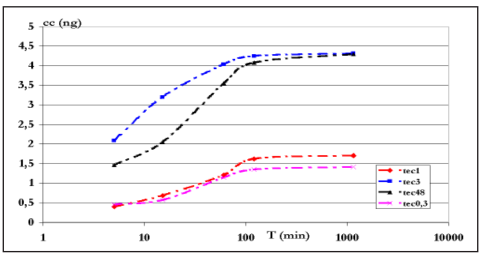

5. ábra. A Tecothane® bevonatú lapka heparinleadása az idő függvényében, az oldat összkoncentrációját tekintve

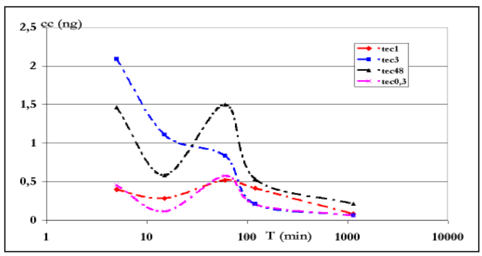

6. ábra. A Tecothane® bevonat mérési időpontok közötti heparinleadása

idő függvényében. A bevonat esetében mindegyik bevonási eljárás esetén megfigyelhető, hogy a teljes vizsgálati idő alatt nem volt folyamatos a hatóanyag-leadás. A bevonatok 120 perc alatt teljes mértékben leadták a megkötött hatóanyagot. A legtöbb heparint a háromrétegű bevonat adta le (5,5 ng), amely 24 órán keresztül volt a heparin 10 mg/ml oldatában. A *4. ábrán* az oldatok időegységenkénti koncentrációváltozása látható a Carbothane® bevonatok esetén.

Az *5. ábrán* a hidrofób tulajdonságú Tecothane® bevonatok heparinleadása látható, az idő függvényében. A bevonat esetében mindegyik bevonási eljárás esetén megfigyelhető a teljes vizsgálati idő alatt a folyamatos hatóanyag-leadás. A legtöbb heparint a háromrétegű bevonat adta le (4,3 ng), amely 48 órán keresztül volt a heparin 10 mg/ml oldatában. A *6. ábrán* az oldatok időegységenkénti koncentrációváltozása látható a Tecothane bevonatok esetén.

Megbeszélés

A leadási görbéket elemezve megállapítható, hogy a legtöbb hatóanyagot a hidrofil Chronoflex® bevonat kötötte meg.

A vizsgálatokkal egyértelmű bizonyítást nyert az a megállapítás, hogy a bevonatok rétegszáma befolyásolja a megkötött hatóanyag mennyiségét. Ennek az oka a bevonatokban keletkező pórusokkal magyarázható, mert a használt híg PUR oldattokkal és a többszöri bevonással az egyes rétegek nagyobb porozitása érhető el, a felület teljes és egyenletes bevonása mellett.

Az eredmények alapján azt is kijelentjük, hogy a töményebb hatóanyagú regeneráló oldatból nagyobb mennyiséget kötöttek meg a háromrétegű bevonatok mind a felületükön, mind a mélyebb rétegeikben, a pórusokban. A vizsgálatok során nem érték el az oldatok azt a koncentrációt, amely a thrombocita aggregációt már teljesen gátolja, de a felhasznált hatóanyaggal lényegesen töményebb oldatok is előállíthatóak.

A leadási görbén az oldatok koncentrációváltozása alapján két szakaszt lehet elkülöníteni, egy gyors első fázist és egy lassú másodikat. A gyors fázis a 0'-tól 60'-ig tart, erre a szakaszra mindhárom bevonat esetében jellemző az oldat gyors koncentrációváltozása, amelyet követ a második szakasz, a lassú koncentrációváltozással jellemezhető 60' utáni elhúzódó leadási görbe. A gyors szakaszt a bevonatok felületén megtapadt és onnan leoldott hatóanyag eredményezi, míg a lassú leadásért a bevonat mélyebb rétegeibe, pórusaiba, bejutott és onnan kioldódó hatóanyag jellemzi.

A Tecothane® bevonat esetében megfigyelt teljes vizsgálati idő alatti hatóanyag-leadás és a 60' után jelentkező másodlagos leadási csúcsok szintén a bevonat porozitásával vannak összefüggésben véleményünk szerint.

Megítélésünk szerint a PUR bevonatok megfelelőek passzív és aktív bevonat kialakítására egyaránt, mert mindegyik alkalmazott PUR bevonat képes volt megkötni a heparint, és a megkötött heparint leadni, valamint a három rétegben alkalmazott bevonatok teljes mértékben befedték a mintadarab felületét. Az elhúzódó leadási görbék alapján arra kelet következtetni, hogy a PUR bevonatok duzzadásra képesek, kifejezetten a hidrofil bevonatok. Ezen eredmények alapján a többrétegű és különböző PUR rétegeket tartalmazó bevonatokkal a felvett hatóanyag mennyisége és időbeli leadása is szabályozható lehet.

IRODALOM

1. *Keltai M.* A gyógyszerkibocsátó coronariastentek alkalmazásának hatásai. Orvosi Hetilap 2007; 148:443–50.

2. *Chen M, John JM, et al.* Bare metal stent restenosis is not a benign clinical entity. Am Heart J 2006; 151:1260–64.

3. *Kotani J, Awata M, Nanto S.* Incomplete neointimal coverage of sirolimus-eluting stents: angioscopic findings. J Am Coll Cardiol 2006;47: 2108–11.

4. *Fülöp G, Berta B, Merkely B.* A gyógyszerkibocsátó stentekkel kapcsolatos legújabb információk. LAM 2008;18(1):39–42.

5. *Maisel WH.* Unanswered questions – Drug-eluting stents and the risk of late thrombosis. N Engl J Med 2007;356:981-4.

6. *Bognár E.* Endoprotézisek passzív és aktív bevonatai és bevonatolási technológiái, 2009. Doktori értekezés.

7. *Wieneke H, Sawitowski T and Wnendt SH et al.* Stent Coating: A New Approach in Interventional Cardiology. s.l.: Herz 2002;Vol. 27:pp. 518–526.

8. *Rzany A and Schaldach M.* Smart Material Silicon Carbide: Reduced Activation of Cells and Proteins on a-SiC:H-coated Stainless Steel. s.l.: Progress in Biomedical Research 2001;Vol. 6: pp. 182–192.

9. *Serruys PW and Gershlick AH.* Handbook of Drug-Eluting Stents. s.l.: Taylor & Francis Group, 2005.

10. *Winslow RD, Sharma SK and Kim MC.* Restenosis and Drug-Eluting Stents. s.l.: Mt Sinai J Med 2005;Vol. 72: pp. 81–89.

11. *Pan CJ, Tang JJ and Shao ZY et al.* Improved blood compatibility of rapamycin-eluting stent by incorporating curcumin. s.l.: Colloids Surf B Biointerfaces 2007;Vol. 59: pp. 105–111.

12. *Tang J, Wang J and Pan C et al.* Anticoagulation and Drug Release Behavior of Curcumin-Loaded PLGA Films. s.l.: Key Engineering Materials 2007;Vols. 342–343: pp. 481–484.

Szabadíts Péter
Budapesti Műszaki és Gazdaságtudományi Egyetem Anyagtudomány és Technológia Tanszék
H-1111 Budapest, Bertalan Lajos utca 7.

Specific biomechanical consideration in trauma cases involving forearm and hand

Miklós Szokoly[1], Petra Aradi[2]
[1] Péterfy S. Hospital and Trauma Center
[2] Budapest University of Technology and Economics
szokoly@gmail.com

Abstract
The rescue of a severed or amputated limb and restoration of the its biomechanical unity after serious hand or forearm injuries is analysed and discussed with two case presentations. Methods of anatomy and surgery in these cases are not part of the everyday practice, the need for improvization during surgery is essential. Ischaemia-reperfusion time is also crucial when a limb has to be saved. The first case reports on the subtotal amputation of a young man's right hand and the successful revascularization and unorthodox restoration of the radiocarpal joint to full function. The second case is of a young woman with a conquassated left forearm. A special aspect in this case is the extremely long ischaemia-reperfusion time. Complete function was restored in this case too, however the patient's refusal of spongiosa-plasty resulted in the fatigue break of the fixation plate, that had to be replaced.

In traumatology it happens quite often, that serious decisions have to made by the operating table without the chance of consultation with colleagues and literature. The two presented cases might help to decide on treatment for those who meet similar cases in their practice.

Keywords: subtotal amputation; conquassation; ischaemia-reperfusion; revascularization; restoration of function

Introduction

Salvaging limbs injured as a consequence of the increasing number of industrial and traffic accidents is a real challenge for surgical teams (traumatologists, hand surgeons, plastic surgeons). Microsurgical skills and the knowledge of necessary techniques allow the revascularization of partly or totally amputated limbs and nerve repair, up to date and continuously improved surgical techniques provide the appropriate care of bones, muscles, tendons and skin defects.

Improvements in surgical technique

Successful revascularization and replantation was made possible by the development of adequate techniques and instruments. Nylen introduced the operating microscope for ear surgery in 1921. Mass production of such microscopes was started by Zeiss in 1953. In 1960 Jacobson and Suarez adapted the operating microscope to the construction still in use, providing better focus, magnification and movement in multiple planes.

The surgical team headed by Ronald Malt performed the first successful replantation in 1962 in Boston. There is a report on successful finger replantation on Rhesus monkeys in 1965, as well as a literature account of the successful blood vessel anastomosis in an avascularized thumb. The first finger replantation was performed by Japanese Komatsu and Tamai in the same year.

In the 1970s replantation centers and microsurgical laboratories were established, and a critical analysis of results was presented. Technique and replantation protocols were refined in the 1980s. At that time the previous practice of nerve and tendon repair months after skeletal stabilization and restoration of blood vessel continuation was stopped. This idea led to today's practice, during replantation each structure is repaired one other the another at the same time.

Surgical technique

Getting the patient into the operating theatre has the ultimate priority. It is beneficial to have two surgical teams. (There is usually no chance for it in domestic conditions.) The amputated body part should first be taken to the operating table, structures should be thoroughly prepared, vessels and nerves suitable for anastomosis should be marked. It is the time to examine the blood vessels to decide whether the replantation could be carried out or not. The next step is the preparation of flexor and extensor tendons.

General or regional anaesthesia is applied to the patient. General anaesthesia is often supplemented with regional, so that peripheral blood perfusion increases. It is important to protect the patient against hypothermia. Then the stump is prepared, blood vessels, nerves and tendons are marked, while the amputated part is kept cold.

Ostheosynthesis follows the thorough preparation and debridement. Kirschner-wires are often used, however in the forearm fixation plates or fixateur extern are recommended.

The next step is the suture of tendons, usually extensors precede flexors, then microvascular anastomoses follow on the artery and vein. During anastomosis it is important to frequently rinse the lumen of vessels with diluted heparin solution, to minimize the removal of adventitia, to carefully grip the proximal and distal ends of blood vessels, to choose appropriate size, non-absorbable, synthetic, monofilament suture and when it is necessary to apply a venous graft to avoid decreased flow rate of the blood. The sequence of unification depends basically on the anatomical situation, literature resources are not uniform on sequence. Nerve suture is last. Skin should be closed without tension.

When replanting burlier limbs unification of arteries takes priority in contrast with veins to decrease the amount of muscle necrosis and to remove toxic metabolites that would otherwise enter the patient's circulation. Extensive fasciotomy is also needed.

Due to the repeated, mindful preoperative and intraoperative reconsideration and the development of microvascular anastomosis techniques, the success rate of replantations improved significantly by now.

Postoperative care begins on the operating table. Anticoagulation is provided with dextran, heparin, LMWH, or thrombocyte aggregation suppressors. Replanted (revascularized) limbs should be bandaged with extreme caution to avoid compression. Similar indication has the fasciotomy at the end of surgery. Loose bandage has to be applied, only the distal part of fingers must be uncovered. It is the place to check the limb's circulation and oxygenization. The limb can not be moved. Sedatives are often given to minimize vasospasm caused by psychic distress. The reduction of pain with appropriate analgetics is also important. The skin color, turgor and temperature has to be checked continuously. The room temperature has to be controlled, too.

Case presentation 1

In 1994 an 18 years old young man subtotally amputeted his right hand with a disc saw *(Figure 1)*. The hand was only attached to the arm dorsally with a piece of skin approximately 3 cm wide. The saw mangled the proximal carpal bones, scaphoid, lunate and triquetral as well as the surface of the radiocarpal joint in the radius. The radial and ulnar arteries, the median, ulnar and radial nerves and the complete flexor and extensor apparatus were damaged. The ambulance crew provided fluids, analgesia, stabilised the arm and transported the patient with pneumatic compression to avoid severe blood loss into our hospital after notifying the accident and emergency department. The transport time was relatively short from the accident site 35 kms from the hospital.

The time of injury was around 10:00 in the morning. The patient arrived to the hospital at 10:45, got into the operating theatre at 11:00. The time of total reperfusion was 13:00, the operation finished at 16:00 after each structure was reconstructed *(Figure 2)*.

The reconstruction of the carpal joint caused some professional dilemma during surgery. In cases of similar severity operation usually starts

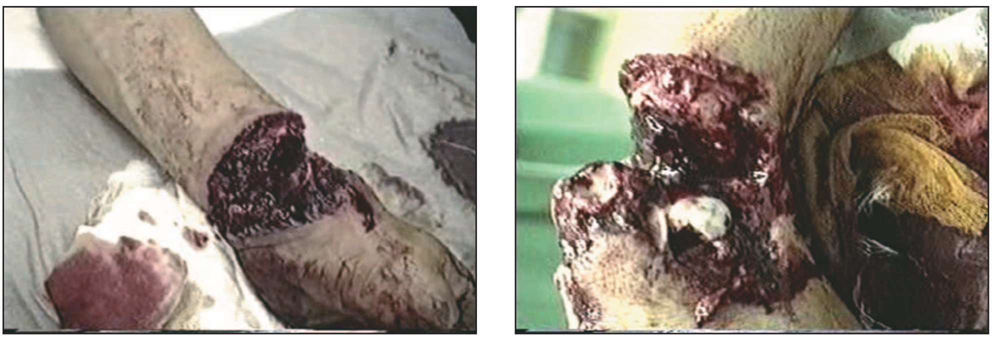

Figure 1. Images at the time of arrival to the hospital

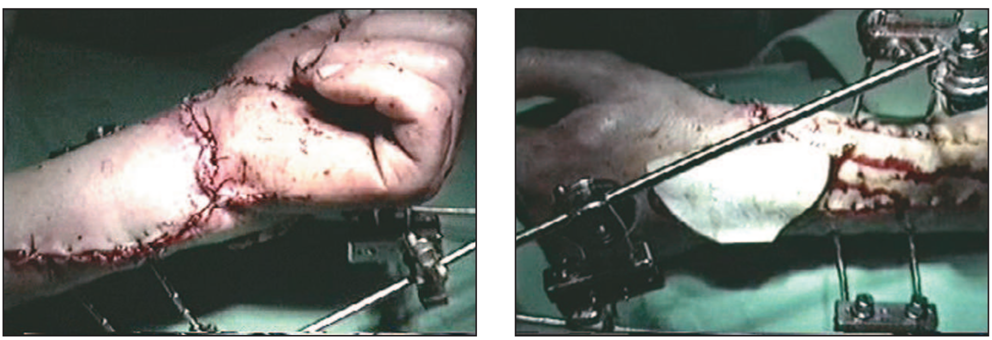

Figure 2. Postoperative images

with arthrodesis, as keeping the joint function is hardly possible. In this case an 18 years old young man was affected, whose wrist function we intended to reconstruct.

The distal carpal bones join the proximal row in an S-shaped arch which is convex proximally and concave distally, and its ulnar end is bulging towards distal, its middle part is domed intensely toward proximal according to the head of the capitate *(Figure 3)*. The joint capsule of the radiocarpal articulation is strengthened by a tight, strong system of ligaments (lig. radiocarpeum palmare et dorsale, lig. ulnocarpeum palmare) *(Figure 4)*.

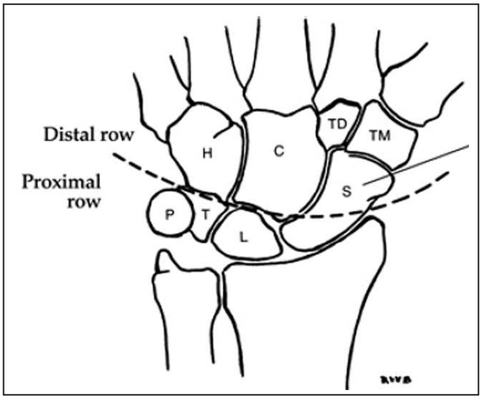

Figure 3. Bones of the radiocarpal joint[1]

The radiocarpal or wrist joint is an ellipsoid joint with two axes formed by the radius and the articular disk proximally and the proximal row of carpal bones distally. The complex movement of the minor articulations could best be observed under a fluoroscope. The splitting of such a structure can have serious consequences both statically and biomechanically. In this case the loss of the proximal row made reconstruction possible, as the disc saw injured major blood vessels, nerves, tendons and soft tissue with a loss of 1–1,5 cm. After a thorough debridement the defect of the joint surface of the radius was detected, as well as a distal piece of the scaphoid. It seemed obvious to use this piece of bone to form a „pin", that was inserted into the pit in the radius *(Figure 5)*. This „biological pinned joint" functions well even now and the hand regained its biomechanically important role *(Figure 6)*.

Considering the weak blood supply of the scaphoid we were afraid of a necrosis in the short run, not to mention the chance of early arthrosis. That is why a fixateur extern was applied at the end of surgery, however it was a technically more complicated fixation method. After restoring blood circulation the wrist stabilizers were cared for, it was possible to rein-

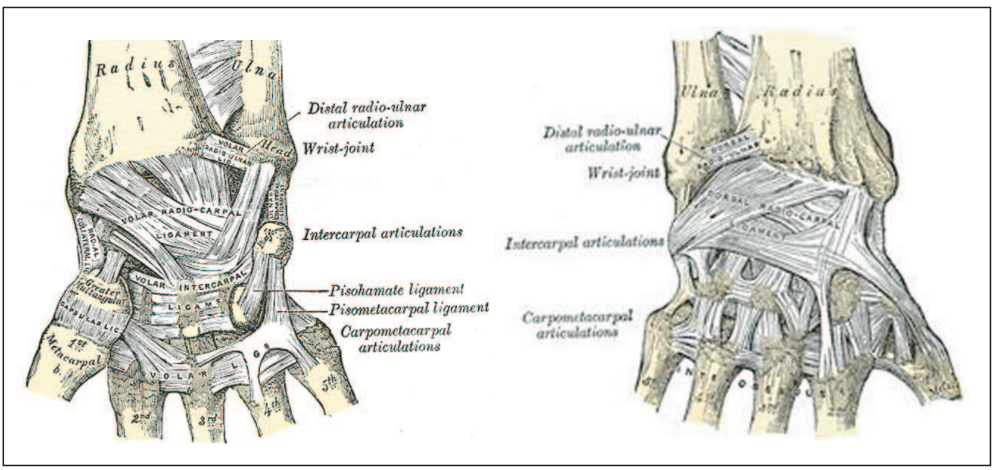

Figure 4. Ligaments of the radiocarpal joint[2]

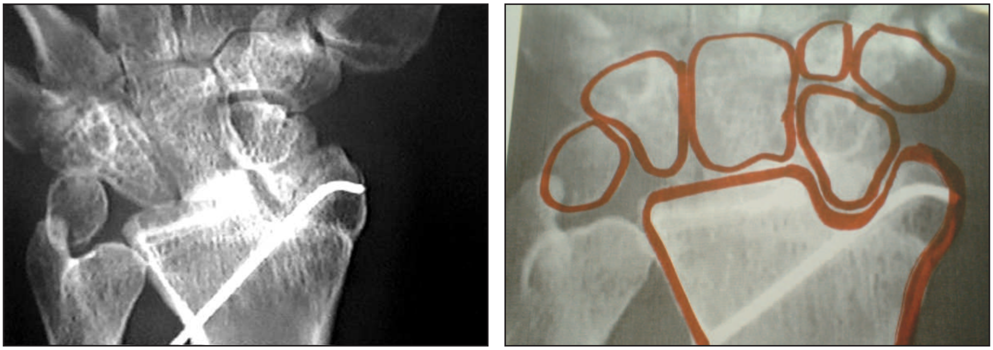

Figure 5. The scaphoid „pin" inserted into the radius

Figure 6. Early functional results

state musculus flexor carpi radialis and extensor carpi radialis longus by attaching them to the base of the 2nd metacarpal. All the other extensor and flexor tendons were systematically cared for and sutured. In this case nerve restoration and soft tissue correction were the final stage of surgery. Fortunately neither bone necrosis, nor early arthrosis did appear for as long as 15 years.

On the postoperative X-ray *(Figure 5)* it is apparent, that the distal carpal row fits well. Initially we had doubts about postoperative functional results because of the desorganization in the system of ligaments, still early physiotherapy began. Fortunately there was no septic complication. The wounds healed per primam. After early rehabilitation we were surprised how good the results were and how well the biomechanics of the hand returned *(Figure 6)*.

We were lucky enough to follow up the young man for many years, we were even able to control him 15 years after the injury in his home. The patient with the subtotally amputated

Figure 7. Late functional results

hand works now as a heavy machinery mechanic. Not just the quality of feeling and function returned, but he is able to lift heavy objects and perform hard physical labour *(Figure 7)*.

Case presentation 2

A 25 years old young woman had a road traffic accident, hit a crash barrier on the highway, the broken pieces of which conquassted her left forearm *(Figure 8)*. She was transported to the regional hospital, then to other institutions, everywhere amputation was recommended.

The diagnosis was as follows: conquassatio antebrachii sinistri, laesio arteriae radialis et ulnaris sinistrae, laesio nervi mediani, ulnaris et radialis rami muscularis sinistri, laesio musculi flexoris et extensoris digitorum antebrachii sinistri, defectus cutis antebrachii sinistri.

The accident happened at 19:40 2001-11-07, the patient arrived to our hospital the next day at 00:22, and about two further hours later reperfusion was ensured. The ischaemic duration was 6 hours 42 minutes. The extensive conquassated forearm injury involving skin and bones provided a professional challenge.

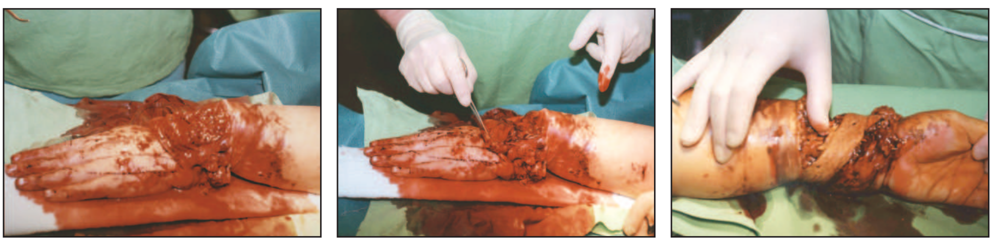

Figure 8. Preoperative images

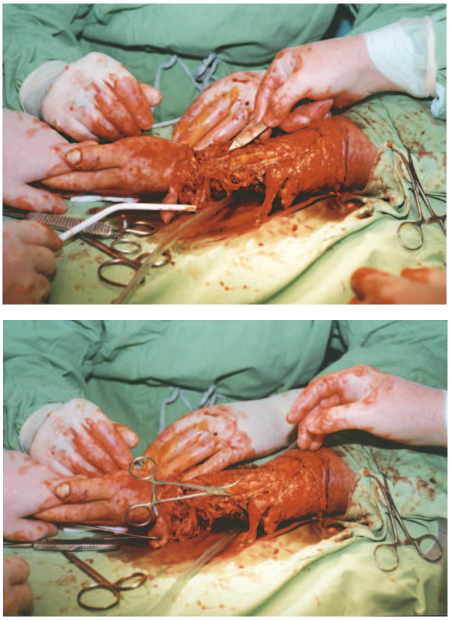

Figure 9. Intraoperative images after plate fixation

Because of the long ischaemic period we had to endeavor a quick solution, so that we could restore arterial circulation as soon as possible.

The extent of conquassation was such, that the identification of bones became very difficult. After fixation plate placement *(Figure 9)* the smaller and larger bone defects were clearly visible, but this problem had to be taken care of at a later date, because the restoration of arterial circulation had absolute priority.

In the postoperative period there was a – luckily superficial – septic complication, so after temporary debridements skin transplantation was performed using mesh-graft *(Figure 10)*.

Early spongiosa plastic surgery was planned to compansate for the bone deficit of the radius, however the patient rejected the operation based on her physical, psychic and familiar difficulties. After physiotherapy the hand's function was totally restored *(Figure 11)*.

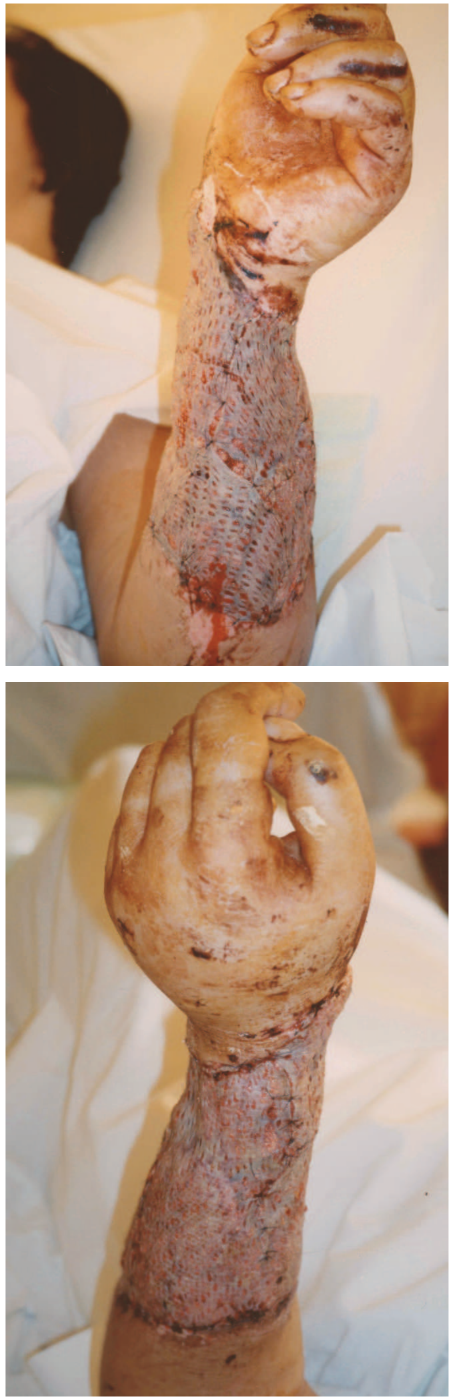

Figure 10. Mesh-graft

Figure 11. After physiotherapy the hand's function was totally restored

Based on the bone deficit the fixation plate's fatigue break was expected, and happened 7 years later *(Figure 12, on the left)*. Repeated reconstruction was also difficult, since the original fixation plate was placed atypically, so it was not possible to know the exact routes of blood vessels and nerves supplying the hand. Tightly and carefully following the metal we succeeded in changing the plate without further complications and spongiosa-plasty was also performed *(Figure 12, on the right)*.

After repeated rehabilitation and physiotherapy final results are almost complete function and a powerful hand, the young woman uses her left hand for everything in her everyday life, even for hard physical labour.

X-rays made in 2010 show the result of spongiosa plastic surgery, the pseudoarticulation disappeared, the radius became full *(Figure 13)*.

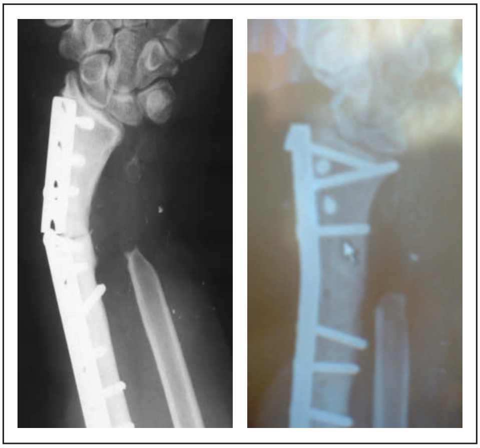

Figure 12. The broken and replaced fixation plates

Figure 13. X-rays made in 2010

Conclusion

Solutions at the operating table play an important role in majority of traumatological procedures, as in the two presented cases. There are no similar cases in textbooks, the surgeon has to improvise.

In the first case not even early surgical results were to be predicted, since quite a number of risks threatened the limb (thrombosis, septic complications, necrosis, suture insufficiency, etc.). Later on the necrosis of the scaphoid was to be expected, requiring early arthrodesis or resulting in early arthrosis, that did not happen. We were lucky with our atypical solution, that is why this method could be used in similar cases.

In our second case the gravest danger was the ischaemia-reperfusion time. The superficial septic complication is most probably a consequence of it, however the extreme contamination of the forearm might as well contributed. It was a mistake to go without spongiosaplasty, despite the fact that the patient kept on hoping that it will not be necessary. The fatigue fracture of the fixation plate was to be expected because of biomechanical reasons.

A surgeon thinks over and over a case and plans each treatment step in vain, if his original plan has to be changed later by the patient's will.

References

1. *Beasley RW.* Beasley's Surgery of the Hand. New York: Thieme, 2003.
2. *Gray H.* Anatomy of the Human Body. 1918. *(http://www.bartleby.com/107/)*

Miklós Szokoly
Péterfy S. Hospital and Trauma Center
H–1081 Budapest, Fiumei út 17.

Biomechanica Hungarica III. évfolyam, 1. szám

Survey among school-aged children with ultrasound-based motion analyzing system at two primary schools in Szolnok

Mária Takács[1], Ervin Rudner[2], Ildikó Juhász[2], Rita M. Kiss[3]
[1] MÁV Hospital, Department of Rheumatology
[2] MÁV Hospital, Department of Orthopedics
[3] Hungarian Academy of Sciences, Research Group of Structures
drtakacsmaria@freemail.hu

Abstract

Aim: The use of ultrasound based motion analyzing systems is harmless and has no side effects. They are applicable among healthy people and children as well. Since 2007 we have been surveying children who suffer from spine and foot deformities and participate in adapted physical education. With three-year experience we decided to broaden the scope of the survey. In September last year we started a survey among primary school pupils aged 6-10 with the goal to follow up their state. At first we examined the children's initial state when their usual annual medical examination was made at school. The survey is planned to take at least three years. During the survey we pay special attention to reveal spine and foot vault deformities at an early stage, because these deformities are most common in the age group and after discovery conservative therapy-based correction can be started without procrastination.

Material and Method: After the orthopaedic examination, we performed a static posture examination and sole pressure distribution examination among 210 pupils from the two primary schools. By analysis with the Zebris CMS-HS ultrasound-based system and using Win Spine program we defined the degree of dorsal kyphosis and lumbar lordosis, the total trunk inclination in the sagittal and frontal planes and the degree of scoliosis.

Results: Two children with innate locomotor disorders and a boy with neurological problems were excluded from the survey. Out of the remaining 207 children the orthopaedic examination found 75 healthy ones, 55 with bad back posture and 9 with flat back. 16 times the diagnosis was scoliosis, mostly functional but could be corrected properly. 53 children had no spine deformity but were positively flat-footed. Following the recommendation of the GKE 2008 annual congress, we divided each group into subgroups according to the degree of curvatures in the sagittal plane. Dorsal kyphosis between 30 and 60 degrees and lumbar lordosis between 30 and 40 degrees were considered normal. Because of this consideration the healthy group was not homogeneous, either. 37.3% of them had flat lumbar lordosis, 4% of them had flat lumbar lordosis and thoracic kyphosis, too. Among children with bad back posture these ratios were 50.9% and 3%, respectively.

Conclusion: Continuous control over different age groups makes it possible for us to search diagnosis-specific signs in the results of ultrasound-based motion analysis. The sign can be, for example, unbending of the curvature. The results of adapted physical education can be measured numerically. We can call the attention of teachers and parents for the need of posture correction built into physical education and everyday life.

Introduction

Medical literature describes children's low back and back pains as multi-factorial problems. The body mass index, the mobility and flexibility of muscles and joints, muscular strength, sports, the furniture in schools, heavy school backpacks, psychological factors and smoking – although in different ways – play an important role in children's spine development[3]. In most cases, children's back pain experiences are mild and do not affect their daily life[2,5,6]. The number of complaints is always higher than the actual structural changes. Psychological factors play an important role in children's back pain[2]. Low endurance of trunk flexors and extensors can lead to abnormal posture, which condition later becomes permanent and leads to health problems[7]. Data in the medical literature prove that back pain reports in childhood and early adolescence are significantly related to back pain in adulthood[2,8]. It is important to discover the reasons at an early stage, so the health problems can be cured in time and further complications can be prevented. Despite this demand, spine deformities in childhood are mostly without symptoms and for the lack of expansive orthopaedical examinations they are discovered late or are not recognized at all. Due to late discoveries, the efficiency of cures is behind expectations, and many times spine anomalies in adulthood are the results of health problems not revealed in childhood. Even a simple bad posture can play a great role in the evolution of a secondary degenerative process. At pupils between the ages of 6 to 10 the required muscular development often lags behind the quick height increase. Diagnosis at an early stage followed by appropriate correction is the first step towards prevention. The use of screening makes it possible to establish an exact diagnosis and to start conservative therapy at the earliest possible moment. With the survey our goal was to reveal and record the spine conditions and the back postures of children between the ages of 6 to 10 and to demonstrate the existence of foot deformities. Using the Zebris CMS-HS system's Win Spine program we received static pictures of the children's spines, and pedographic examinations indicated us the deformities of the foot.

Material and method

The subjects of our research were children from two primary schools in Szolnok from the first to the fourth grades, and it concerned one class from each grade. 210 children were examined; out of them, 4% were six years old, 25% were seven, 29% were eight, 25% were nine and 18% of them were ten years old. Three children's data were removed. Two of them had a genetic defect and congenital neurological anomaly, which influenced the organs of locomotion. At the third one, we found a complex hip, knee and ankle disorder which had a role in spine deformity. After the orthopaedic examination every patient was measured by the CMS-HS system to investigate the shape of their spine and a foot pressure distribution measurement was also performed by the pedograph. When it was required we used X-ray as well. The system consists of a central unit, an ultrasound transmitter, a personal computer and a pointer *(Figure 1)*. The emitters are built

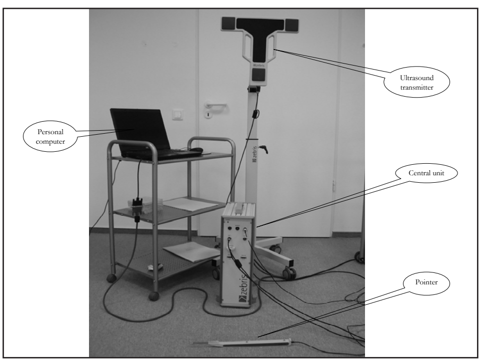

Figure 1. Ultrasound transmitter, Pointer, Central unit and PC

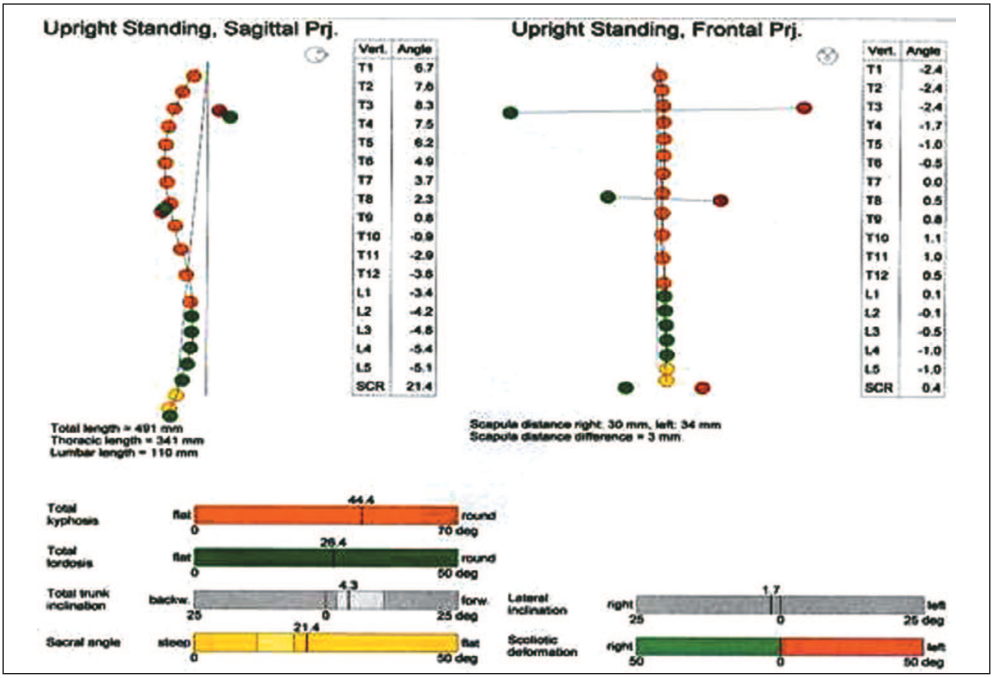

Figure 2. Graphic and numerical data in the sagittal and frontal planes

in the three ends of the T-shaped head of the transmitter in one plane. The pointer contains 2 microphones. By the pointer the anatomical points and the spine can be determined.

The distance between the head and the sensors is calculated in the knowledge of the speed of ultrasound and by measuring time. With the help of the space coordinates of emitters and of the microphones the space coordinates of the determined anatomical points can be calculated. The printed medical report shows numerically and graphically the degree of the dorsal kyphosis, the lumbar lordosis and the scoliosis and the total trunk inclination in the sagittal and frontal planes *(Figure 2)*.

The pedograph has five sensors in each square centimeter. During a 10-second foot examination we received information about the distribution of weight at the left and right legs, back and fore foot *(Figure 3)*.

Results

Without considering the age groups, 36.2% of the patients were healthy *(Figure 4)*. 26.6% of the children had bad posture and 7.7% of them had scoliosis. The flat back was the rarest with 3.9%. 25.6% of them had no spine deformity but a flat foot. In conclusion, it was established that 61.8% of the children had no spine problems at all.

Diagnosis of flat foot with other problems were common in 40.1% out of the total amount of subjects. Flat foot occurrence was 50% among 6-year-olds, which is not surprising *(Table 1)*. The medical arch does not develop until the sixth to tenth year of life. This decreasing tendency is clearly visible till the age of nine, but from that point the tendency veers round.

When diagnoses are analyzed according to age groups it is evident that bad posture can be

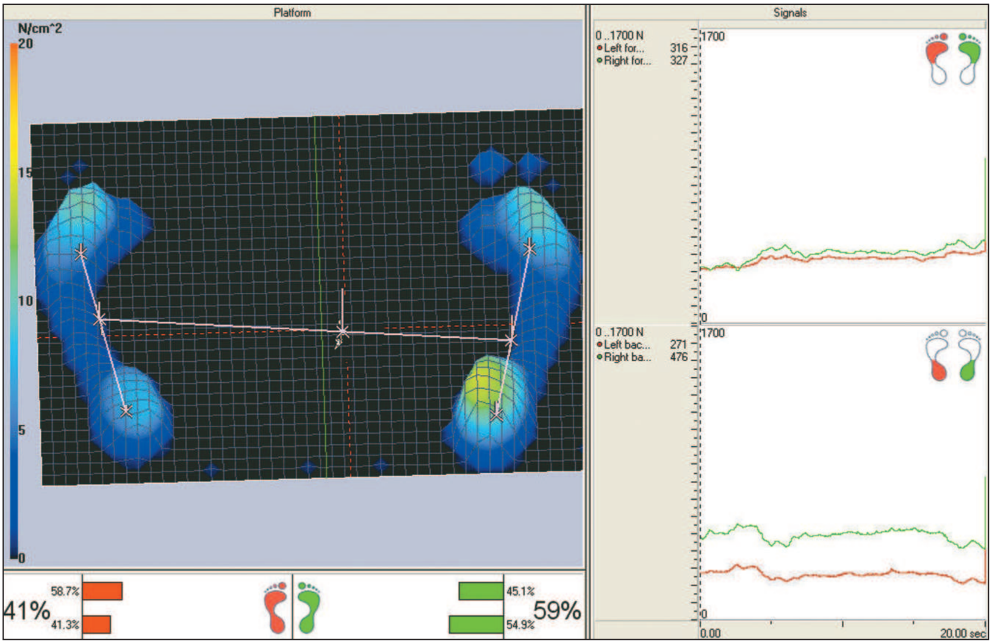

Figure 3. Medical report of the pedograph

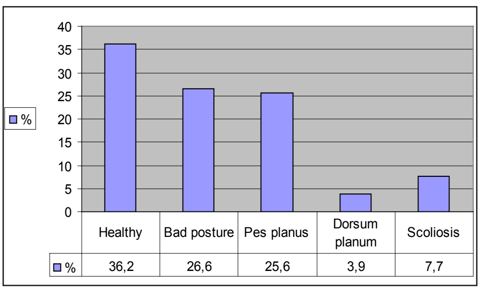

Figure 4. Diagnosis distribution without considering age groups

	6 year	7 year	8 year	9 year	10 year
Flat foot (person)	4	22	12	28	17
%	50%	43%	20%	54%	46%

Table 1. Flat foot according to age groups

	6 years	7 years	8 years	9 years	10 years
Healthy (%)	12.5	33.3	54.2	25	32.4
Scoliosis (%)	0	2	6.7	7.7	16.2
Bad posture (%)	62.5	33.3	22	25	21.6
Flat back (%)	0	5.9	1.7	5.8	2.7
Flat foot (as individual clinical picture) (%)	25	25.4	15.3	36.5	27

Table 2. Diagnosis distribution according to age groups

found in every age group, but it is more frequent among 6-year-old children *(Table 2)*. The age group of eight-year-old children included the healthiest subjects. Scoliosis was always functional.

Following the recommendation of the 2008 GKE congress, we considered dorsal kyphosis between 30 and 60 degrees and lumbar lordosis between 30 and 40 degrees to be normal *(Figure 5)*. Subgroups were created accordingly for every diagnosis. From the eight possible subgroups only three were found as real categories. The occurrence of flat lumbar lordosis was the highest in the groups of flat-footed, bad postured and healthy children.

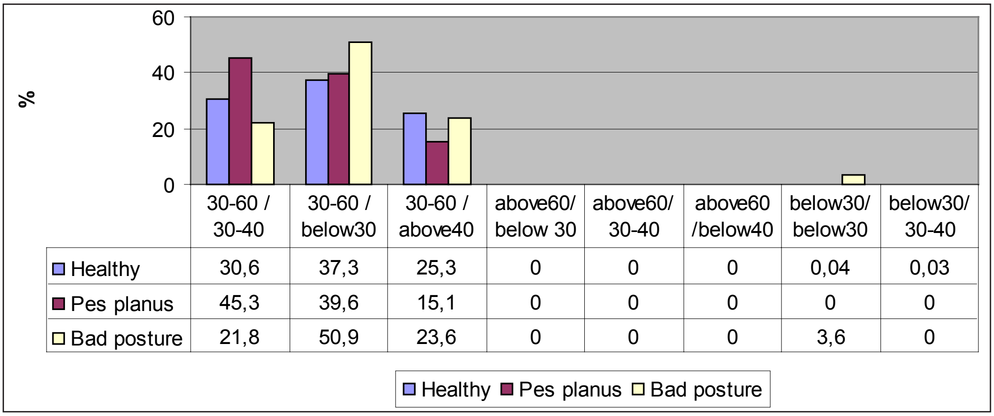

	30-60 / 30-40	30-60 / below30	30-60 / above40	above60/ below 30	above60/ 30-40	above60 /below40	below30/ below30	below30/ 30-40
Healthy	30,6	37,3	25,3	0	0	0	0,04	0,03
Pes planus	45,3	39,6	15,1	0	0	0	0	0
Bad posture	21,8	50,9	23,6	0	0	0	3,6	0

Figure 5. Subgroups according to thoracic kyphosis and lumbar lordosis

Discussion

With the survey among schoolchildren we wanted to turn attention to the importance of screening of the organs of locomotion. The main characteristic of posture problems is that in the ages examined they do not generate complaints, but later on they can lead to several rheumatological and orthopaedic problems.

The other main characteristic is easy remedy. With more care, children are able to correct a part of sagittal problems, but cannot hold them back permanently. That is why special attention and strengthening of the trunk's musculature are so important. Beside physical education, regular trainings for good back posture are essential. Children with scoliosis require individual exercise programs. Adapted physical education at school is also important to develop the appropriate muscular strength, which doubles the effect of exercise programs. The cure of children with spine deformities is more efficient when it is backed from several sides. The search for foot deformities is just as important as the examination of the spine. In these age groups, foot problems can be corrected by special physical exercises.

References

1. *Geldhof E, Cardon G, Bourdeaudhuij I De et al.* Effects of back posture education on elementary schoolchildren's back function. Eur Spine J 2007; 16:829–839.
2. *Geldhof E, Cardon G, Bourdeaudhuij I De, Clercq D De.* Back posture education in elementary schoolchildren: a 2-year follow-up study. Eur Spine J 2007;16:841–850.
3. *Cardo G, Balagué F.* Low back pain prevention's effects in schoolchildren. What is evidence? Eur Spine J 2004;13:663–679.
4. *Kratenová J, Zejglicová K, Maly M, Filipová V.* Prevalence and risk factors of poor posture in school children in the Czech Republic. Journal of School Health March 2007;77(3):131–137.
5. *Jones MA, Stratton G, Reilly T, Unnithan VB.* Biological risc indicators for recurrent non-specific low back pain in adolescent. Br J Sports Med 2005;39:137–140.
6. *Jones MA, Stratton G, Reilly T, Unnithan VB.* A school-based survey of recurrent non-specific low back pain prevalence and consequences in children. Health Educ Res 2004;19:284–289.

7. *Salminen JJ, Erkintalo M, Laine M, Pentti J.* Low back Pain int he young a prospektive 3 year follow-up-study of subjekts without low-back-pain. Spine 1995;20:2101–2107.

8. *Brattberg G.* Do pain problems in young school children persist into early adulthood? A 13-year follow-up. Eur J Pain 2004;8:187–199.

Mária Takács
MÁV Hospital Department of Rheumatology
H–5000 Szolnok, Verseghy u. 6–8.

Biomechanica Hungarica III. évfolyam, 1. szám

Analysis of the mechanical behavior of discrete elements in fluids (from the continuum to the discrete)

Brigitta Krisztina Tóth, Imre Bojtár
Department of Structural Mechanics
Budapest University of Technology and Economics (BME)
brigitta.toth@mail.bme.hu

Keywords: motion of red blood cells; stresses of artery-walls; continuum modelling; discrete element method; endothelium cells

1. Introduction

In the last few years there is increasing interest in numerical models of human blood vessels. The new computer-based systems can help already to come to a decision, if it is necessary to operate a diseased segment of a blood vessel, and if it is so, how urgently.

In the past years I have measured material parameters for different constitutive models of human artery vessels, and in the course of this work the medical doctors raised a very interesting issue: *is it possible to give an estimation* with engineering models, what *collision-forces* are effected in the endothelium cells – covering the vessels wall – from the red blood cells floating in blood plasma arteries? The question is important from biomedical point of view, because the endothelium cells work in some respect as a *"switchboard",* they transfer these internal forces as commands for different biochemical reactions of a segment of vessels. The solution of this problem could help to understand the physiological processes of artery wall.

To understand this problem from engineering point of view we have to know that arteries can be modelled like tubes – with elastic wall –, in which the flowing liquid is the so called blood plasma, and the different bigger-size cells – amongst all in largest number the red blood cells – move in this plasma. The volume percent of the cellular fraction is greatly significant, so we have to examine a relatively densely "filled" fluid. The solid particles can bump with each other or with the vessels wall in the course of their motion in the fluid, and the question is exactly, how can we describe this motion and how can we calculate the contact forces during these collisions?

I would like analyze what kind of numerical model is able to examine this effect of red blood cells streaming in the different type (size) of human arteries. I evaluated in a critical analysis those numerical models, which are used in fluid mechanics nowadays, mainly examined from that point of view, how fare are they able to model the mechanical effects of solid particles floating in blood plasma. I do also computational simulations on different models held suitable – and run-able by me, of course – to calculate collision forces of cells. I have a look at separately those special cases, when the diameter of the examined artery is so small, that the red blood cells pass through them only one after the other. In such cases the mechanical effect on the vessels wall is special, it doesn't refer to the direct collision, it refers to the change is pressure produced in the course of the flow.

We would like to note that this task of biomedical problem has a great number of analogous associate in many field of the life. For instance I can mention different examples: the rock masses transported by stream of lava, as well as ice-floes break off a glacier and travelling in a river, or an alternative, typically analogous task is for example the investigation of solid slime diluted with liquid and streaming in pipes, etc. It is worth mentioning, that can be found engineering-like examples to the analysis the influence of collisions also: the ice-floes bumping against a body of a ship or a river-pier of a bridge, or forces exerted by other solid bodies require similar mechanical investigations, like I need in the solution of my work.

The complex biomechanical analysis of arteries – generally speaking the solution of coupled problems in different numerical techniques – can be solved essentially in two different ways. The one is the *continuum-base modelling,* which can occur by any *FEM* (Finite Element Method) + *CFD* (Computational Fluid Dynamics) software. I note that we have the possibility to investigate also the time-dependent analysis of bigger-size arteries with these types of modelling, since we can keep the cellular elements circulating in blood only as infinitesimal particles. But in another domain of scale, what I want to model too, the effect of the particles having extension is greatly significant. Otherwise there is an interesting question: how can we take into account the presence of cellular elements with the method referred to above, in other words till when can we increase the rate of particles "theoretically" considered in current flow, how many percent of volume occupy those? It is important to note also that at present times further researches exist, which have the aim to expand the applicability of continuum-based modelling to the modelling of particles, too. These are called *"modified finite element methods"* (see the works of *Oñate* and *Liu*).

The alternative practicable analytical method is the so called *Discrete Particle Method* (DPM), which is able to treat the large-sized particles as really independent bodies. Although the behaviour of particles moving in the artery can

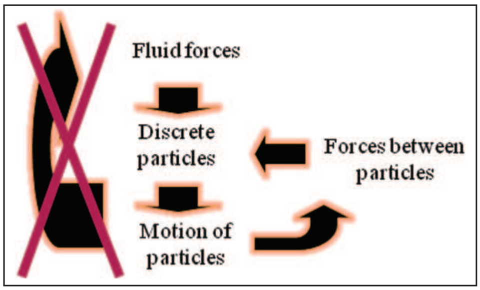

Figure 2. The flow chart of the traditional discrete element method: the motion of particles don't have a reaction on the fluid

Figure 1. Examples to "large-sized" discrete particles in streaming substance: stream of lava, glacier, red blood cells

be modelled with this method, moreover the fluid-forces can be added to the particles, a question arise: have these particles – cellular elements – a reaction on the circulating fluid surrounding them? The answer is of course, that the influence between the liquid and the body attending in continuum medium is mutual; the body has an influence on the relationship of circulation. In our opinion we ought to connect the pure discrete element modelling and the continuum-based fluid mechanics if we want to describe the required problem. Our answer is simple at first sight that we have to consider only *Newton's III. law* of motion what declare the law of action-reaction. Unfortunately this is not so easy, new developments must introduce in this field of science, like for instance the coupled new PFC3D, which connects the program based on the discrete element method with the CFD module.

2. Methods

2.1. Continuum model of particles moving in fluid

The *Computational Fluid Dynamics* (CFD) is suitable to model the behaviour of streaming fluids, heat-transfer or any other complex processes (see *Ferziger et al.*[7]). The CFD solves the equations describing the behaviour of fluid on the investigated domain, and can take into account the prescribed boundary and initial conditions on the domain (see *ANSYS CFX Theory Guide*[1]).

We can talk about multiphase flow in those cases, if more than one fluid is presented. Fluids can occupy independent regions which can partake in the same area of the fluid. The flow consisting of several components is different from these phenomena of course.

There are two available well defined fluid-models: the *Euler-Euler multiphase model* (see *Enwald et al.*[6], *Manninen et al.*[10]) and the so called *Lagrangian Particle Tracking* model. See applications and summaries in *Casey et al.*[3], in *Lun et al.*[9], in *Menter et al.*[11] and in *Clift et al.*[4].

In the next I will talk about the modelling of particle transport. The so called *Particle Tracking* model is able to describe dispersed phases, which appear discretely dispersed in the continuum substance. This model contains the independent calculation of the discrete particles with the essential conditions considering the effect to the continuum, which is made by the particles. From view point of this paper, this includes the circulation of blood and the transported cellular elements in it, too. Thus, the particle transport is attached to the multiphase models, in which case the particles are followed *Lagrangian-manner* during the flow, instead of extra *Euler-phase* modelling. We can model the entire particle-phase by a ideal sample substituting the particles. The tracking of particles is possible by the help of the common differential equations (these equations refer to place, velocity and mass). If we combine these equations with the basic mechanical equations of particles we can describe the complex behaviour of the whole system.

If the fluid contains small particles, it means the injection of millions of particles in every second. Avoid the cost of modelling the whole particles; we have the possibility to inject particles representing the real number of the particles but fewer than that. We can prescribe how many particles have to denote the followed particles. Contrary to the Euler-type multiphase computation, the calculation protection of the continuum phase doesn't contain the volume fraction occupied by the particles. This means, that the model is valid only in case of *small volume fractions.* Moreover in that case, when the model is not reliable, the volume fraction of the particles can be greater than one.

Different diverse forces can cause the motion of a particle in the fluid. We have to take into account the following forces at the equations describing the motion of particles: viscous, fluid *drag force,* buoyancy, virtual mass and pressure gradient forces, centripetal and *Coriolis-forces* in rotating frame of reference. The calculation of viscous drag forces is always important and essential. Apart from that buoyancy, what appears at one-phase flows, the difference between the densities of the particle and the continuous phase results in buoyancy too.

2.2. Discrete element modelling of particles in fluid

We can model the mechanical behaviour of complex systems composed of different particles with the help of the so called *particle-flow model.* Within the frame of this paper, if I use the word *"particle",* I don't think about the particle defined in mechanics, which has an extension negligible, and so it occupies a simple *"point"* in the place. In this paper I will always use the world "particle" as a body with *finite dimensions.* A discrete element model (see the theory from *Cundall et al.*[5]) consists of independent particles, which are able to move independently from each other, and they make interaction with each other only at contact points or by the side of their surfaces, respectively. In so far as we count particles to be rigid, as well as we consider finite normal stiffness in the course of contact problems, the mechanical behaviour of the system will be definable by the motion of particles and the interaction forces between particles (see details in *PFC3D Guide*[2]).

Newton's law of motion gives the basic relations between the motion of particles and the forces causing them. The system of forces can be in quasi-static equilibrium – in which case the motions are remarkably small – or can be so, what causes the flowing of the particles. A much complex behaviour can be modelled, if we allow the adherence of particles by the side of their contact points, up till the time as the forces between particles are in the neighbourhood of the so called contact stiffness necessary for opening the connection. In this manner tension forces can arise between particles, so contact problems among adhered blocks can be modelled too, and in this way there is the possibility of breaking blocks into smaller-sized elements.

In addition to the traditional domain of the particle-flow analysis, by this type of modelling there is a possibility to analyze the solid bodies by specified initial- and boundary conditions. In these models we can consider the solid body as a compact set composed of numerous particles. The stresses and strains can be considered as an averaged value inside a characteristic measurement domain.

All equations of motion have to satisfy for each particle. New connections can create and they can divide in the course of the calculation. The interaction between particles can be considered as dynamic process, in which course, an ambition of continuous equilibrium is noticeable by the help of the balancing of the internal forces. We can handle the dynamic behaviour with a numerical time-stepped algorithm, where the velocity and acceleration can be treated as constant in the individual time-steps.

The course of the solution is just the same, what the explicit method of finite differences applies in case of continuum investigations. The chosen time-step has to be so small, that the error in one time-step happens only by the direct neighbours of particles, so at all times we can determine the forces acting on a particle from the adjacent particles being interaction with it. Since the velocity of the expansion of disturbance is the function of physical properties of the system, we have to choose the time-step in that manner, that it fulfils the above mentioned condition. The application of explicit numerical method opens the door to simulate nonlinear contact problems of numerous particles, without extreme memory requirement or application of iterative solutions.

The *DEM* (Discrete Element Method) calculations apply in rotation *Newton's II. law of motion* to the particles and the force-displacement law to the contacts. Newton's II. law of motion serves for determination of motion derived from contact forces acting on particles and from body forces, while the force-displacement law makes the update of contact forces caused by relative displacements by contact points possible.

3. Results

The relation of artery's diameter to the size of red blood cells determines fundamentally the modelling of discrete elements (red blood cells) streaming in the continuum medium (blood). Since our main purpose is determinate the mechanical effect acting on the so called endothelium cells, we suggest the usage of different methods in the different domains of artery size.

3.1. Middle-large arteries

We begin with the investigation of the blood streaming in an artery having radius: $r = 1.5$ mm, because in this domain of size the red blood cells start to exert significant influence on the wall. We regard as suitable for investigation the *continuum-base modelling* of this domain of size of arteries. We have the foreknowledge, that only these arteries having "larger" diameter can be examined on the basis of pure continuum modelling, when the order

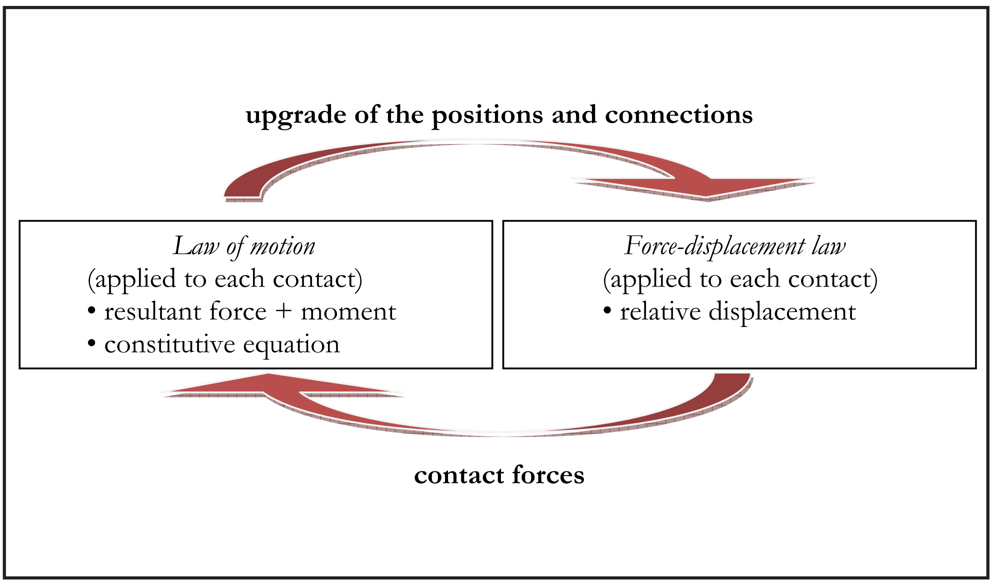

Figure 3. The course of the calculation

of magnitude of red blood cells diameter is not so significant considering the diameter of the blood vessel. We can model the sinker-like shape red blood cells as an particle having approximate diameter $d_{sphere} = 5.56 \cdot 10^{-6}$ *m*.

We want to find out the possibilities and limitations of the modelling by the so called *particle transport* method. The modelling of the whole particle phase in the continuum fluid occurs by the assistance of only a few tracking particles. The red blood cells constitute the predominant majority of the cellular elements flowing in the blood plasma, for this reason we have the primary goal modelling only these elements.

On the *Figure 4* – above on the left side – it can be seen the function of the inflow. We approach the physiological pulsating pressure with this function, which is perceptible by this size of artery. Next to it – to the right – the modelled schematic “artery-elbow” is visible. At the third position of the *Figure 4* it can be seen the path of the tracked particles, which zigzagged motion shows fairly the ability of bumping against each other. The colours of particles tracks signify their velocity. Finally on the fourth place of the *Figure 4* we can see the von Mises-stresses acting on the wall by the red blood cells. (Since this was a short time running of the program, the majority of the particles are still before the bend, for this reason the coloured plots are observable mainly at the entrance part of the artery.)

The so called hematocrit (Ht or HCT) or packed cell volume (PCV) or erythrocyte vol-

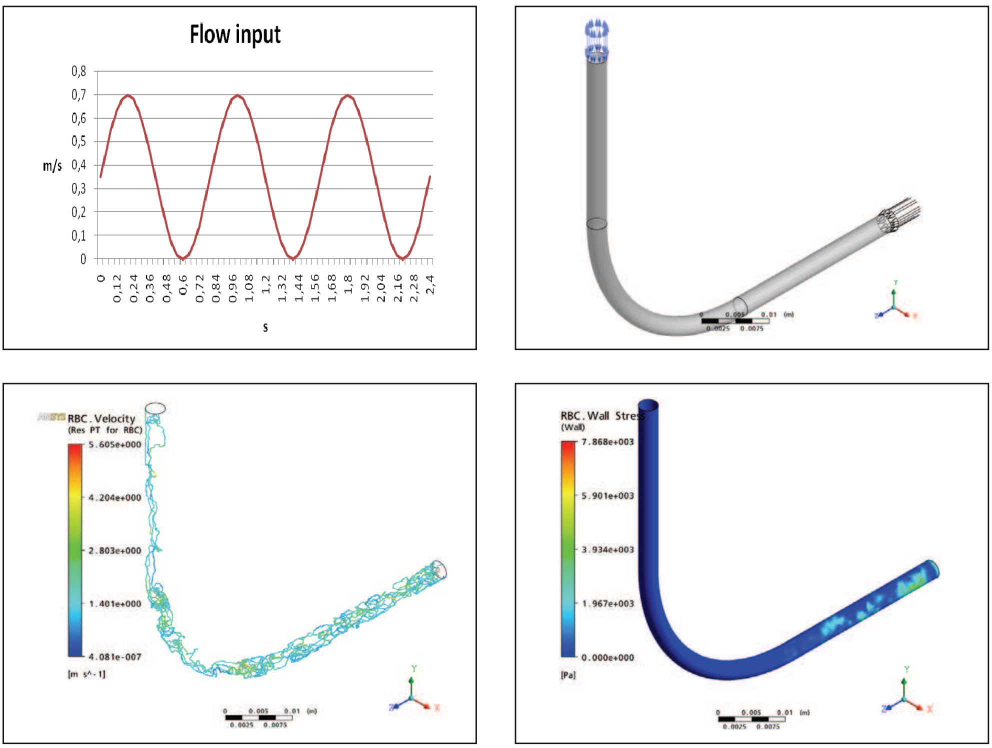

Figure 4. Flow input, schematic model of an artery-elbow, velocity of the tracked particles, wall stresses caused by red blood cells

ume fraction (EVF) is the proportion of blood volume that is occupied by red blood cells. It is normally about 48% for men and 38% for women in the physiological normal range. We had regard to this at the parameter calibration of the following pictures model. I note, that it is necessary to treat cautiously the obtained results, since the pure continuum-base modelling leaves out of consideration the dispersed particle-phase by equation of the continuum phase. Exactly therefore we recommend the application for liquids slightly saturated by particles.

3.2. Arterioles

At the domain of the *arterioles* (small arteries) – which can be considered as the "entrance-door" of the capillary vessels – the shape of the endothelium cells begins to play significant role. The endothelium cells covering the artery-wall are seen in the *Figure 5* below in blue colour, and their nuclei are distinctly visible as bulging in the lumen of the artery. It is observable on the *Figure 5* too, that these cells are in possession of internal stiffening. In the course of the collision of red blood cells to the wall, the endothelium cells give signals by the help of the cellular connecting-structures (modelled by five leglets, piece by piece of the endothelium cells, see also the *Figure 5*) as the results of the forces acting on their faces. These signals determine essentially the answers and reactions of the artery wall. On account of all these we propose the *discrete element method* to model this domain of artery-size. (See other application in *Li et al.*[8] and in *Tipthavonnukul et al.*[12])

On the above mentioned *Figure 5* you can see some results of simulation made by this method. The connected to one another yellow particles represent the "doughnut-shape" of the red blood cells. In the course of the discrete element modelling the red blood cells and the blood plasma are modelled by the help of particles. In so far if as we want to model the continuum phase with fine particles filling closely the entire range of the fluid phase, it will not give correct results, since we will observe the so called "tightness-symptom" of particles. No matter how we reduce the size of the particles modelling the continuum, the countable discrete particles will never substitute the continuum. This is why we advice the modelling the continuum phase only by a few distributed particles (see the small green particles on the *Figure 5*). This gives the possibility can take into account not only the effect of the continuum phase (green particles on the figure below) on the red blood cells (yellow particles on the figure below), but we have the chance to consider the back action, namely the effect of red blood cells on the continuum phase, too.

On the *Figure 6* we can see the forces arising from collision of the red blood cell to the under and to the upper wall. Red colour represents tensile forces and black colour shows the compressive forces. (A small tension is always present in the endothelium cell from the motion of the fluid.)

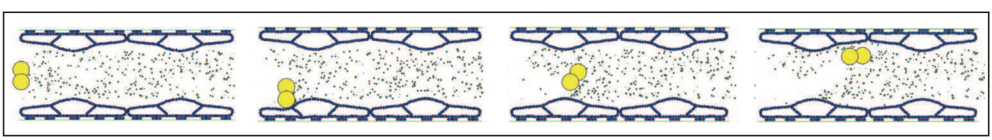

Figure 5. Motion of a red blood cell (yellow particle) in the blood plasma (representing green particles). The walls of the 2 dimensional artery consist of endothelium cells (blue cells with inner stiffening and with 5 leglets)

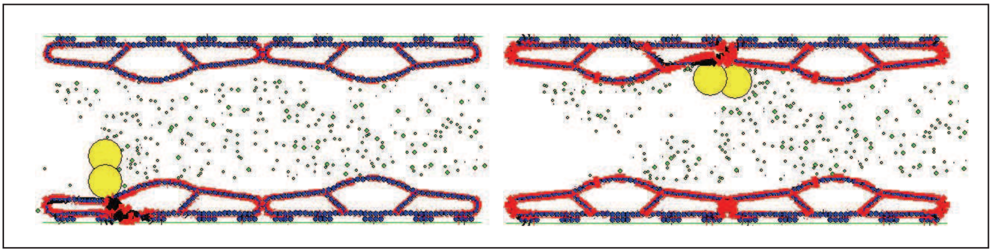

Figure 6. Collision of the red blood cell (yellow particle) to the under and the upper wall. Tensile forces are in red colour and compression in black

3.3. Capillary vessels

In the capillary vessels – smallest blood vessels – the size of the red blood cells can reach (in extreme case it can exceed, too) the diameter of the artery. In the present case it is no longer the collision of the red blood cells to the wall what mainly produce the reaction of the endothelium cells. The red blood cells march through the capillary *one by one,* and the shear forces arising by this motion acting the main role. On account of these we propose to return to the *continuum-based* modelling. We made a simplified mixed model to the investigation the effect of the red blood cells moving in the capillaries. In this model not only the continuum phase takes effect the particle inside it, but the back-action could be model also.

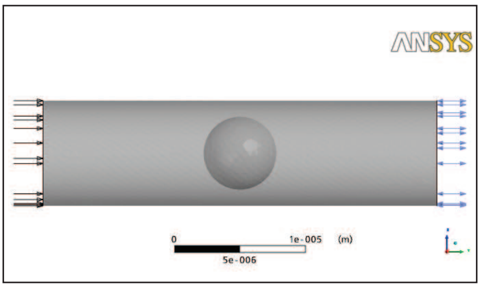

Figure 7. Geometry of a capillary vessel within a schematic red blood cell

4. Discussion

We have the aim to scientific investigate those domains of size of arteries, where the effect of the red blood cells on the wall is significant, and it is impossible to model the whole blood circulating in the blood vessels as continuum medium, thus we have to separate the blood to the plasma and to the cellular elements (mainly the red blood cells) streaming in it. We think different methods are suitable for modelling of different size of arteries. By the middle-large

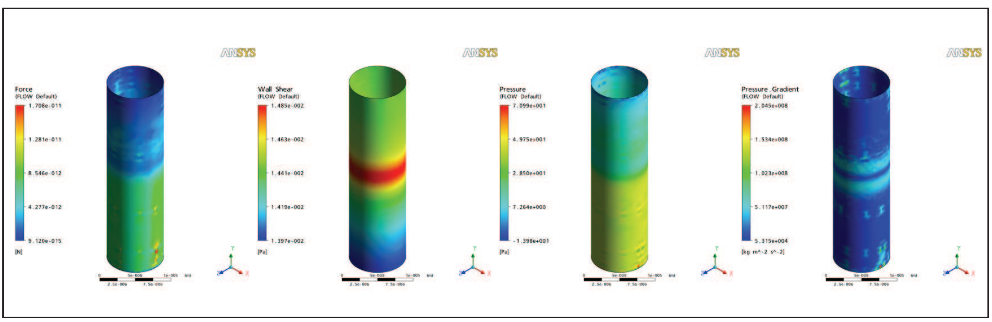

Figure 8. Results on the wall: Force, Wall shear, Pressure, Pressure Gradient

arteries repute convenient the continuum-based modelling, and inside this the so called particle tracking method. As soon as the tube-diameter size decrease and we reach the arterioles, the discrete element method gives the possibility to the modelling, and finally by the capillary vessels according to our suggestion is necessary to return to the continuum-based models.

References

1. ANSYS CFX-Solver Theory Guide. ANSYS CFX Release 11.0., ANSYS Europe, 1996–2006.

2. PFC3D, Particle Flow Codein 3 Dimensions, THEORY AND BACKGROUND, Itasca Inc.

3. *Casey M, Wintergerste W.* Best Practice Guidelines, ERCOFTAC Special Interest Group on Quality and Trust in Industrial CFD, Report, 2000.

4. *Clift R., Grace JR, Weber ME.* Bubbles, Drops and Particles, Academic Press, New York, USA, 1978.

5. *Cundall PA, Strack ODL.* A Discrete Numerical Model for Granular Assemblies, Géotechnique 1979;29:47–65.

6. *Enwald H, Peirano E, Almstedt AE.* Eulerian Two-Phase Flow Theory Applied to Fluidisation, Int. J. Multiphase Flow, Suppl., 1996;22: 21–66.

7. *Ferziger JH, Peric M.* Computational methods for fluid dynamics, Springer, Berlin.

8. *Li L, Holt RM.* Simulation of Flow in Sandstone with Fluid Coupled Particle Model. In: Rock Mechanics in the National Interest (Proceedings of the 38th U.S. Rock Mechanics Symposium, 2001 July; Washington, D.C.), Rotterdam: Balkema, 2001;1:165–172.

9. *Lun CKK, Savage SB, Jeffery DJ, Chepurniy N.* Kinetic Theories for Granular Flow: Inelastic Particles in Couette Flow and Slightly Inelastic Particles in a General Flow Field, J. Fluid Mech., 1984;140:223–256.

10. *Manninen M, Tavassalo V.* On the Mixture Models for Multiphase Flow, VTT Publications, 1996.

11. *Menter F.* CFD Best Practice Guidelines for CFD Code Validation for Reactor Safety Applications, Evaluation of Computational Fluid Dynamic Methods for Reactor Safety Analysis (ECORA), European Commission, 5th EURATOM FRAMEWORK PROGRAMME, 1998–2002.

12. *Tipthavonnukul S, Chan D.* Numerical Simulation of Granular Particles Moving in Fluid Flow. In: Discrete Element Methods: Numerical Modeling of Discontinua (Proceedings of the Third International Conference, 2002 September; Santa Fe), Reston, Virginia; ASCE. 2002;104–106.

Brigitta Krisztina Tóth
Department of Structural Mechanics
Budapest University of Technology and Economics (BME)
H–1111 Budapest, Műegyetem rkp. 3.

Retaining hand biomechanics in case of a hand tumor

Miklós Szokoly[1], Petra Aradi[2]
[1] Péterfy S. Hospital and Trauma Center
[2] Budapest University of Technology and Economics
szokoly@gmail.com

Abstract
The case of a patient with lung cancer is presented whose first metastasis was detected in the 5th metacarpal head. Hand metastasis in lung cancer is a rarity in literature. After the detection of the hand tumor treatment was sidetracked by representatives of other medical specialities. The growing tumor destroyed the 3rd, 4th and 5th metacarpals, thus based on DSA, MRI, CT, PET-CT and X-ray results and thorough planning of the surgical procedures only opposition and grip of thumb and index finger was possible to form. During surgery unexpected difficulties occured partly because of the condtion of tissues, partly because the tumor was infected. It was not possible to plan exactly before the procedure due to the nature of the tumor, and according to the hystological results, the metastasis was cleared only by 6 mm. It was possible to rescue the 2nd metacarpal with the atypical insertion of an AO-plate, so that the final statics of the hand was secured. The postoperative period proved to be reassuring, however due to the quick progression of the underlying disease the patient was lost.

Keywords: metastatic hand tumor; function preservation

Introduction

The hand as a biomechanical unit is extremely sensitive to any small changes that affect the fine motion of thumb and long fingers, especially when a radical amputation becomes unavoidable due to either traumatological reasons or a tumor.

In this case review the treatment of a 51 years old patient with a rare hand tumor is followed from detection, till the function preserving radical intervention, during which we wished to keep the most of the hand's biomechanical unit.

Case presentation

The 51 years old woman was treated with COPD in the local dispensary for lung diseases since 2003.

End of January 2009 she detected a painful swelling on her right hand, in the 5th metacarpal head. The routine X-ray showed a cystous osteolytic degeneration on the 5th metacarpal. She had an accident at work on 2009-02-03, when the same 5th metacarpal was injured. Based on the X-ray *(Figure 1)* a transverse fracture without dislocation just under the head of the 5th metacarpal was described, and a cystous disorganization the size of a small bean was mentioned.

In the beginning of February 2009 a needle biopsy, a repeated chest X-ray and an MRI examination *(Figure 2)* were ordered.

The hypothenar needle biopsy of 2009-03-11 showed small and larger groups of atypical, polymorph tumor cells with wide cytoplasma near the blood elements. Based on the shown image a carinoma metastatis was suspected, and further cytochemical examinations were suggested.

Figure 1. X-ray of right hand after the injury of 2009-02-03

Because of the patient's primary disease and a chest X-ray made in the local dispensary for lung diseases she was transferred to a pulmonology ward, where an exploration started to localize the primary tumor, during which a PET-CT examination was made *(Figure 3)*.

The PET-CT showed a 4×3 cm tumor in the left lower lung lobe with mediastinal and left axillary lymphnode metastases and two suspected 2×1 cm lymphnode metastases in the right armpit.

Oncologists recommended palliative irradiation for the right hand, and the hand metastasis responded well both radiologically and macroscopically. After this treatment the patient was transferred back to the pulmonology ward and lost contact with her hand surgeon. A bronchoscopic test proved the tumor to be malignant. From May 2009 the pulmonary adenocarcinoma was treated with chemotherapy, Gemzar+CDDP. During this period the hand tumor was gradually growing, and the painful, malodorous, loose lump became increasingly intolerable for the patient.

Due to the increasing hand pain the patient was directed to an ambulatory pain center in September 2009. She first came to our hospital in October 18, and based on the hand status *(Figure 4)* and X-ray *(Figure 5)* a repeated checkup was started.

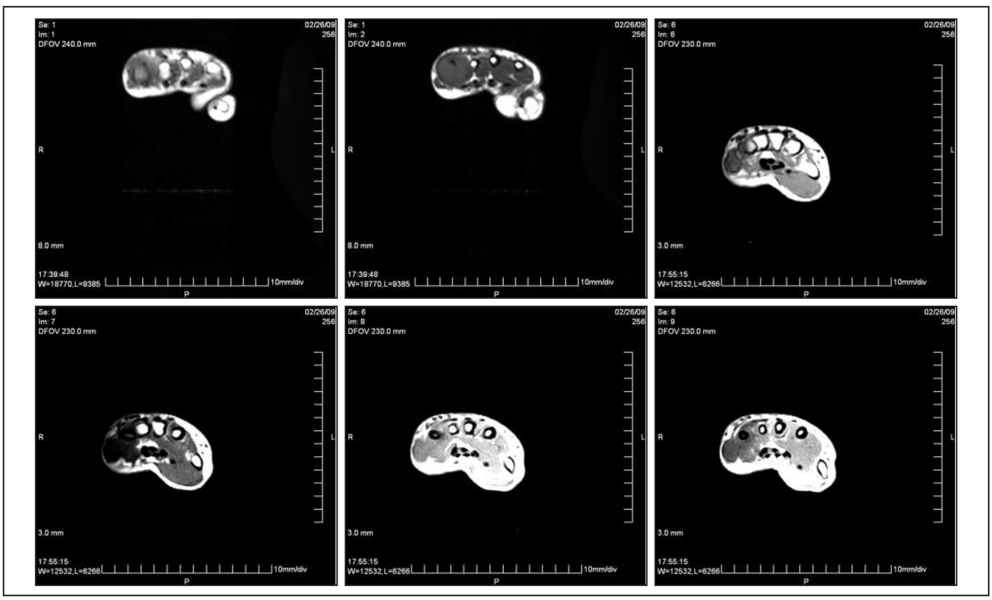

Figure 2. Right hand MRI images of 2009-02-26

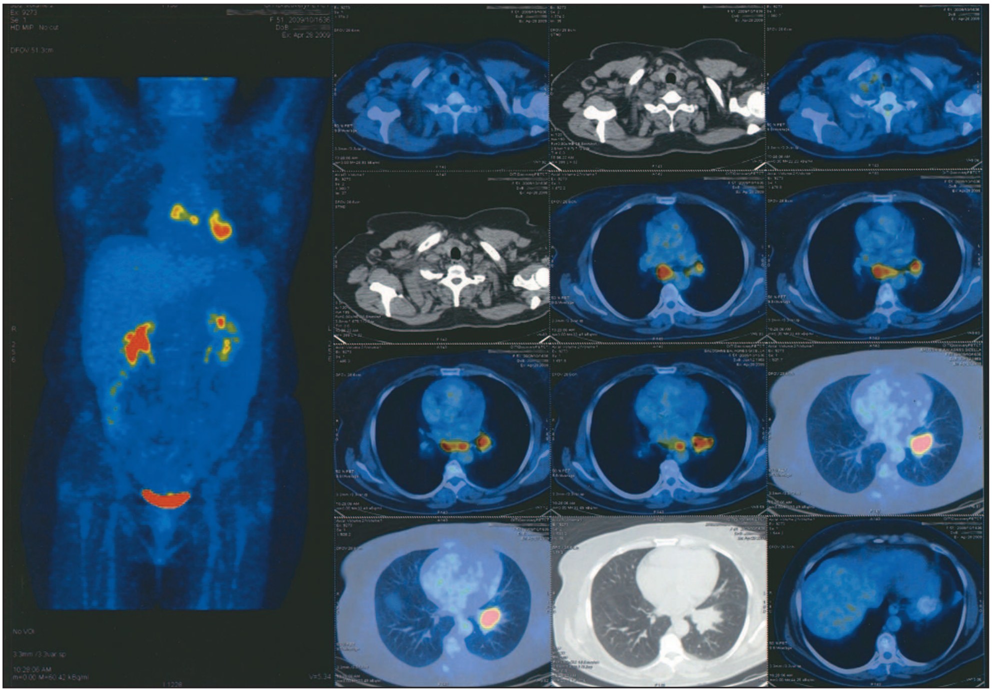

Figure 3. PET-CT images of 2009-04-28

Figure 4. Hand status of 2009-10-18

Compared with the X-rays of February 2009 *(Figure 1)* the new X-rays *(Figure 5)* show the tumor's spreading and the osteolysis.

During the new checkup series beacuse of the urgency a CT was made 2009-10-27 *(Figure 6),* while the cytostatic treatment of the lung tumor continued in the pulmonological institution.

Figure 5. X-ray of 2009-10-19

After the rapid checkup the patient was transferred back to the pulmonology ward where the cytostatic treatment went on. In the beginning of November the patient arrived in a severe septic condition to our hospital, beacuse the hand tumor became infected, disintegrated, malodorous *(Figure 7)* and made the life of not just the patient, but that of her family unbearable.

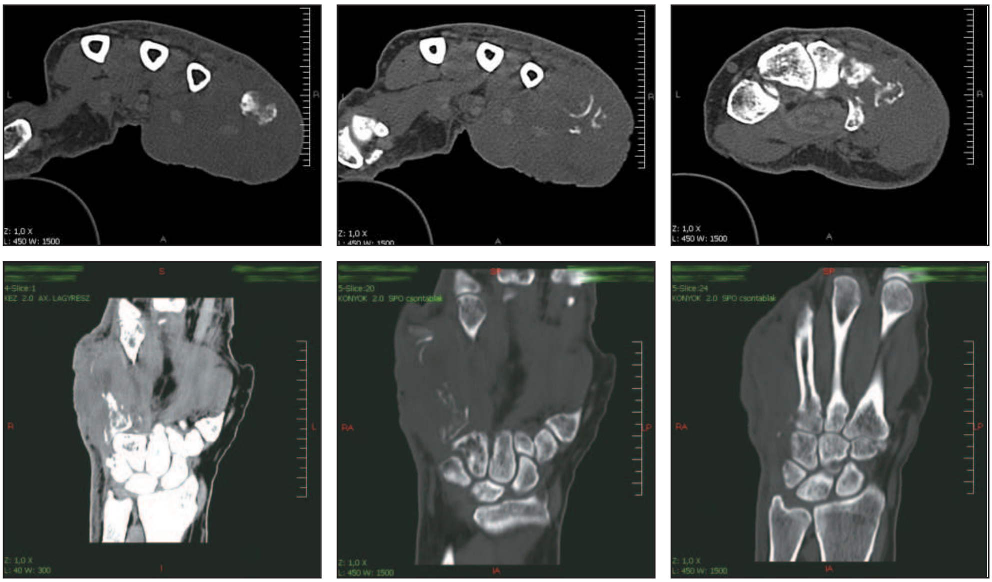

Figure 6. CT images of 2009-10-27

Figure 7. Hand status of 2009-11-03

When planning surgery it was imperative to assess the extent of the tumor and its blood supply, that is why further X-ray *(Figure 8)* and DSA *(Figure 9)* images were made.

According to the DSA results the brachial artery is moderately gracile, spastic, but with intact contours and the branches are retained. The antebrachial arteries fill normally. There are two incomplete arches on the palmar side. In the ulnar third of the palm there is an independent feeding artery coming from the distal

Figure 8. X-ray of 2009-11-13

Figure 9. DSA images of 2009-11-03

third of the ulnar artery towards the macroscopically visible bulge. In the bulge region there is a tumor-specific malformed blood vessel network. The arch of the ulnar artery is slightly deviated towards radial, however the width and route of the digital arteries leading to the ring finger are normal. There is no abnormality in the radial arch. According to the DSA results, it was suggested, that in case of no other contraindications, the middle finger might as well be saved.

According to the DSA findings there seemed to be a good chance to retain opposition and grip. However the surgeon might have to face quite a number of surprises during tumor surgery.

During surgery attention was paid to the stabilization of the radial side and the preservation of the motor apparatus *(Figure 10)*. To achieve it tendons of the brachioradial muscle, mm. extensor carpi radialis longus et brevis, mm. extensor pollicis longus et brevis, mm. extensor indicis longus et brevis and m. extensor pollicis longus, on the palmar side tendons of m. flexor carpi radialis, and flexor tendons, the small thenar muscles and mm. lumbricales had to be preserved.

Special attention was paid to the motor branch of the median nerve, and its direct sequel the digital nerves of the thumb and index finger, that originate partly from this trunk, partly form a separate branch *(Figure 11)*.

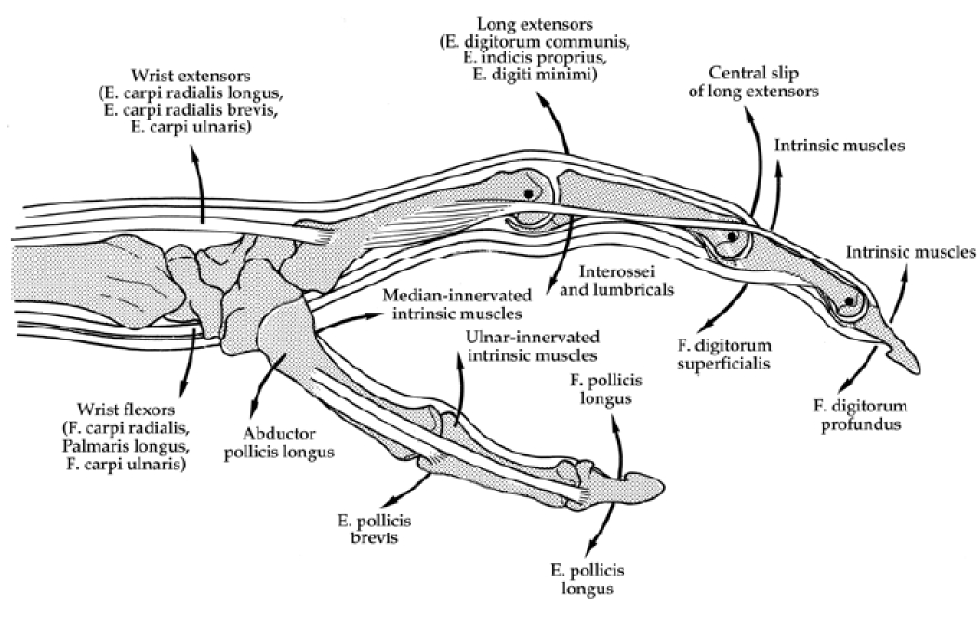

Figure 10. Radial side of the hand's movement apparatus[1]

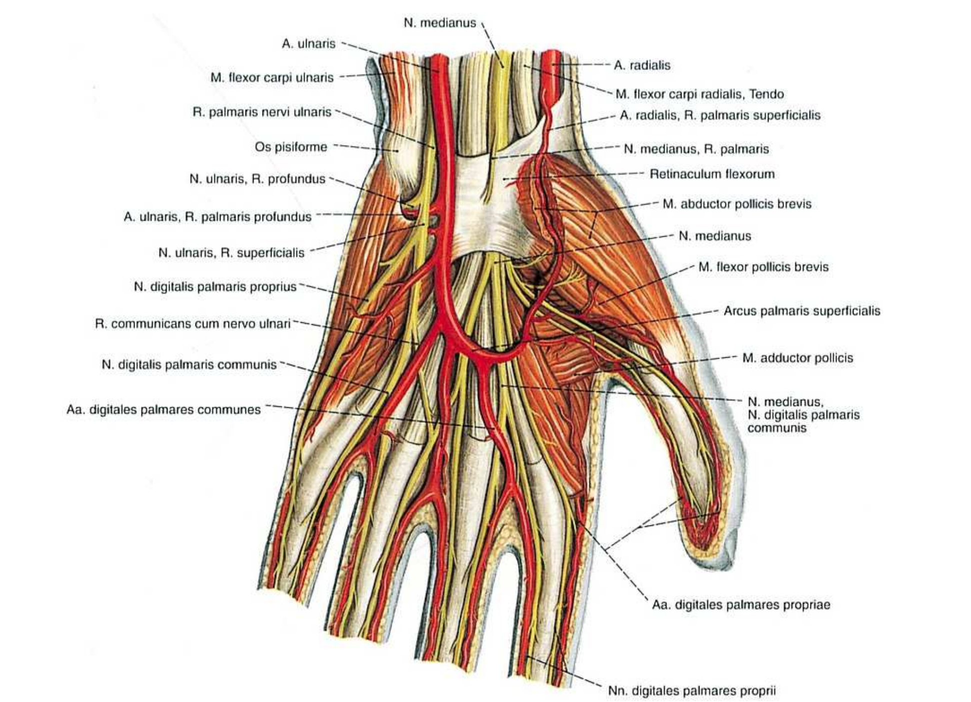

Figure 11. Nerves of the hand[2]

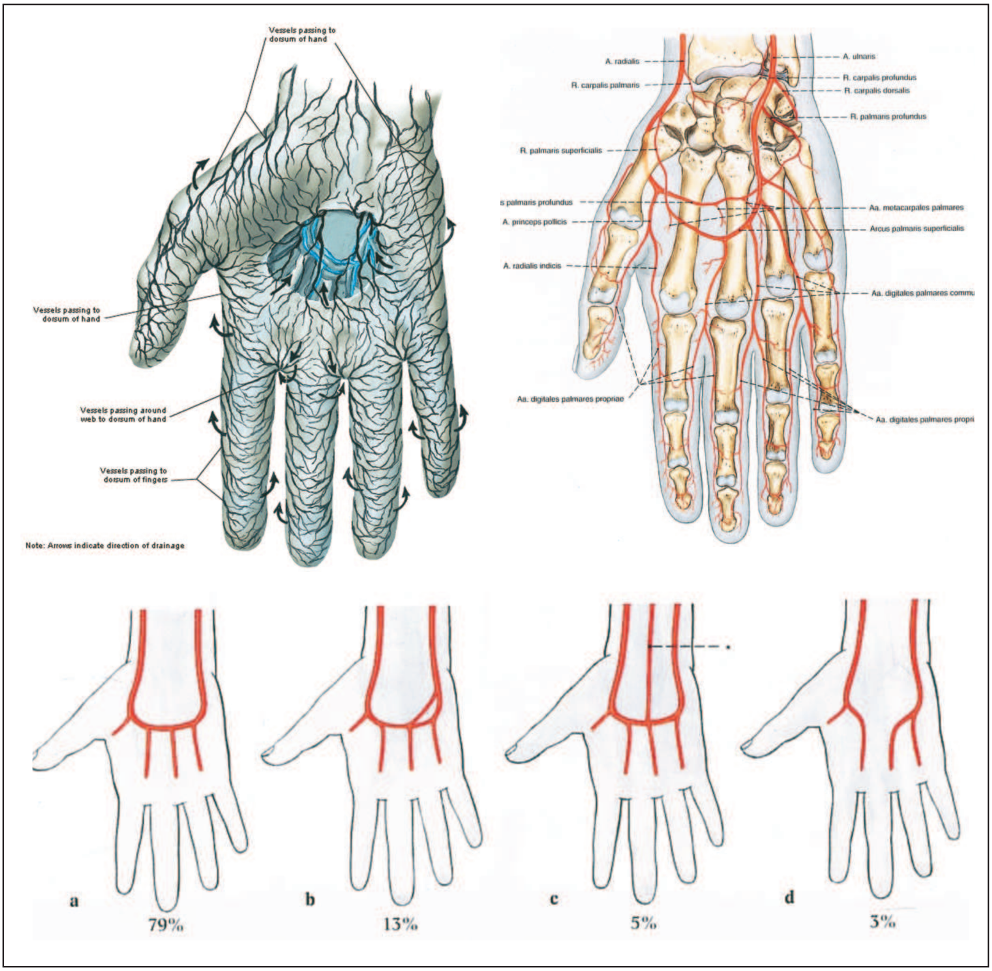

Figure 12. Anatomy of lymphatic vessels and arteries of the palm[2]

The superficial and deep palmar arterial branches had to be identified too, the latter having a large number of anatomical variations as shown in literature *(Figure 12)*.

Figure 13.
Postoperative X-rays of 2009-11-16
showing fixation

The surgery resulted in a resection that cleared the tumor by 6 mm, but left a huge skin defect. The thumb and index finger became unstable due to the size of the resection, that is why an atypically placed AO-plate was used to fasten them to the forearm *(Figure 13)*. The surgery *(Figure 14)* was concluded by using the middle finger as a fillet flap *(Figure 15)*.

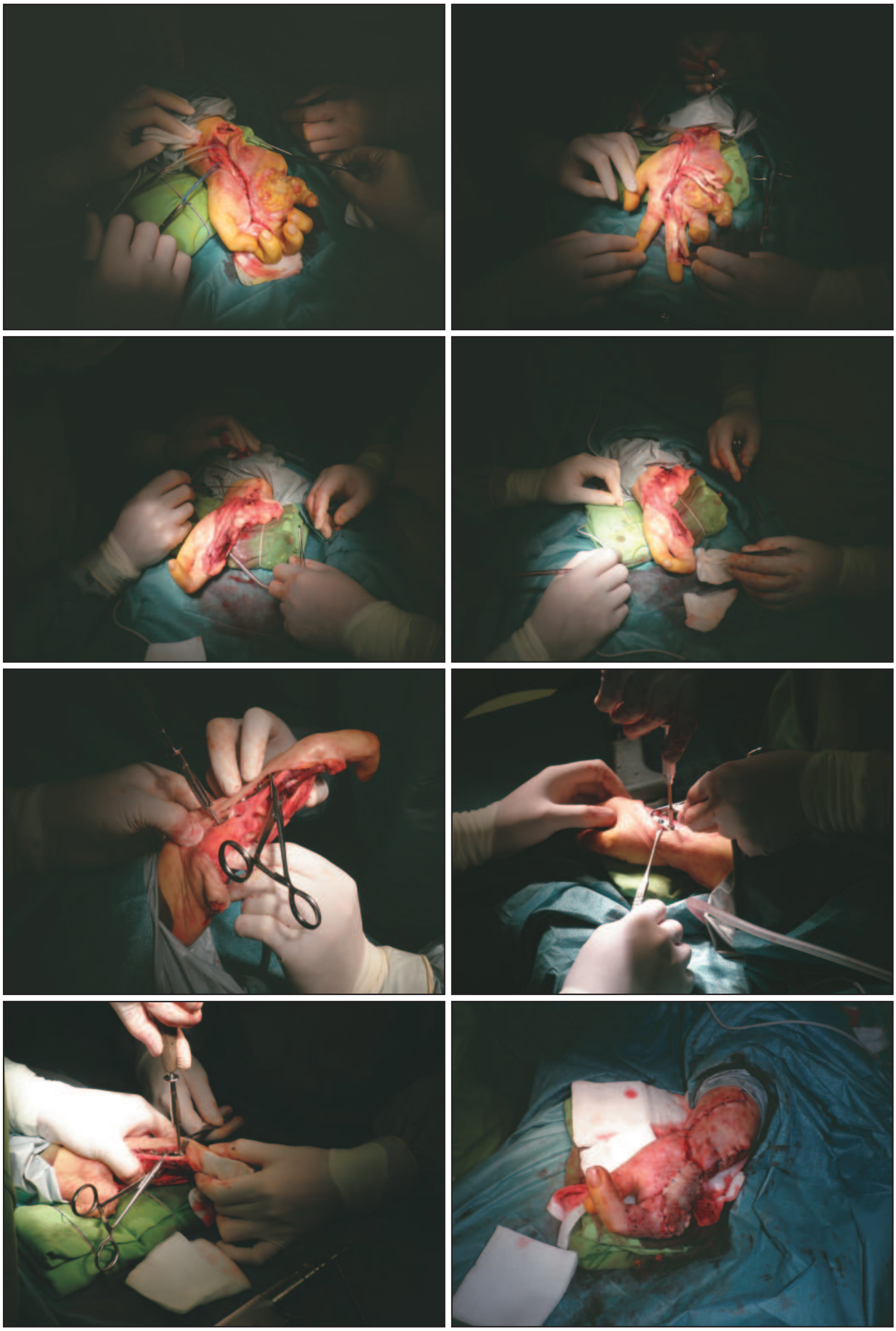

Figure 14. Snapshots from surgery of 2009-11-16

Figure 15. Result of surgery

Tissues of a patient after cytostatic therapy and hand irradiation can not be compared to those of a healthy person, their consistency caused a large number of technical difficulties.

The thorax CT of 2009-12-09 showed that infiltrated lymphnodes that can not be separated form the tumor in the lower left lung lobe dislocate, compress and infiltrate the oesophagus. There was a 2×5 cm probable metastasis in the right suprarenal gland.

Mid-December percutan gastroenteral feeding had to be started because the tumor compressed the oesophagus 30 cm long.

50 days after surgery the patient was able to do opposition and grip with the remaining two fingers, and could handle small objects, like pens *(Figure 16)*.

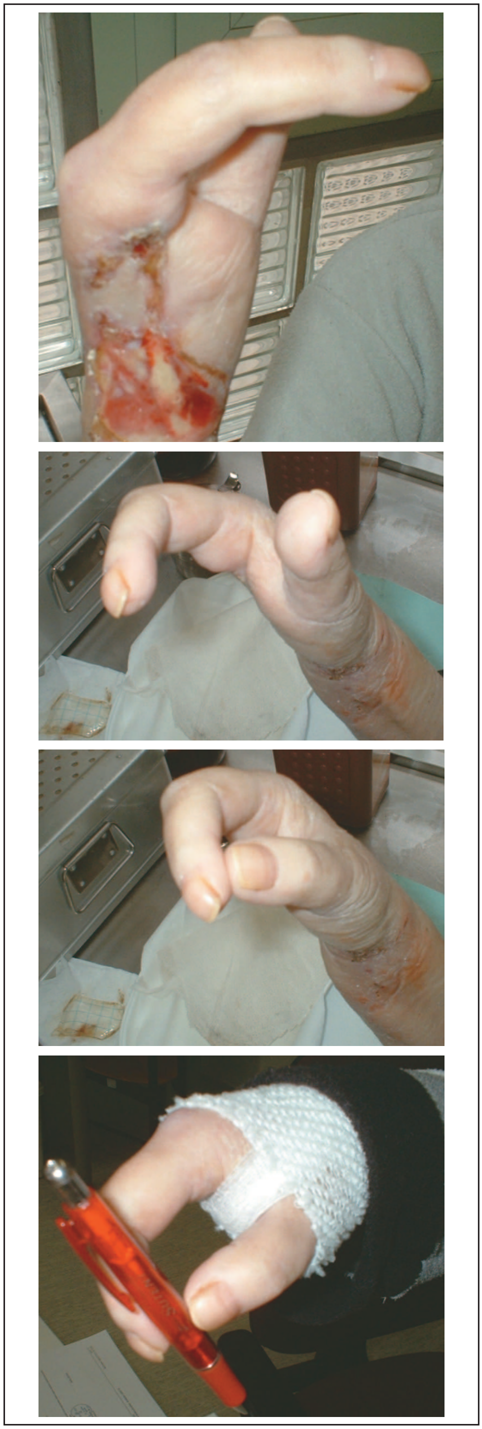

Figure 16. Functional results of 2010-01-04

Unfortunately a few days later the patient died of general circulatory and respiratory insufficiency.

Results & conclusion

It is often necessary to use ad hoc solutions in hand surgery, especially in cases of hand tumors. It is important to choose the ideal method from the repository of osthesynthesis techniques, because in such cases as shown in this paper, there is hardly a chance of a revision.

It is highly recommended to use statically terminal and biomechanically unorthodox solutions, like atypical plate placements.

In the presented case early consideration and the help of other specialists the adequate surgical planning promised the retainment of good function for the hand surgeon. However the patient's treatment nevertheless early recognition and appropriate diagnostic steps sidetracked from the point of hand surgical view, and later on only the severe tumor caused deformation could be treated with sever difficulties.

There seems to be no similar case yet, where the primary metastasis of the lung tumor appeared on the hand in both domestic and international literature.

References

1. *Beasley RW*. Beasley's Surgery of the Hand. New York: Thieme, 2003.
2. *Putz P, Pabst R. Sobotta*. Az ember anatómiájának atlasza I–II. Budapest: Medicina, 2007.

Miklós Szokoly
Péterfy S. Hospital and Trauma Center
H–1081 Budapest, Fiumei út 17.

Human morphologic measurements by photogrammetry

Bence Molnár, Károly Fekete, Péter Schrott
BME, Department of Photogrammetry and Geoinformatics
molnar.bence@fmt.bme.hu

Introduction

One of the most important parts of the human measurements is the facial measurements. A project at our department is to create a facial measurement system. There are several demands to get a high precision facial measurement system. For example, there are security systems at airports, forensic and anthropologic researches. These measurement systems make a 3D model automatically from the living human face. In our project, we choose photogrammetry to perform measurements. In addition to facial measurements the system won't be able to measure the face only, but other part of human body.

To build such a measurement system, there are several problems have to been solved. An important aspect of any close range photogrammetric system is to achieve an optimal photogrammetric network for special purpose, in this case for measurement of the human face. That includes selection of digital cameras, design of camera stations, modeling and calculation methods. This paper will present a solution for the main questions of photogrammetric network, gross error filtering and a processing method on the web.

In close range photogrammetry not photos with parallel axis are used, but ones with convergent axis. With this method more images are used at same processing, and the intersection of beams can be calculated with higher accuracy. The problems of network designing are presented based on Fekete[1].

Constraint of image scale

The image scale is a decisive impact on the accuracy of point determining. The 1. equation describes the maximum object distance, where the required accuracy is assured.

$$d = \frac{\overline{\sigma_c}\sqrt{kc}}{q\sigma} \qquad (1)$$

where σ_c are empiric errors of the X,Y,Z object space coordinates, d is object distance, σ are mean errors of image coordinates, σ_a is the mean error of angle measurements, q is the design factor of network, k are the quotient of independent measurements and number of images, c is the focal length.

Therefore the object distance in our project is mostly fixed; the equation is suitable to determining an ideal camera constant. It is important to select a well applicable camera for the project. The lens and the camera form a single unit; they have to be designed together, because the ratio of object distance and camera constant defines the photo scale. The selected lens is *(Figure 1):* N.E Technology L-SV2514MP (focal length: 25 mm, F: 1.4-C).

Figure 1. The selected lens

Constraint of resolution

The minimum geometric resolution is determined by the standards for mean errors of image coordinates. The maximum is limited by financial and technical reasons. There are two disadvantages of high resolution: first, if a sequential camera is used, the amount of data will exponentially rise. The duration of the human body measurement is critical, because of the movements. The time of data gathering should be minimized. The other disadvantage is that the geometric size of the sensor is constant for technical reasons; a pixel is smaller if the resolution is higher. The charge of pixels has effect on each other; the noise will increase in higher resolution.

The critical key issue of photogrammetry is the automatic point identifying. The currently used methods for identifying are working unreliable with homogenous textured surfaces, such as in case of human face. The identifying can be improved by projecting a pattern on the surface. If more images are available with different patterns from the same object, accuracy can be improved. That means, sequenced images have to be used, therefore a high speed camera is needed.

When the camera model was selected it was an important issue that the full control of cameras has to be done by computer. The camera is programmable with an SDK (Software Development Kit), developed by the manufacturer. The selected camera is *(Figure 2):* PicSight GigE P202B-GigE-AR color camera (sensor size: 1/1.8" CCD, resolution: 1624×1236 pixel, speed: 14 fps).

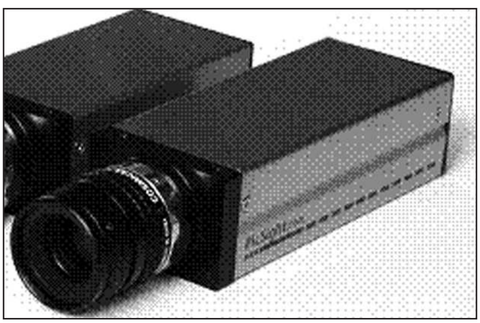

Figure 2. The selected camera

Depth of field constraint

High accurate measurement results in a sharp image. If the projection of a point is smaller than the physical size of the pixel, the projection is sharp, otherwise a blur circle (circle of confusion) occurs. In most cases a blur circle bigger than a pixel is allowed, if the digitizing mean error is still acceptable. The depth of field (DOF) is determined *(Figure 3)* by the camera constant and the aperture size (f-number).

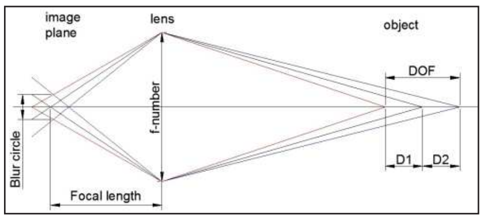

Figure 3. Depth of field

Facial measurement system requires a low object distance, compared to the relatively large size of the head. That's why the system should cope with large DOF. The object distance will be approximately 1.5 m and the f-number will be 5.6 to get an optimal result.

Constraint of intersection and incidence angles

The accuracy of a point identifying depends on the incident angles. Since the face is a complex surface, this constraint requires applying more cameras. In photogrammetry usually more cameras are used, typically two. In this case due to the complexity of the face, four cameras are needed. The accuracy of spatial measurements will be higher if the intersection angle of camera axis is the maximum that can be set. The best camera configuration is equilateral triangle-sided, square-based pyramid, on the base are the cameras, and on the peak is the object[2].

Constraint of lighting

The big f-number and the sequential photography require a bright object surface. Therefore not only the camera stations but light sources should be designed too. The lighting should be homogenous at all parts of the face. The bright object can cause difficulties if a pattern is projected to the object. The projector has to be very bright, to highlight the contrasts on the object, and support the automatic point identifying.

Gross errors and robust estimation

The automatic point identifying is a critical point of the measurement system. The automatic algorithms are based on contrast difference calculation. Due to lighting and homogenous texture of skin there can be several errors during recognition. The false recognized point pairs are called gross errors in literature. If gross errors still exist in final calculation, the final accuracy will be very low. The calculation in photogrammetry usually made by Least Squares Method (LSM), which is especially sensitive to gross errors[3]. LSM is a very good method to minimize residuals in a fast and easy way. If the base equations of a system are linear, the LSM gives the result in one step, no other calculation and linearization is needed.

In photogrammetry beam equalization is the classical calculation method, but it uses non-linear equations, that are not ideal for LSM. There is an other calculation method, called Direct Linear Transformation (DLT), which gives a direct connection between image coordinates and spatial coordinates[4], as shown in equation 2 and 3. As the name shows, it is based on linear equations, therefore if LSM is used, no linearization is needed.

$$L_1X+L_2Y+L_3Z+L_4-xL_9X-xL_{10}Y-xL_{11}Z-x=0 \tag{2}$$

$$L_5X+L_6Y+L_7Z+L_8-yL_9X-yL_{10}Y-yL_{11}Z-y=0 \tag{3}$$

where x,y are image coordinates, X,Y,Z are spatial coordinates and L_i are DLT parameters. An other advantage of DLT is that, no calibrated camera is needed. It enables to change settings on camera system, without a new calibration.

Other disadvantages of LSM are gross errors that have to been eliminated. Estimating methods that are insensitive for gross errors, named are robust estimations. Some methods make gross error filtering before estimation; other ones make it an iterative way, and continuously reweight the measurements. To make an automatic processing algorithm, the second way is a better choice.

The goal of these methods, that LSM can be used iteratively, with new weight matrices based on previous estimation residuals. The theoretical backgounds of these methods is that the clean (without gross error) measurements have normal distribution, but if gross error exits, the distribution differs[3].

$$F=(1-\varepsilon)\Phi+\varepsilon H \tag{4}$$

where F is the distribution model of errors, Φ is normal distribution function, H is the unknown distribution of gross errors, ε is the probability of gross errors.

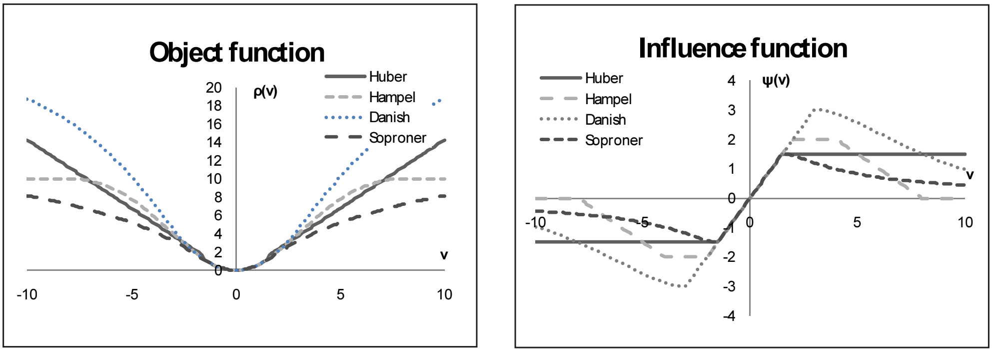

Figure 4. Density and influence function

These methods define one or more threshold, where other distribution is used in the probability density function. The first threshold always defines the part of objective function with normal distribution. The main objective functions are Huber-, Hampel-, Danish- and Sopproner-functions[5].

The influence function is the derivation of objective function. It shows the errors' effect on the global estimation. Influence function divided by x forms the weight matrix.

The objective functions are shown on the left side of *Figure 4.* The only one objective function which is convex is the Huber function[6]. (A non-convex object function has the disadvantage that, it is not convergent. A non convergent calculation is not ideal for an automatic method, that's why Huber method is chosen for estimation.

$$\psi(x) = \begin{cases} x & ,|x| \le a \\ a\dfrac{x}{|x|} & ,|x| > a \end{cases} \qquad (5)$$

where ψ is the influence function and a is the threshold for gross errors. The value of a is usually 1.5 but can be changed. The estimation steps are as follows: first an initial estimation with an identity weight matrix has to be done. The following estimations are based on previously calculated errors. Iteration runs while the optimized result is calculated. At the

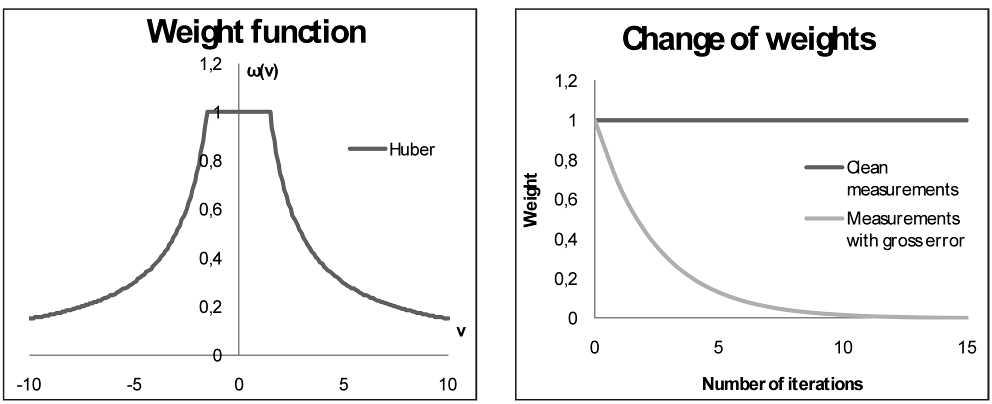

Figure 5. Weight function and weights during iterations

end the measurements with gross errors have weights around zero, all other measurements around one *(Figure 5)*. That means LSM can be used for estimation, the gross errors do not have effect on the final result.

To test the algorithm a web based photogrammetry application was developed. This application can be reached web, therefore available for everybody and everywhere. Own photos can be uploaded and the measurements can be done. Inexperienced users produce large amount of data that are often corrupted by gross errors. These kind of data sets are useful for testing the method and for selecting a proper threshold for the Huber method.

Conclusion

For development of a facial measurement system the best applicable equipment should be used. The best affordable cameras and lens were selected for the project. The good camera and light source configuration was defined to improve accuracy. A properly working calculation algorithm was developed for the spatial measurements, and gross errors were filtered out.

In the future a new algorithm should be developed for identifying points on the homogenous skin. Finally the photogrammetric network should be realized.

References

1. *Fekete K.* Network design issues in close range photogrammetry (in Hungarian). Geodézia és Kartográfia III, 2006;12–23.

2. *Mason S.* Conceptual Modell of the Convergeent Multistation Network Configuration Task. Photogrammetric Record 15(86), 1995;277–299.

3. *Detrekői Á.* Adjustment calculation (in Hungarian), Budapest: Tankönyvkiadó, 1991.

4. *Abdel-Aziz YI, Karara HM.* Direct Linear Transformation from Comparator Coordinates into Object Space Coordinates ASP Symposium on Close-Range Photogrammtery, Falls Church, VA, 1971;1–18.

5. *Závoti J.* Robust estimation methods in geodesy, Dr Habil Thesis, 1996;1–35.

6. *Huber PJ.* Robust Statistics, John Wiley & Sons, New York, 1981.

Bence Molnár
BME, Department of Photogrammetry and Geoinformatics
H-1111 Budapest, Műegyetem rkp. 3.

Intermediate biomechanical analysis of the effect of physiotherapy only compared to capsular shift and physiotherapy in multidirectional shoulder instability

Péter Nyiri[1], Árpád Illyés[1], Rita Kiss[2], Jenő Kiss[1]
[1] Saint John's Hospital, department of Orthopedics and Traumatology
[2] Budapest University of Technology and Economics, Department of Structures
nyirpet@vipmail.hu

Abstract

Purpose: The aim of study is to compare the kinematic parameters and activity pattern of muscles around the glenohumeral joint in multidirectional instability (MDI) treated by only physiotherapy and by capsular shift and physiotherapy, before and after treatment.

Materilal and method: The study was carried out on 32 patients with MDI treated with only physiotherapy (29 patients after 2 years, and 21 patients after 4 years), 19 patients with MDI treated by capsular shift and physiotherapy (19 patients after 2 and 4 years), and 50 healthy subjects as control group. The investigated kinematic parameters were the range of the humeral elevation (HE) in the scapular plane, the scapulothoracal and glenohumeral angle, the scapulothoracal (ST) and glenohumeral (GH) rhytms, and relative displacement between the rotation centers of the humerus and the scapula. The muscle activity was modeled by the on-off pattern of muscles around the shoulder.

Results: Before treatment the increased relative displacement between the rotation centers of the scapula and the humerus and different ST and GH rhythms were observed in MDI patients. The physiotherapy strengthened the rotator cuff, biceps brachii, triceps brachii, deltoid muscle, but ST and GH rhytms remained monolinear. Capsular shift and physiotherapy resulted bilinear ST and GH rhytms and normal relative displacement between the rotation center of scapula and humerus was restored. After surgery and physiotherapy the activity pattern of muscles around the shoulder was almost normal.

Conclusion: The significant alterations in kinematic parameters in MDI patients cannot be restored by physiotherapy only. After the capsular shift and postoperative physiotherapy the bilinear ST and GH rhytm (angulation at 60 degree), the normal relative displacement between the rotation centers of scapula and humerus and the normal muscular activity pattern can be restored.

Keywords: multidirectional instabiliy; shoulder joint; kinematics; physiotherapy; capsular shift; muscular activity; middle-term results

Introduction

MDI of the shoulder is a complex condition, it is characterized by symptomatic global laxity of glenohumeral joint[4,15]. It may or may not be caused by trauma, may be uni-, or bilateral. Subjects with MDI subluxate or dislocate anteriorly, posteriorly or inferiorly, with current reproduction of symptoms in at least two directions[2,18]. Most authors agree that patients with MDI initially should be treated by physiotherapy to increase the muscle strenght and coordination[1,4,16,18].

Neer and Foster in 1980 first recognized the MDI as a separate condition from unidirectional instability (frequency of MDI is undepended from the age, the sex, or physical activity)[17]. They developed the inferior capsular shift for the treatment of MDI. Nowadays if the physiotherapy is unsuccessful, the widely accepted surgical treatment is the anterior-inferior capsular shift (open or arthroscopic), followed by physiotherapy [7,13].

The aim of this study was to compare the changes in motion before and after different treatment, by kinematic and elektromyographic analyses during humerus elevation in the plane of the scapula. Three groups were investigated: the healthy control group (1), MDI patients treated with physiotherapy only ("physiotherapy group") (2) and MDI patients treated with open capsular shift followed by physiotherapy ("surgery group") (3). On the base of the previous investigation our hypothesis was that the "surgery group" is going to demonstrate better kinematic and muscle activity that is more consistent to the normal characteristics, compared to the "physiotherapy group".

Materials and methods

Patients

Thirty-two patients with MDI were treated non-surgically, by physiotherapy only (physiotherapy group), 19 patients with MDI were treated by open capsular shift followed by postoperative physiotherapy (surgery group), and 25 control subjects with normal, healthy shoulders participated the study.

The control group was tested once. The physiotherapy group was tested before starting the conservative treatment, 36 weeks, 2 and 4 years after the rehabilitation was started. The surgery group (capsular shift with postoperative physiotherapy) was tested before the surgery, 42 weeks, 2 and 4 years after surgery. Compared to the first investigation in the physiotherapy group after 2 years one patient died, other two patient (one male and one female) required surgical treatment. After 4 years additional eight patient (six male and two female) required surgery.

Anthropometric data of each group is summarized in *Table 1*.

Physiotherapy

The program[13] concentrated on proprioceptive input to improve the sense of joint position, and on relearning correct movement patterns with the development of strength and endurance in the scapulothoracic and glenohumeral muscles. Increased stability

	Control group		Physiotherapy group		Surgery group	
	Male	*Female*	*Male*	*Female*	*Male*	*Female*
Number (N)	32	18	15	12	5	9
Age (years)	28.1 ± 5.1	24.6 ± 6.12	24.5 ± 3.4	23.5 ± 4.5	26.4 ± 4.8	28.4 ± 3.6
Height (cm)	175.9 ± 14.9	168.9 ± 22.3	176.2 ± 4.7	158.4 ± 5.2	170.4 ± 6.7	165.3 ± 8.5
Mass (kg)	77.1 ± 8.4	66.1 ± 5.5	79.9 ± 2.1	58.4 ± 2.5	70.1 ± 1.7	58.4 ± 4.9
Duration of symptoms (months)	–	–	13.2 ± 2.2	12.9 ± 2.5	69.1 ± 11.5	75.9 ± 17.1

Table 1. Patient characteristics (no significant differences compared to the control group)

of muscle balance and proprioception were targeted by using strengthening exercises, closed-chain exercises, and stamina training. Home exercise program were used to promote and maintain the functional capacity of the shoulder.

Capsular shift with postoperative physiotherapy

The patients underwent Neer type antero-inferior capsular shift[17] performed by the same surgeon.The shoulder was immobilized by a sling for 3 weeks in tied up position. The post-operative rehabilitation program for the group began on the first postoperative day. Elbow movement and gentle pendulum exercises were allowed during the first 3 weeks. After 3 weeks assisted active elevation and gradual external rotation were allowed. After 6 weeks a maximal, pain-free external rotation position was allowed. The 36-week rehabilitation protocol was identical to the one described above.

Method of biomechanic measurement

The structure of the Zebris CMS-HS movement analysis system (Zebris, Medizintechnik GmbH, Germany) and of the measurement control software enabled us to measure changes in electric potential generated in muscles in the course of movement simultaneously with recording the kinematic characteristics of movements (without subsequent synchronization) by surface electromyography. The measurement was performed at the Biomechanical Laboratory of the Department of Applied Mechanics at the Budapest University of Technology and Economics, and Szolnok Hospital of Hungarian Railways. The detailed ultrasound-based shoulder kinematic and electromyographic measurement method is described by the same authors previously[8,9].

Assessment parameters

The range of humeral elevation (HE), scapulothoracic angle (ST), and glenohumeral angle (GH) were used for motion. For the dynamic analysis of motion, the position of the scapula and the humerus relative to each other was analyzed in terms of the relative displacement of rotation centers. The motion parameters are described in *Table 2.*

The kinematic and muscular parameters were calculated at the motion cycle where the final humerus elevation was around 80°. The number of cycles taken into account was more than 6 at all subjects.

Parameter	Definition
Humeral elevation (HE)	Angle formed by spatial vectors between the proximal and distal points of the sternum, and between the insertion points of deltoid muscle and radial humeral epicondyle
Range of humeral elevation	Differences in the humeral angle at initial and final positions
Scapulothoracic angle (ST)	Angle formed by spatial vectors between the proximal and distal points of the sternum, and the angulus acromialis and trigonum spinae
Range of scapulothoracic angle	Differences in the scapulothoracic angle at initial and final positions
Glenohumeral angle (GH)	Angle formed by spatial vectors between the insertion points of deltoid muscle and the radial humeral epicondyle, and the angulus acromialis and trigonum spina
Range of glenohumeral angle	Differences in the glenohumeral angle at initial and final positions
Glenohumeral rhythm	Glenohumeral angle as a function of humeral elevation
Scapulothoracic rhythm	Scapulothoracic angle as a function of humeral elevation
Relative displacement between the rotation centers of the humerus and scapula (ε_{SH})	Difference between the maximal and minimal distance of the rotation centers projected to a unit of length (calculation method is described in[16])

Table 2. Characteristic parameters describing motion patterns

The five parameters representing the bilinear regression line of a scapulothoracic and glenohumeral rhythm. The calculation method of these curves are described by the same authors previously[9,10].

Electromyographic analysis, time-based processing had to be applied and the purpose was to generate a linear cover curve to determine the motion pattern of each muscle group during movement.

Statistical analyses

Data processing was carried out using a Microsoft Excel™-based software which was developed by Illyés Á and Kiss R[9]. The average and standard deviation were calculated from the measurement results of the motion cycles. The parameters of the dominant and non-dominant shoulder were averaged (i.e., dominance was not considered).

The data were analyzed using two-factor ANOVA with one repeated measure; processing was carried out using a "Statistica" (v.7.0 StatSoft) software. Two factors were involved in these experiments: the groups and the time of observations. The factor of the groups had three levels, namely the control group, the physiotherapy group and the surgery group. The time of observations was the repeated factor, and had up to three levels: the control group was observed once, and the physiotherapy and surgery group was observed four times (before treatment, after 36-weeks physiotherapy, resp. 2 and 4 years after the rehabilitation came to an end); The post hoc comparison was made by a Student t-test for multiple comparisons. The significance level at statistical analysis (p) was set at 0.05.

Results

For the sake of transparency, the results of angular kinematics are summarized in *Figure 1* and *Figure 2*. The results of relative displacement are visible in *Figure 3* and *Figure 4.* The parameters of regression lines are shown in *Table 3. a* and *3. b,* and the p-values of different statistical comparisons in *Tables 4. a, 4. b* (in the physiotherapy and surgery group). The average regression lines of scapulothoracic and glenohumeral rhythms in the control group, before treatment, and after 2 and 4 years in each group are shown in *Figure 5.* The duration of muscle activities of each group is shown in *Figure 6.*

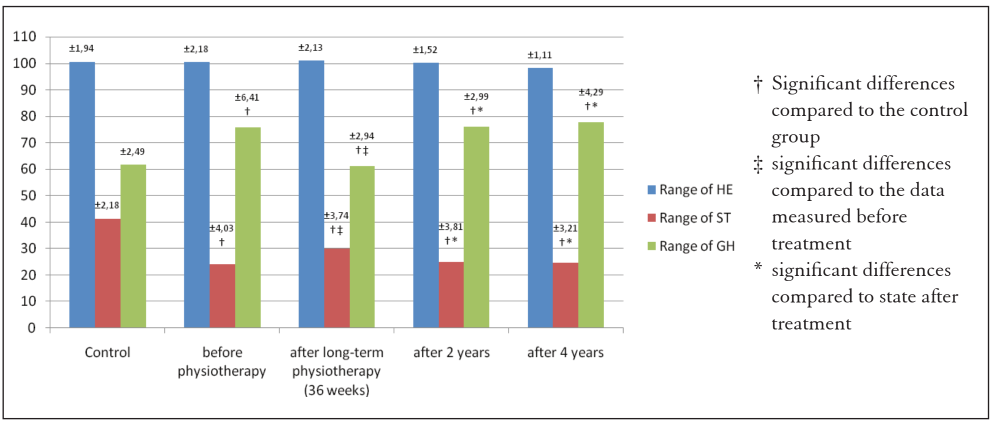

Figure 1. Range of humeral elevation (HE), scapulothoracic angle (ST) and glenohumeral angle (GH) for **physiotherapy group** at different observation times, with the standard deviation values

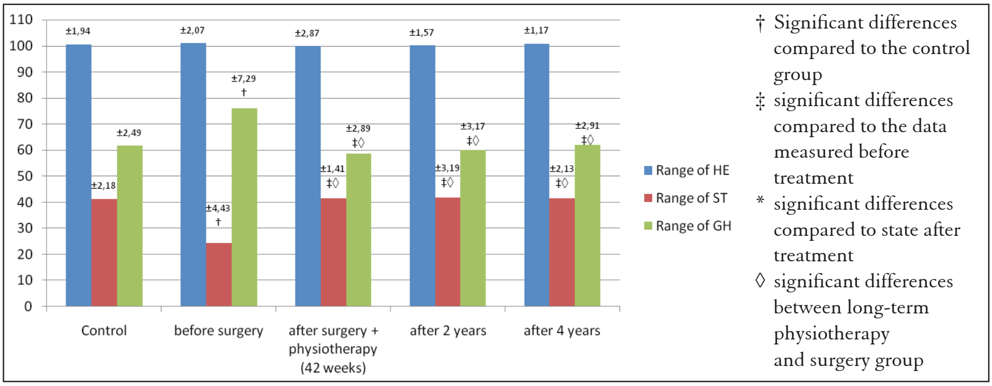

Figure 2. Range of humeral elevation (HE), scapulothoracic angle (ST) and glenohumeral angle (GH) for **surgery group** at different observation times, with the standard deviation values

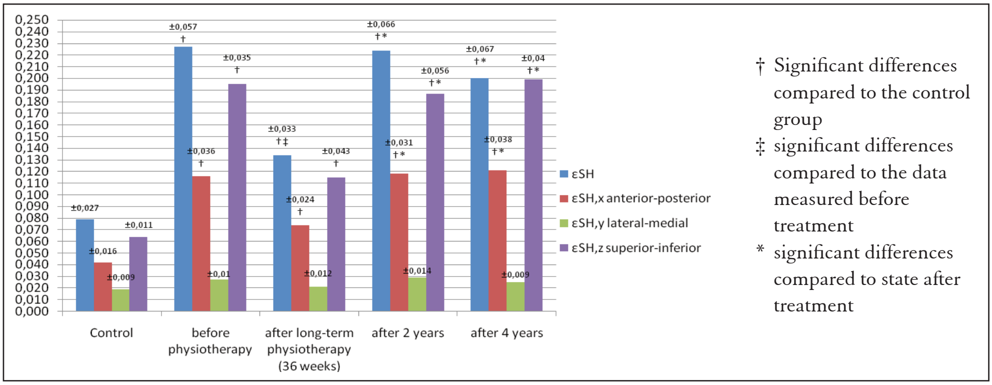

Figure 3. Relative displacement (ε_{SH}) and components in directions X, Y, and z of the relative displacement (ε_{SH}) between the rotation centers of the scapula and humerus for **physiotherapy group** at different observation times, with the standard deviation values

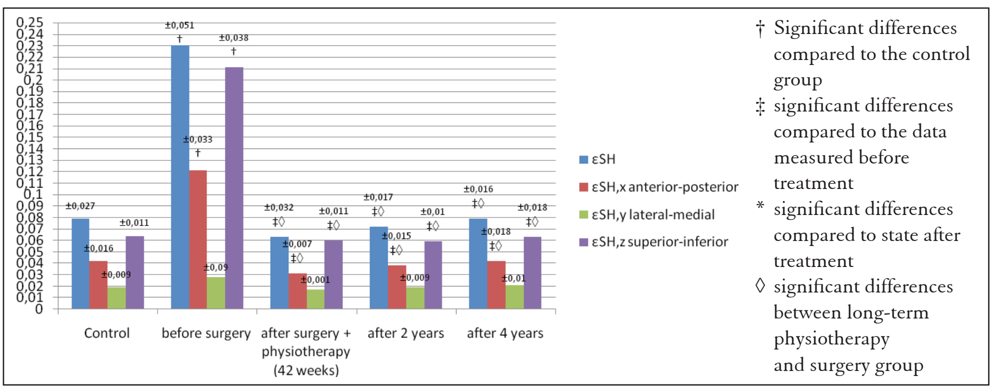

Figure 4. Relative displacement (ε_{SH}) and components in directions X, Y, and z of the relative displacement (ε_{SH}) between the rotation centers of the scapula and humerus for **surgery group** at different observation times, with the standard deviation values

Parameters			Control group	Physiotherapy group			
				before physiotherapy	*after long-term physiotherapy*	*after 2 years*	*after 4 years*
			mean ± SD	mean ± SD	mean ± SD	mean ± SD	mean ± SD
scapulothoracic rthym	until the intersection	m_{ST}	0.303 ± 0.015	0.248 ± 0.023†	0.299 ± 0.024‡	0.252±0.022†,*	0.246 ± 0.029†,*
		b_{ST}	75.08 ± 1.04	98.78 ± 2.15†	81.23 ± 2.11†,‡	99.01 ± 2.18†,*	99.10 ± 2.58†,*
	humeral elevation at intersection		59.87 ± 0.35				
	over the intersection	m_{ST}	0.557 ± 0.025				
		b_{ST}	59.95 ± 0.85				
glenohumeral rthym	until the intersection	m_{GH}	0.673 ± 0.021	0.759 ± 0.037†	0.612 ± 0.027‡	0.761 ± 0.040†,*	0.777 ± 0.042†,*
		b_{GH}	86.86 ± 1.68	57.98 ± 2.19†	60.17 ± 1.88‡	58.15 ± 2.22†,*	56.18 ± 2.49†,*
	humeral elevation at intersection		60.13 ± 0.29				
	over the intersection	m_{GH}	0.547 ± 0.018				
		b_{GH}	94.49 ± 2.28				

Table 3. a Slope and intercept parameters of regression lines characterizing scapulothoracic and glenohumeral rhythms for physiotherapy group at different observation times.

m_{ST}: slope of regression line of scapulothoracic rhythm; m_{GH}: slope of regression line of glenohumeral rhythm; b_{ST}: y-intercept of regression line of scapulothoracic rhythm; b_{GH}: y-intercept of regression line of glenohumeral rhythm; The linear regression line characterized by two parameters (slope and intercept), the other three parameters (humeral elevation in intersection, slope and intercept over the intersection) shown as a blank cell. † Significant differences compared to the control group, ‡ significant differences compared to the state before treatment, * significant differences compared to the state after treatment

Parameters			Control group	Surgery group			
				before surgery	*after surgery + physio.*	*after 2 years*	*after 4 years*
			mean ± SD	mean ± SD	mean ± SD	mean ± SD	mean ± SD
scapulothoracic rthym	until the intersection	m_{ST}	0.303 ± 0.015	0.244 ± 0.028†	0.308 ± 0.020‡	0.307±0.018‡,◊	0.305±0.12‡,◊
		b_{ST}	75.08 ± 1.04	99.14 ± 1.99†	73.22 ± 2.27‡,◊	74.15±1.97‡,◊	75.15±0.98‡,◊
	humeral elevation at intersection		59.87 ± 0.35		60.03 ± 0.72	58.87±0.55	60.10±0.44
	over the intersection	m_{ST}	0.557 ± 0.025		0.535 ± 0.027	0.547±0.023	0.558±0.024
		b_{ST}	59.95 ± 0.85		60.19 ± 0.61	60.02±0.67	59.88±0.74
glenohumeral rthym	until the intersection	m_{GH}	0.673 ± 0.021	0.761 ± 0.040†	0.683 ± 0.029‡,◊	0.679±0.028‡,◊	0.677±0.018‡,◊
		b_{GH}	86.86 ± 1.68	56.12 ± 1.69†	87.87 ± 2.14‡,◊	87.15±1.95‡,◊	86.75±1.12‡,◊
	humeral elevation at intersection		60.13 ± 0.29		59.69 ± 1.07	60.01±0.87	60.69±0.20
	over the intersection	m_{GH}	0.547 ± 0.018		0.550 ± 0.024	0.549±0.024	0.548±0.019
		b_{GH}	94.49 ± 2.28		92.28 ± 2.97	94.96±2.17	94.58±2.31

Table 3. b Slope and intercept parameters of regression lines characterizing scapulothoracic and glenohumeral rhythms for surgery group at different observation times.

m_{ST}: slope of regression line of scapulothoracic rhythm; m_{GH}: slope of regression line of glenohumeral rhythm; b_{ST}: y-intercept of regression line of scapulothoracic rhythm; b_{GH}: y-intercept of regression line of glenohumeral rhythm; The linear regression line characterized by two parameters (slope and intercept), the other three parameters (humeral elevation in intersection, slope and intercept over the intersection) shown as a blank cell. † Significant differences compared to the control group, ‡ significant differences compared to the state before treatment, * significant differences compared to the state after treatment, ◊ significant differences between physiotherapy and surgery group

	Parameters		Physiotherapy group: *before physio-therapy*	*after long-term physio-therapy*	*after 2 years*	*after 4 years*
	Range of HE		0.602	0.605	0.588	0.495
	Range of ST		0.005	0.016	0.008	0.004
	Range of GH		0.004	0.037	0.027	0.006
Relative displacement	ε_{SH}		<0.001	0.003	0.002	<0.001
Relative displacement	$\varepsilon_{SH,x}$ *anterior-posterior*		0.003	0.014	0.008	0.001
Relative displacement	$\varepsilon_{SH,y}$ *lateral-medial*		0.654	0.652	0.657	0.581
Relative displacement	$\varepsilon_{SH,z}$ *superior-inferior*		0.001	0.009	0.004	0.001
ST and GH rhythm	*until the intersection*	m_{ST}	0.014	0.054	0.035	0.028
ST and GH rhythm	*until the intersection*	b_{ST}	0.004	0.041	0.005	0.002
ST and GH rhythm	*humeral elevation at intersection*					
ST and GH rhythm	*over the intersection*	m_{ST}				
ST and GH rhythm	*over the intersection*	b_{ST}				
ST and GH rhythm	*until the intersection*	m_{GH}	0.003	0.018	0.007	0.004
ST and GH rhythm	*until the intersection*	b_{GH}	0.001	0.002	0.001	<0.001
ST and GH rhythm	*humeral elevation at intersection*					
ST and GH rhythm	*over the intersection*	m_{GH}				
ST and GH rhythm	*over the intersection*	b_{GH}				
on-off pattern of muscles	*m. deltoideus anterior*		<0.001	0.14	0.005	<0.001
on-off pattern of muscles	*m. deltoideus medius*		<0.001	0.12	0.06	<0.001
on-off pattern of muscles	*m. deltoideus posterior*		0.009	0.004	0.008	0.007
on-off pattern of muscles	*m. supraspinatus*		<0.001	0.001	<0.001	<0.001
on-off pattern of muscles	*m. infraspinatus*		<0.001	<0.001	<0.001	<0.001
on-off pattern of muscles	*m. biceps brachii*		<0.001	0.04	0.003	<0.001
on-off pattern of muscles	*m. triceps brachii*		<0.001	0.008	0.002	<0.001

Table 4. a P-values of difference in biomechanical parameters between the physiotherapy group and the control group

	Parameters		Surgery group: *before surgery*	*after surgery + physio.*	*after 2 years*	*after 4 years*
	Range of HE		0.602	0.592	0.588	0.645
	Range of ST		0.006	0.271	0.288	0.228
	Range of GH		0.004	0.225	0.256	0.267
Relative displacement	ε_{SH}		<0.001	0.283	0.274	0.214
Relative displacement	$\varepsilon_{SH,x}$ *anterior-posterior*		0.003	0.333	0.337	0.338
Relative displacement	$\varepsilon_{SH,y}$ *lateral-medial*		0.654	0.681	0.701	0.707
Relative displacement	$\varepsilon_{SH,z}$ *superior-inferior*		0.001	0.367	0.333	0.398
ST and GH rhythm	*until the intersection*	m_{ST}	0.014	0.294	0.301	0.299
ST and GH rhythm	*until the intersection*	b_{ST}	0.004	0.265	0.308	0.278
ST and GH rhythm	*humeral elevation at intersection*			0.346	0.348	0.347
ST and GH rhythm	*over the intersection*	m_{ST}		0.319	0.321	0.328
ST and GH rhythm	*over the intersection*	b_{ST}		0.279	0.288	0.293
ST and GH rhythm	*until the intersection*	m_{GH}	0.003	0.311	0.304	0.312
ST and GH rhythm	*until the intersection*	b_{GH}	0.001	0.397	0.385	0.391
ST and GH rhythm	*humeral elevation at intersection*			0.473	0.460	0.468
ST and GH rhythm	*over the intersection*	m_{GH}		0.282	0.281	0.283
ST and GH rhythm	*over the intersection*	b_{GH}		0.351	0.350	0.346
on-off pattern of muscles	*m. deltoideus anterior*		<0.001	0.136	0.147	0.151
on-off pattern of muscles	*m. deltoideus medius*		<0.001	0.125	0.131	0.126
on-off pattern of muscles	*m. deltoideus posterior*		0.009	<0.001	0.001	0.002
on-off pattern of muscles	*m. supraspinatus*		<0.001	0.24	0.21	0.19
on-off pattern of muscles	*m. infraspinatus*		<0.001	<0.001	<0.001	<0.001
on-off pattern of muscles	*m. biceps brachii*		<0.001	0.35	0.39	0.37
on-off pattern of muscles	*m. triceps brachii*		<0.001	0.41	0.34	0.26

Table 4. b P-values of difference in biomechanical parameters between the surgery group and the control group

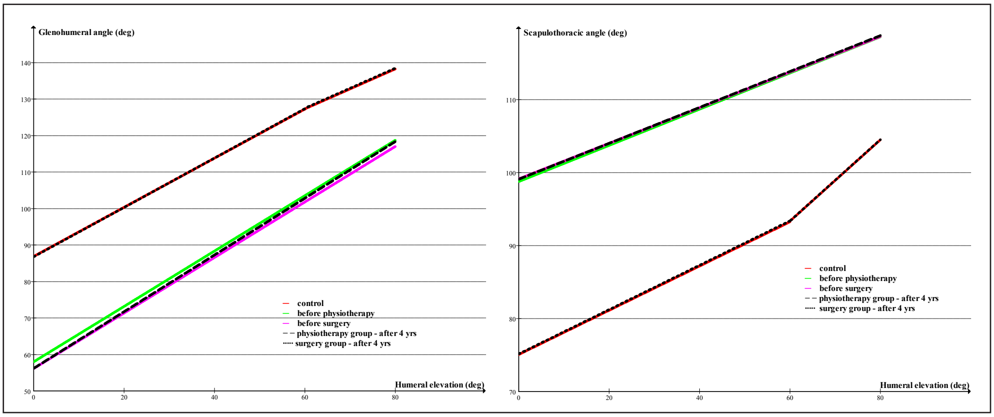

Figure 5. The average of regression lines of glenohumeral and scapulothoracic rhythms in the control group, before treatment and after 4 years in the physiotherapy and surgery group

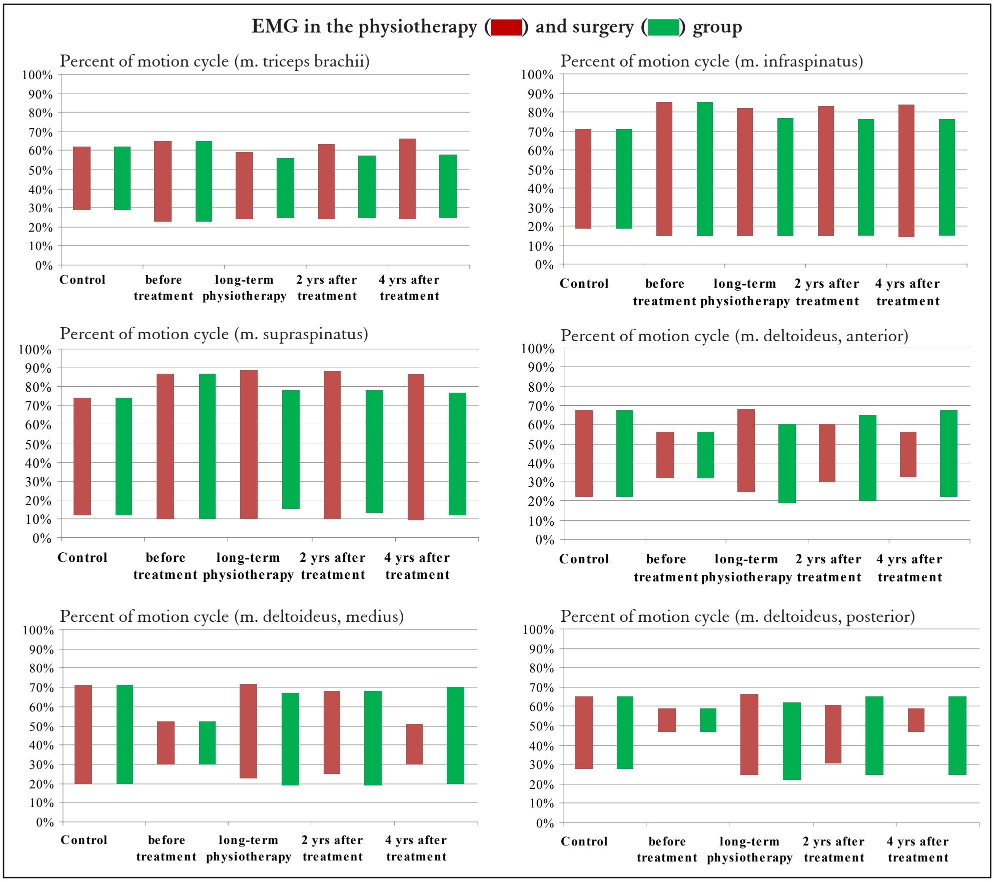

Figure 6. The on-off patterns of muscle activity generated by normalization with modified muscle contraction during elevation in the physiotherapy and surgery group at different times

Discussion

The investigated motion (elevation in the scapular plane) was continuous (motion was not stopped for recording the position of different anatomic points), so we determined potential changes in the motion pattern of skeletal elements and changes in muscle activity. The motion pattern of skeletal elements was characterized by kinematic parameters: range of HE, ST, GH, relative displacement between the rotation centers of the scapula and the humerus, and scapulothoracic and glenohumeral rhythms. The pattern of muscle activity was characterized by the on-off pattern of muscles, which modeled intramuscular coordination. Patients with MDI had significant alterations in shoulder kinematics (up to about 80° elevation) and in muscle activity compared to the controls, which is in accordance with earlier reports[1,10,11,17,18]. The ST and GH rhythms were linear and did not show angulation at 60° as in controls (where ST motion gradually takes over from GH motion during elevation), confirming the hypothesis of An and Friedman[1] and Matsen[14] *(Figure 5)*. Long-term physiotherapy only, by strengthening the rotator cuff, triceps, serratus and deltoid muscles did not restore the motion and duration of the muscular activity of the shoulder joint and at the control in the 2. and 4. years these values were near to the values measured before physiotherapy. In this investigation capsular shift and postoperative physiotherapy restored the motion and the muscular activity pattern of the shoulder joint and at the control in the 2. and 4. years the kinematic parameters approached the control group, respectively these have shown improvement compared to the end-values of the rehabilitation. Our comprehensive set of functional tests indicated that surgery with postoperative physiotherapy resolved ligamentous abnormalities by surgical treatment, and restored impaired muscular control with consequent postoperative rehabilitation, whereas physiotherapy restored muscular control only.

Conclusion

In the MDI patients observed different scapulothoracic and glenohumeral rhythms and increased relative displacement between the rotation centers of the scapula and humerus cannot be restored by physiotherapy only. After 2-4 years the on-off pattern of muscles in the physiotherapy group turns same to EMG in MDI group before treatment. Later was necessary to execute operation on some patients from this group. The duration of kinematic parameters and muscular activity also can be restored to normal after surgery with postoperative physiotherapy and after two and four years the measured biomechanic parameters are nearly similar to control group.

References

1. *An YH, Friedman RJ*. Multidirectional instability of the glenohumeral joint. Orthop Clin North Am 2000;31:275–85.
2. *Beasley L, Faryniarz DA, Hannafin JA*. Multidirectional instability of the shoulder in the female athlete. Clin Sports Med 2000;19:331–49.
3. *Brown GA, Tan JL, Kirkley A*. The lax shoulder in females: issues, answers but many more questions. Clin Ortop 2000;372:110–22.
4. *Cooper RA, Brems JJ*. The inferior capsular-shift procedure for multidirectional instability of the shoulder. J Bone Joint Surg Am 1992;74: 1516–21.
5. *Illyés Á, Kiss R*. Method for determining the spatial position of the shoulder with ultrasound-based motion analyzer. Journal of Electromyography and Kinesiology 2006;16:79–88.

6. *Illyés Á, Kiss R.* Kinematic and muscle activity characteristics of multidirectional shoulder joint instability during elevation. Knee Surg Sports Traumatol Arthrosc. 2006;14:673–685.

7. *Illyés Á, Kiss R.* Shoulder joint kinematics during elevation measured by ultrasound-based measuring system. Journal of Electromyography and Kinesiology 2007;17:355–364.

8. *Illyés Á, Kiss R.* Shoulder muscle activity during pushing, pulling, elevation and overhead throw. Journal of Electromyography and Kinesiology 2005;15:282–289.

9. *Kiss J, Damrel D, Mackie A, Neumann L, Wallace WA.* Non-operative treatment of multidirectional shoulder instability. Int Orthop. 2001;24(6): 354–7.

10. *Matsen FA. Stability. In: Matsen FA, Lippit SB, Sidlers JA, Harryman DT,* editors. Practical evaluation and management of the shoulder. Philadelphia: W.B. Saunders; 1994. p. 59–109.

11. *McFarland EG, Kim TK, Park HB, Neira CA, Gutierrez MI.* The effect of variation in definition on the diagnosis of multidirectional instability of the shoulder. J Bone Joint Surg Am 2003;85:2138–44.

12. *Morrey BF, An KN.* Biomechanics of the shoulder. In: Rockwood Jr CA, Matsen FA, editors. The shoulder 1990; vol. 1. Philadelphia: W.B. Saunders; 1990. p. 208–45.

13. *Neer CS, Foster CR.* Inferior capsular shift for involuntary inferior and multidirectional instability of the shoulder. A preliminary report. J Bone Joint Surg Am. 1980 Sep;62(6):897–908.

14. *Sidles JA, Harryman DT, Harris SL.* In vivo quantification of glenohumeral stability. Trans Orthop Res Soc. 1991;16:646.

Péter Nyiri
Saint John's Hospital
Department of Orthopedics and Traumatology
H–1125 Budapest, Diós árok 1–3.

Application of fingertip support technique in microsurgery

Gergely Csókay[1], Gergely Pataki[2], Attila Óvári[3], István Valálik[4], András Csókay[5]

[1] Semmelweis University Department of Maxillo-facial Surgery, Budapest, Hungary
[2] St. Steven Hospital Department of Plastic and Reconstructive Surgery, Budapest, Hungary
[3] Department of Otorhinolaryngology, Head and Neck Surgery, University of Rostock, Germany
[4] St. Johns's Hospital Department of Neurosurgery, Budapest, Hungary
[5] B.-A.-Z. County Hospital Miskolc, Department of Neurosurgery, Miskolc, Hungary
csokaya@gmail.com

Abstract

Objective

The physiological tremor which may extend up to 0.4–0.6 mm on the instrument tip in case of a well-skilled microsurgeon may cause difficulties in any field of microsurgery, in spite of using different armrests. The limit of correctness of medical robots is about 0.1 mm so far, but the application of these machines is expensive and not convenient for surgeons because the direct touch via microinstruments with living tissues is impossible.

Method

The effectiveness of the fingertip support technique has been proven by randomized analysis by exact measuring of the reduction of tremor.

Results

The 0.1 mm precision could be reached by fingertip support. This extra precise work has not been available by hand so far.

Conclusion

The significant effect of fingertip support technique in neurosurgery has been certified and published by exact measuring and clinical data.

Our hypothesis could be the indication for trials in any microsurgical work.

Keywords: fingertip support technique; micromanipulation; microsurgery; revascularisation

Introduction

The precise microsurgical work can be complicated when more than 5–10× magnification is necessary (microneurosurgery, microvascular procedures in plastic and hand surgery, retineal surgery in ophtalmology, cardiac surgery, ear surgery). The most obstructive problem is the physiological tremor which expands up to 0.4–0.6 mm even in the case of, well skilled microsurgeons us well[3,4,5,6] *(Figure 1)*.

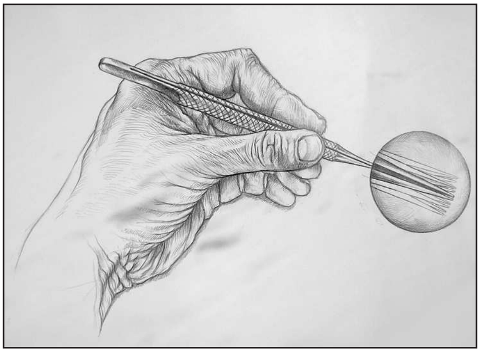

Figure 1. There is a shift caused by the tremor on the end of micro instruments, by the traditional technique

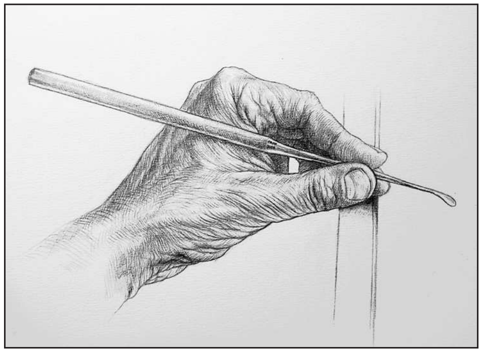

Figure 2. The fingertip support technique reduces the tremor at the end of the instruments

The problems originate from the fact that between the operation point and the last supporting point (end of IV–V fingertip) the carpal joints transmit micro movements (tremors originated neurogenic and mechanical from breathing and heart beat transmitted by circulation to hand) which cause tremors at the end of micro instruments. The fingertip support technique consists of support of I–III fingertip on the crossing bridge (called Bethlehem bridge) above the operating (working) point[1,2,3,4] *(Figure 2)*.

The end of the bridge rests on the cushions which are fixed on the edge of the exposure. By this technique there are no carpal and finger joints between the last supporting points and the end of instruments which could transmit the tremor. The bridge is necessary because the closest fixed points on the skull or any part of body including the well known armrest devices could be placed so far too far to balance and drive the microinstruments to the operating point only by the fingertip. The fingertip support technique was introduced at different microneurosurgical approaches[1,2,3,4] *(Figure 3)* and gives significant reduction of postoperative complications[3,4].

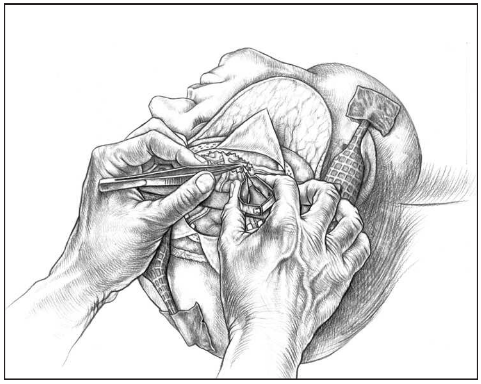

Figure 3. The application of robot hand method in the course of microneurosurgery

Randomized trial of tremor reduction by robot hand technique has not been performed so far. Our hypothesis states that this technique could be introduced in any field of microsurgical approach.

Method

Effectiveness of the fingertip support technique has been proven by randomized analysis by exact measuring of the reduction of tremor. To measure the difference between the traditional and the new method, we used tracking the instrument tip movements in case of 8 microsurgeons. (3 neurosurgeons, 3 opthalmologists, 1 hand and plastic surgeon, 1 facial and neck surgeon, (aged 30–50), (male and female ratio (6/2). The subjects were asked to hold the tip of the instrument above a fixed point with visual control under the microscope with 20× magnification. At a distance of 5 mm from the tip of the instrument an adhesive retroreflective marker (2 mm in diameter) was fixed. The position of the marker was registered in a 100×72 mm field of view in the infrared range with the real-time passive marker-based analyser of movement- PAM[5] at a sampling rate of 50/s. Coordinates of the marker positions, evaluated from the images were recorded by a two-dimensional analyzer[8].

The digital camcorder was positioned on the axis of the forearm of the subject, the elevation angle was approximately perpendicular to the instrument axis. The markers X and Y position data then were processed with the MATLAB 7.1 (The Math Works, Inc.). The marker trajectories and displacement data were compared, concerning the two methods of holding the instrument. With each method 3 recording were captured from a subject.

Results

Comparison of marker trajectories showed a significant regress of trajectory field ranges *(Table 1)* with the new instrument holding (fingertip support) technique. The significant reduction of tremor (3,0–4,4) was measured at each subject by fingertip support technique.

The displacement intensity, and the mean displacement values showed significant regress. The maximal displacement with the new method improved from 0.61 mm to 0.27 mm. The most impressive effect was observed in the vertical maximal value with regress from 0.53 mm to 0.18 mm.

Conclusion

The significant reduction of tremor (3.0–4.4) was measured at each subject by fingertip support technique, so we stopped the randomized analysis after the 8 person. The microsurgical work one of the hardest manual work in medicine. Unfortunately microsurgical work practice is hardly affordable in most part of the

	Traditional (mm)	Traditional (mm)	P
Trajectory field horizontal	0.53±0.054	0.15±0.030	0.000
Trajectory field vertical	0.46±0.044	0.13±0.020	0.000
Displacement RMS	0.36±0.046	0.10±0.013	0.001

Table 1. Comparison of measurement data with traditional and fingertip support methods recording of a microsurgeon. The new method resulted highly significant ($P<0.005$) reduction of vertical and horizontal trajectory field and root-mean-square (RMS) of displacement

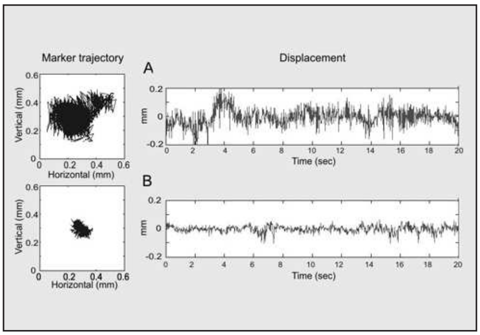

Marker trajectories and displacement curves registered with passive marker based analyser of movements with sampling rate of 50 Hz. The trajectory field and the displacement oscillations with the new method (B) are significantly reduced compared to traditional (A) technique world. The continuous practice, peaceful spirit helps the surgeon's hand "to stay quiet" during the operations. Even so the tremor may cause difficulties or damages.

There are trials to introduce the medical robots[7,9] into microsurgery, but their application has not been spread in the microsurgical practice. The preciseness of the most modern robots are 0,1 mm[9]. The preciseness the of fingertip support technique reduces the tremor close to 0,1 mm as well. The manipulation by the surgeons' hand is easier than by the robots.

The contact of instruments with the living tissues is also very important during surgery. The new technique guarantees it. By fingertip support technique the microsurgical procedures could be available to more surgeons to avoid the postoperative complication. Moreover the mental load on the microsurgeon could be reduced. Our hypothesis suggests the introduction of this technique in any other field of microsurgery *(Figure 4, 5, 6, 7)*.

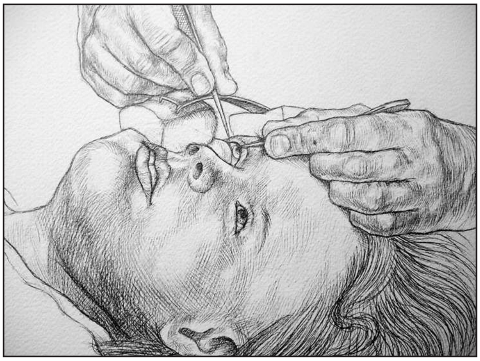

Figure 4. The application of fingertip support method in the course of ophthalmic (retinal) surgery

Figure 5. The application of fingertip support method in the course of microrevascularisation of free skin flap transplantation in plastic surgery. The place of Bethlehem bridge is similar in oto surgery (implantation of ear bones)

Figure 6. The application of fingertip support method in the course of finger replantation (revascularization in hand surgery)

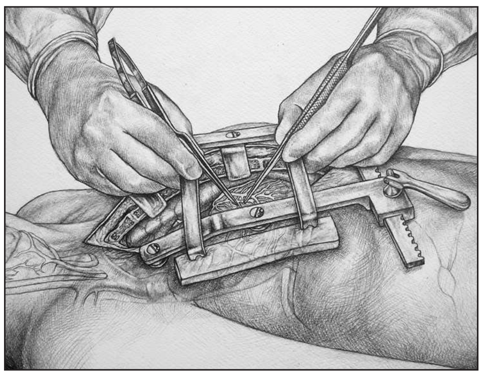

Figure 7. The possible application of robot hand technique in the course of coronary surgery

References

1. *Csókay A, Csókay G.* Catch fingertip support in microsurgery to reduce the tremor: Technical note (in Hungarian). Hungarian Medical Journal 2006;147:21.

2. *Csókay A.* A novel microsurgical technique reduces hand tremor in the course of lateral suboccipital approach. Surgical Neurology 2007;67: 392–94.

3. *Csókay A, Valálik I, Jobbágy Á.* Early experiences with a novel (robot hand) technique in the course of microneurosurgery. Surgical Neurology 2009; 71:469–472.

4. *Csókay A, Valálik I, Jobbágy Á.* Application of robot hand technique in the course of microneurosurgical operations (in Hungarian). Clinical Neuroscience 2009;62:48–52

5. *Ferguson RL, Jobe K.* A quiet hand for microneurosurgery: twiddle your thumb. J Neurosurgery 2004;101:541–544.

6. *Hartwell RC, Ferguson RL.* Physiologic tremor and microsurgery. Microsurgery 1983;4:187–192.

7. *Hubschman JP, Bourges JL, Choi W, Mozayan A.* "The Microhand": a new concept of micro-forceps for ocular robotic surgery. Eye 2009 Mar 20; S1476–5454

8. *Jobbágy Á, Harcos P, Károly R.* Analysis of finger-tapping movement. J Neurosci Methods 2005; 141:29–39.

9. *Russel HT, Stoianovici D.* Medical Robotics in Computer-Integrated Surgery. IEEE Transactions on Robotics and Automation 2003;19: 765–82.

Special thanks for the medical illustrations to Balázs Sándor Muhari-Papp

Gergely Csókay
Semmelweis University Department of Maxillo-facial Surgery, Budapest, Hungary
H–1085 Budapest VIII., Üllői út 26.

Force measurement of hand and fingers

Károly János Bretz[1], Ákos Jobbágy[1], Károly Bretz[2]
[1] Budapest University of Technology and Economics
[2] Semmelweis University TF
bretzkarl@hotmail.com

Abstract
Objective: To determine forces of hand and fingers in model situations.

Methods: Subjects were 16 university students (males). Dyna-8 force measuring system was used, which is equipped with transducers making the measurement of handgrip strength and forces of fingers possible. The maximum force value is displayed digitally and simultaneously, the complete force diagram is shown on the computer monitor.

Results: Right and left hand strengths and forces of all fingers were recorded, and descriptive statistics, correlation analysis, and t-test were executed. Forces of right and left hand strengths correlate, but differ significantly when their means are compared. Forces of the same fingers on the right and left hand correlate significantly with the exception of the middle and index fingers.

Conclusion: Hand and finger force data are used in numerous sport types, industrial design, ergonomics, and rehabilitation.

Keywords: dynamometers; hand strength; finger force; ergonomics; rehabilitation control

Introduction

The application field of hand and finger force measurements is related to the industrial design of hand tools, workstations, vehicles, and human-machine interfaces requiring force while manipulating these means *(Figure 1)*. Taking into account the data of the above-mentioned forces and the construction requirements, one can improve comfort and minimize hand injuries (Valero-Cuevas, 2000). Development of hand and finger force is worthy of attention in several types of sport, e.g., judo, wrestling, weightlifting, hammer throw, discus throwing, tennis, gymnastics, rock climbing, etc. Devices and computerized measuring systems are in the available literature, which are capable of recording isometric, isotonic, and isokinetic forces. (Yokogawa, Hara, 2002, Zatsiorsky, 2002, Kiung Ki Uk et al., 2004)

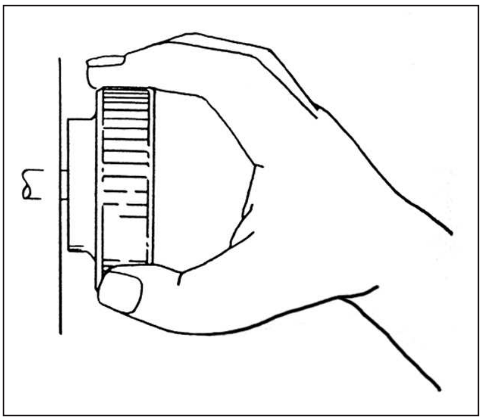

Figure 1. Setting a turning button

The purpose of the present study was to focus on our special measuring system and typical data regarding whole-hand grasp forces and finger pinch exertions.

Methods

Sixteen healthy subjects, university students (males), consented to participate in the study; aged: 21.2 ± 1.48 years, body height: 182.7 ± 9.19 cm, body mass: 77.85 ± 10.03 kg.

A Dyna-8 type general purpose, portable measuring system was developed, allowing the user to selectively collect numeric data and diagrams on hand and finger forces. The system can be connected to a host PC via USB to serial converter.

During the recording the maximum force value is fixed by a microcontroller and shown digitally on the electronic unit display. The force diagram is displayed simultaneously on the computer monitor (Bretz KJ et al., 2006).

Range of finger force measurement:	2–120 N
Range of all-purpose force measurement:	20–1,200 N
Linearity:	±1.5%
Hysteresis:	±1.5%
Sampling frequency:	300 Hz
Dimensions:	
Hand grip adapter:	250 × 150 × 30 mm
Finger force adapter:	∅ 22 × 100 mm
Electronic unit:	200 × 150 × 80 mm
Complete mass:	4.2 kg
Battery:	9 V
Power supply with mains adapter:	9 V

Performance of the measuring system
Force diagram recording time with PC: 240 s.
Manual scanning function.
Zoom function.

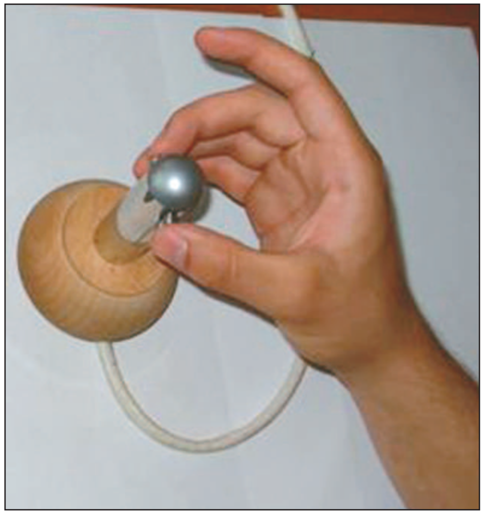

Figure 2. The selective finger force measurement. Middle finger–thumb. (At right)

Automatic maximum force value with time and slope value displaying.
Storage function, data bank.
Text file produced for Excel.

During the finger force measurement, the lower arm was on the table *(Figure 2)*. In this lower arm position the subjects pressed their fingers on the flat surfaces of the two screws on the adapter- one screw with the thumb and the opposite screw with any other finger *(Figure 2 and 3)*. During the measurement the subjects shaped a circle with their fingers in a horizontal plane.

They could easily do it in the given situation, since the height of the adapter of the two press-buttons was about 100 mm, which ensured a comfortable handling of the instrument. A visual feedback was also applied during the experiment. The subjects could see the formation of the force diagram on the computer screen simultaneously with the force exertion.

The next task was the measurement of the hand grasping force.

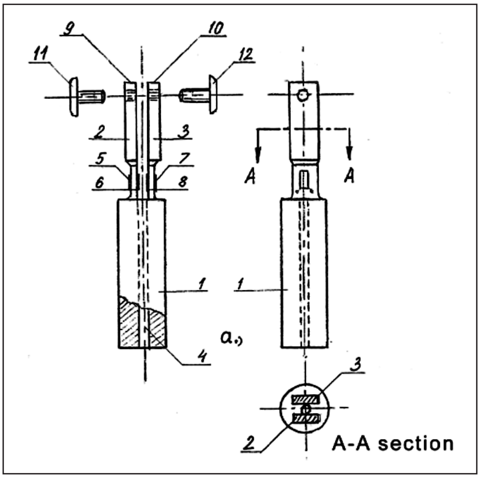

Figure 3. The fork-shaped measuring element built in the adapter *(Figure 2 and 4)*

Figure 4. The finger force sensor adapter and the electronic unit

Figure 3 illustrates the lateral view, front-view, and cross-sectional view of the fork-shaped measuring element (1), built in the adapter *(Figure 4)*. The strain gauges (5, 6, 7, 8) connected in a Wheatstone bridge, are stuck to the measuring plates (2, 3), in which screws (11, 12) produced with pressure surface are fixed. During measurement, as shown in *Figure 2,* the middle finger and the thumb grasp and press the screws on the pressure surfaces.

Results

Table 1 summarizes the hand and finger force values (16 male subjects). *Tables 2, 3* and *4* show the correlations between maximum finger forces.

Force measurement, right hand (N)						
	Hand	Little finger	Ring finger	Middle finger	Index finger	Thumb
Average	551.2	30.8	37.9	55.1	56.7	107.7
St. deviation	74.5	11.57	10.08	17.3	12.62	30.68
Force measurement, left hand (N)						
	Hand	Little finger	Ring finger	Middle finger	Index finger	Thumb
Average	505.2	28.4	37	53.7	60.4	109.5
St. deviation	112.7	10.26	11.26	12.04	14.6	28.9

Table 1. Results of force measurements: averages and standard deviations

Correlation coefficients & significances	Little finger Right	Ring finger Right	Middle finger Right	Index finger Right	Thumb Right
Little finger (Right)	1				
Ring finger (Right)	0.790** $p<0.000$	1			
Middle finger (Right)	0.647** $p<0.007$	0.744** $p<0.001$	1		
Index finger (Right)	0.349 $p<0.185$	0.564* $p<0.023$	0.242 $p<0.366$	1	
Thumb (Right)	–0.454 $p<0.077$	–0.253 $p<0.343$	–0.079 $p<0.772$	–0.371 $p<0.158$	1

Table 2. Correlations between right hand finger forces

Correlation coefficients & significances	Little finger Left	Ring finger Left	Middle finger Left	Index finger Left	Thumb Left
Little finger (Left)	1				
Ring finger (Left)	0.610* p<0.012	1			
Middle finger (Left)	0.439 p<0.089	0.661* p<0.005	1		
Index finger (Left)	0.446 p<0.084	0.537* p<0.032	0.642** p<0.007	1	
Thumb (Left)	–0.228 p<0.396	0.120 p<0.659	0.063 p<0.816	0.394 p<0.131	1

Table 3. Correlations between the left hand finger forces

Correlation coefficients & significances	Little finger Left	Ring finger Left	Middle finger Left	Index finger Left	Thumb Left
Little finger (Right)	0.719** p<0.002	0.565* p<0.023	0.408 p<0.117	0.453 p<0.078	–0.151 p<0.591
Ring finger (Right)	0.665** p<0.005	0.626** p<0.01	0.572* p<0.021	0.502* p<0.047	0.028 p<0.919
Middle finger (Right)	0.341 p<0.196	0.427 p<0.099	0.469 p<0.068	0.427 p<0.099	–0.098 p<0.717
Index finger (Right)	0.409 p<0.116	0.32 p<0.227	0.601* p<0.014	0.393 p<0.132	–0.254 p<0.342
Thumb (Right)	–0.695** p<0.003	–0.507* p<0.045	–0.465 p<0.069	–0.197 p<0.465	0.506* p<0.045

Table 4. Correlations between the right and left finger forces

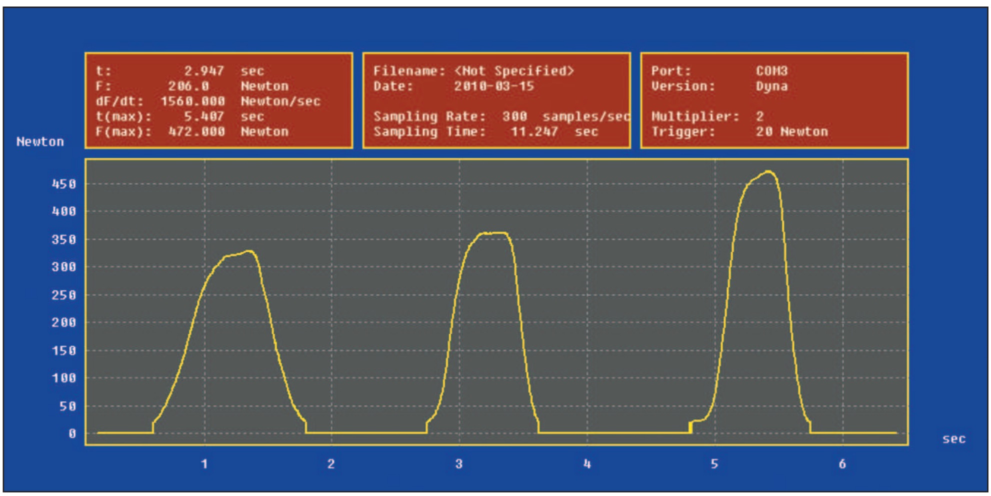

Figure 6. Diagram of hand grasping forces.
The following data are displayed: forces related to time elapsed; slope of the diagrams (dF/dt) at any time during measurement; maximum force and the moment when it occurred; sampling rate; measuring time; zoomed part; (adjustable) trigger level (20 N), etc.

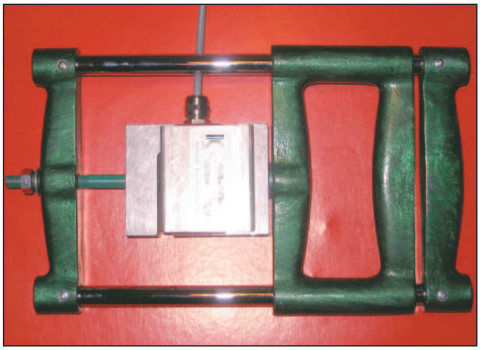

Figure 5. Hand grip adapter with force sensor

Discussion

The first goal of this study was to describe hand and finger force capabilities in relation to various couplings with handles and levers. The knowledge of grasping force makes it possible to create an estimation of the general neuromuscular power of the subject. Body dimensions correlate with maximum hand force (Roman-Liu et al., 2004).

Many researchers have already dealt with the measurement of finger forces. They have developed various methods in order to do this (Yokogawa and Hara, 2002). In some cases they applied the kind of sensors which simultaneously measured the exertions between the thumb and the other four fingers. The transducers are up-to-date, almost all of them are accurate and linear (Zatsiorsky, 2002, Gorniak et al., 2007).

In earlier solutions, there are four sensors opposing the thumb, but in some cases, none of these is opposite the sensor of the thumb. The axis of this sensor is coincident with the vector of the pressure force of the thumb, and is projected to the midpoint of the distance between the sensors of the middle finger and the ring finger on the opposite side of the sensor equipment. In the case of a fixed transducer this fact would not cause any problems. Using an elegant solution, the sensors were built in a table (Latash et al., 2007). If the reaction force against the other four fingers occurs due to the press of the thumb, and the sensor equipment is not fixed, then really only the (maximum) force of the thumb can be measured. The total force exerted by the four fingers could be greater than that of the thumb. As a consequence, with this method the maximal force exertion of the thumb, as well as the force distribution between the other fingers could be measured.

In order to determine the forces and torques of the other four fingers and their maximal values, the vector of the pressing force of the thumb has to coincide with the vector of the pressing force of one of the other fingers. While pinching with the thumb and any other finger, the force of the index, middle, ring, or little finger can be measured since the thumb is able to exert a greater force than any other finger due to its muscular and anatomical structure.

Bearing in mind the above mentioned conditions, the force measuring adapter was constructed in a way that it makes the selective measuring of the forces of fingers possible. According to this design, the uniaxial arrangement satisfies the original aim (Bretz et al., 2006).

Hand and finger force data can be used in numerous types of sport, industrial design, ergonomics, and rehabilitation.

References

1. *Bretz KJ, Jobbágy Á, Bretz K.* (2006) Equipment for investigation of hand and finger tremor and finger forces. Utility model, Hungarian Patent Office. Reg. No: 3 305. 1–11 p. (in Hungarian)

2. *Gorniak SL, Zatsiorsky VM, Latash ML.* (2007) Hierarchies of synergies: an example of two-hand multi-finger tasks. Exp. Brain. Res., 179:167–180.

3. *Kiung KU, Kwon D-S, Choi HJ et al. (*2004) Mouse interface device transmitting reaction force to user's arm and finger Patent No.: JP2004220593 and US2004140953, and DE102004001870.

4. *Lee M, Chien M* (TW) (2004) "Finger gripping force measuring or testing device" Patent No.: US6725728 1–3.p.

5. *Roman-Liu D, Tokarski T, Wojcik K.* (2004) Quantitative assessment of upper limb muscle fatigue depending on the conditions of repetitive task load. J. of Electromyography & Kinesiology, 14(6):671–682.

6. *Valero-Cuevas FJ.* (2000) Predictive modulation of muscle coordination pattern magnitude scales fingertip force magnitude over the voluntary range. The Journal of Neurophysiology, 83(3): 1469–1479.

7. *Yokogawa R, Hara K.* (2002) Measurement of distribution of maximum index-fingertip force in all directions at fingertip in flexion/extension plane. Journal of Biomechanical Engineering, 124:(3) 302–307.

8. *Zatsiorsky VM* (2002) Kinetics of human motion, ISBN 0-7360-3778-0. Human Kinetics, Champaign, IL USA.

9. *Zhang W, Zatsiorsky VM, Latash ML.* (2007) Finger synergies during multi-finger cyclic production of moment of force. Exp. Brain. Res., 177: 243–254.

Károly Bretz
Semmelweis University TF
Dept. of Biomechanics
H–1123 Budapest, Alkotás u. 44.

KÖSZÖNTŐ / GREETINGS

Csernátony Zoltán
a tudományos bizottság elnöke

Zoltán Csernátony
chief of the scientific committee

Illés Tamás
a szervezőbizottság elnöke

Tamás Illés
chief of the organization committee

A hagyományteremtés sikerének ünnepeként tekintünk a 4. Magyar Biomechanikai Konferencia elébe. Külön öröm számunkra, hogy a konferencia nem vált egy Budapest–Debrecen pingpongrendezvénnyé, hiszen a 2010-es évben Pécs vállalta a házigazda szerepét. Ez valahol az eszkaláció révén emel a rendezvény színvonalán, és reméljük, szerénytelenség nélkül mondhatjuk, hogy talán hozzáad valamely csekély értéket Pécs Európa kulturális fővárosi szerepéhez is.

Mint sokak számára ismeretes, legközelebb 2013-ban tervezzük megrendezni a konferenciát, azon egyszerű oknál fogva, hogy a páros évekre jelentősen nagyobb számban esnek tudományos ülések a biomechanika iránt esetlegesen érdeklődésre számot tartó szakterületeken. Így mindenkit arra buzdítunk, hogy „ürítse ki” szakmai tarsolyát, tegye azt közkinccsé, gazdagítva ezzel a magyar biomechanikai tudásbázis divatos kifejezéssel élve: hozzáadott értékét, tegye le a biomechanika műhelyasztalán szakmai névjegyét, hogy annál nagyobb várakozással tekintsenek az érdeklődők a 2013-as szereplésükre is.

Mindenkit szeretettel várunk tehát 2010 Európa Kulturális Fővárosában, Pécsett, szakmai örömöket ígérő részvételt kívánva.

Jelen digitális kiadványunk a konferencia kapcsán beküldött cikkeket tartalmazza.

It is with great joy to announce the 4th Hungarian Biomechanics Conference, which by now has become a tradition. It is an especially high honor that this year the conference is held in Pécs, and not in Debrecen or Budapest like in the previous years. This escalates the level of the program even more, as in 2010 Pécs is the Cultural Capital City in Europe.

As many people know the next conference will be held in 2013, for the simple reason that there is much more biomechanics related conferences in even years. That is why we encourage everyone to present their professional investigations, idea, and hypothesis to enrich the Hungarian Biomechanical knowledge so that in 2013 there will be a greater interest towards the realization of their research.

We give a warm welcome for everyone in the 2010 European Cultural Capital Pécs, and good luck in the conference.

Present digital issue contains the articles sent us in connection with the conference.

Lumbálisgerinc-szegmentumok degenerációjának numerikus szimulációja: I. Az életkorral járó degeneráció

Kurutzné Kovács Márta[1], Oroszváry László[2]
[1] Budapesti Műszaki és Gazdaságtudományi Egyetem, Budapest
[2] Knorr Bremse Hungaria Ltd, Budapest
kurutzm@eik.bme.hu

Absztrakt

A numerikus szimuláció olyan jelenségek és folyamatok követésére is alkalmas, amelyek kísérleti úton nem vizsgálhatók. Ilyenek például a gerinc öregedéssel járó degenerációs folyamatai. A jelen dolgozatban az emberi lumbálisgerinc-szegmentumok nyomóteherből eredő, öregedéssel járó károsodási folyamatainak a végeselemes szimulációját mutatjuk be 3D végeselem-modellek alapján. A korral járó degenerációs folyamatot a szegmentumot alkotó egyes szervek anyagi tulajdonságainak változásával modellezzük. A kidolgozott végeselem-modelleket húzásra és nyomásra egyaránt úgy validáltuk, hogy a számítási eredményeinket összehasonlítottuk a saját és a szakirodalomból rendelkezésre álló kísérleti mérési adatokkal. Öt degenerációs fokozatot dolgoztunk ki a teljesen egészségestől a teljesen degeneráltig. A degenerációs folyamat két legfontosabb tényezőjének, a porckorong nucleusában lévő hidrosztatikus nyomásnak és a nucleus keményedésének a hatását külön-külön vizsgáltuk az öregedési folyamat során, és azt tapasztaltuk, hogy a degenerációs folyamat kezdeti szakaszában a hidrosztatikus nyomás megszűnésének van domináns hatása, míg a későbbiekben a nucleus keményedése a döntő. Ez azt mutatta, hogy a nyomómerevség az alig degenerált fiatal szegmentumnál a legkisebb, vagyis az instabilitás kockázata ekkor a legnagyobb, és a stabilitás esélye a további öregedéssel és degenerációval megnő. Kimutattuk, hogy a szegmentum merevségében a nucleusnak van domináns szerepe. Ahhoz, hogy a nucleus folyadékszerű, kezdeti egészséges állapotát pontosan modellezni tudjuk, a rugalmassági modulusát 1 MPa értéknél kisebbre, célszerűen 0,1 MPa értékre kell felvenni. A lumbális gerinc degenerációs folyamatainak végeselemes szimulációja segít megérteni e folyamatok kialakulását és lefutását, annak okait, de segít a lumbális porckorongproblémák konzervatív kezelési eljárásainak tökéletesítésben is.

Kulcsszavak: emberi lumbális mozgásszegmentum; korral járó degeneráció; porckorong; végeselem-modell; numerikus szimuláció; nyomási merevség

Abstract

Numerical simulation is an effective tool for analyzing phenomena that cannot be clarified by experimental methods, like spinal degeneration processes. 3D finite element simulation of age-related degeneration processes of lumbar functional spinal units was investigated in axial compression. Aging degeneration was modeled by the material properties of the components of the segment, validated both for compression and tension, by comparing the numerical results with experimental data. Five grades of aging degeneration were distinguished from the healthy to fully degenerated case. By systematic numerical analysis of the separated effect of the mechanical components of aging degeneration it was proved that at the beginning phase of aging process the effect of loss of hydrostatic stress state had a dominant effect, while in further aging the hardening of nucleus dominates, leading to the largest deformability and the smallest compressive stiffness, consequently, to the risk of segmental instability at mildly degenerated case, while stiffness and stability increased with further aging. In the numerical modeling of hydrostatic state of a healthy nucleus, smaller than 1 MPa Young's modulus of nucleus must be considered to cut down the nuclear stress divergence below 10%. For healthy nucleus, E=0.1 MPa seems to be acceptable. FE simulations of degeneration processes of lumbar segments may help clinicians to understand the initiation and progression of disc degeneration and to treat lumbar discopathy problems even more effectively.

Keywords: human lumbar functional spinal unit; age-related degeneration; intervertebral disc; finite element model; numerical simulation; compressive stiffness

1. Bevezetés

A gerincdegeneráción annak felépítésében, szerkezetében és működésében beálló káros elváltozásokat értjük. A degeneráció általános fogalom, a gerinc degenerációi két alapvető osztályba sorolhatók: (1) a hosszú idejű, *életkorral járó degenerációk,* és (2) a külső hatásra kialakuló rövidebb idejű ún. *környezeti degenerációk*. Ilyen környezeti hatások elsősorban a mechanikai hatások, a különféle terhek, a fiziológiai, a sportolási vagy munkavégzési terhek, vagy éppen a balesetből eredő traumatikus terhek. További környezeti degenerációt okozhat a fagyás, égés, vegyi-, vagy sugárkárosodás stb. A mechanikai eredetű degenerációk a környezeti degeneráció külön osztályát képezik, ezek a rövid idő alatt, rendszerint váratlanul fellépő mechanikai túlterhelésből adódó ún. *hirtelen degenerációk*. Ilyen lehet például az elesés, vagy éppen egy rossz mozdulat[1]. Ebben a tanulmányban csak az életkori károsodásokkal foglakozunk; a hirtelen károsodást a tanulmány második részében elemezzük[2].

A porckorong a szegmentum legkritikusabb alkotórésze, amelynek bármilyen károsodása jelentősen befolyásolhatja a szegmentum teherbírását és stabilitását[3]. Az öregedéssel járó károsodás a porckorong nucleusában jelentkezik először. A nucleus kezdi elveszteni folyadékszerű viselkedését, és megszűnik benne a hidrosztatikus nyomás feszültségállapota, a száradással egyidejűleg keményedni kezd, merevsége növekszik[4,5,1]. Eközben a teherbírás átrendeződése és irányváltozása miatt egyéb károsodási formák is megjelenhetnek, például az annulus felhasadása, a belső annulus kihajlása, a véglemezek berepedése, vagy a csontritkulásos csigolyák megroppanása[6,7]. Az utóbbi idők kutatásai, valamint a derékfájós, porckorongbántalommal orvoshoz forduló betegek életkori statisztikái kimutatták, hogy a fiatal, kevéssé degenerált szegmentumokat fenyegeti inkább a stabilitásvesztés, míg az idősödés során a stabilitás egyre inkább biztosított[1,8,9]. Az okok numerikus szimulációval történő kimutatása ennek a tanulmánynak az egyik célja.

Az utóbbi időben számos tanulmány foglalkozik a lumbális gerinc degenerációjának a numerikus, végeselemes modellezésével. Iatridis és munkatársai[10,11] kimutatták, mint válik a nucleus folyadékból szilárd halmazállapotúvá az öregedés során. Natarajan és munkatársai[6,12] poro elasztikus végeselem-modellt alkalmaztak az életkorral járó degeneráció szimulálására. Polikeit és munkatársai[13] több degenerációs fokozatot definiáltak: először a nucleus keményedett, majd az egész porckorong, azután a belső annulusban lévő szálakat távolították el, végül az annulus külső szálait is legyengítették. Rohlmann és munkatársai[8] három degenerációs fázist különböztettek meg: csökkentették a porckorong magasságát a nucleusban lévő hidrosztatikus nyomással arányosan. Tang és munkatársai[14] a porckorong magasságával együtt az anyagállandókat is változtatták a degeneráció szimulálására. Schmidt és munkatársai[15,16] a degenerációs fokozatokat a magasság csökkentésével, a nucleus rugalmassági modulusának növelésével, a véglemezek görbületének növelésével, a kisízületek irányának változtatásával és csontkinövések beiktatásával alakították ki. E tanulmányok legtöbbje leszögezi, hogy az instabilitás leginkább a gyengén degenerált fiatalabb szegmentumokat veszélyezteti.

A jelen tanulmány célja az életkori degenerációs folyamat numerikus követése, a degeneráció kialakulására vonatkozó következtetések levonása, és annak – a sokak által felvetett – kérdésnek a megválaszolása, hogy miért a fiatal felnőtteket veszélyezteti leginkább a porckorongbántalom.

2. Módszerek

2.1. A lumbális szegmentum végeselemes modellje

A 3D geometriai modellt egy tipikus lumbális szegmentum méretei alapján vettük fel. A csigolyatest modelljénél külön kezeltük a corticalis és trabecularis csontszakaszokat és a nyúlványokat *(1. a ábra)*. A porckorongnál külön szerkezetet képezett a nucleus és az annulus; az annulust kompozitnak tekintve, ahol a mátrixot és a szálakat több gyűrűszerű rétegből építettük fel *(1. b ábra)*. Mind a hét gerincszalagot és ezek különféle kapcsolódási viszonyait is figyelembe vettük. A végeselemes hálózatot Pro/Engineer, ANSYS Workbench és ANSYS Classic programok segítségével vettük fel *(1. c ábra)*.

A végeselem-modellnél az egyes szervekre más-más elemtípust alkalmaztunk. Az annulus mátrixot, a nucleust és a szivacsos csontot, a nyúlványokat és a kisízületeket, továbbá bizonyos kapcsolatokat térfogatelemekből, a csontos véglemezeket és a csigolya corticalis részét, valamint a szalagokat héjelemekből, végül az annulus szálait rúdelemekből építettük fel.

1. ábra. A szegmentum geometriai és végeselemes modellje

A csontok rugalmas anyagállandóinak felvételénél elsősorban a szakirodalomra támaszkodtunk[17–23]. A nucleus collagen szálait csak húzásra dolgozó lineárisan rugalmas anyagúnak feltételeztük, radiálisan kifelé növekvő rugalmassági modulussal[17–20,24–30]. Mind a hét szalagot csak húzásra dolgozó lineárisan rugalmas anyaggal vettük figyelembe[18,31,32]. Az egészséges szegmentum anyagállandóit az *1. táblázat* mutatja.

A szegmentum alkotórészei	Rugalmassági modulus [MPa]	Poisson-tényező
Corticalis héj	12000	0,3
Szivacsos csont	150	0,3
Csigolyanyúlványok	3500	0,3
Véglemezek	100	0,4
Annulusmátrix	4	0,45
Annulusszálak	500/400/300**	–
Nucleus	1	0,499
Elülső hosszanti szalag	8*	0,35
Hátulsó hosszanti szalag	10*	0,35
A többi szalag	5*	0,35

1. táblázat. Az egészséges szegmentum anyagállandói
*húzás, **külső/közbenső/belső szálak, húzás

2.2. A lumbális szegmentum életkori degenerációs modellje

Az öregedéssel járó degeneráció modellezése során a nucleusban megszűnő hidrosztatikus nyomást a Poisson-tényező csökkenésével, a nucleus fokozatos keményedését pedig a rugalmassági modulusa növekedésével modelleztük[33,34]. Öt degenerációs fokozatot állítottunk fel az egészségestől a teljesen degenerált állapotig, amelyekben figyelembe vettük a belső annulus kihajlását, ezért az annulus öregedésénél csak kismértékű keményedést vettünk figyelembe. A modellben a szivacsos csont és a véglemezek korral járó gyengülését is figyelembe vettük.

A numerikus szimulációt 1000 N nyomóteherre végeztük, amelyben figyelembe vettük, hogy a lumbális nyomóerőt egyrészt a felsőtest súlya, amely a testsúly mintegy 60%-a[35,36], másrészt a gerincet egyensúlyban tartó izomerők alkotják, mely utóbbi megközelítőleg ugyanakkora, mint a felsőtest súlya.

2.3. A lumbális szegmentum végeselemes modelljének validálása

Az egészséges és a degenerált végeselemes modell validálását húzásra és nyomásra egyaránt elvégeztük[37]. Nyomás esetén a porc-

Degenerációs fokozatok	1. fokozat egészséges		2. fokozat		3. fokozat		4. fokozat		5. fokozat teljes deg.	
	E (MPa)	ν	E (MPa)	ν	E (MPa)	ν	E (MPa)	ν	E (MPa)	ν
Nyomás										
nucleus	1	0.499	3	0.45	9	0.4	27	0.35	81	0.3
annulusmátrix	4	0.45	4.5	0.45	5	0.45	5.5	0.45	6	0.45
szivacsos csont	150	0.3	125	0.3	100	0.3	75	0.3	50	0.3
véglemezek	100	0.4	80	0.4	60	0.4	40	0.4	20	0.4
Húzás										
nucleus	0.4	0.499	1.0	0.45	1.6	0.4	2.2	0.35	2.8	0.3
annulusmátrix	0.4	0.45	1.0	0.45	1.6	0.45	2.2	0.45	2.8	0.45

2. táblázat. A degenerált szegmentum anyagállandói korong szagittális középsíkjában keletkező függőleges nyomófeszültségek számításból kapott nagyságát és eloszlását hasonlítottuk össze Nachemson[35], Adams és munkatársai[1,5], Dolan és Adams[38], Adams és Dolan[39] porckorongba szúrt tűre szerelt feszültségmérő műszerrel mért, ún. stress-profilometriával nyert kísérleti eredményeivel. Az eredmények meggyőző egyezést mutattak. Húzás esetén az L3–S1 lumbális szakaszhoz tartozó szegmentumra számított megnyúlási eredményeinket hasonlítottuk össze Kurutz[40] és munkatársai[41] a súlyfürdőben in vivo mért kísérleti eredményeivel. Nemcsak a megnyúlási értékek, hanem azok életkori megoszlását mutató függvények is nagy hasonlóságot mutattak. Ezek szerint tehát a fenti táblázatok szerint felvett anyagállandók elfogadható alapot képeznek az öregedési degenerációs folyamatok numerikus szimulációjához.

3. Eredmények

A szegmentum porckorongjának 1000 N centrikus nyomóerőre bekövetkezett összenyomódását mutatja a *2. ábra.* A *2. a ábrá*n valamennyi degenerációs tényező együttese hatására létrejövő összenyomódásokat látjuk a degeneráció előrehaladtával. A *2. b* és *2. c ábrá*n külön-külön látjuk a nucleusbeli hidrosztatikus feszültségállapot csökkenésének és a nucleus szilárdulásának hatását. A *2. b ábrá*n a Poisson-tényező csökkenésének hatása látható adott rugalmassági modulusok mellett, a *2. c ábrá*n a rugalmassági modulus növekedésének hatása látható adott Poisson-tényezők mellett.

A *2. a ábrá*n látható, hogy a porckorong összenyomhatósága a 2. degenerációs fokozatnál, az alig degenerált, fiatal porckorongnál a legnagyobb. A *2. b ábrá*ról azt látjuk, hogy a nucleusban uralkodó hidrosztatikus nyomás megszűnésével monoton növekszik a porckorong összenyomhatósága bármely rugalmassági modulus mellett. A *2. c ábra* azt mutatja, hogy a nucleus keményedésével monoton csökken a porckorong összenyomhatósága a megszűnő hidrosztatikus nyomás bármely stádiumában. A *2. a* és *2. b ábrá*k összevetéséből látjuk, hogy a degenrációs folyamat kezdetén a nucleusban lévő hidrosztatikus nyomás megszűnésének van domináns hatása; míg a *2. a* és a *2. c ábrá*k egybevetése azt mutatja, hogy a további degeneráció során a nucleus keményedésének a hatása a döntő. A *2. a ábrá*n azt látjuk, hogy az életkori degenerációs folyamat során a *2. b* és *2. c ábrá*kon látható ellentétes hatások harca zajlik, emiatt a porckorong degenerációs deformációja nem monoton függvény.

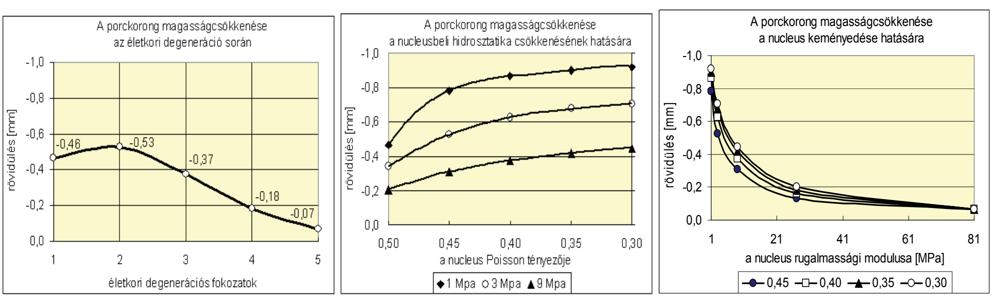

a) *b)* *c)*

2. ábra. A porckorong összenyomódásának változása *a)* a degenerációs folyamat során, *b)* a nucleus Poisson-tényezőjének csökkenése függvényében különböző rugalmassági modulusok mellett, *c)* a nucleus rugalmassági modulusának növekedése függvényében különböző Poisson-tényezők mellett

Minden szempontból hasonló viselkedést mutatott a porckorong kihasasodása elülső, hátulsó és oldalsó irányban egyaránt, és különösen az annulusban a maximális posterolaterális szálerők, amint azt a *3. ábra* mutatja.

A *4. ábrá*n a függőleges nyomófeszültségek változását láthatjuk a degenerációs folyamat során a porckorong szagittális középsíkjában a nucleus közepén. A *4. a ábrá*n látható, hogy a nucleus közepén a függőleges nyomófeszültségek a 2. degenerációs fokozatnál, az alig degenerált, fiatal porckorongnál a legkisebbek.

A *4. b ábrá*ról azt látjuk, hogy a nucleusban uralkodó hidrosztatikus nyomás megszűnésével e feszültségek monoton csökkennek bármely rugalmassági modulus mellett. A *4. c ábra* azt mutatja, hogy a nucleus keményedésével viszont növekszik a nyomófeszültség a megszűnő hidrosztatikus nyomás bármely stádiumában, és csak extra kemény nucleusnál csökken kissé. A *4. a* és *4. b ábrá*k összevetéséből látjuk, hogy a degenerációs folyamat kezdetén a nucleusban lévő hidrosztatikus nyomás megszűnésének van domináns hatása; míg a *4. a* és a *4. c ábrá*k egybevetése azt mutatja, hogy a további degeneráció során a nucleus keményedése a döntő. A *4. a ábrá*n azt látjuk, hogy az életkori degenerációs folyamat során a *4. b* és *4. c ábrá*kon látható ellentétes hatások ütköznek egymással, emiatt a nucleus közepén a nyomófeszültségek degenerációs változása nem monoton függvény.

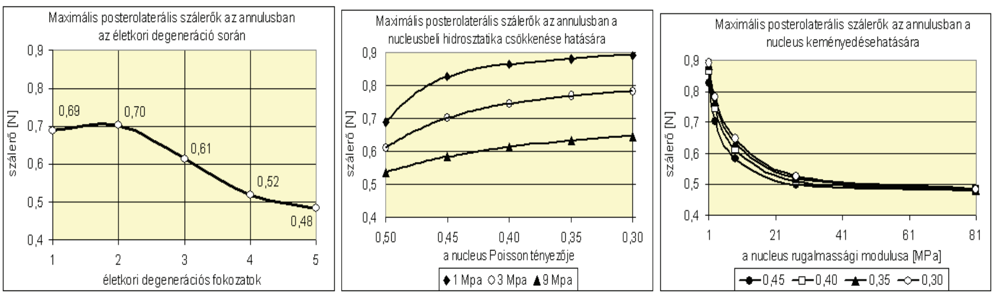

a) *b)* *c)*

3. ábra. Maximális posterolaterális szálerők az annulusban
a) az életkori degenerációs folyamat során, *b)* a nucleus Poisson-tényezőjének életkori csökkenése hatására, *c)* a nucleus rugalmassági modulusának életkori növekedése hatására

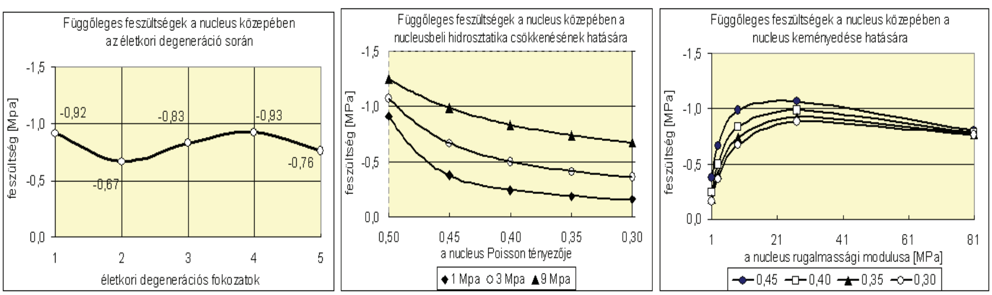

a) *b)* *c)*

4. ábra. Függőleges nyomófeszültségek változása a nucleus közepén
a) az életkori degenerációs folyamat során, *b)* a nucleus Poisson-tényezőjének életkori csökkenése hatására, *c)* a nucleus rugalmassági modulusának életkori növekedése hatására

A *4. ábrá*t a *2.* és *3. ábrá*val összevetve látható, hogy a nucleus közepén fellépő nyomófeszültségek a porckorong deformációival éppen ellentétes viselkedést mutatnak a degenerációs folyamat során.

Az *5. ábrá*n a függőleges nyomófeszültségek degenerációs változását láthatjuk a nucleus peremén a szagittális középsíkban. Az *5. b* és *5. c ábrá*k szerint ezek a feszültségek monoton csökkennek a nucleus Poisson-tényezője csökkenésével, és monoton növekednek a nucleus keményedésével. A komplex degenerációs folyamat során e feszültségek a 2. degenerációs fokozatnál a legkisebbek, később monoton nőnek az *5. a ábra* szerint. A degenerációs folyamat kezdetén most is a nucleus Poisson-tényezője csökkenésének a hatása a döntő.

A *6. ábrá*n a belső annulusban ébredő függőleges nyomófeszültségek változását láthatjuk a degenerációs folyamat során a szagittális középsíkban. A *6. b ábra* szerint a belső annulus érzékeny a nucleus rugalmassági modulusára, vagyis csak akkor csökken benne a függőleges nyomófeszültség a hidrosztatika megszűnésével, ha a nucleus valóban lágy (E=1 MPa), egyébként alig változik. A nucleus keményedésével azonban a belső annulusban a függőleges nyomófeszültségek monoton csökkennek a *6. c ábra* szerint. A komplex degenerációs folyamat során e feszültségek szinte lineárisan csökkennek.

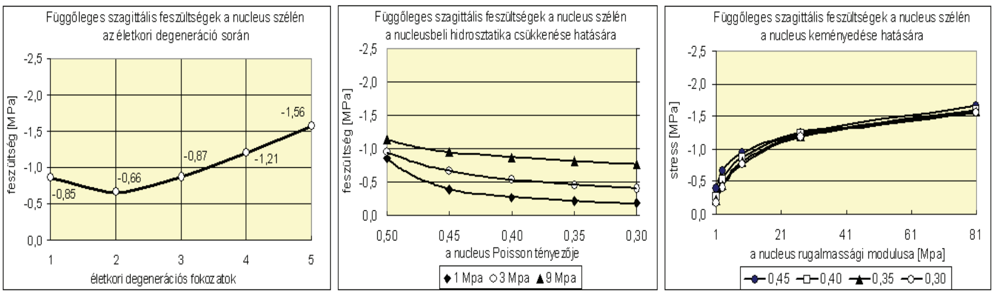

a) *b)* *c)*

5. ábra. Függőleges nyomófeszültségek változása a nucleus szagittális peremén
a) az életkori degenerációs folyamat során, *b)* a nucleus Poisson-tényezőjének életkori csökkenése hatására, *c)* a nucleus rugalmassági modulusának életkori növekedése hatására

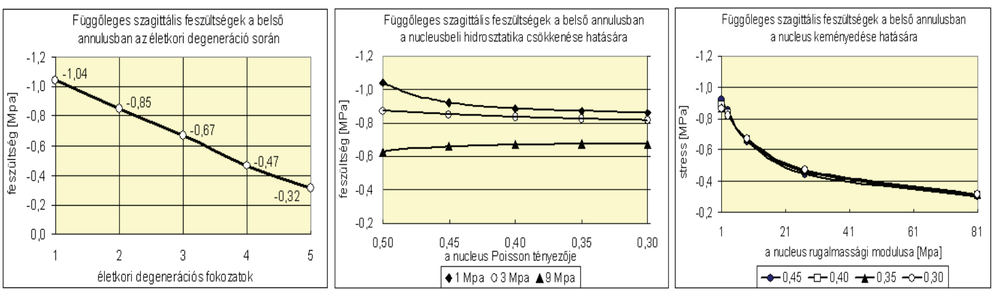

a) *b)* *c)*

6. ábra. Függőleges nyomófeszültségek változása a szagittális belső annulusban
a) az életkori degenerációs folyamat során, *b)* a nucleus Poisson-tényezőjének életkori csökkenése hatására, *c)* a nucleus rugalmassági modulusának életkori növekedése hatására

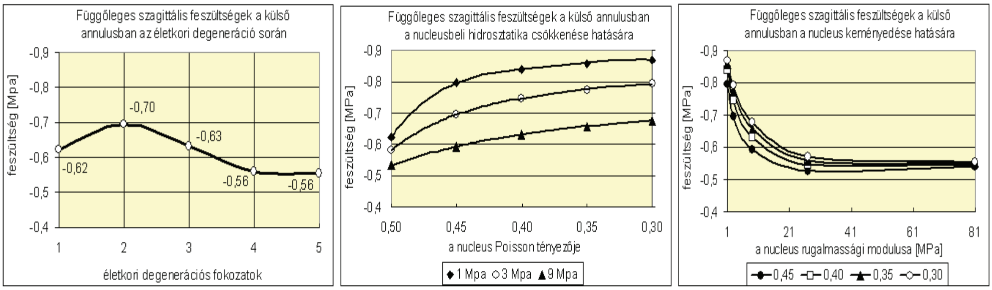

a) *b)* *c)*

7. ábra. Függőleges nyomófeszültségek változása a szagittális külső annulusban *a)* az életkori degenerációs folyamat során, *b)* a nucleus Poisson-tényezőjének életkori csökkenése hatására, *c)* a nucleus rugalmassági modulusának életkori növekedése hatására

A *7. ábra* a külső annulusban mutatja a függőleges nyomófeszültségek változását a degenerációs folyamat során a szagittális középsíkban. A *7. b* és *7. c ábrá*k szerint ezek a feszültségek monoton növekednek a nucleus Poisson-tényezője csökkenésével, és monoton csökkennek a nucleus keményedésével. A komplex degenerációs folyamat során e feszültségek a 2. degenerációs fokozatnál a legnagyobbak, és később csökkennek a *7. a ábra* szerint.

A *7. ábra* és a *4. ábra* összevetéséből látjuk, hogy a külső annulusbeli függőleges nyomófeszültségek a nucleusközepi feszültségekkel ellentétesen viselkednek. Ha a nucleusban csökken a feszültség, akkor a külső annulusban megnő, és ez fordítva is igaz. A degenerációs folyamat kezdetén most is a nucleusbeli hidrosztatika csökkenésének a hatása a döntő. A *7. ábrá*t a *2.* és *3. ábrá*val összevetve látható, hogy a külső annulusban fellépő nyomófeszültségek a porckorong deformációival megegyező viselkedést mutatnak a degenerációs folyamat során.

A *8. ábrá*n a porckorong alkotórészeinek átlagos függőleges merevségét tüntettük fel az öregedési degenerációs folyamat során. Az öt degenerációs fokozatban a nucleus átlagos merevsége 710, 460, 830, 2090 és 5510 N/mm; a belső annulusé 1210, 1020, 1220, 1980 és

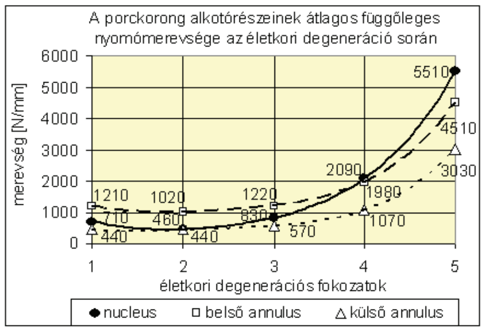

8. ábra. A porckorong alkotórészeinek átlagos függőleges nyomómerevsége az életkori degeneráció során

4510 N/mm; a külső annulusé pedig 440, 440, 570, 1070 és 3030 N/mm volt. A teljes porckorong függőleges nyomómerevsége 2400, 1900, 2600, 5100 és 13000 N/mm értékre adódott. A *8. ábra* mutatja, hogy valamennyi alkotórész és a teljes porckorong merevsége a 2. degenerációs fokozatban, a gyengén degenerált fázisban a legkisebb.

4. Megbeszélés

A porckorong életkori degenerációs folyamatának numerikus modellezésénél a belső annulus kihajlását figyelembe kell venni. Ha a nucleus keményedésével párhuzamosan az annulusnál is jelentős keményedést feltételezünk, akkor a kísérleti eredményekkel ellentétes feszültség-megoszlást tapasztalunk a porckorongban[1, 39].

A porckorong életkori degenerációs folyamatának numerikus modellezésénél az egészséges nucleus rugalmassági modulusát 1 MPa értéknél kisebbre célszerű felvenni, hogy a hidrosztatikus feszültségi állapot biztosítható legyen. Ennél nagyobb értéknél a különböző irányú feszültségek 10% fölé divergálnak. A legcélszerűbb érték 0.1 MPa, ezt a szakirodalomban azonban kevesen használják[20,45], Néhányan[30,42–44], az $E=4$ MPa és $\nu=0.499$ értékpárt, többen[17,19,23,46] az $E=1$ MPa és $\nu=0.499$ adatokat használják a numerikus szimulációnál.

Amíg a függőleges feszültségek lényegesen változnak a degeneráció során, a vízszintes feszültségek alig változnak. Ennek az a magyarázata, hogy míg a függőleges nyomófeszültségek érzékenyen reagálnak a nucleus hidrosztatikus feszültségállapotának megszűnésére, a vízszintes feszültségek kevésbé. A hidrosztatika megszűnésével járó feszültségdivergenciát éppen a függőleges feszültségek erőteljesebb megváltozása idézi elő.

Az életkori degeneráció két legfontosabb tényezője a nucleusban uralkodó hidrosztatikus feszültségi állapot megszűnése és a nucleus keményedése. E két tényező lényegében a nucleus folyadékszerű állapotának a szilárd halmazállapotba való áttérésének letéteményese. E két összetevő hatásának az elkülönített elemzése kizárólag numerikus szimulációval végezhető, kísérleti úton nem.

A degenerációs folyamat kezdeti szakaszán a hidrosztatika megszűnésének a hatása dominál, a folyamat további fázisaiban a keményedés a döntő. Ennek oka az, hogy hidrosztatikus feszültségállapotban csak folyadék lehet, szilárd anyag nem, és mivel a nucleus csak fiatal, egészséges állapotában mutat folyadékszerű viselkedést, ennek megváltozása csakis a kezdeti szakaszra eshet, amikor a nucleus még kellően lágy. Ezt a nyilvánvaló tényt numerikus kísérleteinkkel igazoltuk *(2–7. ábrák)*.

A nucleus összenyomhatatlansága fokozatos megszűnésének a kezdeti degenerációs szakaszbeli dominanciája következtében a nucleus nyomási teherbírása a fiatal, gyengén degenerált porckorongnál a legkisebb *(4–5. ábra),* ugyanekkor a porckorong deformációja, összenyomódása, kihasasodása a legnagyobb *(2. ábra)*. Következésképpen a kettő hányadosaként előálló nyomási merevség és teherbírás a nucleusban ekkor a legkisebb *(8. ábra)*. Hasonlóan ebben a korai degenerációs fázisban van minimuma a belső annulus merevségének is, míg a külső annulus merevsége ebben a szakaszban állandó. Valóban, a porckorong alkotórészeinek átlagos merevsége egészséges porckorongban 400–1200 N/mm, gyengén degenerált porckorongnál 400–1000 N/mm, közepesen degenerált esetben 500–1200 N/mm, súlyosan degenerált esetben 1100–2100 N/mm, teljesen degenerált porckorongban 3000–5500 N/mm közötti értékre adódott *(8. ábra)*.

A teljes porckorong merevségében a nucleus merevségének döntő szerepe van. Következésképpen a teljes porckorong fiatal, gyengén degenerált állapotában rendelkezik a legkisebb függőleges nyomási merevséggel, vagyis az instabilitási kockázat a fiatal, gyengén degenerált porckorongnál a legnagyobb, majd a degenerációs folyamat további fázisaiban a merevség és a stabilitási esély szignifikánsan növekszik *(8. ábra)*. Valóban, a teljes porckorong merevsége az öt degenerációs fázisban mintegy 2400, 1900, 2600, 5100 és 13000 N/mm értékben változott. Schmidt és munkatársai[15] kimutatták, hogy a porckorongsérv, a disc prolapsus előfordulása a gyengén degenerált porckorongoknál a leggyakoribb, míg a közepesen vagy súlyosan degenerált eseteknél egyre kevésbé fordul elő. Tang és munkatársai[14] szerint a gyenge degeneráció instabilitáshoz vezet, de a tovább erősödő degeneráció javítja a stabilitási esélyt, mert a porckorong merevsége gyengén degenerált esetben a legkisebb, és a további degenerációval egyre növekszik. Adams és munkatársai[1] kísérletei azt mutatták, hogy a 40–50 évesek sérvre hajlamos cadaver porckorongjai nem voltak degeneráltak, míg a sérvre nem hajlamos porckorongok súlyosan degeneráltak voltak.

Numerikus szimulációval igazoltuk, hogy a nucleus teherbírása gyengén degenerált stádiumban a legkisebb, deformációja a legnagyobb, következésképpen a porckorong kompressziós merevsége, ellenállása ekkor a legkisebb, ami a szegmentum instabilitásához, sérülésekhez, fájdalomhoz vezet fiatal felnőtt korban. Ez a magyarázata annak, hogy a derékfájás, a sokféle porckorongbántalom elsősorban ezt a generációt sújtja. Ezt bizonyítja Bender és munkatársai[47] tanulmánya is, miszerint a hazai reumatológusok és balneológusok tapasztalatai szerint a discopathiás betegek oroszlánrészét a 40–55 év közötti populáció képezi.

IRODALOM

1. *Adams MA, Bogduk N, Burton K, Dolan P.* 2002. The Biomechanics of Back Pain. Churchill Livingstone, Edinburgh, London, New York, Oxford, Philadelphia, St Louis, Sydney, Toronto, 238 p.

2. *Kurutz M, Oroszváry L.* 2010. Lumbális gerincszegmentumok degenerációjának numerikus szimulációja: II. Hirtelen fellépő degeneráció. A IV. Magyar Biomechanikai Konferencia, Pécs, 2010. május 8-9.

3. *Ferguson SJ, Steffen T.* 2003. Biomechanics of the aging spine. European Spine Journal, Suppl 2: S97–S103.

4. *McNally DS, Adams MA.* 1992. Internal intervertebral disc mechanics as revealed by stress profilometry. Spine, 17:66–73.

5. *Adams MA, McNally DS, Dolan P.* 1996. Stress distributions inside intervertebral discs. The effects of age and degeneration. J. Bone Joint Surg. Br. 78(6):965–972.

6. *Natarajan RN, Williams JR, Andersson GB.* 2004. Recent advances in analytical modelling of lumbar disc degeneration. Spine, 29:2733–2741.

7. *Little JP, Adam CJ, Evans JH, Pettet GJ, Pearcy MJ.* 2007. Nonlinear finite element analysis of anular lesions in the L4/5 intervertebral disc. Journal of Biomechanics, 40:2744–2751.

8. *Rohlmann A, Zander T, Schmidt H, Wilke HJ, Bergmenn G.* 2006a. Analysis of the influence of disc degeneration on the mechanical behaviour of a lumbar motion segment using the finite element method. Journal of Biomechanics, 39: 2484–2490.

9. *Schmidt H, Heuer F, Simon U, Kettler A, Rohlmann A, Claes L, Wilke HJ.* 2006. Application of a new calibration method for a three-dimensional finite element model of a human lumbar annulus fibrosus. Clinical Biomechanics, 21:337–344.

10. *Iatridis JC, Wedenbaum M, Setton LA, Mow VC.* 1996. Is the nucleus pulposus a solid or a fluid? Mechanical behaviours of the nucleus pulposus of the human intervertebral disc. Spine, 21(10): 1174–1184.

11. *Iatridis JC, Setton LA, Wedenbaum M, Mow VC.* 1997. Alterations in the mechanical behavior of the human lumbar nucleus pulposus with degeneration and aging. Journal of Orthopaedic Research, 15(2):318–322.

12. *Natarajan RN, Williams JR, Andersson GB.* 2006. Modeling changes in intervertebral disc mechan-

ics with degeneration. Journal of Bone and Joint Surgery Am. 88(4), Suppl. 2:36–40.

13. *Polikeit A, Nolte LP, Ferguson SJ.* 2004. Simulated influence of osteoporosis and disc degeneration on the load transfer in a lumbar functional spinal unit. Journal of Biomechanics, 37:1061–1069.

14. *Tang XJ, Chen QX, Liu YS, Li FC.* 2008. Analysis of lumbar disc degeneration using three-dimensional nonlinear finite element method (Article in Chinese). Zhonghua Yi Xue Za Zhi, 88(23):1634–1638.

15. *Schmidt H, Kettler A, Rohlmann A, Claes L, Wilke HJ.* 2007. The risk of disc prolapses with complex loading in different degrees of disc degeneration – a finite element analysis. Clinical Biomechanics, 22(9):988–998.

16. *Schmidt H, Heuer F, Wilke HJ.* 2009. Dependency of disc degeneration on shear and tensile strains between annular fiber layers for complex loads. Medical Engineering Physics, 31(6):642–649.

17. *Shirazi-Adl SA, Shrivastava SC, Ahmed AM.* 1984. Stress analysis of the lumbar disc-body unit in compression. A three-dimensional nonlinear finite element study. Spine, 9(2):120–34.

18. *Goel VK, Monroe BT., Gilbertson LG, Brinckmann P.* 1995. Interlaminar shear stresses and laminae separation in the disc. Finite element analysis of the L3–L4 motion segment subjected to axial compressive loads. Spine, 20(6):689–698.

19. *Cheung JTM, Zhang M, Chow DHK.* 2003. Biomechanical responses of the intervertebral joints to static and vibrational loading: a finite element study. Clinical Biomechnaics, 18:790–799.

20. *Denoziere G, Ku DN.* 2006. Biomechanical comparison between fusion of two vertebrae and implantation of an artificial intervertebral disc. Journal of Biomechanics, 39:766–775.

21. *Rohlmann A, Bauer L, Zander T, Bergmann G, Wilke HJ.* 2006b. Determination of trunk muscle forces for flexion and extension by using a validated finite element model of the lumbar spine and measured in vivo data. Journal of Biomechanics, 39:981–989.

22. *Noailly J, Wilke HJ, Planell JA, Lacroix D.* 2007. How does the geometry affect the internal biomechanics of a lumbar spine bisegment finite element model? Consequences on the validation process. Journal of Biomechanics, 40:2414–2425.

23. *Williams JR, Natarajan RN, Andersson GBJ.* 2007. Inclusion of regional poroelastic material properties better predicts biomechanical behaviour of lumbar discs subjected to dynamic loading. Journal of Biomechanics, 40:1981–1987.

24. *Shirazi-Adl A, Ahmed AM, Shrivastava SC.* 1986. A finite element study of a lumbar motion segment subjected to pure sagittal plane moments. Journal of Biomechanics, 19(4):331–350.

25. *Spilker RL, Jakobs DM, Schultz AB.* 1986. Material constants for a finite element model of the intervertebral disc with a fibre composite annulus. Journal of Biomechanical Engineering, 108: 1–11.

26. *Shirazi-Adl A.* 1989a. On the fibre composite material models of the annulus – comparison of predicted stresses. Journal of Biomechanics, 22:357–365.

27. *Shirazi-Adl A.* 1989b. Strain in fibers of a lumbar disc. Analysis of the role of lifting in producing disc prolapse. Spine, 14(1):96–103.

28. *Rao AA, Dumas GA.* 1991. Influence of material properties on the mechanical behaviour of the L5–S1 intervertebral disc in compression: a nonlinear finite element study. Journal of Biomedical Engineering, 13(2):139–151.

29. *Fagan MJ, Julian S, Siddall DJ, Mohsen AM.* 2002b. Patient specific spine models. Part 1: finite element analysis of the lumbar intervertebral disc – a material sensitivity study. Proceedings of the Institution of Mechanical Engineers, Part H: 216(5):299–314.

30. *Lavaste F, Skalli W, Robin S, Roy-Camille R, Mazel C.* 1992. Three-dimensional geometrical and mechanical modelling of lumbar spine. Journal of Biomechanics, 25(10):1153–1164.

31. *Zander T, Rohlmann A, Bergmann G.* 2004. Influence of ligament stiffness on the mechanical behaviour of a functional spinal unit. Journal of Biomechanics, 37:1107–1111.

32. *Noailly J, Lacroix D, Planell JA.* 2005, Finite element study of a novel intervertebral disc substitute. Spine, 30(20):2257–2264.

33. *Kim YE, Goel VK, Weinstein JN, Lim TH.* 1991. Effect of disc degeneration at one level on the adjacent level in axial mode. Spine, 16:331–335.

34. *Kurowski P, Kubo A.* 1986. The relationship of degeneration of the intervertebral disc to mechanical loading conditions on lumbar vertebrae. Spine, 11:726–731.

35. *Nachemson A.L.* 1981. Disc pressure measurements. Spine, 6(1):93–97.

36. *Sato K, Kikuchi S, Yonezawa T.* 1999. In vivo intradiscal pressure measurement in healthy individuals and in patients with ongoing back problems. Spine, 24(23):2468–2474.

37. *Kurutz M, Oroszváry L.* 2010, Finite element analysis of weightbath hydrotraction treatment of degenerated lumbar spine segments in elastic phase. Journal of Biomechanics, 43(3):433–441.

38. *Dolan, P, Adams MA.* 2001. Recent advances in lumbar spinal mechanics and their significance for l. Clinical Biomecanics., 16, Suppl.(1):S8–S16.

39. *Adams MA, Dolan P.* 2005. Spine biomechanics. Journal of Biomechanics, 38(10):1972–1983.

40. *Kurutz M.* 2006. Age-sensitivity of time-related in vivo deformability of human lumbar motion segments and discs in pure centric tension. Journal of Biomechanics, 39(1):147–157.

41. *Kurutz M, Bene É, Lovas A.* 2003. In vivo deformability of human lumbar spine segments in pure centric tension, measured during traction bath therapy. Acta of Bioengineering and Biomechanics, 5(1):67–92.

42. *Goel VK, Kong W, Han JS, Weinstein JN, Gilbertson LG.* 1993. A combineg finite elelent and optimization investigation of lumbar spine mechanics with and without muscles. Spine, 18: 1531–1541.

43. *Fagan MJ, Julian S, Mohsen A.* 2002a, Finite element analysis in spine research. Proceedings of the Institution of Mechanical Engineers. Part H: 216(5):281–298.

44. *Li H, Wang Z.* 2006. Intervertebral disc biomechanical analysis using the finite element modelling based on medical images. Computerized Medical Imaging and Graphics, 30:363–370.

45. *Ruberté LM, Natarajan RN, Andersson GB.* 2009. Influence of single-level lumbar degenerative disc disease on the behavior of the adjacent segments – a finite element model study. Journal of Biomechanics, 42(3):341–348.

46. *Zhang QH, Zhou YL, Petit D, Teo EC.* 2009. Evaluation of load transfer characteristics of a dynamic stabilization device on disc loading under compression. Medical Engineering and Physics, 1(5):533–538.

47. *Bender T, Karagülle Z, Bálint GP, Gutenbrunner C, Bálint PV, Sukenik S.* 2005. Hydrotherapy, balneotherapy, and spa treatment in pain management. Rheumatology International, 25(3):220–224.

A szerzők köszönik az OTKA K-075018 projektbeli támogatását, továbbá Kutrik Attila végeselemes modellezésben nyújtott segítségét.

Kurutzné Kovács Márta
Budapesti Műszaki és Gazdaságtudományi Egyetem, Budapest
H–1111 Budapest, Műegyetem rkp. 3.

New aspects in grouping typical injuries from road traffic accidents

Petra Aradi[1], Miklós Szokoly[2]
[1] Budapest University of Technology and Economics
[2] Péterfy S. Hospital and Trauma Center
petra.aradi@gmail.com

Abstract
Typical mechanisms and specific injuries of people involved in road traffic accidents are presented. Injury patterns specific to occupants of vehicles with enclosed passenger compartment, as well as unprotected participants of traffic (pedestrians, bicyclists, motorcyclists, etc.) are grouped.

Injury severity classification, treatment planning and outcome prediction is usually done based on various scoring systems, both internationally and in Hungary. The enormous number of such scoring systems make a thorough survey difficult and conversion among these scores has limitations. However prehospital care providers and hospital emergency staff need a “common language”, preferably a system that utilizes the advantages of scoring systems. There is no uniform practice of this communication and data transfer in Hungary now, that is why part of the important data from the incident scene might not get to the hospital together with the patient.

The documentation of prehospital care providers both in Hungary and abroad are discussed and analyzed. Score systems in prehospital and emergency medicine, as well as outcome prediction measures are covered. Data collection schemes especially the Utstein-Style for documenting major trauma and the German MIND2 (Minimale Notarztdatensatz, minimal prehospital care data set) are also presented.

A suggestion is introduced for the data content of prehospital documentation, so that it could further help hospital admission and care. The main aspects of the suggestion are road traffic accidents, because the creation of such a widely accepted and used document (a prehospital patient report form) requires a team of experts from various – mainly medical – specialties. Technical aspects, such as digital data collection are also covered. Future directions of development are named, too.

Keywords: road traffic accidents; prehospital care; emergency medicine; scoring systems; patient report form

Introduction

Accidents are an epidemic in our fast-paced, motorized era. Injuries and the consequent and definitive loss of health are an enormous financial and political problem for societies all over the world.

Road traffic accidents become more and more common, that is why various efforts are made to reduce their number and severity. Injury mechanisms, typical patterns and severity could be examined and relationships defined. These analyses and statistics might further help to fine treatment protocols, so that the best possible ways are used throughout patient care (on-site prehospital treatment, hospital admission and definitive medical attendance, and later on rehabilitation) to provide best outcome.

Communication between prehospital care providers and admitting hospitals needs an upgrade in aspects of transmitted patient data, as well as circumstances and characteristics of the accident.

A brief overview of road traffic accidents and injury mechanisms specific to such events is given. Prehospital care, documentation requirements, scoring systems and data collection schemes are discussed and analyzed, to help consider a new prehospital patient report form with modern data content, processability and ease of use.

Road Traffic Accidents

Road traffic accidents (RTA) are as old as mankind. The severity of injuries from RTAs is in proportion to the "development level" of vehicles. So long as people walked, it was easier to avoid a traffic accident and the consequences of accidents were milder, compared to the emergence of vehicles. The introduction of animal power, and later on mechanization significantly increased accident and injury risks. Spread of motorization together with increase of people's need/urge to locomotion caused significant changes is traffic habits. The rise of speed and the congestion of roads resulted in enormous growth of traffic accident occurrences. In the beginning of the 1960s US President John F. Kennedy said, that "traffic accidents are one of the greatest, perhaps the greatest of the nation's public health problems".

RTAs are responsible for the death of at least 1.3 million people yearly, the number of injured is at least 50 million. The majority of injured and dead are pedestrians. More the 85% of victims (and 96% of dead children) is a citizen of low- and middle-income countries.[1] WHO (World Health Organization) forecasts traffic accidents to be the primary cause of premature death and permanent impairment of children of 4 years and older by 2015. This "hidden epidemic" is going to cause a crisis in the public health system. Predictions suggest today's 1.3 million RTA deaths per year to reach 1.9 million by 2020. Commission for Global Road Safety claims that global, regional and national development of public road traffic could prevent 5 million deaths and 50 million serious injuries in a year worldwide by 2020.

Injuries Related to Road Traffic Accidents

Human body is a complex system of tissues with various mechanical properties. Damage resulting from impacts of certain magnitude, direction and duration on the human body depend on properties such as elasticity and resistance of individual tissues and organs. Beside general governing laws there is a huge effect of individual variations, that are partly consequences of inherited factors, are acquired like illnesses, however the role of age, general physical and mental status could neither be neglected. When a certain body part is injured, tissues with different properties get different damages.

During impact there is a significant amount of energy transferred to the injured person in a usually very short time. The amount of energy transferred could be estimated in view of the mechanism and circumstances of injury. In road traffic accidents the speed of the vehicle at the time of impact is in direct connection with the vehicle's kinetic energy. Vehicle's speed at impact could be estimated from deformations of vehicle body. Statistics show that a deformation greater than 35 cm usually cause serious injuries, a deformation over 50 cm is usually lethal for the person involved. These data are not universal, just an estimated average, because vehicle type, construction, mass and materials vary largely.

Kinetic energy transferred to the person appears as a shock wave at contact. Energy transfer produces cavitation, shock wave is transmitted by particles in tissues and hollow organs. Cavitation is either temporary or permanent. Energy transfer depends on the amount of particles involved, composition of bodies in contact, and area of contact that is connected to the shape and position of the object. Typical examples are lungs filled with compressible air, the gastrointestinal system partly filled by air, vascular system and bladder filled with non-compressible liquid, liver, spleen, kidneys and muscles partly filled by liquid, as well as solids in bones, road surface, steel, etc.

Energy transfer might induce blunt or penetrating injuries. Blunt injuries do not penetrate tissues, cavity is generated farther from the impact site, in impact direction. Penetrating injuries as the name suggests break through tissues, cavity is perpendicular to the direction of the penetrating object that damages tissues getting into its way.

Some injuries are classified as open wounds of mechanical origin ranging from simple abrasions to cuts, stabs, conquassations, often in a combined form. When there is a fire, burn of different severity might appear on the body surface and inside airways. Smoke and chemical inhalation are a risk too. Electrical injuries might also cause burns and life threatening heart rhythm irregularities. Mechanical effects might lead to injuries and tissue damages without visible bleeding. Closed injuries range from relatively simple suffusions, to more serious haematomas under the skin or inside the skull. Blunt forces might cause contusion, commotion, compression or crush, multiple fractures, nerve and spinal lesions. Special soft tissue damage is the usually closed decollement, its more serious form is however an open injury (degloving). It is usually the result of the body or extremities getting stuck between the road surface and the relatively elastic tire moving tangentially. Compartment syndrome arises when tissue pressure increases in muscle compartments of extremities. Typical injury patterns of inner organs are contusion, commotion and rupture, especially of liver, spleen, lungs and kidneys, and perforation of stomach, intestines and bladder. Secondary ruptures occur sometimes days after the accident leading to a serious life-threatening situation. In body cavities (skull, thorax, pleural cavity, pericardium, mediastinum and different parts of the abdominal cavity in relation with the peritoneum) not only blood, but air might cause space-occupying lesions, that compress organs in the affected body cavity. Fractures are bone injuries when the continuity of bones gets broken. Fractures can have both internal and external origins. Latter are magnitude, direction, duration and speed of increase of force causing the fracture. Internal aspects are the bone's energy dissipation capacity, elasticity, density, and resistance against fatigue breaks. Dangers of fractures are severe blood loss, nerve- and vascular injuries and infection. Fractures have various classifications available, e.g. dislocated or not, closed or open, number of broken parts, shape of the fracture, amount of collateral soft tissue damage, etc. Injuries of joints connecting bones range from contusion, and distorsion to luxation. Vascular injuries occur when the continuity of blood vessels is damaged, and result in bleeding. Three main groups of them are direct and indirect vascular injuries, and chronic damages as consequences of traumatic injuries.

Oedema appear usually at the site of and near to the injury. Such space-occupying processes in the skull are life threatening, because intracranial pressure increases rapidly.

Injuries can be classified based on their number and extent. Monotrauma is the injury of one body part, multitrauma is multiple injuries. Multiple injuries apply to polytrauma too, however polytrauma has qualitative attributes compared to quantitative. According to Tscherne polytrauma is the simultaneous injuries of multiple body parts or organ systems, among which at least one injury or a combination of injuries is life-threatening. Most polytraumatised patients have serious injuries of body cavities (skull, thorax, abdomen)[2]. Ahnefeld's extension is also valid in prehospital and emergency medicine, namely certain life-threatening monotrauma (isolated intracranial or severe thoracic injuries) has to be treated as polytrauma, because other, on the scene invisible injuries can not be excluded with absolute certainty[3]. Authors of a recent study categorized polytraumatised as patients suffering such (mostly) blunt injuries of multiple body regions or organs, that disturb normal function and consequently lead to functional disturbances in other, non-injured organs. Morbidity and mortality is higher in polytraumatised than the summed morbidity and mortality of their individual injuries. Major cause of death after polytraumatisation is the vicious circle of the lethal triad of hypothermia, coagulopathy and acidosis.

In traffic accidents forces proportional to the rate of speed change, namely acceleration or deceleration, the mass of vehicle and injured people cause deformation not only in the vehicle, but might lead to injuries of various severity (in extreme lethal) in people. The reason why injuries occur are either directly or indirectly the increase in kinetic energy. The rise in speed and kinetic energy are responsible for increased breaking distance, time to avoid the accident, magnitude of destructive forces, severity of injuries and probability of death. Kinetic energy is proportional to the square of velocity, the faster the speed, the shorter the reaction time, distances and time of effects of forces. A small difference in speed is a huge distinction in injury severity.

The spread and development of motorization result in new types and combinations of injuries in road traffic accidents, the number of polytraumatised grows. Typical injuries have to be graded to help prehospital care providers choose the appropriate facility, where treatment is organized along specific protocols, to safely predict outcome, as well as to serve scientific data collection, processing and comparison.

The knowledge on the course of the accident supports diagnostics (and later on therapy), because the knowledge of typical injury mechanisms help to look for or exclude damage specifically. In oxyology (prehospital emergency medicine) victims of road traffic accidents belong to either the protected or unprotected groups[3]. Protected are drivers and passengers of vehicles with enclosed passenger compartment, that shields occupant from direct impact. Unprotected participants of traffic (pedestrians, bicyclists, motorcyclists, etc.) are covered only by their garments.

It is obvious, that similar mechanisms cause more severe injuries in unprotected participants of traffic, and polytrauma is more frequent among them, than among members of the protected group. The evaluation of WHO underpins this thesis, it lists children, pedestrians, bicyclists and elderly as the most vulnerable.

In a road traffic accident the vehicle usually slows rapidly down before stopping, while people inside it continue to move with their original speed, because of their inertia. Forces acting upon occupants are proportional to change of speed, and their direction is governed by the area of collision. During collision driver and passengers suffer injuries in more than one phases. During primary collision vehicle's speed changes suddenly, however occupants' speed does not. Passive and active protection (safety belts, airbags, etc.) decrease occupants' original speed, however when they are not present or not applied, then parts of the vehicle body that the occupant hits take up their role. The sudden change of speed has different effects on body parts and tissues of various physical properties and attachments. The effect of impact and injuries depend upon, whether the occupant was the driver or a front seat passenger or someone sitting in the back row, as well as s/he perceived the accident situation in time and whether s/he was able to protect her/himself as a reflex action or voluntarily, or by chance s/he was asleep with toneless muscles.

Sudden deceleration makes lower limbs with tightened muscles hit the dashboard (front seat occupants), dashboard and steering column (driver), or the back of front row seats (back seat passengers). Contact areas suffer soft tissue damage, tightened muscles may lead to knee, thighbone and pelvic injuries, pedals are responsible for typical injuries, too. Body's inertia causes the head to swing forward, hit some part of the vehicle with resulting facial and head injuries, while cervical spine is injured by hyperflexion. Next the thorax dashes forward, resulting in extensive bone- and soft-tissue injuries. Cervical spine hyperextends and typical whiplash injury arises. The next phase is the repeated forward motion of head and torso, aggravating head, abdominal, thoracic and extremity injuries.

Organs suspended in body cavities and the brain in the hard skull boost forward from the sudden deceleration, than bang back. Suspension system gets damaged, and organs are injured because of the repeated hits. Localized brain oedema appears below the place of impact (coup) or farther from it (contre-coup).

The driver is usually in a more favorable situation than the front seat passenger, because s/he usually perceives the situation sooner, and may better prepare to avert it. Head and chest of back seat passengers hit the upholstered seat back, causing significantly milder injuries than dashboard, windscreen, steering wheel and column A. When the head of an unrestrained ack seat passenger hits the head of a restrained front seat passenger, both suffer severe head trauma. Typical injuries of back seat passengers are severe pelvic injuries, fractures and dislocated hip. When front seat occupants not properly use safety belts or do not use at all, their injuries are more complicated, especially when airbags inflate.

In case of a rollover accident unrestrained occupants fall out, suffering further severe, often life-threatening injuries. When the occupant gets stuck under or inside the vehicle s/he might suffer crush injuries. By side impacts typical glass shard injuries of face, shoulder and arm occur.

Generally speaking motor vehicle occupants suffer injuries in three levels: head, thorax and abdomen, and knee-thigh-hip region.

Pedestrian accidents were analyzed in connection with hit speed, and a significant relationship was proven between hit speed and injury severity. Over 40 km/h life-threatening injuries are expected, over 60 km/h death is almost imminent. Beside hit speed, there are a number of other factors to concern, too. Probably the most important is the pedestrian's age, and in tight connection with it the state of the skeletal system, its rigidity and elasticity, the eventual osteoporosis, and the frequency of injury complications. Injury severity depends not just on the magnitude, but the duration of impact. There is a significant difference in speed and mass and physical properties of pedestrian and vehicle, kinetic energy could be enormous. Pedestrian's "deformation" is highly complex, and it has three phases: pedestrian acquires the vehicle's speed when contact is made, gaining a huge amount of extra kinetic energy, then usually the body separates from the vehicle and after an airborne period crashes into the ground and skids or rolls until stop, losing the kinetic energy. The third phase is occasional, the pedestrian might crash into an other object or is hit or run over again. Pedestrian hits happen in a few seconds, that is why victims do not have enough time to react and try to avoid the accident.

The mechanism of total frontal hit is described by Waddell's triad: thighbone fracture, intrathoracic or intraabdominal injuries and head trauma on the opposite side.

Bicyclists suffer their injuries when they tip over, brake suddenly, or when a motor vehicle hits them. Different mechanisms might appear in combination, but magnitude and direction of impact force and change of speed is significant to each of those. Primary collision is often with a part of the bicycle, transmitting the force indirectly to the bicyclist. When the collision is is from the back, the bicycle accelerates, its driver falls to the motor vehicle or the ground and suffers injuries. The bike tumbles upon its rider causing further extremity injuries. Handlebar and its equipment, brakes and levers hurt hands. Handlebars might also cause severe abdominal injuries. Saddle and frame cause typical injuries in the perineal region in cyclists riding the bike. When a car overtaking the bicycle hits the biker from the left, the left lower extremity is injured and secondary injuries occur on the cyclist's other (right) side. When a bike turns in front of a motor vehicle its rider suffers similar injuries, however secondary injuries are on the same sides as the primary, because the biker's body contacts the front side and bonnet of the vehicle.

The speed of motorcyclists is comparable to the speed of cars and trucks, however the probability of death is almost 30 times that of occupants of a car. Size and mass of motorcyclists is much less, and their garment provide less protection than body and safety devices of a vehicle. Compared to pedestrians, bicycles and motorcycles with their riders on are unstable systems. Motorcycles are sometimes orders of magnitude heavier, more powerful and harder to control than bikes. Injury patterns are similar to those of bicyclists, but knee, elbow and shoulder injuries are frequent. Lower limb degloving injuries and conquassations, severe fractures are common, often resulting in the loss of the limb. Head injuries are also common, however safety helmets helped reduce the number and severity of head injuries since their wide-spread introduction. Thoracic injuries are also prevalent. Burns from the hot parts of the motorcycle are also common.

Prehospital Care

Prehospital care is organized around different schemes worldwide. These schemes integrate local rescue and ambulance systems and health network in a various scale. In Europe rescue services and ambulance services are usually clearly separated. The so-called Franco-German model operates with highly skilled doctors (in Hungary oxyologists and other specialists) on site. In Anglo-Saxon systems prehospital care is provided by well educated paramedics, who work by protocols with equipment appropriate to their skills. The basis of emergency care is the system of emergency departments and trauma centers. However simultaneous existence of personal and objective terms are needed in both systems. The main philosophical difference between these to systems is "scoop and run" and "stay and play". Today both principles are applied in a locally fitting proportion in a large number of countries.

In a trauma scene injury severity can not always be determined because of circumstances (e.g. jammed victim), the relatively spare diagnostic apparatus (e.g. no on site imaging and laboratory) and the shortness of time available. Severe injuries are presumed, based on the suspected injury mechanism determined by anamnesis and a quick look at the scene, significant changes in basic vital functions, injury patterns. Today Dr. R Adams Cowley's "golden hour of shock" refers rather to urgency and emergency in the care of severely injured, and not the strictly 60 minutes. Principles and educational systems of ATLS® (Advanced Trauma Life Support® for in hospital providers) and ITLS (International Trauma Life Support for on site providers) are accepted and applied in a large number of countries in the world. Checklists help prehospital providers worldwide to choose the appropriate treatment strategy based on quick and accurate decisions. Scoring systems are integral parts of some checklists.

The Methodological Guide of the Hungarian National Ambulance Service (Országos Mentőszolgálat, OMSZ) also refers to the mechanism of the event leading to the injury as a measure of injury severity.[6] Injury mechanism informs prehospital providers whether a high energy, full body impact (run over, fall from height, frontal collision, fall from a vehicle), or the isolated injury of one or more body parts occurred, as well as about priority of transport or on site primary care.

In traffic accidents severe injury has to be assumed, when the pedestrian or bicyclist is run over or hit the ground, was dragged, high speed motorcycle or car accident happened (at least 50 km/h with safety belt, at least 30 km/h without safety belt or motorcycle, at least 5 km/h by bicyclists), falling or flying out of a vehicle, falling from a vehicle in motion, turnover of a vehicle, victim is jammed (rescue can take long and delays definitive care), indirect signs (severely damaged passenger compartment, engine crushing into passenger compartment, serious frontal axle damage, inflated airbag, death in the same passenger compartment), fall from height (over 3 m), explosion.[6] A quick examination can also reveal severe injuries: unstable thorax, fracture of two or more long bones and/or pelvic fracture, high limb amputation, penetrating abdominal, thoracic, pelvic, neck or skull injury, smoke inhalation and at least 15% of body surface with 2nd- or 3rd-degree burns.[3]

Scoring Systems

Scoring systems are used worldwide to assign one or more numbers to injury or illness severity. There are three basic groups of scoring systems: anatomical, physiological and outcome based, however in practice these categories can not be clearly separated. Creating numeric descriptors has more than one goals: the quick handover of information on the patient's status and the change of status during medical attendance between prehospital providers and hospital staff helps choosing appropriate treatment schemes (protocols), and later on it can be used in a scientific study that uses statistics. Scoring systems have to be simple, quick, and should support quality of treatment and outcome.

Today's trauma scoring systems together with anatomical and physiological scales help outcome prediction. One application area is prehospital triage, however quality control and assurance of groups of injured people, organization and development of trauma care systems also appear useful.

In the prehospital environment scoring systems are primarily patient's assessment, measurement and control of diagnostic and therapeutic efforts, outcome prediction and decision support in triage and therapy. Prehospital and emergency department scoring systems need to be based on such general vital parameters, that might be obtained throughout the whole system of care.

When a scoring system is applied, the patient's complex and diverse data have to be compiled into one or some representative severity measures (numbers). Scoring always means information loss. Efforts for more and more exact mappings resulted in an enormous number of scoring system with advantages and disadvantages. Inaccuracy in mapping is partly because of patients' different anatomical and physiological characteristics. Exact outcome prediction *(Eq. 1.)* must refer to earlier medical problems, that adversely affect patients' healing reserves.

$$\text{outcome} = \text{function}\,(\text{anatomical injuries, physiological injuries, patient reserves}) \qquad (Eq.\ 1)$$

MedAL (The Medical Algorithms Project) chapter 29 "Trauma & Emergency Medicine" has 59 topics with 562 scoring systems.[7] Chapter 38 "Forensic Medicine" has 44 topics, among which only one ("Evaluation of Transportation Accidents") has only one traffic accident related scoring system ("Findings That May Identify the Driver in an Automobile or Pilot in an Airplane Accident").[7]

Everyday practice uses a lot less scoring systems. Prehospital trauma scoring systems have to safely identify high- and low-risk patients, have high face-validity and inter-rater reliability, be easy to use, allow quick and accurate measurements. These systems are mostly physiological, while anatomical systems are good for forecasting mortality and hospital care, as well as post-processing. The most widely applied physiological scoring systems have a minimal instrument need, could be quickly determined, supporting triage and repeated retriage.

Glasgow Coma Scale (GCS) was developed to check people with head injury. GCS 13 corresponds to minor brain injury, GCS 9–12 is a moderate, GCS 8 or less corresponds to severe brain injury. GCS is the sum of three values, eye opening (1–4 points), verbal response (1–5 points) and motor response (1–6 points), ranging from 3 to 15 points, the more points representing better condition, however individual components are noted as well. GCS is widely used both in prehospital environment and in hospitals. GCS 8 or less is indication for assisted airway (endotracheal intubation and mechanical ventilation in most cases). Hospital admission GCS has one of the most important prognostic values, however it is to be evaluated only with additional neurological examinations. A change of 2 or more in GCS points means a significant change in the patient's status.

Revised Trauma Score (RTS) uses three parameters, respiratory rate, systolic blood pressure and the sum of GCS points. All three parameters can have 0–4 points (worst-best), the sum of which is the RTS value. RTS of 11 or less indicates transport to a trauma center. RTS is hard to determine when exact GCS and spontaneous respiratory rate is not available, because the patient is intubated or is under medications, alcohol or drugs.

Effects of injuries depend on many parameters, quantity of tissue damage, physiological responses to the injury and other aspects, such as age, physical status, etc.. Tissue damage can be classified with the anatomical Abbreviated Injury Scale (AIS) and its descendants. ICD (International Classification of Diseases) based systems help in outcome prediction. There are more detailed scoring systems for organs and organ systems, such as AAST (American Association for the Surgery of Trauma) and AO/OTA (Arbeitsgemeinschaft für Osteosynthesefragen, Orthopaedic Trauma Association) scales.

Abbreviated Injury Scale (AIS) was created in 1969 by American Medical Association (AMA), Society of Automotive Engineers and Association for the Advancement of Automotive Medicine (AAAM). Since the publication of the first AIS version, the International Injury Scaling Committee (IISC) organizes its development. AIS uses a severity score of 1–6 (light to severe) for seven body regions, with 9 as the measure of unknown severity. Injury Severity Score (ISS) is also an anatomical scoring system, that uses AIS severity points (1–6) and it is used to classify people with multiple injuries. ISS uses 6 body regions and has a disadvantage of considering only one injury per body region. New Injury Severity Score (NISS) corrected this problem, more than one serious injury in the same body region can be taken into account.

Data Collection Schemes

Quality assurance and documentation are strongly connected, the first provide that the latter maintains its function, documentation serves the basis of quality assurance. Until the end o the 20^{th} century there was no general demand to prepare fact-based studies on quality and efficiency of prehospital care.

In Hungary ambulance care documentation is regulated by law. Currently there are two generally used documents of the National Ambulance Service and the volunteer Ambulance Service of the Hungarian Maltese Charity Service. One of the documents used by both organizations is the so-called log sheet, that contains mostly technical details (name, address of the patient and the description of the problem, times, distances, materials used). Prehospital care is documented in a prehospital patient report form. Legal regulations govern the handling and keeping of these (and other connected) documents.

To strengthen the link between prehospital and institutional care, new uniform administration schemes should be used to provide hospitals with every possible details of the circumstances of the injury, as well as details of prehospital and in-transport care. This link is supposed to provide and develop professional standards of patient care, and could help clearing legal aspects (e.g. complaints).

The prehospital patient report form of OMSZ is an A5 sized paper with both sides to fill *(Figure 1)*. Data content is not very extensive, the form has to be filled with handwriting and there is not much help in the form of checklists and drawings. The only scoring system used is GCS. The main characteristics of this form is written information.

Figure 2 shows the prehospital patient report form of the Ambulance Service of the Hungarian Maltese Charity Service, that provides a completely volunteer, but professional high-level ambulance 4 days a week in Budapest. This single A4 sized form is more user-friendly from the point of filling out, quite a number of checklists and a trauma figure are present, where injuries can be marked. Originally it had two copies with carbon-paper technology, so that a copy could remain with the patient in the hospital.

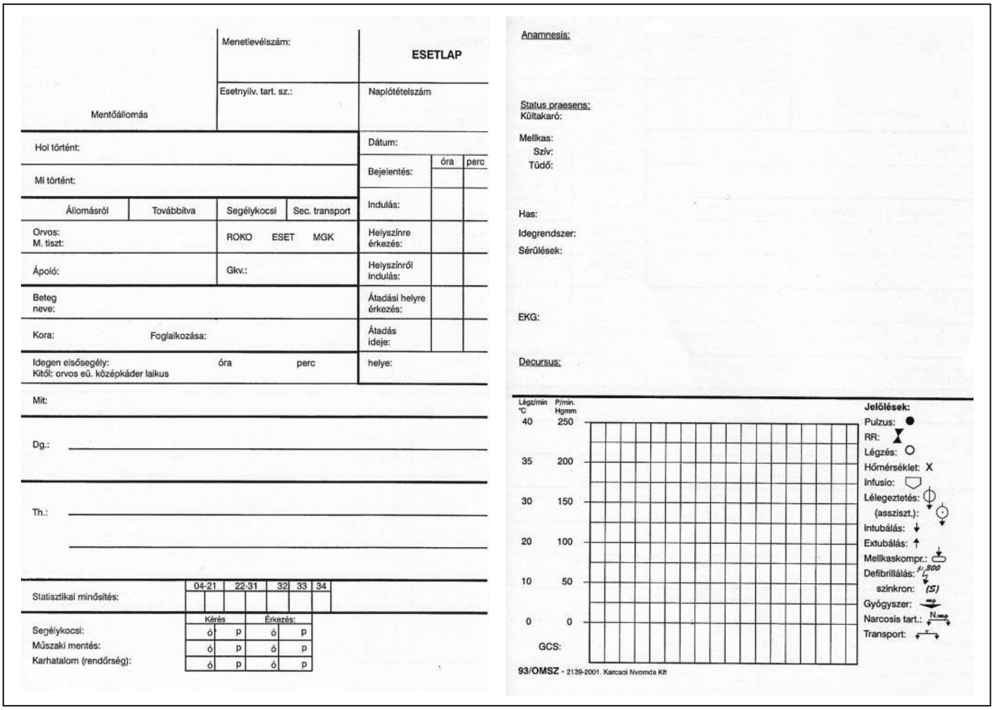
Menetlevélszám:
ESETLAP
Esetnyilv. tart. sz.:
Naplótételszám
Mentőállomás
Dátum:
Hol történt:
Bejelentés: óra perc
Mi történt:
Indulás:
Állomásról | Továbbítva | Segélykocsi | Sec. transport
Orvos: M. tiszt: | ROKO ESET MGK
Helyszínre érkezés:
Ápoló: | Gkv.:
Helyszínről indulás:
Beteg neve:
Átadási helyre érkezés:
Kora: Foglalkozása:
Átadás ideje:
Idegen elsősegély: óra perc
Kitől: orvos eü. középkáder laikus
helye:
Mit:
Dg.:
Th.:
Statisztikai minősítés: 04-21 22-31 32 33 34
Kérés Érkezés:
Segélykocsi: ó p ó p
Műszaki mentés: ó p ó p
Karhatalom (rendőrség): ó p ó p

Anamnesis:
Status praesens:
Kültakaró:
Mellkas:
Szív:
Tüdő:
Has:
Idegrendszer:
Sérülések:
EKG:
Decursus:
Légz/min °C | P/min. Hgmm
40 250
35 200
30 150
20 100
10 50
0 0
GCS:
Jelölések:
Pulzus:
RR:
Légzés:
Hőmérséklet: X
Infusio:
Lélegeztetés:
(asszriszt.):
Intubálás:
Extubálás:
Mellkaskompr.:
Defibrillálás:
szinkron: (S)
Gyógyszer:
Narcosis tart.:
Transport:
93/OMSZ - 2139-2001. Karcagi Nyomda Kft

Figure 1. Prehospital patient report form of the National Ambulance Service

When a patient is handed over in a trauma center or emergency department in Hungary, some institutions require the filling out of their own A4 or A5 size patient registration forms, reporting the prehospital events, diagnosis and treatment. In other institutions parts of these data (what happened, when and where) is recorded by an administrator and additional more detailed verbal description is given to the doctor who admits the patient. Other hospitals require a narrative, they usually give a piece of blank A4 paper and the leader of the ambulance team writes about the what, when, where (happened) and about treatment.

The variety of documentation, and the multiple recording of patient data, especially physiological parameters and treatment raises a justifiable demand on the development of a uniform patient report form, that is both a prehospital documentation for ambulance services and contains enough and relevant information about the patient, the mechanism of injury (or illness) and the prehospital treatment for hospital admission. Data collection and statistics should also be included in the scheme in the long run, which is inherent to a well organized form, that has a number of checkboxes and selection lists.

Prehospital documentation has multiple overlapping components. Structured data content helps minimizing overlaps, support electronic data storage and processing, and last but not least helps on site providers by securing logical diagnostic sequences. That is why protocols were developed in accordance with these goals. An example of a Franco-German prehospital care system was chosen, because Hungarian prehospital care is organized along this scheme. In Germany DIVI (Deutsche Interdisziplinäre Vereinigung für Intensiv- und

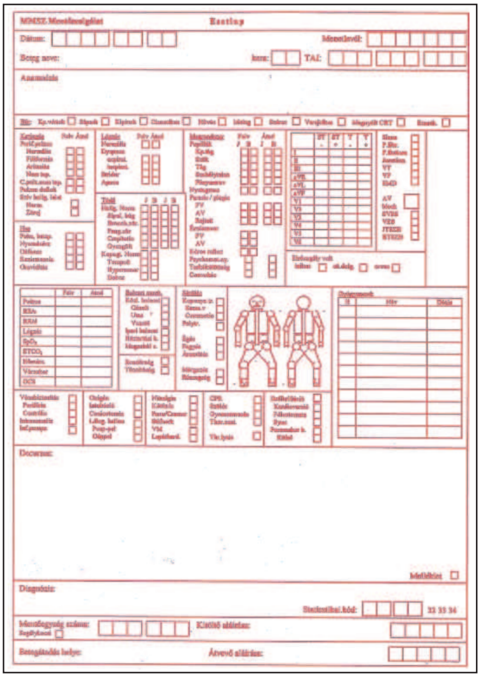

Figure 2. Prehospital patient report form of the Ambulance Service of the Hungarian Maltese Charity Service

Notfallmedizin, German Interdisciplinary Society for Intensive and Emergency Medicine) coordinated the development of the uniform national protocol for high-level ambulance units (the ones with a doctor or a college graduate paramedic) in 1991, and in 1994 it was followed by the protocol for basic level ambulance units. A large number of emergency services use these protocols from the beginning. Their success is proven by translation to various other languages. In 1994 version 4, in 2000 version 4.2 came out, the latter did not cover structural changes, just optimized some details.

Documents, and patient report forms based on the DIVI protocol have a uniform data structure that is the result of collaboration of each professional bodies working in connection with prehospital care. First MIND (Minimale Notarztdatensatz, Minimal Prehospital Care Data Set) appeared in 1996, followed by MIND2 in 2003. MIND's contents map the DIVI protocol, it has a structured format, and is suitable for each ambulance unit levels from basic to highest. Patient registration forms based on MIND2 are widely used (when necessary with local modifications), can be used as a transfer documentation and facilitate data recording on computers. DIVI has a patient report form, that uses MIND2 as its basis, however it contains slightly more data, than that MIND2 requires.

MIND2 is an XML-based (Extensible Markup Language), hierarchical text document, transparent to and editable by both humans and computers. Core data come from multiple sources (e.g. prehospital care providers, hospitals). Part of data covers circumstances of the incident (scene, etc.), ambulance characteristics and some information about the hospital. Patient and prehospital care data is covered in a timeline structure, utilizing scoring systems as often as possible. MEES (Mainz Emergency Evaluation Score) is used, which covers individually marked physiological parameters and other data (age, consciousness, GCS, systolic blood pressure, ECG, heart rate, respiratory rate, oxygen-saturation, pain according to the visual analog scale, blood sugar level, respiration characteristics, etc.). Diagnosis is listed according to organ groups. Trauma cases cover number and severity of injuries (monotrauma, multitrauma, polytrauma), type (blunt or penetrating) and location. Injury mechanism (fall from height, pedestrian, motor vehicle occupant, motorcyclist, bicyclist, other mechanism) and time of injury are covered too. Resuscitation data are in accordance with the current Utstein-template. Therapy can be chosen from the listed 30 interventions. Medications can be detailed in a timeline scheme. On-site and handover score values help evaluate patient's status and the effects of interventions during prehospital care.

German company DokuFORM *(http://www.dokuform.de/)* produces ambulance patient report forms in accordance with DIVI 4.2 (MIND2) both as mass product *(Figure 3),* and according to specific individual needs. There are traditional and modern paper-based versions, the latter to be filled with a digital pen to facilitate quick and exact data storage and transfer. DIVIDOK®-Online is a client-server system to store these forms, that can be scanned or filled with a digital pen. During patient admission in the hospital a copy of the patient form is ready to be handed over together with the patient.

Theoretical and clinical experts of many fields collaborate in the ongoing knowledge base development of injury prevention and resuscitation. Their work resulted in the Utstein-Style (or Utstein-template) for out-of-hospital resuscitations, in 1990. Utstein-Style contains uniform definitions, terminology and data sets. Utstein-Style is continuously revised and updated since then, and new areas have Utstein-Styles developed in the meantime (Pediatric Advanced Life Support, major trauma, drowning, etc.). The Utstein-Style for Major Trauma appeared in 1999, as the result of the extensive work of International Trauma Anaesthesia and Critical Care Society (ITACCS). This version covered prehospital and early hospital phases, previous illnesses and outcome prediction in an object-oriented model structure. In accordance with earlier Utstein-templates this template has Core and Optional data variables. Model elements are divided into five categories, one about the healthcare network, one about the patient, data about treatment and outcome, as well as ethical aspects, documentation and methodology. Type, severity and mechanism of injury, the site where it happened are all recorded. Prehospital and in hospital provider data are similar to those in the resuscitation template.

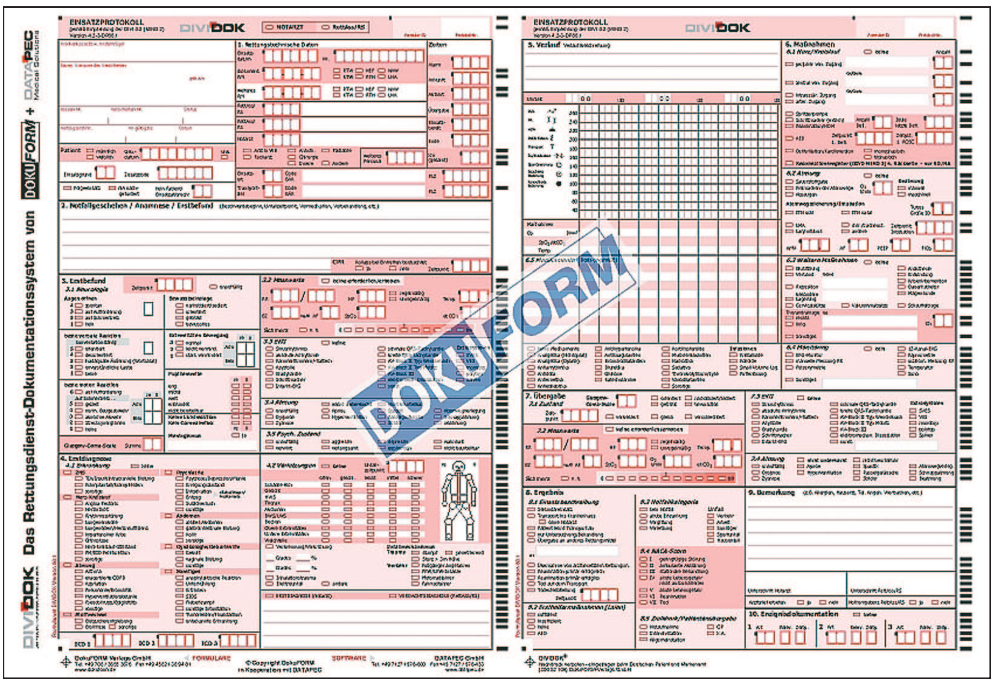

Figure 3. DokuFORM ambulance patient report form in accordance with DIVI 4.2 (MIND2)

Patient data include age, gender, estimated height and weight, previous illnesses, physical status, results of prehospital examinations, treatment, and other categories when necessary (e.g. bicyclist, pedestrian, passenger of driver of a vehicle, etc.) Documentation and methodology chapter covers data collection techniques (e.g. GPS – Global Positioning System data for time and location). The purpose of the 1999 Utstein-Style for major trauma was data collection and statistical processing. This goal was not met, because there was no international consensus about application and applicability, besides the amount and nature of required data were to complicated. A revision followed in 2007 as a collaboration of some of the most important European Trauma organizations: Scandinavian Networking Group for Trauma and Emergency Management (SCANTEM), TARN (Trauma Audit & Research Network) from the United Kingdom, the German Society for Trauma Surgery (Deutsche Gesellschaft für Unfallchirurgie, DGU) and their trauma register (DGU-TR), and the Italian National Register of Major Trauma (Registro Intraospedaliero Multiregionale Traumi Gravi, RITG). The revision resulted in only one inclusion criterion (New Injury Severity Score [NISS] value of 15 or more), 5 exclusion criteria, and 35 exactly specified and compulsory core data variables divided into 3 groups. Core data variables were chosen in accordance with the following considerations: they have to be unambiguous and easy to fill. Core data variable groups are Predictive models (23 variables), System Characteristic Descriptors (8 variables) and Process Mapping (4 variables).

National trauma registers are established in quite a number of countries worldwide, however the comparison is extremely difficult among their data. A typical trauma register is UK's TARN , which served as a model for the EuroTARN Group having 18 member states at the time of this writing (Austria, Belgium, Bosnia-Hercegovina, Croatia, Denmark, Germany, Greece, Ireland, Italy, Macedonia, the Netherlands, Norway, Portugal, Slovakia, Spain, Sweden, Switzerland, and the United Kingdom). A 2007 EuroTARN study examined whether it is possible to compare European trauma registries. The result was positive, minimal additional infrastructure is needed to build a web-based system for this task. There is a wide support across Europe, to make comparisons of efficiency and outcome. The variety of national trauma registers urges unification, which leads to a uniform data set, coding rules, inclusion and exclusion criteria. Utstein-Style is such a scheme. Its 2007 revision is not a final version, the system is continuously checked and updated when necessary.

Conclusion

According to literature review and the study of solutions form various countries, and our everyday practice in ambulance work and in-hospital trauma care, we concluded that the new patient report form for Hungarian ambulance services should follow these aspects:

– logical setup, transparency, support for diagnostic steps
– support for scoring systems
– easy to fill with drawings and lists
– injury mechanisms are detailed
– road traffic accident specialties are drawn (a schematic car, where location of injured, collision sites, etc. can be marked)
– everything “compressed” into one document (single or multiple pages)
– paper-based version, with the support of electronic data processing
– a (carbon-)copy could be handed over with the patient in the hospital, or ideally can get to the hospital before the patient with an electronic communication system
– data content in accordance with reanimation and other specific registers

– legal and ethical aspects fully covered
– equally emphasized documentation for trauma and illnesses (neurological, cardiological, etc.)

Data content has to be a consensus of many disciplines and professional bodies. It is important to study international examples and local circumstances. Patient report form has to cover the professional principles of prehospital care, with data relevant to examination and treatment methods and devices. Integration of protocols helps provide uniform high-level medical attendance, and ensures that no important diagnostic or treatment phase drops out.

References

1. *Andrianopoulos N.* Moscow fuel. Traffic Technology International [Internet]. 2010 Jan; Forrás: *http://viewer.zmags.com/publication/6e26c868#/6e26c868/6*

2. *Tscherne H,* editor. Unfallchirurgie – Trauma Management. Springer, Heidelberg, 1997.

3. *Gorove L, Szegeczky D, Szokoly M.* Politraumatizáltak és súlyos sérültek helyszíni ellátása. In: Oxiológia. Medicina. 2006; pp. 511–526.

4. *Butcher N, Balogh ZJ.* The definition of polytrauma: the need for international consensus. Injury, Int. J. Care Injured [Internet]. 2009 Nov; 40(Supplement 4):S12–S22.

5. WHO | Road traffic injuries [Internet]. Forrás: *http://www.who.int/violence_injury_prevention/road_traffic/en/*

6. *Dr. Márton E, Dr. Gorove L.* A súlyos sérült kórházon kívüli ellátása. Az Országos Mentőszolgálat Módszertani útmutatója. 2008.

7. The Medical Algorithms projekt [Internet]. *http://www.medal.org/*

8. The Trauma Audit & Research Network Procedures manual [Internet]. 2009 Sep; *https://www.tarn.ac.uk/content/downloads/53/Full%20Procedures%20-%20Sept%202009.pdf*

9. *Lossius H.* Erratum to “Reporting data following major trauma and analysing factors associated with outcome using the new Utstein style recommendations”: [Resuscitation 50 (2001) 263-2729]. Resuscitation [Internet]. 2004 11;63(2):227.

10. *Ringdal K, Coats T, Lefering R, Di Bartolomeo S, Steen P, Røise O et al.* The Utstein Template for Uniform Reporting of Data following Major Trauma. A joint revision by SCANTEM, TARN, DGU-TR, and RITG. Scand J Trauma Resusc Emerg Med [Internet]. 2008;16(7).

11. *Brohi K.* The Utstein template for uniform reporting of data following major trauma: A valuable tool for establishing a pan-European dataset. Scand J Trauma Resusc Emerg Med [Internet]. 2008;16(8).

12. *Ringdal K, Coats T, Lefering R, Di Bartolomeo S, Steen P, Røise O, et al.* The Utstein Trauma Template for Uniform Reporting of Data following Major Trauma: Data Dictionary. Version 1.1.1. [Internet]. 2009 May 19; Forrás: *http://www.scantem.org/misc/pdf/Revised_Utstein_Template_-_Data_Dictionary_v1.1.1.pdf*

13. The revised Utstein Template for Uniform Reporting of Data following Major Trauma: User manual (Version: 1.1).

14. *Wolfgang F.* Dick. Anglo-American vs. Franco-German Emergency Medical Services System. Prehospital and Disaster Medicine [Internet]. 2003;18(1):29–37.

15. *Probst C, Paffrath T, Krettek C, Pape HC.* The German Trauma Registry. Comparative Update on Documentation of Trauma in Seven National Registries. Eur J Trauma [Internet]. 2006 8;32(4):357–364.

16. Confronting "Death on Wheels" Making Roads Safe in Europe and Central Asia [Internet]. Forrás: *http://go.worldbank.org/DR6NO0B0P0*

17. *Vaca FE, Anderson CL, Herrera H, Patel C, Silman E, DeGuzman R et al.* Crash Injury Prediction and Vehicle Damage Reporting by Paramedics: A Feasibility Study. WestJEM [Internet]. 2009 May 21;10(2):62–67.

18. *Messelken M, Schlechtriemen T.* Der minimale Notarztdatensatz MIND2. Notfall & Rettungsmedizin [Internet]. 2003 May;6(3):189–192.

19. *Lefering R.* Development and validation of the revised injury severity classification score for severely injured patients. Eur J Trauma Emerg Surg [Internet]. 2009 9;35(5):437–447.

20. *Moecke H, Dirks B, Friedrich H, Hennes H, Lackner C, Messelken M et al.* DIVI-Notarzteinsatzprotokoll, Version 4.2. Notfall & Rettungsmedizin [Internet]. 2004 Jun;7(4):259–261.

21. *Kuisma M, Väyrynen T, Hiltunen T, Porthan K, Aaltonen J.* Effect of introduction of electronic patient reporting on the duration of ambulance calls. The American Journal of Emergency Medicine [Internet]. 2009 10;27(8):948–955.

22. *Pohlman TH, Bjerke HS, Offner P.* eMedicine Trauma: Trauma Scoring Systems [Internet]. eMedicine Trauma. 2009 Jul 23.

23. *Johnson D, Wilson M.* Improving prehospital information for trauma patients. Australian Emergency Nursing Journal [Internet]. 1998 10;1(5):12–13.

24. *Laudermilch DJ, Schiff MA, Nathens AB, Rosengart MR.* Lack of Emergency Medical Services Documentation Is Associated with Poor Patient Outcomes: A Validation of Audit Filters for Prehospital Trauma Care. Journal of the American College of Surgeons [Internet]. 2009 12.

25. *Reinhardt T, Hennes H.* Mainz Emergency Evaluation Score (MEES). Notfall & Rettungsmedizin [Internet]. 1999 Oct;2(6):380–381.

26. Make Roads Safe [Internet]. Forrás: *http://www.makeroadssafe.org/publications/Documents/decade_of_action_report_lr.pdf*

27. *Bouamra O, Wrotchford A, Hollis S, Vail A, Woodford M, Lecky F.* Outcome prediction in trauma. Injury, Int. J. Care Injured [Internet]. 2006 Dec;37(12):1092–1097.

28. *Jenkin A, Abelsonmitchell N, Cooper S.* Patient handover: Time for a change? Accident and Emergency Nursing [Internet]. 2007 7;15(3):141–147.

29. *Gorove L, Szegeczky D, Szokoly M.* Politraumatizáltak és súlyos sérültek helyszíni ellátása. In: Oxiológia. Medicina. 2006; p. 511–526.

30. Präklinische Erfassung der Verletzungsschwere aufgrund technischer Parameter am Unfallort. Notfall Rettungsmed [Internet]. 2007 6;10(5):372–374.

31. *Senkowski C.* Trauma scoring systems: a review. Journal of the American College of Surgeons [Internet]. 1999 11;189(5):491–503.

Petra Aradi
Budapest University of Technology and Economics
Department of Mechatronics, Optics and Engineering Informatics
1111 Budapest, Műegyetem rkp. 3.

Sensitivity investigation of three-cylinder model of human knee joint

István Bíró[1], Béla M. Csizmadia[2], Gábor Katona[2]
[1] University of Szeged, Faculty of Engineering, Szeged, Hungary
[2] Szent István University, Faculty of Mechanical Engineering, Gödöllő, Hungary
biro-i@mk.u-szeged.hu

Abstract

The operation is unavoidable in a certain part of patients suffering from arthrosis. The contact surfaces of wide-spread applied human knee joint prostheses can be described with simple geometrical elements. The relative motion realized by knee joint and as its results the stability of the whole body is harmonic ensured by complicated condyle surfaces. For this reason the implanted prostheses comply with requirements limited and it causes additional load on the diseased bony tissue. According to observations at the fastening of the prostheses the bony tissues become inflamed which after some years need new operation.

At present it is a general aim in biomechanics to create a better mechanical model of human knee joint which can approach the natural motion and on its basis to make new prostheses. The motion of the human knee joint have been studying by many biomechanical research groups for decades. The problem is very complex and specific from technical point of view. The cause of complexity is partly the elaborateness of elements, partly the typical rheological properties of the components (bones, cartilages and other soft tissues).

Authors as members of the Szent István University Biomechanical Research Group in order to describe the motion of knee joint at first joined coordinate-systems on the basis of anatomical landmarks to the femur and tibia moreover joined a three-cylindrical mechanism as mechanical model to the axes of coordinate-systems.

The aim of the investigation is to determine the six independent kinematical parameters of tibia compared to the fixed femur during flexion and extension. The experimental examinations were carried out on cadaver knees in cooperation with doctors of Szent János Hospital. The positioning was tracked by optical positioning appliance. Needed parameters can be obtained from the recorded data determined by the kinematical model.

Considering the irregular shapes of femur and tibia the anatomical coordinate systems can be joined with more or less position mistake. The aim of this paper is the determination of the effects of position mistakes on kinematical parameters.

Keywords: knee joint; kinematical model; optical positioning; accuracy; sensitivity investigation

Introduction

Different constraints enable relative motion of joined rigid bodies referring to each other. The constraints depending on their shapes have one or more degree of freedom. In case of joints the degree of freedom cannot be always determined. It is expedient to treat the human knee joint as six degree of freedom because of its complicated shape. In this case to the precise description of motion achieved by knee joint we need six independent position parameters[1,7].

In recent years the number of kinematical models of anatomical joints has increased. In case of certain models so many researchers have measured and described joint motion with less than six degrees of freedom. Obviously the treatment of six degree of freedom models is the most difficult. The motion of human knee joint can be described by following components: The flexion-extension is defined around the medio-lateral axis, internal-external rotation around the tibial axis and the abduction-adduction around the anterior-posterior (floating) axis. The medio-lateral translation is measured along the medio-lateral axis, proximal-distal translation along the tibial axis and antero-posterior translation along the mutually perpendicular floating axis.

Description of motion components in such a way a little bit subjective. In order to descript the motion components precisely it is needed to join coordinate-systems to the femur and tibia consequently.

In recent decades to measure kinematical parameters of human knee joint different methods have been developed. In these methods it is measured and processed the motion of markers fastened to femur and tibia referring to each other. In vitro mechanical investigations are mainly phantom or simulated computer models or cadaver motion experiments[7].

The visual examinations were based on marker technique to sign single points or axis of the extremities delineating their motion. In spite of that the newly introduced techniques developed in an enormous numbers in the last decades e.g. the radiology, fluoroscopy, three-dimensional CT, MRI, stereophotogrammetry, ultrasound, etc. most of the results were unreliable, inconsistent with other published data[3,4,5,6]. The range of the tibia out and in-rotation along the flexion-extension motion of the knee had been established by different authors as between 5 up to 17 degrees, moreover the character of this diagram is variable[8,9]. On the basis of difference of published results it is quite difficult to establish exact character concerning the motion of knee joint.

Method

Authors developed a special appliance[10,11,12] in order to make a serial experiments. The aim of them was the determination of change of six independent kinematical parameters of tibia (shin bone) compared to femur (thigh bone) during of motion of human knee joint. From recorded data needed parameters can be determined by the aid of kinematical model.

To the presented sensitivity investigation it is necessary to determine anatomical landmarks on femur and tibia moreover coordinate-systems joining to the determined anatomical landmarks. Details of this process can be found in paper of Katona et al[13,14,15]. Considering the biological characters of femur and tibia the optical positioning of anatomical landmarks can be achieved with more or less position mistakes. The aim of this paper is the determination of the effects on kinematical parameters of position mistakes during flexion-extension of human knee joint.

Authors on the basis of current international standards and conventions (e.g. from the Inter-

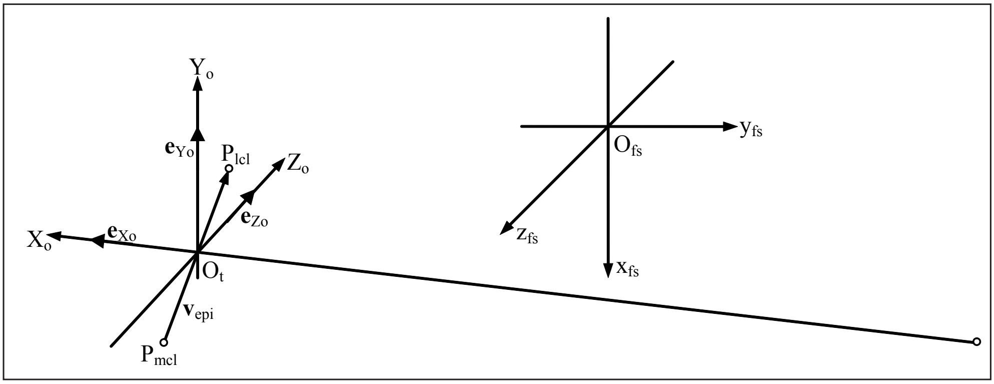

Figure 1. Position of anatomical coordinate-system $X_oY_oZ_o$ joined to femur in coordinate-system *fs* (cadaver lying on his back, investigated right leg, view from medial side)

national Society of Biomechanics)[16] using the above mentioned anatomical landmarks joined coordinate-systems to femur and tibia.

At first to the processing of recorded positioning coordinates it is necessary to take the anatomical coordinate-system on anatomical landmarks of femur in coordinate-system *fs* (*fs* in the appliance, joined to femur rigidly) *(Figure 1)*.

Needed data determining anatomical coordinate-system $X_oY_oZ_o$ (in coordinate-system *fs*):
– centre of the femoral head *(fh)*
– medial and lateral epicondyles (P_{mcl}, P_{lcl}).

The origin of this anatomical coordinate-system *(O_t)* coincides with middle point of line between medial and lateral epicondyles. Axis X_o of coordinate-system is on the line pointed out by points O_t and *fh (Figure 1)*. Vector $\mathbf{v}_{\mathbf{epi}}$ is between medial and lateral epicondyles.

Unit vectors of axes of coordinate-systems can be obtained as results of following vector operations:

$$\mathbf{e}_{Xo} = \frac{\mathbf{v}_{Ot-fh}}{\left|\mathbf{v}_{Ot-fh}\right|}, \quad \mathbf{v}_{epi} = \mathbf{r}_{Plcl} - \mathbf{r}_{Pmcl}, \quad \mathbf{e}_{epi} = \frac{\mathbf{v}_{epi}}{\left|\mathbf{v}_{epi}\right|},$$

$$\mathbf{e}_{Yo} = \mathbf{e}_{epi} \times \mathbf{e}_{Xo}, \ \mathbf{e}_{Zo} = \mathbf{e}_{Xo} \times \mathbf{e}_{Yo}.$$

Determining coordinate-system joined to anatomical landmarks on tibia: Needed data for coordinate-system $x_sy_sz_s$ (in appliance):
– apex of the head of the fibula *(hf)*,
– prominence of the tibial tuberosity *(tt)*,
– distal apex of the lateral and medial malleolus *(kb, bb)*.

The origin of the anatomical coordinate-system *(O_s)* coincides with middle point of line between distal apex of the lateral and medial malleolus. Unit vectors of axes of coordinate-systems can be obtained as results of next vector operations *(Figure 2)*:

$$\mathbf{e}_{kb-bb} = \frac{\mathbf{v}_{kb-bb}}{\left|\mathbf{v}_{kb-bb}\right|}, \quad \mathbf{e}_{kb-hf} = \frac{\mathbf{v}_{kb-hf}}{\left|\mathbf{v}_{kb-hf}\right|}, \quad \mathbf{e}_{Os-tt} = \frac{\mathbf{v}_{Os-tt}}{\left|\mathbf{v}_{Os-tt}\right|},$$

$$\mathbf{e}_{xs} = \mathbf{e}_{kb-bb} \times \mathbf{e}_{kb-hf}, \quad \mathbf{e}_{zs} = \mathbf{e}_{xs} \times \mathbf{e}_{Os-tt}, \quad \mathbf{e}_{ys} = \mathbf{e}_{zs} \times \mathbf{e}_{xs}.$$

During motion investigation of knee joint we follow the change of position of coordinate-system ts joined to tibia compared to coordinate-system fs joined to femur. We had to describe anatomical coordinate-systems in coordinate-systems joined to femur and tibia for the sake of following: in this way the posi-

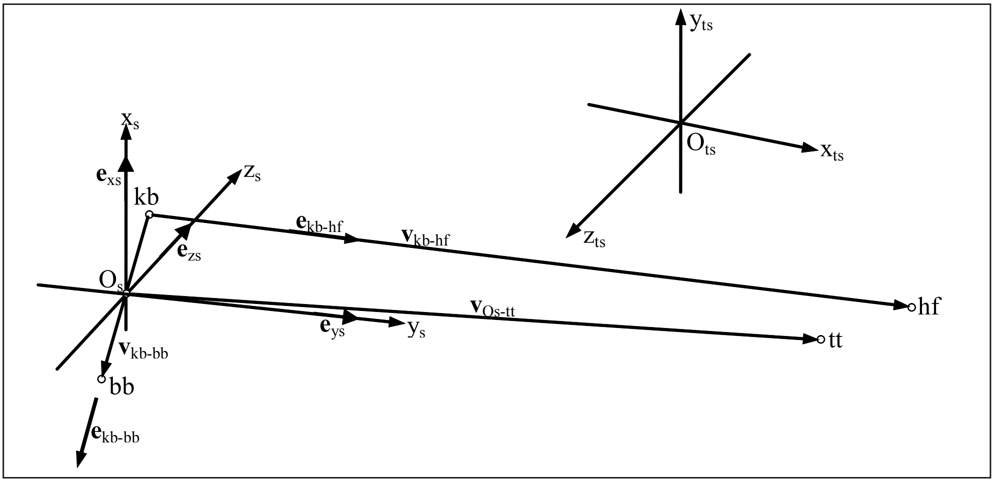

Figure 2. Position of anatomical coordinate-system $x_s y_s z_s$ joined to tibia in coordinate-system *ts* (cadaver lying on his back, investigated right leg, view from medial side)

tion of anatomical coordinate-system joined to tibia in anatomical coordinate-system joined to femur will be known.

If the anatomical landmarks on femur and tibia are determined with some position mistake the kinematical parameters of knee joint will be modified. These kinematical parameters can be obtained by the aid of three-cylindrical mechanism put in between the above defined anatomical coordinate-systems.

Three-Cylindrical mechanism

Putting the origin of coordinate-system $X_3Y_3Z_3$ (without modification of direction of axes) into the origin of coordinate-system $x_s y_s z_s$ unit vectors will be the followings:

$$\mathbf{e}_{X3} = \mathbf{e}_{zs}, \quad \mathbf{e}_{Y3} = -\mathbf{e}_{xs}, \quad \mathbf{e}_{Z3} = -\mathbf{e}_{ys}.$$

The position of coordinate-system $X_3Y_3Z_3$ in the coordinate-system $X_oY_oZ_o$ is described by the next matrix-equation:

$$[\mathbf{T}_{0-3}]=[\mathbf{T}_{ts-3}][\mathbf{T}_{abs-ts}][\mathbf{T}_{abs-fs}]^{-1}[\mathbf{T}_{fs-0}]^{-1}$$

in which the transformation matrices

- $[\mathbf{T}_{ts-3}]$ which contains six position parameters describing the position of anatomical coordinate-system *($X_3Y_3Z_3$)* joined to tibia in coordinate-system *ts,*
- $[\mathbf{T}_{abs-ts}]$ which contains six position parameters describing the position of coordinate-system *ts* in absolute coordinate-system *(XYZ),*
- $[\mathbf{T}_{abs-fs}]^{-1}$ inverse transformation matrix which contains six position parameters describing the position of coordinate-system *fs* in absolute coordinate-system *(XYZ),*
- $[\mathbf{T}_{fs-0}]^{-1}$ inverse transformation matrix which contains six position parameters describing the position of anatomical coordinate-system $X_oY_oZ_o$ joined to femur in coordinate-system *fs.*

Transformation matrix $[\mathbf{T}_{0-3}]$ can be written down in another way:

$$[\mathbf{T}_{0-3}] = \begin{bmatrix} \mathbf{e}_{X3} & 0 \\ \mathbf{e}_{Y3} & 0 \\ \mathbf{e}_{Z3} & 0 \\ \mathbf{r}_{O3} & 1 \end{bmatrix},$$

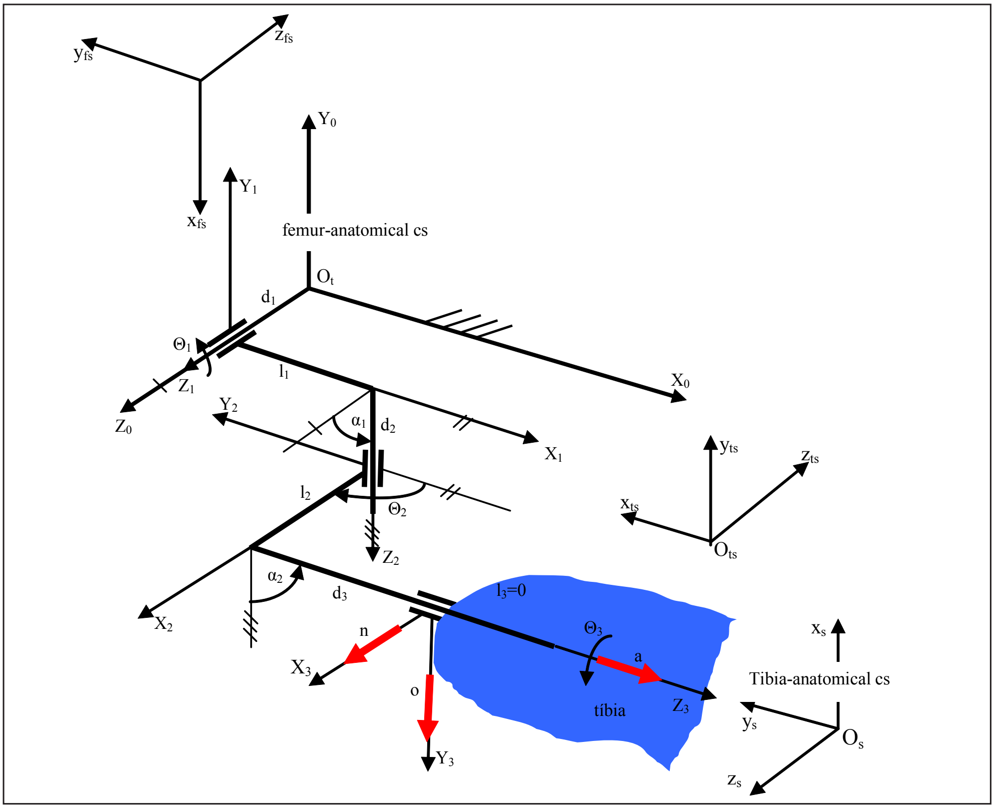

Figure 3. Three-cylindrical mechanism with the defined coordinate-systems (extended position)

where $\mathbf{e}_{X3}$, $\mathbf{e}_{Y3}$, $\mathbf{e}_{Z3}$ are unit vectors of axes X_3, Y_3, Z_3 in coordinate-system $X_oY_oZ_o$ and vector $\mathbf{r}_{O3}$ contains the coordinates of origin of coordinate-system $X_3Y_3Z_3$ in coordinate-system $X_oY_oZ_o$.

In case of similar spatial structures the so-called Denavit–Hartenberg *(HD)* coordinates can be applied *(Figure 4)*. The advantage of the application of HD coordinates: the transformation matrix contains – instead of six – four $(\Theta_i, d_i, l_i, \alpha_i)$ variable physical quantities joining to geometrical characters of bodies and their constraint.

In Figure 3 the *HD* coordinates can be seen in extended position of the leg. In the mechanism α_i, l_i, $(i=1,2,3)$ can be adjustable optionally according to the special geometry of knee joint. On the basis of published recommendations next data are proper approaching: $\alpha_1=\alpha_2=90°$, $\alpha_3=0°$, $l_1=l_2=l_3=0$.

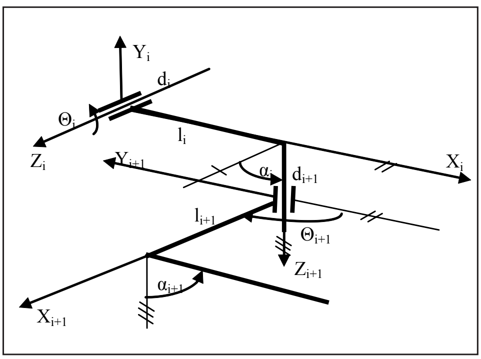

Figure 4. Connection of *i*th and *i+1*th bodies and joined coordinate-systems

The application of the model enables the calculation of following quantities:
– Θ_1 – flexion, in drawn position *0* degree,
– Θ_2 – ab/adduction, in drawn position *90* degree,
– Θ_3 – rotation of the tibia, in drawn position *0* degree,
– d_1, d_2, d_3 – moving on accordant axes.

On the basis of approaching $\alpha_1=\alpha_2=90°$, $\alpha_3=0°$, $l_1=l_2=l_3=0$ for the kinematical chain of *Figure 3* the following matrix equation can be written down where **n, o, a** are unit vectors of coordinate-system $X_3Y_3Z_3$ in coordinate-system $X_0Y_0Z_0$ and P_x, P_y, P_z are coordinates of origin of coordinate-system $X_3Y_3Z_3$ in coordinate-system $X_0Y_0Z_0$.

$$\begin{bmatrix} \cos\Theta_1 & 0 & \sin\Theta_1 & 0 \\ \sin\Theta_1 & 0 & -\cos\Theta_1 & 0 \\ 0 & 1 & 0 & d_1 \\ 0 & 0 & 0 & 1 \end{bmatrix} * \begin{bmatrix} \cos\Theta_2 & 0 & \sin\Theta_2 & 0 \\ \sin\Theta_2 & 0 & -\cos\Theta_2 & 0 \\ 0 & 1 & 0 & d_2 \\ 0 & 0 & 0 & 1 \end{bmatrix} *$$

$$* \begin{bmatrix} \cos\Theta_3 & -\sin\Theta_3 & 0 & 0 \\ \sin\Theta_3 & \cos\Theta_3 & 0 & 0 \\ 0 & 0 & 1 & d_3 \\ 0 & 0 & 0 & 1 \end{bmatrix} = \begin{bmatrix} n_x & o_x & a_x & P_x \\ n_y & o_y & a_y & P_y \\ n_z & o_z & a_z & P_z \\ 0 & 0 & 0 & 1 \end{bmatrix}$$

Roots of equation system: Θ_1, Θ_2, Θ_3, d_1, d_2, d_3, which determine precisely the position of tibia compared to femur.

Sensitivity investigation of results

As results obtained kinematical parameters and diagrams depend partly on method of measurement and anatomical specialties cadaver however principally on determination of coordinate-systems joined to femur and tibia.

Considering the irregular shapes of femur and tibia the anatomical landmarks can be determined with more or less position mistake for this reason the anatomical coordinate-systems joined to anatomical landmarks have more or less position mistake as well[15]. The following anatomical landmarks must be measured:
– centre of the femoral head *(fh),*
– medial and lateral epicondyles (P_{mcl}, P_{lcl}),
– apex of the head of the fibula *(hf),*
– prominence of the tibial tuberosity *(tt),*
– distal apex of the lateral and medial malleolus *(kb, bb).*

The optical positioning of above mentioned anatomical landmarks was made by a special appliance using pointer. The position mistakes of middle point of femur, apex of the head of the fibula and prominence of the tibial tuberosity cause small angular mistakes because these point are located relative far from origins of coordinate-systems.

The origins of coordinate-systems are determined between epicondyles and apices of the lateral and medial malleolus therefore the effect of position mistakes on position and orientation of coordinate-systems is quite significant. Considering the different shapes of investigated cadaver femur and tibia and position mistakes of measurements – depending on cadaver ones – more or less different kinematical functions can be obtained.

As first step of sensitivity investigation the positions of epicondyles were modified in coordinate-system *fs* step by step *(±2 mm)* approximately in the vertical plane *(Figure 1).* In second phase the position of apices of the lateral and medial malleolus were modified in coordinate-system *ts* step by step *(±2 mm)* approximately in the vertical plane as well *(Figure 2).* Difference from basic function (thickened curve) can be seen in *Figure 5–6.* (The basic function contains some mistakes because it was calculated from measured data.)

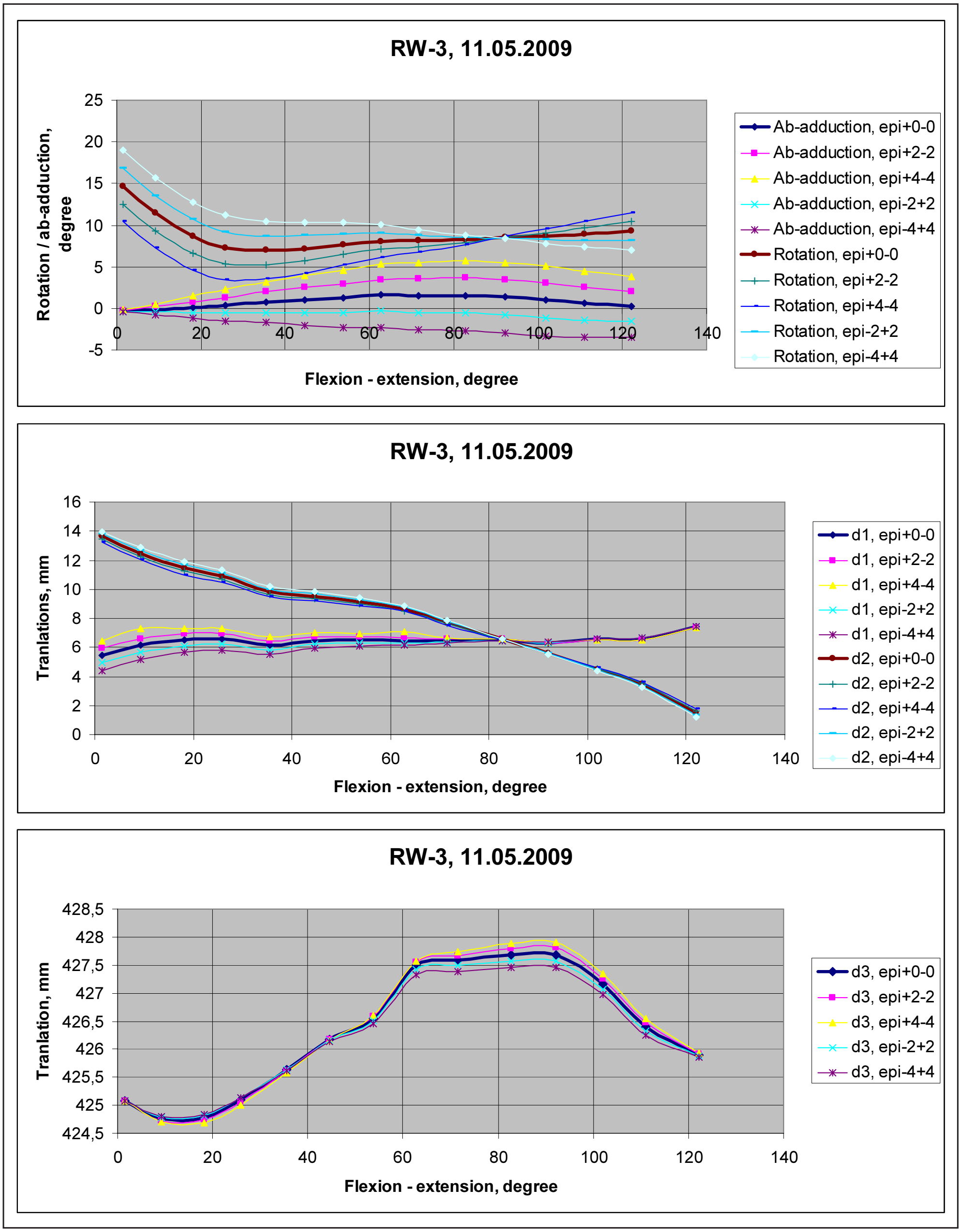

Figure 5. Effect of modification of position of epicondyles on kinematical functions

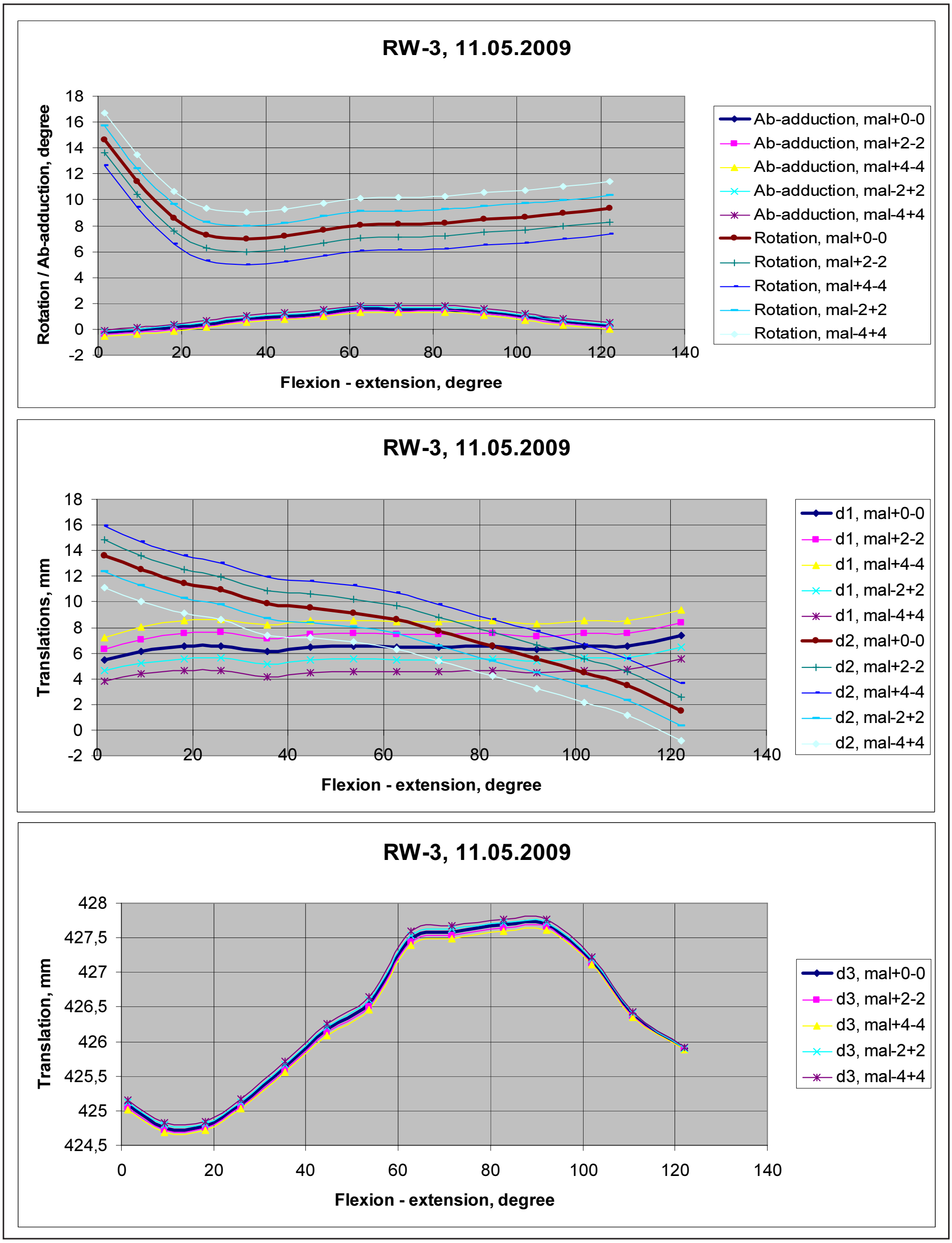

Figure 6. Effect of modification of position of apices of the lateral and medial malleolus on kinematical functions

Conclusion

As result of sensitivity investigation the followings are established:

- The flexion-rotation and flexion-ab/adduction diagrams depend strongly on position mistakes of determined coordinate-systems, for this reason it is important to determine the anatomical landmarks.
- The cause of modification of diagrams is first of all the position mistake in direction of *Y* axis of epicondyles.
  - Its effect can be seen over *60* degree in flexed position. In this part the diagrams are approximately linear, their gradient variable depending on position mistakes of epicondyles.
  - The shapes of ab/adduction diagrams are strongly deformed.

Summing up it can be established that the using of anatomical coordinate-systems enables the comparison and generalization of results of different motion investigation of human knee joints. On the basis of above mentioned it can be decided which parts of obtained results are acceptable certainly which parts and its conclusions need chary treatment. By more precise prescription of taking up of anatomical coordinate-system the comparison of results can be intensified.

References

1. *Grood ES, Suntay WJ.* A joint coordinate system for the clinical description of three-dimensional motions: application to the knee. J. Biomech. Engng 1983;105: pp. 136–144.

2. *Pennock GR, Clark KJ.* An anatomybased coordinate system for the description of the kinematic displacements in the human knee. J. Biomechanics 1990; Vol. 23, No. 12: pp. 1209–1218.

3. *Blankevoort L, Huiskes R, Lange A.* Helical axes of passive knee joint motions. J. Biomechanics 1990; Vol. 23, No. 12, pp. 1219–1229.

4. *Hollister AM, et al.* The axes of rotation of the knee. Clinical Orthopaedics and Related Research 1993;(290): p. 259.

5. *Fujie H, Livesay GA, Fujita M, Woo SLY.* Forces and Moments in six-dof at the Human Knee Joint: Mathematical Description for Control. J. Biomechanics 1996; Vol. 29, No. 12:1577–1585.

6. *Churchill DL, et al.* The transepicondylar axis approximates the optimal flexion axis of the knee. Clinical Orthopaedics and Related Research, 1998;(356): p. 111–118.

7. *Bull AMJ, Amis AA.* Knee joint motion: description and measurement Proc Instn Mech Engrs 1998;Vol 212, Part H.

8. *Iwaki H, Pinskerova V, Freeman MAR.* Tibiofemoral movement 1: the shapes and relative movements of the femur and tibia in the unloaded cadaver knee. The Journal of Bone and Joint Surgery [Br] 2000;82-B:1189–1195.

9. *Wilson DR, Feikes JD, Zavatsky AB, O'Connor JJ.* The components of passive knee movement are coupled to flexion angle. Journal of Biomechanics 2000;33:465–473.

10. *Bíró I.* Kinematical investigation of human knee joint. 21th Working Meeting of the IFToMM Permanent Commission for Standardization of Terminology, Proceedings of the sientific seminar, June 27–July 2, 2005. Bardejov Spa, Slovakia, 91–96. p.

11. *Szakál Z.* Mérőberendezés térdízület mozgásvizsgálatához. GÉP, 2006; LVII. évfolyam 1. szám: 37–40.

12. *Katona G, M. Csizmadia B, Fekete G.* Kísérleti vizsgálatok térd mechanikai modelljének meg-

alkotásához. 2. Magyar Biomechanikai konferencia, Debrecen, 2006. június 30–július 1. p. 49–50.

13. *Bíró I, M. Csizmadia B, Katona G.* New approximation of kinematical analysis of human knee joint. Bulletin of the Szent István University, ISSN 1586-4502 2008; p. 330–338

14. *Bíró I.* Az emberi térd három-hengeres kinematikai modellje. Elektronikus Műszaki Füzetek VII. DAB Műszaki Szakbizottság, ISBN 978-963-7064-22-7, Debrecen 2009; p. 107–112.

15. *Katona G, M. Csizmadia B, Bíró I, Andrónyi K, Krakovits G.* Cadaver térdek mozgásának értékelése anatómiai koordináta-rendszerek felhasználásával. Proceedings of 4th Hungarian Conference on Biomechanics, Pécs, May 7–8, 2010.

16. http://www.ulb.ac.be/project/vakhum

Biomechanica Hungarica III. évfolyam, 1. szám

Mechanical properties of coronary vein – in vitro evaluation of longitudinal and transversal samples

Tibor Balázs[1], Eszter Bognár[1], Endre Zima[2], János Dobránszky[3]
[1] Budapest University of Technology and Economics (BUTE), Department of Materials Science and Engineering
[2] Semmelweis University, Cardiovascular Clinic
[3] Research Group for Metals Technology of the HAS and BUTE, Department of Materials Science and Engineering
balazs.tibor@freemail.hu

Abstract

Aims: Even though several publications are available and experiments were done in the topic of the mechanical properties of vessels there is no data for special veins like coronary veins. Previously a few rectangular coronary vein parts had been examined and the results show that probably there is a difference between the transversal and longitudinal direction of coronary vein. The aim of this study is to investigating the differences in the mechanical properties of the two directions with in vitro tensile tests.

Method: Coronary veins from six pig hearts were tested within one hour after explantation. Five transversal and nine longitudinal coronary vein samples were prepared from these hearts and kept in physiologic solution until the tests. The samples were evaluated in 37 °C physiologic solution with tensile equipment and the force-displacement curves were recorded. Based on these curves and the tearing results the longitudinal and transversal tensile strengths, relative extensions and Young's modulus were calculated.

Results: The evaluation squarely proved the differences of mechanical properties between the longitudinal and transversal directions of coronary vein samples. Transversal direction had higher elongation properties (248±117% vs. 137±37%) but lower resistance to mechanical loading (0.99±0.16 MPa vs. 2.55 ± 0.46 MPa) than the longitudinal direction.

Conclusion: The experiments are successfully investigated the mechanical differences of coronary vein directions. These are important parameters, because in case of special application the maximal elongation capability and the maximal force that the vein can tolerate without injury had to be known. With the result of these experiments the maximal loading concerning to coronary veins can be modelled. However there are still question to answer for example the individual role of the different layers of coronary veins which is not known during the mechanical testing. Further investigations are necessary to perform in order to have a complete analysis of mechanical properties of coronary veins.

Keywords: coronary vein; mechanical properties; in vitro testing

Introduction

Recently a new kind of in vitro testing of coronary vein was published (Balázs et al., 2008) with limitations and raised questions regarding to the method. It was necessary to carry out because the previously performed vessel examinations tested only saphenous veins and arteries from different areas of the body. The literature of mechanical properties of blood vessels are quite large and it is already known that the arteries can be modelled as two-layer model (Holzapfel GA et al., 2000; Holzapfel GA et al., 2002; Matsumoto T et al., 2002) and also founded that blood vessels have incremental Young's modulus even if they were investigated both for laws of elasticity and laws of viscoelasticity (Xiao Lu et al., 2004; Fung YC et al. 1995). It is also well known that the wall thickness and isobaric elastic properties of vein grafts increase after a few days and rearrangement of the elastic structures occurs (Monos E et al. 1995; Jenny S et al., 2006).

It is not enough to have experimental results for arteries from all over the body because the structural differences between arteries and veins cause differences in the mechanical properties as well. It is well known that the vein has three layers. The first is a strong outer cover of the vessel and consists of connective tissues, collagen and elastic fibres. The second one is the middle layer and consisting smooth muscle and elastic fibres, which is thinner in veins. The third one is consists of smooth endothelial cells. These three layers have three different mechanical properties and three different behaviours under mechanical loading.

Monos and his colleagues investigated the elastic modulus of different veins based on the Laplace–Frank equation (Monos E 2004). They used intravascular pressure to measure the tangential elastic stress and the relative displacement.

There are some similar investigations that concentrate on the blood flow simulation of the vessel systems (Molnár F et al. 2005; Till S et al., 2004; Till S et al., 2004) but these don't focus on mechanical properties on the complete modelling of blood circuit in arteries and veins as well.

Large coronary veins are placed on the outer surface of the heart between fat and pectoral muscle and the elongation mainly possible via diameter increasing. This suggests that the mechanical properties of longitudinal and transversal direction of coronary veins could be different.

In certain developments the initial data should be the mechanical properties of coronary veins such as the development of left ventricular pacemaker leads or electrophysiology diagnostic catheters that are placed in the coronary vein. From the view of electrophysiology and pacemaker lead fixation mechanisms, it is more important to know the maximal force and stress that may cause coronary vein dissections. This maximal force can be determined by tensile tests. The force required to tear a material and the amount it extends before tearing are point of interest. Typically, the testing involves taking a small sample with a fixed cross-section area, and then pulling it with a controlled, gradually increasing force until the sample changes shape or breaks. Analysis of force-displacement or strength-relative strain curves can convey much about the material being tested, and it can help in predicting it's behaviour.

The aim of this investigation is to evaluate the differences between the mechanical properties of transversal and longitudinal directions of coronary veins with in vitro tensile tests.

Methods

Six pig hearts were received from slaughterhouse and had been delivered within one hour after explantation to the Semmelweis University in physiologic solution (Baxter Viaflo, Natrium Clorid 0,9% "Bieffe" infusion). Coronary veins were prepared form these hearts immediately after receiving from slaughterhouse and kept in a physiologic solution until testing. The total time between explantation and testing phase was less than two hours.

Bartels-Stringer M et al suggest that after 3 hour storage in physiologic solution and normal saline solution, contractile and relaxant vascular responses are similar in isolated saphenous veins (Bartels-Stringer M et al., 2004 and Boerboom LE et al., 1992) proved that cold storage for 24 h did not affect vascular reactivity of blood vessels.

The diameters of coronary sinus (CS) were between 4 and 5 mm. Longitudinal and transversal samples were prepared. Optimal size would be 5 mm width and 10 mm length without side branches. Finally 9 longitudinal and 5 transversal CS sample were prepared and stored in a physiologic solution until the testing. The length, width and thickness of prepared samples were measured immediately after preparation and recorded together the calculated cross sections *(Table 1)*.

The longitudinal direction was defined as the longitudinal plane of the vein and the transversal direction was perpendicular to this, the plane of crosssection *(Figure 1)*.

Sample	Transversal samples				Longitudinal samples			
	Width a_t (mm)	Thickness h_t (mm)	Length l_t (mm)	Cross section A_{0t} (mm^2)	Width a_l (mm)	Thickness h_l (mm)	Length l_l (mm)	Cross section A_{0l} (mm^2)
1	6.30	0.55	9.87	3.47	6.60	0.38	22.53	2.49
2	6.10	0.48	9.97	2.91	8.83	0.34	17.87	2.97
3	6.37	0.47	10.87	2.97	8.10	0.40	18.53	3.21
4	6.70	0.52	7.97	3.48	6.80	0.40	16.10	2.74
5	5.90	0.40	8.93	2.36	7.73	0.53	22.30	4.10
6	–	–	–	–	6.77	0.42	23.53	2.84
7	–	–	–	–	7.83	0.48	19.07	3.76
8	–	–	–	–	9.03	0.48	17.70	4.37
9	–	–	–	–	8.93	0.43	15.77	3.87
Mean±CI	**6.27±0.35**	**0.48±0.06**	**9.52±1.30**	**3.04±0.47**	**7.85±0.80**	**0.43±0.05**	**19.27±2.38**	**3.37±0.55**

Table 1. Width, thickness, lengths and cross sections of the rectangular vein samples

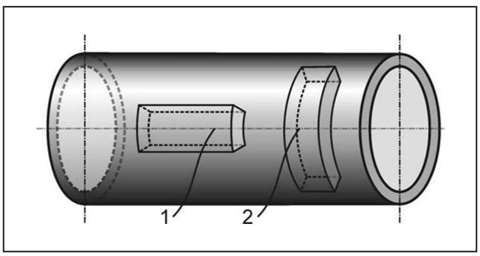

Figure 1. Definition of sample directions
(1: longitudinal; 2: transversal)

The tensile tests were performed at Budapest University of Technology and Economics, Faculty of Mechanical Engineering, Department of Polymer Engineering with Zwick Z020 tensile test machine.

A new type of grip was developed, because the previously applied grips and fixation modes caused the sample rupture just after fixation. Two different types of surfaces were used in

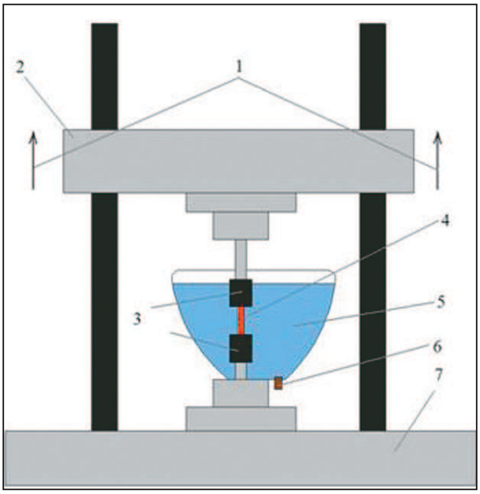

Figure 2. Testing equipment:
1– direction of tensile force; 2 – upper clamp; 3 – grips; 4 – vein sample; 5 – physiologic solution on 37 °C; 6 – plug; 7 – lower clamp

one grip for fixating the coronary vein parts, one side was silicone and the opposite was reticulated metal. This combination of materials was appropriate and the fixation was stable.

A 37 °C degree physiologic solution (Baxter Viaflo, Natrium Clorid 0,9% "Bieffe" infusion) was used *(Figure 2)* to modelling the original surround and after every single testing phase it was drained via the plug and replaced with new 37 °C degree physiologic solution.

Tearing tests were performed with fixed lower camp and a moving upper camp with a constant stretching speed about 20 mm/min. The distance between the grips was 5 mm in case of the longitudinal samples and it had to be decreased because of size limits to 3 mm for the transversal samples. These distances were used as the starting length (L_0) for the relative extension calculations.

Maximal force and the inherent travel distance values from the recorded force in function of displacement curves were used as initial values of the calculations *(Table 2)*.

Relative extension as it shown in Equation 1 is the percentage of elongation during the tensile test. It was calculated as the ratio of the starting distance and the displacement.

$$\varepsilon = \frac{\Delta L}{L_0} \cdot 100\% \qquad (1)$$

Where is ε –relative extension, L_0 – starting length, ΔL – displacement (recorded by the test machine during test).

Sample	Transversal		Longitudinal	
	Displacement ΔL_t (mm)	**Maximal force F_{tmax} (N)**	**Displacement ΔL_l (mm)**	**Maximal force F_{lmax} (N)**
1	11.16	3.76	6.25	5.94
2	4.22	3.19	7.31	7.05
3	11.03	3.29	5.84	9.54
4	6.95	3.39	7.60	4.94
5	3.90	1.68	10.06	9.50
6	–	–	4.57	8.66
7	–	–	6.33	11.68
8	–	–	9.10	9.27
9	–	–	7.37	11.18
Mean±CI	**7.45±4.17**	**3.06±0.95**	**7.16±1.4**	**8.64±1.89**

Table 2. Travel distance and maximal force values for longitudinal and transversal samples based on the force-displacement curves

Typically the cross section at the time of rupture is necessary to define the tensile strength. In case of veins only the starting cross section was available because after tearing the necessary sizes at the time of rupture couldn't be measured. To evaluate the maximal strengths (tensile strength as it is shown in Equation 2) can be tolerated by the veins, the recorded maximal forces and the previously calculated original cross section was used.

$$\sigma = \frac{F_m}{A_0} \qquad (2)$$

Where is σ – tensile strength, F_{max} – maximal force (recorded by the test machine during test), A_0 – original cross section.

To evaluate the elastic properties it was important to measure the degree of the elastic deformation of veins under loading. Based on the tensile strength and relative extension, the Young's modulus (elastic modulus) of the coronary veins had been estimated with Equation 3.

$$E = \frac{\sigma}{\varepsilon} \qquad (3)$$

Where is E – Elastic modulus, σ – tensile strength, ε – relative extension.

Each prepared coronary sinus sample was successfully evaluated. The fixation mode was proved to be stable however the first transversal sample seemed to be instable. The force – displacement curves were recorded and the tensile strength in function of relative extension curves were made based on the previously defined equations for the transversal and longitudinal directions of coronary veins.

Results

Tensile strength in function of relative extension curves for the longitudinal samples were prepared *(Figure 3)*.

The initial parts of the curves were identical, showing the same elastic properties. On the curves of the 1, 4 and the 9 samples there were notches which could be connected to the partional tearing of fat tissue which can not be elongate as much the vein layers can. Except these three curves, the others had continuous running-up, elastic phase until the maximum forces and the maximal tensile strengths were reached. At the point of the maximum loading the veins had the first injury and after that a fast dive was observed in all of the cases. The reason was the damage of the strongest layer and a much lower force was needed to keep the elongation.

As the vein consists of three layers and fat tissue on the surface, after a certain elongation only the tearing force of fat tissue was recorded. These parts were removed from the curves in *Figure 3*.

Testing of transversal samples was much more complicated because of the smaller sizes. Different curves of the samples were received *(Figure 4),* basically two types were represented. The first type what could be connected to the 2. and 5. samples was similar to the longitudinal curve characteristic. The others had different running up phases with slower increasing of the strength. Injury of the vein happened at the peak of the curves where is the maximal loading and the end of the elastic phase. Slow decreasing trend was observed in the loading force and strength after the damage caused by the maximal load.

Based on the recorded curves and the defined equations the relative extension, tensile strength and elastic modulus of the coronary veins were calculated and detailed in *Table 3*.

There are differences in the mechanical properties of the longitudinal and transversal sam-

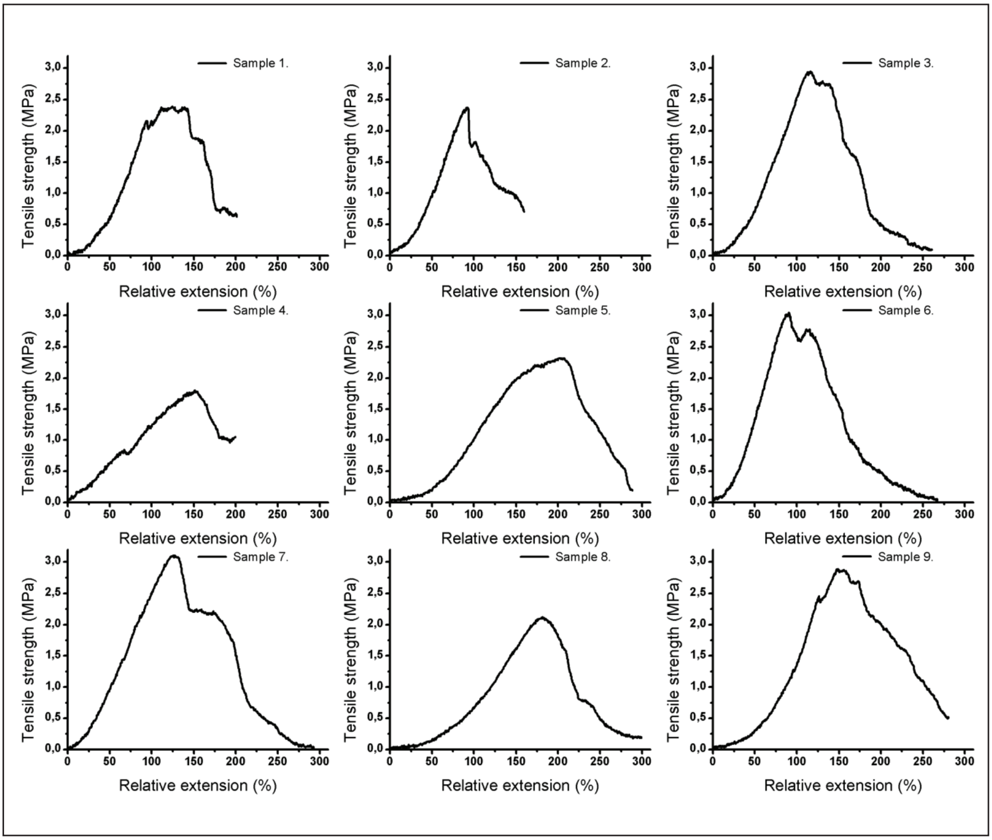

Figure 3. Tensile strength – Relative extension curves of longitudinal samples

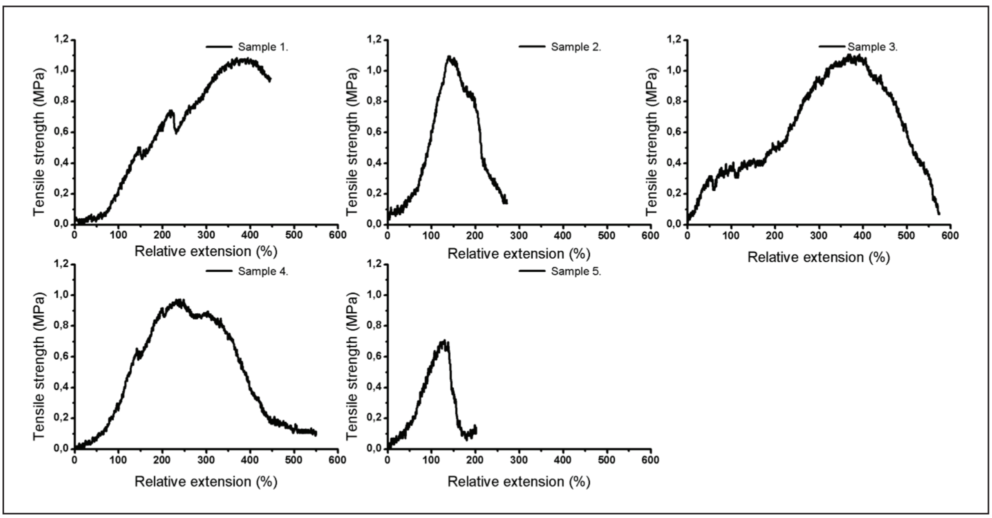

Figure 4. Tensile strength – Relative extension curves of transversal samples

Sample	Transversal samples			Longitudinal samples		
	Relative extension ε_t (%)	Tensile strength σ_t (MPa)	Elastic modulus E_t (MPa)	Relative extension ε_t (%)	Tensile strength σ_t (MPa)	Elastic modulus E_t (MPa)
1	372	1.09	0.29	125	2.39	1.91
2	141	1.10	0.78	92	2.37	2.56
3	368	1.11	0.30	117	2.97	2.54
4	232	0.97	0.42	152	1.80	1.18
5	130	0.71	0.55	201	2.32	1.15
6	–	–	–	91	3.05	3.33
7	–	–	–	127	3.11	2.45
8	–	–	–	182	2.12	1.17
9	–	–	–	147	2.89	1.96
Mean±CI	**248±138**	**0.99±0.19**	**0.47±0.30**	**137±31**	**2.55±0.38**	**2.03±0.64**

Table 3. The calculated mechanical properties of coronary veins

ples. The averages and the standard deviations of the mechanical properties were calculated for the two directions. First of all the relative extension was almost twice higher for the transversal direction.

The tensile strength of the transversal sample was less than half of the longitudinal sample and the Young's modulus was almost the quarter of the longitudinal direction.

In order to have the visual comparison between the two directions, one longitudinal and one transversal curves were chosen closest to the average of the calculated mechanical properties. Finally the sample 4. of transversal direction and the sample 9. of longitudinal direction were compared in one diagram *(Figure 5)*.

Based on the comparison it was obvious that the longitudinal samples need higher force to tear than the transversal, but they had worse relative extension and worse elongation properties. There is another important issue, the question of damage. The longitudinal samples after the maximal loading had a fast dive and complete rupture, but the transversal samples had a plateau phase and kept the strength after

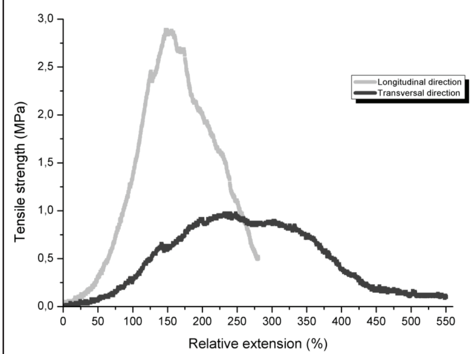

Figure 5. Comparison of the longitudinal sample and transversal sample characteristic

the injury and the maximal strength were reached. The curve was much flatter and extended in case of the transversal sample than the longitudinal.

Conclusions

The results obviously prove the mechanical differences between the longitudinal and transversal properties of the coronary veins. These are important parameters, because in case of special application the maximal elongation capability and the maximal force that the vein can tolerate without injury had to be known.

The mechanical properties of the coronary veins were tested and defined however there are still some questions. The elastic phase is the zone wherein the veins don't have any kind of injury and if the loadings stopped the vein retakes again it's original size. However it is not known whether the veins are able to reshape after loading or they remain in the extended size reached by testing. The individual role of the different layers of coronary veins is not known during the mechanical testing. These questions should be investigated in order to have a complete analysis of the mechanical properties of the coronary veins.

Conflict on interest statement

We wish to confirm that there are no known conflicts of interest associated with this publication and there has been no significant financial support for this work that could have influenced its outcome.

References

1. *Balázs T, Bognár E, Zima E, Dobránszky J.* 2008. Mechanical Properties of Coronary Veins. Gépészet 2008, Proceedings of Sixth Conference on Mechanical Engineering, n7.pdf.

2. *Holzapfel GA, Gasser TC, Ogden RW.* 2000. A new constitutive framework for arterial wall mechanics and a comparative study of material models. Journal of Elasticity, 61:1–48.

3. *Holzapfel GA, Gasser TC, Stadler M.* 2002. A structural model for the viscoelastic behaviour of arterial walls: continuum formulation and finite element analysis. European Journal of Mechanics A/Solids, 21:441–463.

4. *Matsumoto T, Sato M.* 2002. Analysis of stress and strain distribution in the artery wall consisted of layers with different elastic modulus and opening angle. JSME International Journal Series C, Mechanical Systems, Machine Elements Manufacturing, 45:906–912.

5. *Xiao L, Aditya P, Ghassam SK.* 2004. Biaxial incremental homeostatic elastic moduli of coronary artery: two layer model. American Journal of Physiology, Heart and Circulatory Physiology, 287:H1663–H1669.

6. *Fung YC, Liu SQ.* 1995. Determination of the Mechanical Properties of the Different layers of Blood Vessels in vivo. Proceedings of the National Academy of Sciences of the United States of America, 92:2169–2173.

7. *Monos E, Berczi V, Nádasy Gy.* 1995. Local controls of veins: biomechanical, metabolic, and humoral aspects. Physiological reviews.

8. *Jenny S, Ghassam SK.* 2006. A novel strategy for increasing wall thickness of coronary venules prior to retroperfusion. American Journal of Physiology, Heart and Circulatory Physiology, 291:H972–H978.

9. *Molnár F, Till S, Halász G.* 2005. Arterial blood flow and blood pressure measurements at a physical model of human arterial system. Embec 2005, 3rd Europian Medical & Biological Engineering Conference, ISSN 1727–1983.

10. *Till S, Halász G.* 2004. The effect of different artery wall models on arterial blood flow simulation. Proceedings of the first conference on biomechanics, Budapest, Hungary, page 480–485.

11. *Till S, Halász G.* 2004. Modelling and numerical computation of arterial blood flow. Proceedings of the 4. conference on mechanical engineering, Budapest, Hungary, Volume 2, page 769–773.

12. *Bartels–Stringer M, Terlunen L, Siero H, Russel FG, Smits P, Kramers C.* 2004. Preserved vascular reactivity of rat renal arteries after cold storage. Cryobiology, 48(1):95–8.

13. *Boerboom LE, Wooldridge TA, Olinger GN, Rusch NJ.* 1992. Effects of storage solutions on contraction and relaxation of isolated saphenous veins. J Cardiovasc Pharmacol, 20 Suppl 12:S80–4.

Tibor Balázs
Budapest University of Technology and Economics
Department of Materials Science and Engineering
H–1111 Budapest, Bertalan Lajos 7. MT.
Tel.: (+36) 30 420-2643
Fax: (+36) 1 326-4945

Development of bone tissue-analogous implant of functional capacity and of integration range, microscopic incorporation examination of animal experiment implantation series

Lajos Borbás, János Molnár
Cooperation Research Centre for Biomechanics of Budapest University of Technology and Economics
borbas@kge.bme.hu

Introduction

A widely known fact is that the number of joint damage caused by osteoporosis – outstandingly that of the fracture of the femoral neck – is constantly growing.

In addition to several factors among the causes there are the unfavorable side effects of medicines, which are indispensable in case of certain diseases, but as a side effect they weaken bones. Taking this fact into account the social-health importance of the growing lifetime of the implanted joint implants and its economic-financial significance is very great.

Justification of development

The lifetime of different metal-based implants used in medical practice is basically determined by the extent of adherence to bone tissues (excluding their fracture, of course). Today one of the most important tasks of implant developers is to reach the possible strongest and most durable contact between bone tissues and implants. It is well-known that the micromotions developing between the implants and bone tissues under load lead to the degradation of bone tissues, which necessarily will result in the replacement of the implant.

Nowadays there are several procedures, which promote the possible greatest embedment of the bone tissue, in this way the adherence of the implant to the bone tissue can be increased. All of these procedures try to ensure the most favorable conditions for the bone tissue by developing the surface structure of the implant. Favorable surface structures can be developed by using alloys of favorable grain structure in material, with special surface machining and by applying additional layer on the surface of the implant[1,2].

The above-mentioned procedures – although certainly will measurably increase lifetime – have not led to breakthrough (significantly longer increase of lifetime) in the past 25 years[3,4].

We have started our research – which may be regarded credible on the basis of the demonstrated in vivo animal experiments – in a different direction. In mechanical practice, theoretically connection types are divided into two groups: force and shape closing connections. Our goal was to create a connection between the implant and the bone tissue with suitable geometric characteristics, which, compared to the previous methods, in shape closing way increases its stability by an order of magnitude (through bone tissue growing fully into the implant.

We have developed an implant of internationally new integration range, where in course of changing loads of different ways of life, as a result of very complex, heterogeneous load conditions developing in the vicinity of the implant, bio-analogous, transformed state can develop in the integration range. On the surface of the created implant of integration range there are notches of different forms and directions, on that surface there is a micro-lattice structure (Patent: registration number P0401232, catalogue number 225906).

Following implantation, different load oriented bone tissue parts develop in this integration range, based on our examinations they indicate 100% filling (growing in).

Method

Our research-development was carried out in four work phases. The first: planning and preparing the implant of integration structure (basic body + structure), then their in-vitro stability examinations under bone analogous conditions. The second one: producing and preparing pre-in-vivo implants, and surgery plans. The third one: building test implants into sheep (32 implants, 16 sheep), into femur, upper arm and thigh bone places. The fourth: taking out the built in 32 implants, detailed examinations of their state of implantation, evaluation of results.

The implants were made of Ti6A14V-ASTMF 136/ISO 5832-3 bio-compatible basic body and titanium structure of ASTM F 67 material[5]. The integration structure was made with stamping die. Regarding the basic body and the structure, we have tested assemblies with several geometric parameters. The control of the elasticity features, assembly stability, behavior under load of the basic body and the integration structure made in this way (including the control of implant bodies which are analogous to bone growth, cast with epoxy resin) was carried out with tensile – compression tests (experiments) in the Accredited Laboratory of BME Biomechanical Cooperation Research Centre (Identity No.: NAT-1-1614).

Discussion

Figure 1. shows an example of the elastic behavior of the integrated structure using Instron 8872 universal servo-hydraulic test machine.

Pre-in vivo experiments were carried out for implantation. *Figure 2* shows an example of that in cadaver environment.

When preparing the integration structure, an important task regarding the final surface features is to avoid the exaggerated immune load and blood circulation load. Therefore we have

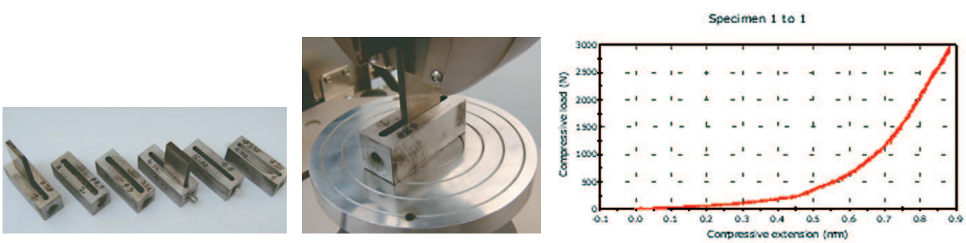

a) Instruments to determine radial elastic behavior

b) Instruments on the pressure plate of the loading machine

c) A typical diagram of radial elastic behavior

Figure 1. Determination of the elastic behavior of the implant structure

Figure 2. Pre-in vivo implantation experiments in cadaver environment

to solve the removal of non-desirable microscopic surface particles coming from manufacturing technology. To this end electrochemical post-machining was deemed to be suitable.

Figure 3 shows the microscopic image of a surface machined with electrochemical treatment.

Merino sheep have been used for the in-vivo experiments of implants, which have been implanted into the locations of upper arm and femur. The operations were performed in PRIMAVET animal hospital on the basis of previously prepared surgery plans. (We have attached a detailed research plan to our experiment and animal husbandry application to the Animal Hygiene and Control Station in the capital (Budapest) indicating the outstanding human justification of the experiment series, highlighting the lifetime problems of big joint implants. (The permission was given for sheep as operation subjects.)

In case of each animal, before implantation hematological and bio-chemical data sheets were made about each animal and their heart action was recorded on ECG.

Figure 4. a shows a picture about a phase of the operations, while *Figure 4. b* shows the X-ray following implantation. The implantations were carried out between March and August, 2007 in seven phases.

Following building in (operations) of joint implants, promoting bone recovery with gradual, moderate, physical motion is the routine.

The promotion of bone recovery, however, by so-called oriented foods is unknown in human medical, veterinary and animal feeding fields.

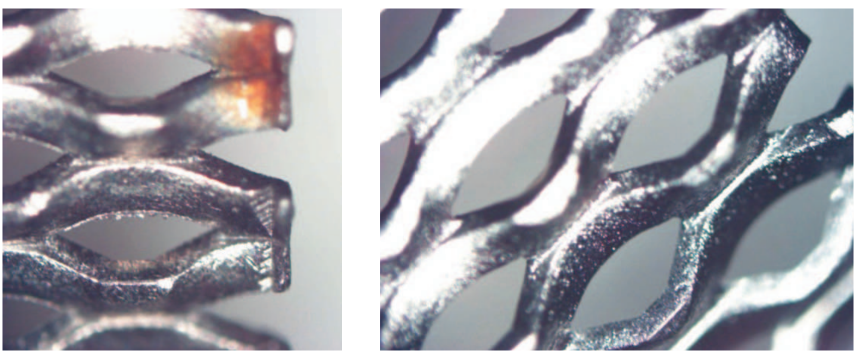

a)
Surfaces before
electrochemical machining (50×)

b)
Surfaces after
electrochemical machining (50×)

Figure 3. Surface features developed with electrochemical machining

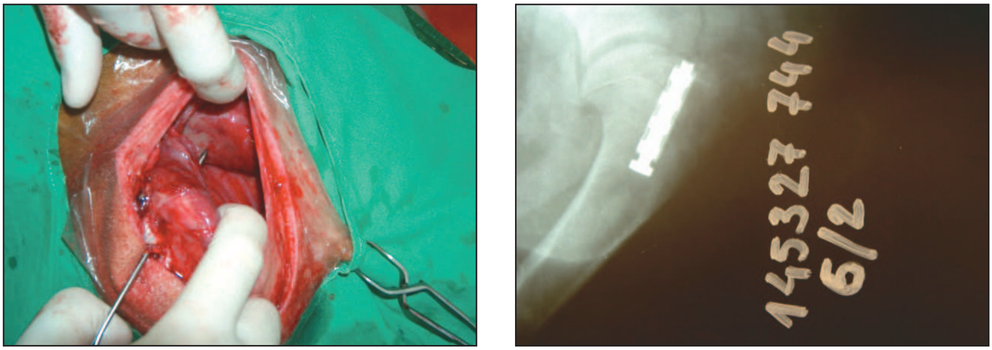

a)
Operation phase of building in implant

b)
X-ray of built-in implant

Figure 4. Building in implant and X-ray

Regarding our project, we deemed it expedient and prospective to carry out primary experiments also in this field for sheep.

Since no scientific experiment is known in this subject, oriented food supply based on the most important mineral and vitamin needs of bone recovery and bone building was provided for sheep (this time we will not go into details in this field).

Following implant operations each sheep stayed in animal hospital for 5 days for medical observation. We can conclude and it justifies the success of operations that all the 16 animals were transported in good post-operative condition to open-air site in the country.

The operated animals did not show any negative behavior during the whole period.

The bones containing implants were taken out continuously after 7–11 months.

The 32 bones containing implants were shaped by cutting as they are needed mainly for mechanical preparation of microscopic examination sections, safe gripping and also for making them suitable to be gripped with grip unit made by us into test machine for pull-out examination.

The sections for microscopic examination were prepared by ISOMET 1000 precision cutting machine. Several sections from bones were made that the building in of the implant basic body and the integration structure could be examined under different environmental venous access and different bone structure conditions. It was necessary since X ray indicating only planar position about the implants was at our disposal.

The bone/implant sections were made approximately perpendicular to the axis of the implant that the bone integration could be examined in the whole periphery of the implant.

The implant/bone pictures indicate that integration, the growing of the bone into the inner part of the lattice-like structure constituting part of the implant on the side of the implant is complete in the whole range.

(BMS 143 stereo microscope was used for the pictures with digital camera.)

Results

Figure 5 shows the incorporation sections of implants marked 5 and 9 as examples in 1:1 and 45 times magnifying.

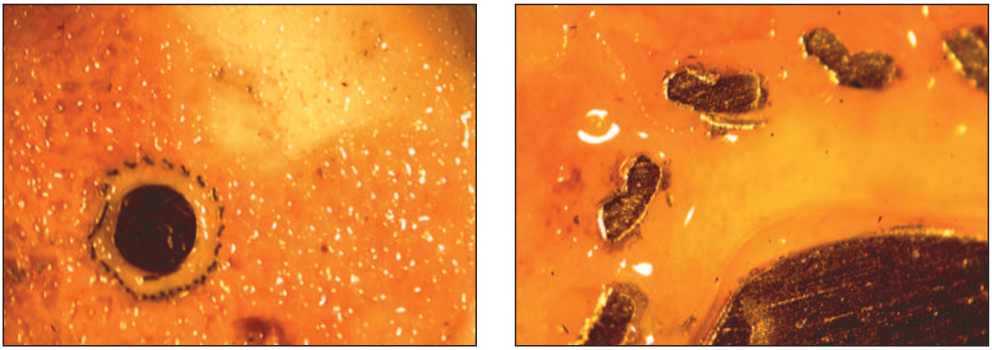

M 1:1 scale M 45:1 scale

a) Section pictures of implant marked 5

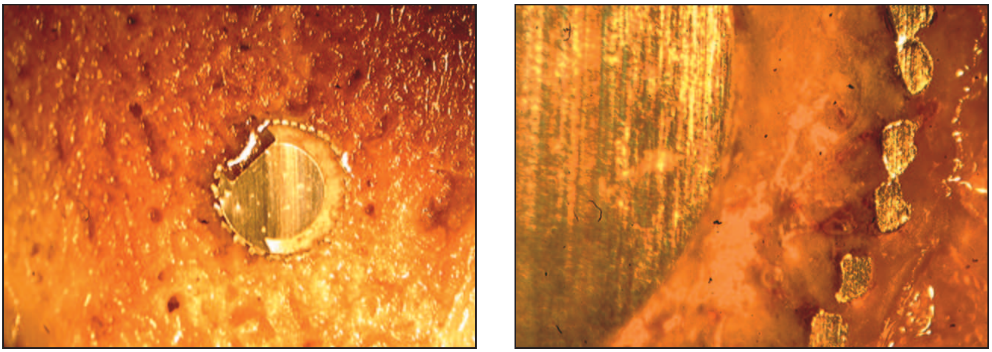

M 1:1 scale M 45:1 scale

b) Section pictures of implant marked 9

Figure 5. Incorporation of implants following their removal on the basis of pictures taken about the sections

Then, the load bearing capacity of bone integration, the behavior of implant under load and the upper limit of load were examined.

The bones containing implants were shaped by cutting for these examinations that the "outer" end part of the implant would become free.

Gradually growing load was used for this end part. (The other, inner ends of the implants were in the medullary cavity.)

(This load direction is similar to the physiological load direction of human medullary cavity implants.)

Load was increased until connection among bone integration developed with bone incorporation, the implant and the bone was broken.

The speed of load was 0.01 mm/sec.

The diagrams show the displacement of implants from their original positions as a function of load until connection-breakage from the bone surrounding the implant.

Figure 6 shows the load taking capacity of implants marked 1 and 4 as examples.

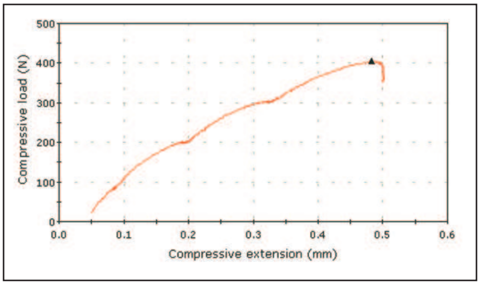

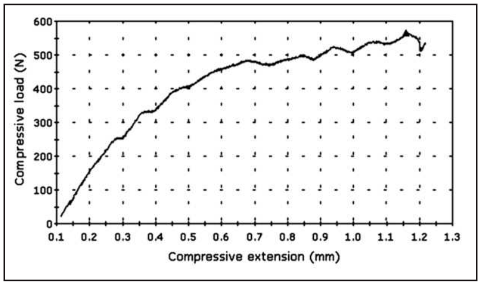

a) Implant marked 1 *b)* Implant marked 4

Figure 6. Determination of load taking capacity of implants with compression examination

The diagrams in *Figure 6* indicate that the loading limit of implants was between 360 N and 550 N. This difference comes from the fact that the four implants were in bone tissue parts to different extents. Since the medium diameter of the integration range of the implant is 6 mm and the length of the part integrated by the bone is 15–20 mm, the measured load limit values are very high. These load limit values are qualified very high since incorporation of bones in 90% took place in spongiosus(-like) bone.

These results, extended to human field, can be interpreted in the following way:

The diameter of the implant part of intermedullar position, which has contact with incorporation bone for human purposes is about double, its incorporation length is 5-6-fold of the implants examined previously.

To this extent the loadability of the implant of integration range according to the project means a capacity of load limit between 3600 N and 5500 N (of 351 kg and 541 kg mass).

On the basis of the microscopic examination series according to the previous pattern and load testing diagrams, we can conclude that the developed joint implant structure of spatial integration range ensures smooth blood supply, in this way undisturbed ossification through full biological bone incorporation and it is able to take very great load.

References

1. *Takács J, Ozsváth P.* Surface Modification of Metal Implants with Plasma Sprayed Layers, Anyagok Világa. VII. évf. 2. szám, 2007. október, (Volume 2 – № 1 – October 2007). Magyar Anyagtudományi Egyesület kiadványa, ISSN 1586 0140.

2. *Herczeg Sz, Takács J, Csanády Á, Kakuk Gy, Sólyom J, Tranta F, Sajó I, Papp K, Hargitai H.* Solid-state Transformation Produced by Laser Treatment and Mechanical Alloying of Fe-Ni-Cu(P) Powders. Material Science Forum, vol. 589. (2008) pp. 391–396. ISSN 0255-5476. Online at *http://www.scientific.net,* 2008. Trans Tech Publications, Switzerland.

3. *Breusch SJ, Aldinger PR, Thomsen M, Ewerbeck V, Lukoschek M.* Verankerungsprinzipien in der Hüftendoprothetik. Der Unfahlchirurg, 2000/11, p. 918.

4. *Reyes CD, Petrie TA, Burns KL, Schwartz Z, Garcia AJ.* Bio-molecular Surface Coating to Enhance Orthopedic Tissue Healing and Integration. Bio-

materials, Volume 28, Issue 21, July 2007, pp.: 03228…3235.

5. *Pinke P, Zitnansky M, Caplovic L, Réger M.* Biocompatible Titanium Alloys. Proceedings of First Hungarian Conference on Biomechanics, Budapest, 11–12. 06. 2004. pp.: 374…382. ISBN 963 420 799 5.

The presented results were achieved in the framework of the project GVOP-3.1.1 – 2004 – 05 – 0357/3.0 "Research-development of joint implants of biological integration suitable for long lifetime" in the Cooperation Research Centre for Biomechanics of Budapest University of Technology and Economics (BKKK BME).

Lajos Borbás
Cooperation Research Centre for Biomechanics of Budapest University of Technology and Economics
H–1111 Budapest, Műegyetem rkp. 3.

Correspondence of biomechanical changes in respect of pain score and psychological status after the standard and enhanced spine stabilisation trainings

István Bors, Peter Paul Varga, Rita Kiss
National Centre for Spinal Disorders, Budapest, Hungary
borsach@freemail.hu

Abstract

Low back pain is one of the leading causes of disability. Exercise therapy is a management strategy that is widely used in low back pain. The aim of our study was to investigate the results of standard and enhanced exercise therapy. 15 patients who had low back pain were involved in the study, none of the patients had had spinal operations before. In the first group the patients did the exercises every day at home. The patients of the second group did the exercises 3 times a week. For the biomechanical measurement we used the Spinal Mouse, a computer associated device, based on electromagnetic impulses. For estimating pain we used the 3D pain questionnaire (West-Haven-Yale Multidimensional Pain Inventory [WHYMPI]).

In the outline analysis there was a significant rise in the capacity ($p<0,05$) of the thoracic spine. By combined analysis of the two groups in the first group the rise of the capacity in the lumbar region after one month was very intensive. Less significant invers ratio was found between the rise in the capacity of the lumbar spine and the percental change of the pain.

The results show, that though the lumbar stability and the fitness level in the more active group is significantly better, it doesn't result in greater decrease of pain.

Keywords: pain score; stabilisation training; biomechanics of the lumbar spine; pyschological status; Spinal Mouse

Introduction

In our research we have investigated the results of standard and enhanced physiotherapy in patients with low back pain. The study was aimed at biomechanical factors, range of motion, psyhological factors and painscale. According to the literature we have suspected, that the different intensity of spinal-stabilization exercises results in improvement of symptoms differently.

Patients and methods

20 patients who had low back pain were involved in the study, none of the patients had had spinal operations before or had symptoms of radiculopathy or any other neurological symptoms. 5 out of the 20 patients were excluded because of noncompliance. The 15 patients, 8 male (mean age 36 ±5,4 years), 7 female (mean age 32,3 ±5,5 years) had morphological disorder (discopathy, disc degeneration, protusion or instability) in one segment only. The morphological disorders were proven by computer tomography or by MRI.

Neurological involvement (lumbar stenosis or compression), systemic disorders, inflammatory disease and obesity (BMI > 31 kg/m^2) were exclusion criteria. The patients were randomised into two subgroups I/a and I/b. Both groups took part in weekly exercise sessions for one month on spinal stabilization, where they learned exercises of increasing difficulty every week. In group I/a (10 patients) they did the exercises every day at home. The patients of group I/b (5 patients, 5 patients sceded from the study) did the exercises 3 times a week. We assessed the patients once a week before and after training.

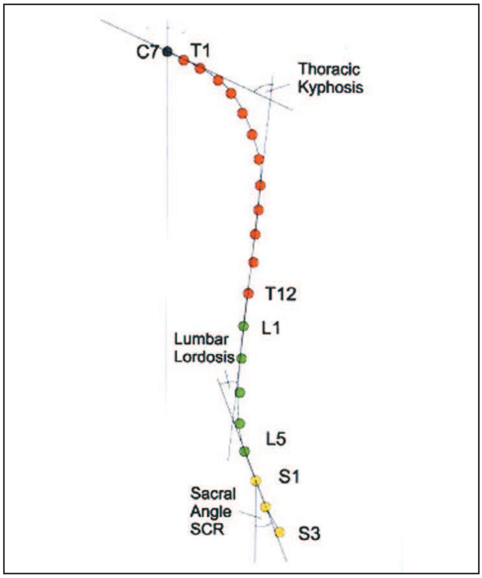

Figure 2. The measurement of thoracic kyphosis and lumbar lordosis

Measurement and parameters

For the biomechanical measurement we used the Spinal Mouse, a computer associated device, based on electromagnetic impulses. The device senses the deflexion of the levels of the spinal processes as it moves along the spinal column. The data is forwarded by bluetooth to a PC. The measured values are processed by the computer, and based on standardized data, the mesaured data are represented in 2-3 dimension. The position of the vertebrae, the functional shift of the vertebrae, and their relation to each other were evaluated by the Spinal Mouse. The kyphotic angle is marked by +, the lordotic by the – sign *(Figure 1, 2)*.

During the study we used the axial endurance test and the Matthias test of the set. The validity parameters of Spinal Mouse *(Figure 3)*.

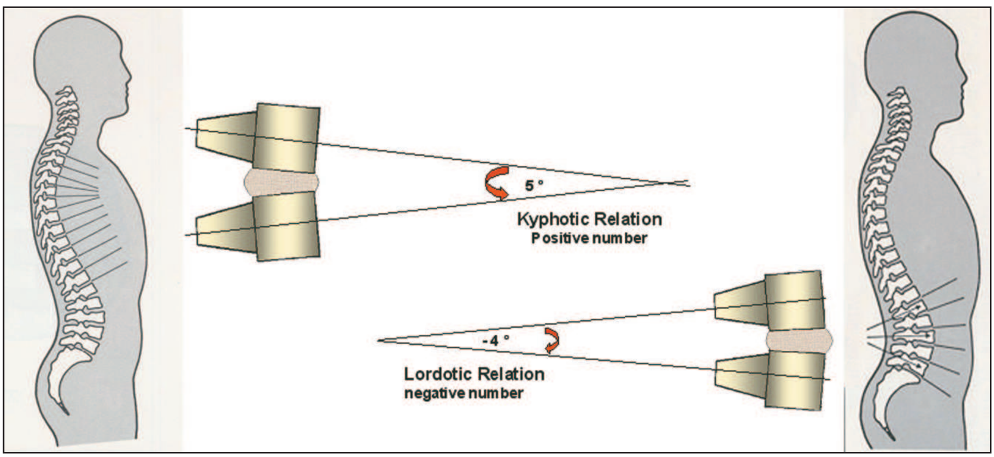

Figure 1. The kyphotic and lordotic angles

Variability (standard deviation SD, n = 50)
(A) = trained (B) = untrained
Systematic (invariant spine shape – laying position)
(A): **SD= +/- 0.8°** (B): **SD= +/- 1.3°**
Intraindividual (repeated upright position after walking)
(A): **SD= +/- 1.3°** (B): **SD= +/- 1.8°**

Intra-rater reproducibility (n = 50)
mean correlation coefficient **r** for segmental angles
(A): **r = 0.97** (B): **r = 0.94**

Inter-rater reproducibility (4 trained raters; 20 healthy probands)
cross-correlation coefficient **r = 0.93**

Comparison with functional radiograph (Th11 to sacrum)
flexion – extension: **r(segm)= 0.84 r(lumb) = 0.95**
upright-flexion: **r(segm)= 0.87 r(lumb) = 0.98**

Figure 3. The variability and reproducibility of the Spinal Mouse

During the study we used the functional test of the set. The validity parameters of Spinal Mouse *(Figure 3)*.

The Spinal Mouse was calibrated by a ZEBRIS ultrasound-based measuring method with WINSPINE software. The accuracy and the reproducibility of the method were appropriate, because the maximum value of intraobserver variation is 0.97 degrees (18.8%), that of interobserver variation is 1.54 degrees (27.1%). The maximum value of the average difference between the angles determined by the two methods is 1.62 degrees (26.6%).

During the measurement we marked the spinous process the C7 vertebra, and the lumbosacral link, we drew a line between these two points, above the spinal processes from C7 to the sacrum. The first measurment was performed with the patient standing in an upright position with his arms down. On the second measurement we gave the patient standard weights, the patient held the dumbbells for 30 seconds, with his arms raised at 90-degrees. We performed the measurement after 30 seconds whilst the patient still held the weight *(Figure 4)*.

The main parameters that we measured were the total thoracic angle [A(Th)] and the total lumbar angle [A(L)], by using expletive angles.

Body weight		Man	Woman
<55 kg	=	2×1,5 kg	2×1,0 kg
56 to 70 kg	=	2×2,0 kg	2×1,5 kg
71 to 85 kg	=	2×2,5 kg	2×2,0 kg
>86 kg	=	2×3,0 kg	2×2,5 kg

Figure 4. Scale of weight

The results were compared with the standardised results of the normal population, which were fixed into the software of Spinal Mouse. This standardised data defines a normal range, we used the limit values and the median value of this range. The axial endurance capacity of the spine is characterized by a change of bend and deviation of the angles, evoked by strain. (M2-M1)

To analyze the changes in time we used the next parameters:

n: deviaton from the normal value (+, –, 0) in degrees
m: deviaton from the median value (+, –, 0) in degrees
th: thoracic spine
l: lumbar spine
DT: the difference between the measurement before (T1) and after (T2) training (T2-T1 +, –, 0) in degrees
b: first measurement
e: last measurement
Dbe: the difference between the first and the last measurement (+, –, 0) in degrees

During the measurement we analyzed the changes of the correction angles during strain (M2-M1). In the first measurement series *(figure)* we assigned the difference of the values between the first and the last measurement Dbe (M2-M1) n,m in the thoracic and the lumbar spine.

In the second measurement series, as the level of taughtness, we defined the balance of the spine stabilizing muscle group from the measured values before and after training DT (M2-M1). We used the difference of the results from the first and last measurements DbeDT (M2-M1) n,m.

Measurement of the pain and psychological involvement, group forming II and III

For estimating pain we used the 3D pain questionnaire (West Haven-Yale [WHYMPI]), and only the part which applied specifically to the pain (I/1, total score: 18) was taken into account. The percental change of the total score demonstrated the amount of improvement.

For the psychological involvement anxiety and depression were measured with the Zung and Spielberger questionnaires, the patients were divided into two groups, the psychologically involved (IIIa) and the not involved (IIIb) group.

Statistical analysis

For the statistical evaluation of groups I. and III. the Kruskal–Wallis one-way analysis of variance was used. We have calculated the H-index from the sum of the Chi-square rank numbers, according to the degrees of freedom of the Chi-square we got the p values.

For the statistical analysis of the pain-scale the Spearman's rank correlation coefficient test was used. After Rho statistical analysis by a permutation test, we got the value of P.

Results

In the outline analysis *(figure)* (2T probe) comparing the mean value (M2-M1) of the first (2.25) and last (–1.5) measurements of the thoracic spine. There was significant rise in the capacity ($p<0,05$). In the lumbar region the difference between the average

Patient's code	Group I.a, b	Changes of pain	Psicho-logical status (III.)	Dbe (M1.M2) th,n	Dbe (M1.M2) th,k	Dbe (M1.M2) l,n	Dbe (M1.M2) l,k	DbeDT (M1-M2) th,n	DbeDT (M1-M2) th,n	DbeDT (M1-M2) l,n	DbeDT (M1-M2) l,k
1	1	6	1	0	5	0	0	0	–3	–1	–1
2	1	0	1	–9	–13	0	7	–8	–8	0	0
3	1	6	2	14	14	3	3	–8	–8	5	4
4	1	11	2	0	2	2	2	0	–2	–6	–5
5	1	6	1	0	5	1	1	0	–1	–3	0
6	1	11	2	2	2	2	2	–1	–11	0	–2
7	2	6	1	0	2	0	6	–13	–8	–2	3
8	2	33	1	0	–1	0	–3	–6	–3	0	1
9	2	11	2	6	6	3	3	–1	–1	0	4
10	1	44	2	–8	–18	6	6	–4	–3	–1	–1
11	2	11	1	0	–5	1	1	0	2	4	4
12	2	17	2	0	–2	1	1	No data	No data	No data	No data
13	1	28	1	0	3	0	1	0	–1	–4	–5
14	1	33	2	–2	–8	–2	–5	–2	–5	–2	–2
15	1	No data	1	11	11	0	0	7	4	–3	–5
16	1	No data	1	–6	–6	0	–2	6	7	0	0

Figure 5. Measured values

value (M2-M1) of the first (2.06) and the last (–0.06) measurement is not significant (p-value = 0.14).

We performed combined analysis of the two groups Ia (daily exercise) and Ib (training 3 times in a week). In the group Ia, the rise of the capacity in the lumbar region after one month was very intensive [DbeDT (M2-M1)m]; (H = 6.3112, df = 1, p-value = 0.01200).

Less significant invers ratio was found between the rise in capacity of the lumbar spine [Dbe(M2-M1)n] and the percental change of pain WHYMPI: I/1. The results seem to be on threshold limit of significancy (Spearman's rank correlation rho –0.3391144, p-value=0.1285).

Summary

The results show, that though the lumbar stability and the fitness level in the more active group is significantly better, it does not influence the improvement of the pain. There is a correlation between the stability of the lumbar spine and the level of pain, but there is no significant difference in the improvement between the two groups who had different intensity exercises. The psychologic factor also didn't have significant impact.

In the long term, the daily exercises seems to have been more effective than exercises 3 times a week, although the patients did improve similarly in the short term.

References

1. *Post RB, Leferink VJM.* Spinal mobility: sagittal range of motion measured with the Spinal Mouse, a new non-invasive device. Arch Orthop Trauma Surg (2004) 124 : 187–192 DOI 10.1007/s00402-004-0641-1 Received: 27 August 2003 / Published online: 14 February 2004.

2. *Seichert N, Senn E.* Sagittal Shape and Mobility of the Spine-Validity and Reliability of the new SpinalMouse®. Rehaklinik Bellikon, CH (2000) European Spine Journal, Vol. 9, No.4, August 2000.

3. *Liebig EM, Kothe R*, Mannion AF, Grob D.* The clinical significance of the lumbar lordosis: relationship between lumbar spinal curvature and low back pain. Schulthess Clinic, Zürich, Switzerland; *University Hospital Eppendorf, Hamburg, Germany.

4. *Mannion[1,2] AF, Knecht[1] K, Balaban[1] G, Dvorak[1] J, Grob[1] D.* Ranges of motion of the spine: reliability of measurements and comparison with data reviewed from the literature. (1) Spine Unit, Schulthess Klinik, Lengghalde 2, 8008 Zürich, Switzerland, (2) Institute of Physical Medicine and Rehabilitation, University Hospital, Zürich, Switzerland .

5. *Guermazi M, Ghroubi S, Kassis M, Jaziri O, Keskes H, Kessomtini W, Ben Hammouda I, Elleuch MH.* Validity and reliability of Spinal Mouse to assess lumbar flexion. Ann Readapt Med Phys. 2006 May;49(4):172–7. Epub 2006 Mar 20.

6. *Bellini CM, Galbusera F, Raimondi MT, Mineo GV, Brayda-Bruno M.* Biomechanics of the lumbar spine after dynamic stabilization. J Spinal Disord Tech. 2007 Aug;20(6):423–9.

7. *Cochrane Group van T. Maurits PhD, Antti M MD PhD, Rosmin E MSc; Koes B PhD.* Exercise Therapy for Low Back Pain: A Systematic Review Within the Framework of the Cochrane Collaboration Back Review Group. Spine: 1 November 2000;Volume 25, Issue 21, pp 2784–2796.

8. *Hayden JA, van Tulder MW, Malmivaara A, Koes BW.* Exercise therapy for treatment of non-specific low back pain. Cochrane Database Syst Rev. 2005 Jul 20;(3):CD000335.

9. *Ferreira PH, Ferreira ML, Maher CG, Herbert RD, Refshauge K.* Specific stabilisation exercise for spinal and pelvic pain: a systematic review. Aust J Physiother. 2006;52(2):79–88.

10. *Mannion AF, Helbling ĆD, Pulkovski ĆN, Sprott ĆH.* Spinal segmental stabilisation exercises for chronic low back pain: programme adherence and its influence on clinical outcome. Eur Spine J. 2009;18:1881–1891.

11. *M. Kiss R.* Verification of determining the curvatures and range of motion of the spine by electromechanical-based skin-surface device. Periodica Polytechnica Civil Engineering. 2008; 52/1:3–13.

István Bors
National Centre for Spinal Disorders, Budapest, Hungary
H–1126 Budapest, Királyhágó utca 1–3.

Biomechanica Hungarica III. évfolyam, 1. szám

Comparison of biomechanical changes in respect of pain scores after lumbar fusion

István Bors, Peter Paul Varga, Rita Kiss
National Centre for Spinal Disorders, Budapest, Hungary
borsach@freemail.hu

Abstract
Low back pain is one of the leading causes of disability, some patients don't respond to conservative therapy, and must undergo surgery. The aim of our study was to investigate the results of lumbar fusion operations, especially considering the changes in the sagittal range of motion (ROM) in the adjacent segments, thoracic, lumbar region and pain. 13 patients were involved, who had lumbar LIV/V rigid fusion (TLIF) operation, and still had low back pain symptoms. For the biomechanical measurement we used the Spinal Mouse, a computer associated device, based on electromagnetic impulses. For estimating the pain we used the 3D pain questionnaire (West-Haven-Yale Multidimensonal Pain Inventory [WHYMPI]).

In the outline analysis we found that the decrease in pain and improvement of symptoms after a lumbar fusion is definitely the result of increased thoracic segment hypermobility, decreased lumbar segment hypomobility, decreased proximal adjacent segment hypomobility and, increase of the distal adjacent segment hypomobility. The sagittal range of motion (ROM) of the whole spine, as the hypomobility is corrected towards the normal ROM resulted in decrease of pain.
In conclusion we can notice when using semirigid systems for bridging adjacent segments, it is important to secure the hypermobility of the thoracic spine, and the mobility of the proximal segment.

Keywords: spinal mouse; lumbar fusion; Range of Motion; hypermobility; hypomobility; adjacent level syndrome

Introduction

In our research we have investigated the results of lumbar fusion operations, especially considering the changes in ROM in the thoracic, lumbar spine, in the adjacent segments of fusions and pain. In the literature the adjacent segment syndrome is known to develop next to the stabilized segment because of the increased shear forces. Our hypothesis is that the changes in the symptoms and pain is in correlation with hypo-and hypermobility and the lack of movement of the fused segment is compensated by other segments of the spine.

Patients and methods:

13 patients were involved, who had had lumbar LIV/V rigid fusion (TLIF) surgery, and still had low back pain symptoms. None of the patients had morphological disorder (proven by CT or MRI), nor had symptoms of radiculopathy. The patient were: 6 male (mean age 36±6 years), 7 female (mean age 34.5±5.5 years). Neurological involvement (lumbar stenosis or compression), systemic disorders, inflammatory disease and obesity (BMI>31 kg/m^2) were exclusion criteria.

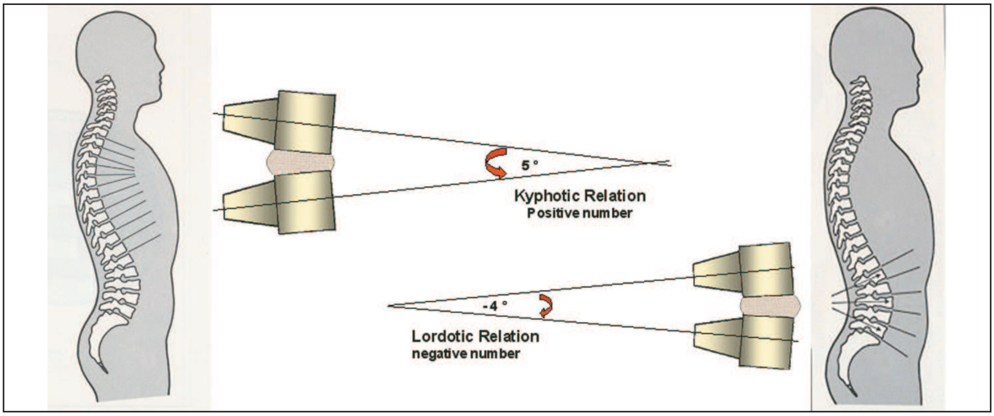

Figure 1. The kyphotic and lordotic angles

Measurement and parameters

For the biomechanical measurement we used the Spinal Mouse, a computer associated device, based on electromagnetic impulses. The device senses the deflexion of the levels of the spinal processes as it moves along the spinal column. The data is forwarded by bluetooth to a PC. The measured values are processed by the computer, and based on standardized data, the acquired data is represented in 2 or 3 dimension. The position of the vertebrae, the functional shift of the vertebrae, and their relation to each other is evaluted by the Spinal Mouse. The kyphotic angle is marked by +, the lordotic by the – sign *(Figure 1, 2)*.

During the study we used the functional test of the set. The validity parameters of Spinal Mouse *(Figure 3)*.

The Spinal Mouse was calibrated by a ZEBRIS ultrasound-based measuring method with WINSPINE software. The accuracy and the reproducibility of the method were appropriate, because the maximum value of intraobserver variation is 0.97 degrees (18.8%), that of interobserver variation is 1.54 degrees (27.1%). The maximum value of the average difference between the angles determined by the two methods is 1.62 degrees (26.6%).

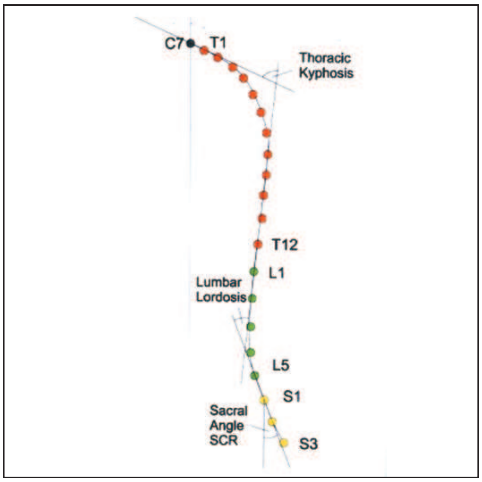

Figure 2. The measurement of thoracic kyphosis and lumbar lordosis

Variability (standard deviation SD, n = 50)
(A) = trained (B) = untrained
Systematic (invariant spine shape – laying position)
(A): **SD= +/- 0.8°** (B): **SD= +/- 1.3°**
Intraindividual (repeated upright position after walking)
(A): **SD= +/- 1.3°** (B): **SD= +/- 1.8°**

Intra-rater reproducibility (n = 50)
mean correlation coefficient **r** for segmental angles
(A): **r = 0.97** (B): **r = 0.94**

Inter-rater reproducibility (4 trained raters; 20 healthy probands)
cross-correlation coefficient **r = 0.93**

Comparison with functional radiograph (Th11 to sacrum)
flexion – extension: **r(segm)= 0.84 r(lumb) = 0.95**
upright-flexion: **r(segm)= 0.87 r(lumb) = 0.98**

Figure 3. The variability and reproducibility of the Spinal Mouse

During the measurement we marked the spinal processes of the C7 vertebra, and the lumbosacral link, we drew a line between these two points, above the spinal processes from C7 to the sacrum. At the beginning of the measurment patient was standing in an upright position with his arms down. The patient must bend over with hanging arms (F:flexion), then we asked them to lean back (E:extension). We got the total sagittal movement range from the difference of flexion and extension, this is the Flexion-Extension Index (FEI: F-E). The FEI was measured on the total thoracic and lumbar region, and in the segments of the lumbar region (Th12/L1, L1/L2, L2/L3, L3/L4, L4/L5, L5/S1). The relation to the normal range is marked with the index **n**, n is + if it is the postive range, – if it is the negative range, 0 if it is the normal range. The relation to the mean value is marked with the index **m** (+ if it is positive, – if it is negative, 0 if it is in the median). For the segmental angles, the FEI values of the segments above and below the fusion were used in the lumbar region. The difference between the values at the follow up after one and three years (FEI n,m) were marked with DFEI (n,m)

Measurement of the pain

We used the 3D pain questionnaire (West-Haven-Yale Multidimensonal Pain Inventory WHYMPI) for estimating pain and only the part which applied specifically to the pain (I/1, total score: 18) was taken into account. The percental change of the total score demonstrated the amount of improvement.

Statistical analysis

For the statistical analysis of the correlation between pain-scale and the DFEI values, the Spearman's rank correlation coefficient test was used. After Rho statistical analysis by a permutation test, we got the value of P.

Results *(Figure 4)*

In the outline analysis we found that the values of the lumbar region were in the negative range or in the normal range. The values were in the positive range, or in the normal range at the thoracic region.

Patient's code	D Pain	DFEI ups;n,m	DFEI dos;m	DFEI dos;n	DFEI th;n	DFEI th;m	DFEI l;n	DFE l;m
1	–1	4	1	0	12	12	8	8
3	–1	5	4	0	0	0	1	1
8	–1	–1	–2	–2	–1	–2	5	5
10	–1	–3	no data	no data	0	1	–5	–10
4	1	–1	2	0	–6	–6	–1	–1
5	1	5	no data	no data	8	22	–3	–3
9	1	3	no data	no data	0	15	10	10
6	2	0	no data	no data	–8	–8	0	4
11	2	0	–1	–1	–3	–3	–5	–5
13	2	–7	7	2	0	5	10	10
12	3	–7	no data	no data	0	–12	–18	–18
2	4	1	–12	0	–18	–18	–7	–7
7	4	–1	–2	0	0	–2	–14	–14

Figure 4. The results of the measurement

1. There is an inverse correlation between the increase of the pain and the positive change from the normal range of the DFEI values in the thoracic region. ($p=0.09366$, $rho=-0.3903177$)

2. There is an inverse correlation between the increase of the pain and the positive change of the mean DFEI values in the thoracic region. ($p=0.02340$, $rho=-0.5595029$)

3. There is an inverse correlation between the increase of the pain and the change of the DFEI values in the lumbar region to the normal range ($p=0.02288$, $rho=-56169$)

4. There is an inverse correlation between the increase of the pain and the positive change from the mean DFEI values in the lumbar region. (p-value$=0.06175$, $rho=-0.4492978$)

5. There is an inverse correlation between the increase of the pain and the positive change from the normal range of the DFEI in the proximal adjacent segment ($p=0.1067$, $rho=-0.3034631$)

6. There is a correlation between the increase of the pain and the positive change from the normal range of the DFEI in the distal adjacent segment ($p=0.09793$, $rho=0.5107458$)

Conclusions

From the significant ($P<=0,05$) – /2,3/ and trendlike ($0,1>=p>0,05$) – /1,4,5,6/ correlations of the above results the following conclusions were made:

The decrease in pain and improvement of symptoms after a lumbar fusion is definitely the result of the increase of the thoracic segment's hypermobility. Hence the range of motion of the spine is controlled by the thoracic segment as it compensates the hypomobility of the lumbar spine with its hypermobility.

The second biomechanical factor contributing to the improvement of symptoms after lumbar fusion is the sagittal ROM of the whole spine, as the hypomobility is corrected towards the normal ROM and these results in decrease of pain.

Similar conclusions can be drawn about the mobility of the proximal segment above the fusion. The distal adjacent level has increased hypomobility after a successful operation .

Summary

The balancing role of the thoracic spine after a lumbar stabilization is of high importance. Hence a decision about such operation or the extension – if required, needs careful planning to preserve the ROM of the thoracic segment. The preoperative ROM of the T-spine is a good indicator of the success of the operation and has to be considered when predicting the results.

When using semirigid systems for bridging neighboring segments, it is important to secure the mobility of the proximal segment. The hypomobility or rigid fixation of the distal segment also has to be considered.

References

1. *Post RB, Leferink VJM.* Spinal mobility: sagittal range of motion measured with the SpinalMouse, a new non-invasive device. Arch Orthop Trauma Surg (2004) 124: 187–192 DOI 10.1007/s00402-004-0641-1 Received: 27 August 2003 / Published online: 14 February 2004.

2. *Seichert N, Senn E.* Sagittal Shape and Mobility of the Spine-Validity and Reliability of the new SpinalMouse®. Rehaklinik Bellikon, CH (2000) European Spine Journal, Vol. 9, No.4, August 2000.

3. *Liebig EM, Kothe R*, Mannion AF, Grob D.* The clinical significance of the lumbar lordosis: relationship between lumbar spinal curvature and low back pain. Schulthess Clinic, Zürich, Switzerland; *University Hospital Eppendorf, Hamburg, Germany.

4. *Mannion*[1,2] *AF*, Knecht[1] *K, Balaban*[1] *G*, *Dvorak*[1] *J, Grob*[1] *D*. Ranges of motion of the spine: reliability of measurements and comparison with data reviewed from the literature. European Spine Journal (2004), Springer-Verlag Heidelberg, Volume 13, Number 2, 122–136.

5. *Kumar MN, Baklanov A, Chopin D.* Correlation between sagittal plane changes and adjacent segment degeneration following lumbar spine fusion. Eur Spine J. 2001 Aug;10(4):314–9.

6. *Chosa, Etsuo; Goto, Keisuke.* Analysis of the Effect of Lumbar Spine Fusion on the Superior Adjacent Intervertebral Disk in the Presence of Disk Degeneration, Using the Three-Dimensional Finite Element Method. Journal of Spinal Disorders Volume 17(2), April 2004, pp 134–139.

7. *Ghiselli G MD, Wang JC MD, Bhatia NN MD, Hsu WK MD, Dawson EG MD.* Adjacent segment degeneration int he lumbar spine. Journal Of Bone and Joint Surgery Volume 86-A(7), July 2004, p 1497–1503.

8. *Lai P-L MD, Chen L-H MD, Niu Ch-Ch MD, Fu T-Sh MD, Chen W-J MD*. Relation Between Laminectomy and Development of Adjacent Segment Instability After Lumbar Fusion With Pedicle Fixation. Spine Volume 29(22), 15 November 2004, pp 2527–2532.

9. *Park P MD, Garton HJ MD MHsc, Gala VC MD, Hoff JT MD, McGillicuddy JE MD.* Adjacent Segment Disease after Lumbar or Lumbosacral Fusion: Review of the Literature [Literature Review]. Spine Volume 29(17), 1 September 2004, pp 1938–1944.

10. *Akamaru T MD*, Kawahara N MD PhD +, Tim YS. MD PhD*, Minamide A MD PhD*, Su KK MD*, Tomita K MD PhD +, Hutton WC DSc*.* Adjacent Segment Motion After a Simulated Lumbar Fusion in Different Sagittal Alignments: A Biomechanical Analysis. Spine. 28(14): 1560–1566, July 15, 2003.

11. *Okuda Sh MD*, Iwasaki M MD*, Miyauchi A MD*, Aono H MD*, Morita M MD*, Yamamoto T MD +.* Risk Factors for Adjacent Segment Degeneration After PLIF. Spine. 29(14):1535–1540, July 15, 2004.

12. *Goldstein JA MD*, Macenski MJ PhD†, Griffith SL PhD†, McAfee PC MD‡.* Lumbar Sagittal Alignment After Fusion With a Threaded Interbody Cage. Spine Volume 26(10), 15 May 2001, pp 1137–1142.

13. *M. Kiss R.* Verification of determining the curvatures and range of motion of the spine by electromechanical-based skin-surface device. Periodica Polytechnica Civil Engineering: 52/1 (2008) 3–13.

István Bors
National Centre for Spinal Disorders, Budapest, Hungary
H–1126 Budapest, Királyhágó utca 1–3.

Biomechanica Hungarica III. évfolyam, 1. szám

STABILOMÉTERREL TÖRTÉNŐ JÁRÁSVIZSGÁLAT TRIMESZTERENKÉNT VÁRANDÓS NŐKNÉL

Dálnoki Éva[1], Hock Márta[2], Dakos Zsófia[3], Kránicz János[2], Bódis József[4]
[1] Szevital Egészségügyi Bt.
[2] PTE ETK Fizioterápiás és Táplálkozástudományi Intézet
[3] Zsigmondy Vilmos Harkányi Gyógyfürdőkórház
[4] PTE ÁOK Szülészeti és Nőgyógyászati Klinika
eva.dalnoki@gmail.com

Absztrakt
Célkitűzések
A várandósság hatással van a testtartásra és így a járásra, mint a dinamikus testtartás egy képviselőjére. Célunk volt bizonyítani ezen élettani változások hatásait a járásra.

Adatok és módszerek
Az utánkövetéses vizsgálatban, melyet a PTE ÁOK Szülészeti és Nőgyógyászati Klinikáján végeztünk 2008 májusától 2009 februárjáig, 42 nő vett részt: 21 várandós az I., a II. és a III. trimeszterben, és 21 nem terhes és még nem szült nő alkotta a kontrollcsoportot.

Eredmények
A stabilométeres mérések szerint a várandósok járása lassabb, mint a kontrollcsoporté (p=0,046), de a lépésciklus ideje a terhesség előrehaladtával csökken. A trimeszterekben mért lengőfázis ideje rövidebb a kontrollcsoporthoz képest. A kettőstámaszok aránya a teljes lépésciklushoz képest, a kontrollcsoporttal összehasonlítva trimeszterenként nőtt. A gördítés vizsgálatánál a kontrollcsoport és a kismamák I. trimeszterben mért adatai között szignifikáns különbséget találtunk (p=0,006). Az I. trimeszterben lévő kismamáknál mért lábszög nagyobb a kontrollcsoporténál (p=0,029). A kismamák I. trimeszterben mért lépésszélessége a kontrollcsoportéhoz képest kisebb (p=0,002). A várandós nők I. és III. trimeszterben mért lépésszélességét összehasonlítva szignifikáns növekedést tapasztaltunk (p=0,049).

Következtetések
Kimutattuk, hogy a járás kinematikája megváltozik a terhesség folyamán, illetve eltérést mutat a kontrollcsoporthoz képest.

Kulcsszavak: várandósság; járás; stabilométer

Examination of pregnant women's gait per trimesters with stabilometry

Abstract
Pregnancy has an impact on posture and so on walking as well, as it is a representative of the dynamic posture. Our aim was to demonstrate the effects of these physiological changes on walking.

The follow-up research was conducted at the Medical School of the University of Pécs Department of Obstetrics and Gynaecology Clinic from May 2008 to February 2009. 42 women participated in it. 21 pregnant women in the I., II. and III. trimester of their pregnancy were involved and 21 non-pregnant women, who had not gave birth yet, formed the control group.

According to the stabilometric measurements the pregnant women's gait is slower than the control group's gait ($p=0.046$), but the period of the gait cycle decreases in course of pregnancy. The duration of the swing phase measured during the trimesters are shorter compared to the control group. The proportion of the double-support stance period in the whole gait cycle, increased during the trimesters in comparison with the control group. The test of the midstance showed significant difference ($p=0.006$) between the control group and the pregnant women in the first trimester. The foot angle of the expectant mothers in the first trimester is bigger than the foot angle of the control group ($p=0.029$). The step width of the pregnant women in the first trimester is smaller than the control group's step width ($p=0.002$). The comparison of the step width of pregnant women in the first and third trimester, showed a significant increase ($p=0.049$).

We have shown that the kinematics of gait changes during pregnancy and differs from the control group.

Keywords: pregnancy; gait; stabilometry

Bevezetés

A terhesség folyamán végbemenő változások a méh alakjának, méretének a változása, az emlők növekedése, az endokrin rendszer, a vízháztartás, az emésztőrendszer, a csontrendszer és a központi idegrendszer változásai kihatnak a testtartásra, a testtartás pedig a járásra, hiszen a járás nem más, mint a testtartás megváltoztatása. A járás a dinamikus testtartás leggyakoribb megjelenési formája. A dinamikus testtartás során a test és/vagy szegmentumai mozgásban vannak. A mozgások kivitelezésében meghatározó szerepe van a mozgás biztonságnak, melyre hatással vannak a cardiovascularis és a muscolosceletalis szervrendszer változásai a várandósság folyamán[2,6].

Szakirodalmi áttekintés során eltérő információk találhatók a várandós nő megváltozott testtartásáról, járásáról. Fontosak és szükségesek a további kutatások, hiszen még olyan evidensnek tűnő változással kapcsolatban, mint a lumbális szakasz lordosisának a fokozódása, sincs egységes álláspont. Még felderítésre vár a kismamák és a nem várandós nők járásmódbeli különbségeinek pontos megállapítása is.

D. Hauswald által 2002-ben publikált tanulmányban a terhes nő járására jellemző változásokat kutatták, leírták, hogy a megnövekedett testsúly miatt a járás sebessége csökken, a lépésszélesség nő[4]. Wu és munkatársai megerősítik tanulmányukban, hogy a várandósok járása lassul a koordinációs hibák elkerülése érdekében[10].

Ezekkel ellentétben található olyan publikáció, melyben arról számolnak be a szerzők, hogy a járás sebessége nő, a megnövekedett lépéstávnak köszönhetően, a lépés szélessége nem változik[5]. Szakirodalomban olvasható még, hogy a vizsgálat során a kinematikus paraméterek nem változtak, a járásmód változatlan maradt, kinetikus értékek között viszont különbség van[9].

A terhesség során a járás kinematikai összetevőit stabilométerrel vizsgálva kimutatható, hogy milyen változás történt, például a lépésszélességben, a lépésciklus idejében, a lengő és támasz fázisban.

Célunk volt stabilométerrel vizsgálni a terhesség alatt trimeszterenként végbemenő változások hatását a járás kinematikai jellemzőire. A várandóssággal együtt járó fiziológiás változások járásra gyakorolt hatásának kimutatása.

A mérési eredmények ismeretében célzott mozgásprogrammal és a testtartás javításával a terhesség kilenc hónapja könnyebbé válhat, a jó kondíció megőrzésével a szülés és a szövődmények megelőzése hatékonyabb, a gyermekágyi időszakban a regeneráció gyorsabb lehet.

Anyag és módszer

Az utánkövetéses vizsgálatban 21 kismama vett részt – az első, a második és a harmadik trimeszterben vizsgálva –, a kontrollcsoportot 21 fiatal felnőtt nő képezte (n=42). Mindannyian önként vállalták a részvételt. Az első mérés a terhesség 10–12. hete között volt (átlag: 11,9), a második mérés a 16–20. hét közé esett (átlag: 18,7), és a harmadik mérés pedig a 28–36. hét között történt (átlag: 30,6). Kizárási kritérium volt a patológiás terhesség (placenta praevia, diabetes mellitus), súlyos mozgásszervi, belgyógyászati, neurológiai betegség, illetve nem korrigált látásprobléma.

A kontrollcsoport beválasztási kritériumai, hogy 18 évesnél idősebb, de 25 évnél fiatalabbak és még nem szült nők legyenek. Kizárási kritériumot jelentett a gestatio megléte, illetve amennyiben a szülés szerepelt az anamnézisben. A mérések 2008. 05. 01-től 2009. 02. 28-ig folytak, a Pécsi Tudományegyetem Szülészeti és Nőgyógyászati Klinikáján.

		Kor (év)	Tömeg (kg)	BMI (kg/m²)
Kontroll-csoport	Átlag Szórás	23±1,04	62,05±9,19	22,09±3,43
	Range	23–25	50–85	16,9–29,41
I. trim.	Átlag szórás	31±3,09	62,95±13,97	22,26±4,59
	Range	25–38	50–107	16,59–37,46
II. trim.	Átlag szórás	31±3,09	65,24±13,02	23,08±4,28
	Range	25–38	51–103	17,55–36,10
III. trim.	Átlag szórás	31±3,09	71,62±11,37	25,35±3,67
	Range	25–38	56–95	19,47–33,26

1. táblázat. A vizsgált várandósok és a kontrollcsoport adatai

A vizsgálat során a kismamák trimeszterenként és a kontrollcsoport összesen 84 db kérdőívet töltött ki, melyek a hozzá tartozó mérési adatokkal feldolgozásra kerültek. A kérdőívek információval szolgáltak a várandósok testi és lelki állapotáról, a terhesség lefolyásáról, a testtartás és járás lehetséges befolyásoló tényezőiről, meglévő társbetegségeikről, terhesség alatti panaszaikról.

A terhességgel kapcsolatos panaszok, fájdalmas testrészek befolyást gyakorolhatnak az egyensúlyra, testtartásra és a fiziológiás járásra[1,7]. A várandós nők trimeszterenként más és más, a terhességgel együtt járó panaszokról, fájdalmas területekről számoltak be. A panaszok és a fájdalom jelentős része az első és a harmadik trimeszterben jelentkezett, leggyakrabban szédüléstől, hányingertől, gyomorégéstől, háti és lumbális gerincfájdalomtól szenvedtek a kismamák *(2. táblázat)*.

A vizsgálatot a stabilometriás mérésekkel folytattuk. A mérőrendszer összetevői: két darab erőmérő platform, méretei 10 cm×50 cm×50 cm, tömege 11,5 kg, platformonként három db erősítő, egy mikrokontroller, személyi számítógép, monitor és egy nyomtató.

	I. trim.	II. trim.	III. trim.
Szédülés	5	1	3
Hányinger	15	3	3
Gyomorégés	6	4	9
Fáradékonyság	2	–	3
Ízületi lazaság	–	1	1
Ödéma	–	2	5
Nincs panasz	4	9	2
Hátfájdalom	4	6	7
Derékfájdalom	–	4	8
Keresztcsonti fájdalom	–	–	1
Csípőfájdalom	–	–	1
Térdfájdalom	1	1	1
Bokafájdalom	–	2	–
Nincs fájdalom	16	11	7

2. táblázat. A várandós nők panaszai
és jellemző fájdalmas testrészek trimeszterenként

A platform a nyomásközéppont helyzetét méri, kimenő feszültsége a deformáció függvénye, azzal arányos. A kimenő feszültség az erősítőkbe jut, az erősített analóg feszültség jeleket a mikrokontroller a számítógép által értelmezhető digitális jellé alakítja. A számítógép ezen jelek segítségével elvégzi a számításokat, és azok eredményét, mint az eredménydiagramokat, az elmozdulásokat és az időfüggvényeket megjeleníti a monitoron, illetve a nyomtatón.

A mérőrendszer kiegészítője még két darab 10 cm magas, 50 cm széles és 1 m hosszú dobogó, mely a két platform előtt és mögött helyezkedik el, és a járás során a platformra lépéskor, illetve arról lelépéskor a szintkülönbséget egyenlíti ki.

A mérőrendszer segítségével a járás analizálható, három eljárási mód szerint:
– Az erővektor időbeni eloszlásának ábrázolása F (t)
– A láb és talaj érintkezési periódusának kimutatása
– A testtömegközéppont pozíciójának grafikonja koordináta-rendszerben (x, y)

1. ábra. Stabilometriás vizsgálat

Stabilometriás vizsgálat során megmértük a kismama testtömegét (kg) illetve a súlyát (N), majd a páciens a dobogó elejéről indulva kényelmes tempóban, zavartalanul végigment a platformokon, *(1. kép)* így a két platform segítségével egy lépésciklus vizsgálható.

A platformok regisztrálták az eredményeket az egyik láb sarokérintésétől a másik láb öregujjának elrugaszkodásáig, végül analizálásra kerültek a gép által megjelenített grafikonok.

Erő-idő grafikon: Folyamatos felvétele a nyomás, illetve a terhelés növekedésének és csökkenésének a járás során.

Erő-pozíció grafikon: Egymás utáni felvétele a testtömegközéppont pozíciójának a járás során. A különböző platformokról származó

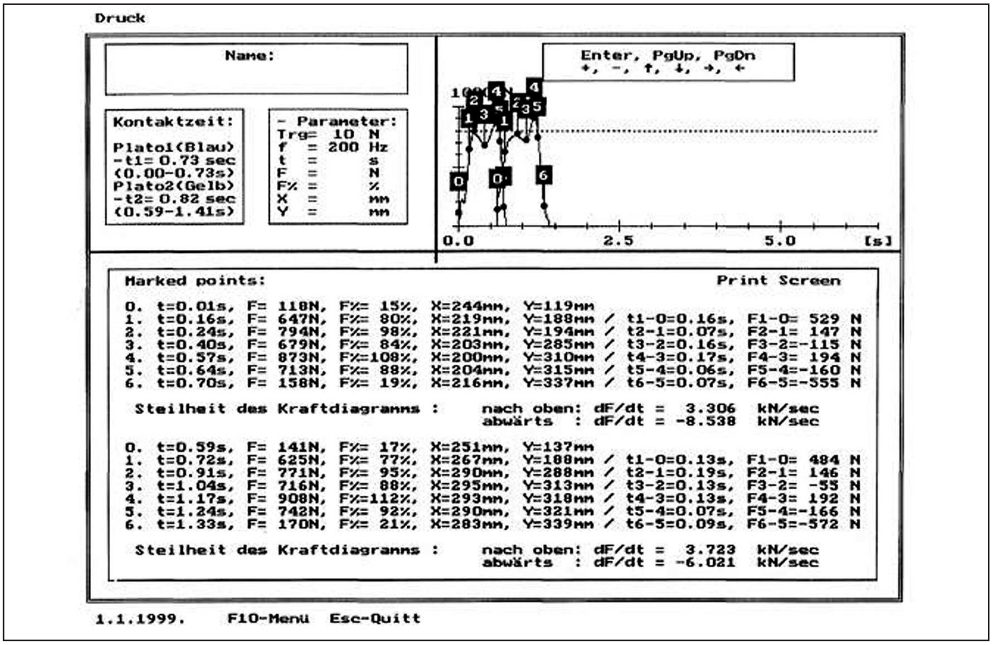

2. ábra. Erő-idő grafikon és táblázat

eredmények egy közös grafikonban, különböző színekkel megkülönböztetve kerülnek megjelenítésre.

A monitoron kijelzésre kerül még a láb-talaj kapcsolat ideje, minden kapcsolat kezdeti és befejezési időpontjaival.

A mérések eredményei rögzítésre és feldolgozásra kerültek egy táblázat segítségével, mely hét darab nevezetes pontot jelöl meg. Az erő-idő grafikonon ábrázolja a hét pontot (0–6), és a táblázatban az ezen pontoknak megfelelő idő-, erő-, erő %-értékeket és az x, y koordinátákat *(2. kép)*.

A vizsgált paraméterek:
– Lépésciklusidő
– Lengőfázis százalékos aránya
– Kettős támasz fázis százalékos aránya
– Gördítés fázisa
– Lábszög
– Lépésszélesség

Eredmények

Lépésciklus ideje: A terhesség előrehaladtával a lépésciklus ideje csökken, az I. trimeszterben átlag=1,32s±0,14, a II. trimeszterben átlag=1,27s±0,16, és a III. trimeszterben átlag=1,26s±0,1, a trimeszterek között nem mutatható ki szignifikáns eltérés. Annak ellenére, hogy a terhesség előrehaladtával a járás gyorsul, a kontrollcsoporthoz képest a várandós nők járása szignifikánsan lassabb az első

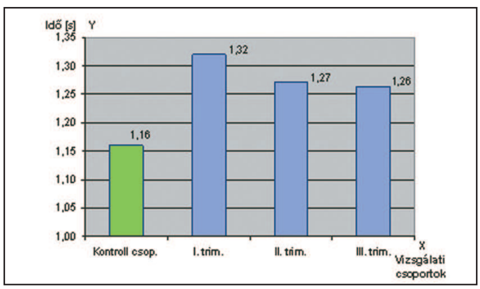

1. grafikon. A kontrollcsoport és a várandós nők trimeszterenkénti átlag-lépésciklusideje trimeszterben (p=0,007), a második trimeszterben (p=0,046) és a harmadik trimeszterben is (p=0,046).

A legnagyobb eltérést a kontrollcsoport, és az első trimeszter eredményeit összehasonlítva tapasztaltunk (p=0,007). A várandós nők járásának sebessége az első trimeszterben jelentősen lecsökken a kontrollcsoporthoz képest *(1. grafikon)*. Magyarázat lehet erre az első trimeszterben előforduló számos panasz, mint a hányinger, gyomorégés, szédülés, fáradékonyság *(2. táblázat)*. Ebben az időszakban pszichés komponensek is hatással vannak a kismamára, a terhesség ténye óvatosságra inti a nőt, ha túlzottan figyel a járás folyamatára, az kímélővé válik, eltérések keletkeznek[4]. Ajánlatos a meditáció, lazító gyakorlatok, melyek lelkileg segítik hozzá a kismamát a változások elfogadásához[8].

Lengőfázis-támaszfázis: Lengőfázisról akkor beszélünk, mikor a lépésciklus alatt az adott láb nem érintkezik a talajjal[3]. Vizsgálatunk szerint a lengőfázisok ideje egy lépésciklus alatt csökkenő tendenciát mutat a kontrollcsoporttól a harmadik trimeszterig *(3. táblázat)*.

A lengőfázisok idejének csökkenése feltételezi a támasz fázisok idejének a növekedését, ami a kettős támasz fázisokban mutatkozik meg.

Kettős támaszok: Összehasonlítva a kontrollcsoport és a kismamák kettős támaszainak időtartamát, egy lépésciklus alatt mindhárom trimeszterhez tartozó értékek esetén szignifikáns különbség állapítható meg (I. trimeszter: p=0,034, II. trimeszter: p=0,003, III. trimeszter: p=0,0009).

A két kettős támasz hányada a teljes lépésciklushoz képest a kontrollcsoporttal összehasonlítva növekedést mutat oly mértében, hogy a harmadik trimeszterben már szignifikáns a különbség (p=0,023). *(4. táblázat)*

	Kontrollcsoport	**I. trim.**	**II. trim.**	**III. trim.**
Első lengőfázis átlag ideje (s)	0,37±0,07	0,40±0,07	0,39±0,05	0,38±0,04
Első lengés %-ban	32,07	30,20	30,46	29,95
Második lengőfázis átlag ideje (s)	0,43±0,08	0,48±0,04	0,47±0,06	0,46±0,04
Második lengés %-ban	36,87	36,55	36,50	36,34

3. táblázat. Lengőfázisok átlagos időtartama, illetve százalékos értékük a teljes lépésciklushoz képest

	Kontrollcsoport	I. trim.	II. trim.	III. trim.
1 kettős támasz átlagidő (s)	0,23±0,05	0,27±0,05	0,26±0,04	0,27±0,04
1 kettős támasz %	20	21	21	21
2 kettős támasz átlagidő (s)	0,13±0,03	0,17±0,04	0,16±0,03	0,16±0,03
2 kettős támasz %	11	12	12	12
∑ kettős támasz átlagidő (s)	0,36±0,08	0,44±0,08	0,42±0,07	0,43±0,06
∑ kettős támaszok %	31	33	33	33

4. táblázat. lépésciklus alatti kettős támaszok ideje és százalékos aránya

Lábszög: Célunk volt még bizonyítani, hogy a két láb által bezárt szög átlagos értéke hogyan változik a terhesség folyamán és a kontrollcsoporthoz viszonyítva.

Az átlaglábszög a kontrollcsoportnál 16,44°± ±7,72°, az első trimeszterben 23,67°±12,31°, a második trimeszterben 21,82°±9,69°, és a harmadik trimeszterben 22,81°±13,11°. Szignifikáns növekedést a kontrollcsoport és az első trimeszter összehasonlításakor kaptunk (p=0,029). A második (p=0,053) és harmadik trimeszter (p=0,064) esetében az eredmény szignifikáns közeli *(2. grafikon)*.

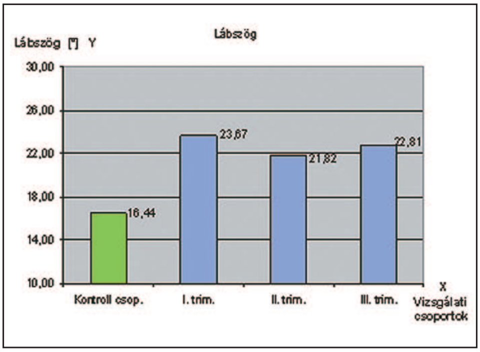

2. grafikon. A kontrollcsoport és a várandósoknál mért átlag-lábszögek mértéke

A gördítés fázisa: A gördítés fázisában a súlypont vertikális tengelyen való elmozdulását súlycsökkenéssel jellemezhetjük. A gördítés fázisában a kontrollcsoportnál létrejövő súlycsökkenés mértéke átlagosan 14,04%±4,05% a kezdő lábnál, a másik lábnál 14,38%±5,83%. A várandós kismamáknál az első trimeszterben 12,52%±3,28% az első lábnál, a másiknál 8,76%±6,83%, a második trimeszterben 12,57%±3,56%, 8,71%±5,04%, a harmadik trimeszterben 12,43% ±4,56%, 12,28%±5,6%.

A gördítőfázis vizsgálatával a járás dinamizmusára következtethetünk. A legnagyobb súlycsökkenés a kontrollcsoport gördítése alatt volt mérhető, a súlypont emelkedése ennél a csoportnál a legnagyobb, minél kisebb mértékben mozdul el a súlypont, annál stabilabb a járás. Szignifikáns különbség mutatható ki a kontrollcsoportot összehasonlítva a kismamákkal az első trimeszterben (p=0,006).

Lépésszélesség: A kontrollcsoport 76,81 mm± ±32,73 mm átlag lépésszélessége a legmagasabb a vizsgált csoportok közül. A várandós kismamák első trimeszterében mért lépésszélessége 45,38 mm±27,63 mm volt, a második trimeszterre ez a távolság 54,76 mm-re ±27,63 mm nőtt meg, a harmadik trimeszterben még jelentősebb a lépésszélesség növekedése: 61,71 mm±30,52 mm, ez a különbség az első trimeszterhez képest már szignifikáns (p=0,049) növekedést mutatott *(3. grafikon)*.

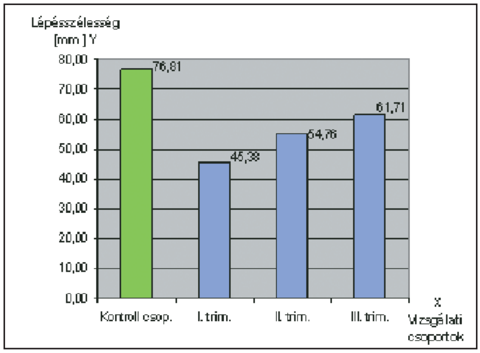

3. grafikon. A kontrollcsoport és a terheseknél mért átlag-lépésszélesség mértéke

Megbeszélés

A vizsgálatunk tárgya, a terhes nők járása, jelenleg kevéssé kutatott terület. A témában jelentek meg tanulmányok, de ezen tanulmányokban kisszámú mintát vizsgáltak (1–15 fő), melyek nem mutatnak reprezentatív képet a várandós nők járásának változásáról. A szakirodalmi háttér feltárása során ellentétes eredményű vizsgálatok is találhatók. A kutatási terület kiaknázatlanságát jelzi az is, hogy nem készült még metaanalízis a témában megjelent vizsgálati eredményekből.

Jelen kutatásban 42 egészséges nő (21 várandós és 21 nem terhes) vett részt, a járásukat 6 szempontból vizsgáltuk. A megfigyelt kinematikus jellemzők: a lépésciklus ideje, lengőfázisok és a kettős támaszok százalékos aránya a teljes lépésciklushoz képest, a lábszögek és a lépésszélesség mértéke, valamint a gördítés fázisában a súlyerő mértéke.

A vizsgált járási paramétereknél a változás megfigyelhető, több esetben szignifikáns eltérést regisztráltunk:

– A kismamák járása valamennyi trimeszterben szignifikánsan lassabb, mint a kontrollcsoporté (I. trimeszterben $p=0,007$, a II. trimeszterben $p=0,046$ és a III. trimeszterben $p=0,046$). Ez egyezést mutat D. Hauswald[4] és Wu[10] eredményeivel, miszerint a kismamák járása lassabb, mint a kontrollcsoporté, de eltér a trimesztereket összehasonlító vizsgálattól, ahol azt tapasztaltuk, hogy a várandós nők járásának sebessége fokozatosan nőtt, ez az eredmény E. Butler[5] publikációját támasztja alá.
– Az I. trimeszterben mért lábszög szignifikánsan nagyobb a kontrollcsoporténál ($p=0,029$).
– A kismamák I. trimeszterben mért lépésszélessége a kontrollcsoporthoz képest kisebb ($p=0,017$), de a terhesség során fokozatosan nő.
– A várandósok I. és III. trimeszterben mért lépésszélességének értékei között szignifikáns a növekedés ($p=0,049$), tehát jelentős a változás a lépésszélesség mértékében, így E. Butler[5] tanulmányának ellentmond, de D. Hauswald[4] vizsgálatát megerősíti.

A terhesség alatt végbemenő változások nem kórosak, az értékek a terhesség előrehaladtával változtak, és a kontrollcsoporthoz viszonyítva eltérést mutattak, mégis mindvégig a normál járással foglalkozó szakirodalom által egészségesnek tekintett tartományban maradtak. A harmonikus, kontrollált járás látványos megváltozása csökkentené a járás hatékonyságát, és növelné az energiaigényét.

A vizsgálat eredményei azt mutatják, hogy a változások jelen vannak, még ha sok egyéni eltérést is mutatnak. A fizioterapeutáknak szükséges ismerniük a lehetséges eltéréseket a fiziológiás járástól a terhes nőknél, hiszen egy megfelelően korrigált tartásnak, járásnak az elváltozások kialakulásában jelentős prevenciós szerepe van. A fiziológiás járás jellemzői ismeretében fontos a helyes állás megéreztetése, betanítása, a helyes járás betanítása és a korrekció.

Irodalom

1. American College of Sports Medicine: Várandós mamák edzésprogram-ajánlata, 2007.
2. *Ángyán L.* Az emberi test mozgástana, 2005, Motio Kiadó, Pécs
3. *Magee DJ.* Orthopedic physical assessment, 2008, Saunders Elsevier, St. Louis
4. *Hauswald D.* (2002) Der gang einer Schwangeren-Analyse des Bewegungsablaufs mittels der FBL Klein-Vogelbach, Krankengymnastik – Zeitschrift für Physiotherapeuten, 54(8):1244–1252.
5. *Butler E, Colón I, Druzin M, Rose J et al.* (2006) An investigation of gait and postural balance during pregnancy, Gait & Posture, 24 (S2):128–129.
6. *Illei Gy.* Klinikai ápolástani ismeretek, 2006, II. Pécsi Tudományegyetem Egészségtudományi Kar, Pécs

7. *Grunfeld N.* Terhesség hétről hétre. 2004, Glória Kiadó, Budapest

8. *Dahlke M, Dahlke R, Zahn V.* Út az életbe – a születés teljessége, 2001, Holistic Kiadó, Budapest

9. *Foti T, Davids JR, Bagley A et al.* (2000) A Biomechanical Analysis of Gait During Pregnancy, The Journal of Bone and Joint Surgery, 82(5): 625–63.

10. *Wu W., Meijer O, Lamoth C et al.* (2004) Gait coordination in pregnancy: transverse pelvic and thoracic rotations and their relative phase, Clinical Biomechanics, 19(5):480–488.

Dálnoki Éva
Szevital Egészségügyi Bt.

The effects of gradual dynamization on fracture healing

Peter Fröhlich
OSEI, Budapest
frohlichp@osei.hu

The verified conditions of fracture healing are: vascularity of the injured bone, repositon of the fracture and proper casting. Opinions about casting and stabilization have been changed in the course of time.

There has been gradual development. At the beginning external fixation, splints and casting, then constant extension, later stable compression osteosynthesis were used. Nowadays elastic internal fixation is thought to be the best solution. All these methods mean non-changing stabilization from the beginning of the treatment to complete healing.

To reach a constant biological stimulus on fracture healing during treatment, the degree of fixation should gradually be reduced, dynamized. Furthermore, the question if gradual dynamization should be only axial or complex has not been answered yet. In addition to this, we've got positive clinical experiences about single dynamization, but we miss comparative examinations, objective methods to verify the right degree of stabilization and the effects of dynamization.

In my study I compared the effects of 3 different methods of casting/splinting (A: permanently stable, B: gradually dynamized, C: gradually stabilizing).

I created standardized conditions on femurs of rabbits by osteotomy in the 3 groups. I examined the 'fractures' of 5 rabbits in each group in the course of week 3, 4, 5 and 6. I used external fixation and influenced the stability of the bars by changing the number of the 5 connecting Kirschner-wires. In advance, I checked the stability of the fixators by load test.

Control methods

Control measurings happened once a week. I measured the following factors:
– the electric voltage of tissue metabolism and the resistance of the tissues;
– the weights of the rabbits;
– the quantity of the callus (per week) by vital dyeing in hard segments (polychrome sequens-marked hystomorphometria);
– sizes and density of the osteons;
– the signs of healing on x-rays of the femurs.

I used planimetry to measure quantity of the callus, changes in the periphery and density of the callus. Furthermore I compared the fracture resistance of prepared femurs and the non-injured sides and recorded sound emission during loading the femurs. In this lecture I'll evaluate the histological segments, the x-rays and the measurement results of flexibility strength of the callus.

Results

I recorded the evaluation results numerically and this method offered the possibility of biostatistical (correlation and significance) calculations.

In the hard segments I recorded the diameter of the osteons; the surface of differently coloured osteon rings that had developed in a week's time and the number of osteons to be seen in a visual field of a 0.25 square millimetre. The surface growth of the rings decreased exponentially in all of the 3 groups.

Most callus developed in group C. (In both A and B the quantities were smaller.) The difference between group C and group A or B was significant in the course of week 2. The number of osteons in group A was significantly higher than in groups B and C in week 2 and 3; there was no statistical difference in the rest of the weeks. As for the number of osteons, group A contained significantly more osteons – there were no more differences between the groups.

The x-rays of the femurs were evaluated by 3 experienced specialists. They classified the healing process in 5 categories. The specialists considered the healing process of group B to be significantly better (α=0.05). The findings began to get closer to each other in weeks 5, 6 and 7. Group C seemed to be significantly worse compared to group A in weeks 6 and 7.

The prepared femurs were submitted to a 3-point flexibility test loaded by a speed of 2.5 mm/minute on a 4-centimetre section; comparing the healthy and the 'broken' side in the same way. The stability in group B was significantly better in weeks 3, 4, 5, 6 and reached the domain of health. The difference between groups A and C developed as late as in week 7 for group A.

Discussion

The experimental model provided equivalent local conditions for fracture healing. The only variable was the stability of fixators. This factor made it possible for us to compare the effects of different kinds of stabilization without any restrictions. The measure of stability and the pace of the changes were chosen arbitrarily. These factors were only guided by the known total time of healing, and they followed also the possibilities of the fixator's structure . I think that complex-direction stability changes get closer to the mechanism of the biological stimulus in the tissues than an exclusive one-direction axial loading-model does[3,5].

If healing means for the patient to regain loadbearing, continuous dynamization (group B) can shorten time of the healing process in rabbits by 2 weeks – compared to constant stability fiixation (group A). In the reciprocal group (group C) I could not verify that increasing fixation (that is continuous reduction of mechanical stimulus) had curbed healing process. As this group starts out with flexible fixation (2-wire bars), in histological segments – compared to stable groups – the healing process begins to produce higher quantities of callus and a rougher osteon structure. The reduction of stimulus probably results in decreased calcification some weeks later, so the callus produces a relatively lower stability, weaker bone scar.

The stable conditions in groups A and B at the beginning start with developing identical histological structures (osteon sizes and density). The advantages of gradual dynamization turn up after week 3 (group B). These advantages come probably from the optimal structure and quality of collagen fibres and the earlier formation of apatite.

Accepting the results given, implant development should be directed towards absorbing – that is gradually dynamizing – fixation. On this way, the axial mechanical stimulus accompanying the present-day implantates can only represent an intermediate phase.

References

1. *Basset CAL.* Influence of oxygen concentration and mechanical factors on differentation of connective tissues in vitro. Nature 1961;(190):460–461.

2. *Blietz R.* Die biologische Reaktion der Knochen-Kortikalis auf definierte mechanische Spannungen, als piezoelektrisches Verhalten interpretiert. Nova Acta Leopoldina 1976;(44):95–100.

3. *Claes L, Wolf S, Augat P.* Mechnical modification of callus healing, Chirurg. 2000;(9):989–994.

4. *Fröhlich P.* Untersuchungen zu Biomechanik der Frakturheilung am Fixateurmodell. Disseration, MTA Budapest 1989.

5. *Goodship AE, Lawes TJ, Rubin CT.* Low-magnitude high-frequency mechanical signals accelerate and augment endochondral bone repair: prelimenary evidence of efficacy. J. Orthop. Res. 2009 Jul;(7)922–930.

6. *Takashi M, Cornell ChN.* Biomechnaics of bone healing, Clin Orthop Relat Res 2009;(467):1937–1938.

7. *Uhthoff HK, Finnegan MA.* The role of rigidity in fracture fixation. Arch. Orthop. Traum. Surg. 1984;(102):163–166.

Peter Fröhlich
OSEI, Budapest
1123 Budapest, Alkotás u. 48.

Biomechanica Hungarica III. évfolyam, 1. szám

Scoliosis testing features on the basis of electronically generated moire patterns

Zselyke Gaal, Ákos Antal, Tamás Péter
Budapest University of Technology and Economics
zsgaal@gmail.com

Abstract
The Dept. of Mechatronics, Optics and Information Engineering, within the project team, had built an electronic moire equipment to visualize and diagnose scoliosis. The device generates a computerized moire phenomenon, which can be viewed and save for later examination. The applicability of the system was tested with statistical method from the moire patterns, which was created by the prototype device. The results of the calculations – to determine the rate of scoliosis by moire patterns – are promising and comparable with X-ray examinations.

Keywords: moire; scoliosis

1. Introduction

The Budapest University of Technology and Economics, Department of Mechatronics, Optics and Information Engineering as part of a team had won subvention on a tender of the National Office of Research and Technology to develop a new optical measuring family of orthopedical applications, to ensure more reproducible and more appropriate sampling and monitoring of orthopedic deformities (TECH 08-A1/2-2008-0121). The Salus-Orthopedtechnique Surgical Appliances Manufacture and Trade Ltd., The Department of Polimertechnique from Budapest University of Technology and Economics, The Orthopedic Clinic of the Semmelweis University, Varinex Informatics Ltd. and the Aga IT Ltd. are also the members of the winning consortium. The prototype of the moire measuring system, the target of the project, has been finished. The device's primarily purpose is screening and diagnostic, but it can be used for improve 3D modelling of orthopedic deformities and aid designing and controlling the manufacturing process of corrective tools.

The tasks of the project were the followings:

1. Calibration and error analysis of the prototype of the developed and installed moire equipment.
2. Test of the calibrated equipment, analysis of the possibility to determining the angular characteristic of idiopathic scoliosis from moire patterns on the basis of practical measurements.

2. Methods

A) The moire technique

The moire phenomenon is the result of the interaction between two periodic structures with different space frequencies. The measured or tested surface is similar to the contour lines of the maps but described in more general manner. Moire stripe is the manifestation of the moire phenomenon. These are generally the points of a surface with a given distance from the reference plane. Generally, moire surface is a set of points with a specific distance from a reference surface where distance is function of the fixed parameters of the layout. Moire stripes are the section lines of the measured and moire surfaces. The picture created via any capturing method, represents the section lines of moire and measured surfaces in two dimensions called moire pattern.

This optical method is one of the most modern ways for measuring the shape of the human body in space. The advantage is the simultaneity and touch-freeness, so the measured body is not charged with measuring pressure at all, information can be obtained all of its points at the same time. Its measurement applicability is wide[1–5]. This technique can also be used to measure deformation caused by pressure or by temperature change, when measurement with mechanical process cannot be carried out. It is also suitable to check dimensional accuracy of products made in production in series or in robotics[33,34,35].

B) Using Moire technique in orthopedics

The moire patterns' orthopedic – scoliosis testing – application is primarily used for screening by visual evaluation or diagnosing, as the back surface's asymmetry is very characteristically shows up[22]. The orthopedic applications are comprehensive, because the reproduction is simple but the result is very impressive and convincing[7,16–18]. In particular, it is used in combination with X-ray[19], but only making a moire pattern is not cause radiation pressure on the patient, which is a serious benefit of moire technique. The moire technique with computing, image processing and pattern recognition background is already a serious factor in this area[29–31].

The professional protocol on the physiotherapy of the structural idiopathic scoliosis prepared by the Professional College of Nursing and the Hungarian Society of Physiotherapists recommends moire topography beside diagnostic or imaging tests, bi-directional, stationary made X-ray image, the Cobb-angles (lateral size of curves), the rotation, the torsion, the sagittal profile view, the Risser sign, spiroergometric examination and the surface analysis.

3. The build device

The moire measuring equipment was designed and constructed in consultation with an orthopedical specialist to fit in the tender. The prototype of the device was tested in the Heim Pal Hospital, and in the Salus Orthopedtechnique Surgical Appliances Manufacture and Trade Ltd. In essence, that is a moire equipment with classic projection. The novelty is so far, that video projector used to project out the stripes to the reference and the test surface instead of a traditional projector. During the measurement, firstly a picture of the reference surface is taken, which is stored in computer memory or in mass storage. Then the test object takes the place of the reference surface, while the grating is projected with the same settings. The lattice is deforming on the examined surface depending on its shape. An other picture is taken from this, then the software prepare the moire pattern from the pictures of the reference surface and the test surface. The resulting moire pattern can be displayed or stored.

4. The examination and treatment of scoliosis

The idiopathic scoliosis's origin is unknown, the prevention of its formation is not yet known. However the disease can be recognized early with screening and it can be stopped and a significant and lasting improvement can be achieved with appropriate treatment.

A) The definition of the disease

By definition, the idiopathic scoliosis is the lateral curvature of the spine with structural changes, which forms without traceable reason before bone ageing. The structural changes of idiopathic scoliosis come about in all directions of space. The spine is curved, not only on the frontal plane, but also twists on the horizontal plane and become concave on the sagittal plane. The disease may begin in different ages and can appear in any part of the spine. The date of commencement of the disease is significantly affects the size of the curve. The earlier starting age of idiopathic scoliosis, the worse prognosis what patients can be expect. Thus, the lateral curvature of the spine is the scoliosis. The mobility of the vertebrae are often significantly reduced, so that the inward rectifying of the vertebra column is no longer possible. The lateral curvature of the spine is usually associated with the roll – torsion – of the vertebrae which results the so-called rib hump dorsal, and hump in the lumbar section.

B) The types of idiopathic scoliosis

The disease has two main groups, the functional and the structural scoliosis.

1. *Functional scoliosis:* The type of lateral curvature of the spine, which was not followed by torsion. The deformity can be corrected advanced state. It can develop without detectable reason which called primary functional scoliosis and also in the alternative, when some other reason lies in the background, such as lower limb length difference, muscle paralysis or herniated discs. Functional scoliosis is not three-dimensional change in the spine. Generally it can be well managed.

The therapy consists corrective physiotherapy maintenance. The primary treatment of functional scoliosis is to strengthen the back musculature. This type of functional scoliosis usually do not worsen and not transformed to structural scoliosis. The secondary functional scoliosis forming cause is one of the lower limb's real or apparent shortening. The half-pelvis on the shorter side is lower and because of the compensation of the inclined pelvis orientation, it become the convex lumbar scoliosis for the shortened side. It can be corrected with the limb length differential correction, for example with heel rise.

2. *Structural scoliosis:* It means the three-dimensional spine deformities, in clinical practice, the vast proportion of cases are in this group. The causes of scoliosis may be quite different, but it can develop without any known cause. Overall, the earlier year of life, the worse is the prognosis.

Characteristic of the deformity, is the so-called Cobb-angles *(Figure 1)*. This angle by definition is the exterior angle of the lines, perpendicular to the lines laying on the end plates of the beginning and ending vertebrae of scoliosis. 80–90% of structural scoliosis are idiopathic, 4:1 ratio girls are affected.

C) Consequences

Due to disease the motion of the vertebra column is greatly reduced and the chest is deformed. Beyond the aesthetic problems, sco-

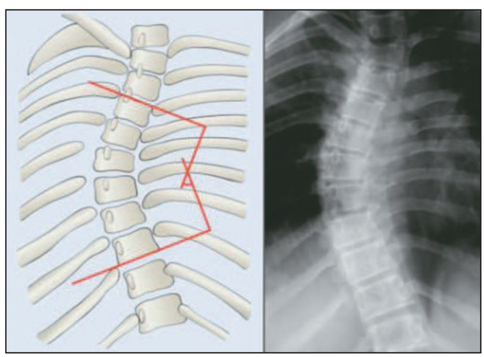

Figure 1. Definition of the Cobb-angle

liosis can lead to significant pain in the back, in very severe cases the consequences are heart and circulatory disorders. It should be noted that due to inappropriate static load the risk of herniated discs and other degenerative spine disorders increase as well.

D) Diagnosis

To determine the type of idiopathic scoliosis and curvature of the spine bi-directional X-ray is used, made of the total size of the standing patient's spine. The Cobb method is for determining the angle of curvature *(Figure 1).* The prevalence around 10 Cobb-angles of idiopathic scoliosis is 2–3%. The bigger curves are significantly less frequent, incidence of curves above 30 Cobb-angles occur in 0.1–0.3%.

E) Treatment

The treatment of idiopathic scoliosis has essentially three options:

1. *Gymnastics:* Special gymnastics has developed to correct the scoliosis; the so-called Schroth therapy, which beside the active spinal stretching, strengthening the muscles asymmetrically in a corrected position, which is accompanied by a three-dimensional corrective breathing exercise. The regular long-term treatment occurs long lasting results.

2. *Corset:* Wearing corset become necessary, if the curative treatment is not sufficient in itself to correct the curvature. This is normally over 20 degrees considered.

3. *Surgery:* Above 50 degrees surgical approach is recommended.

5. Experiments

During the experiments an answer was sought – supported by measuring results – whether the determination of Cobb-angle with moire patterns – accepted by orthopedic specialists – is as accurate as the determination with X-ray pictures.

Well-known from the literature, that the rate of scoliosis is well characterized with a number which descript the figure of the spine shape. This defines the rate of disease severity, and also the possible treatment or intervention.

Three main techniques are known[25], Cobb, Ferguson and Tidestrom method In Hungary, the protocol uses the Cobb method, and rate is determined by X-rays.

Kamal[24] developed the algorithm to determinate Cobb-angles on the basis of the moire patterns.

A) The algorithm for determining the Cobb-angle

Using the the publication referred to[24] the figure the definition of Cobb-angle from moire stripes is the following *(Figure 2):*

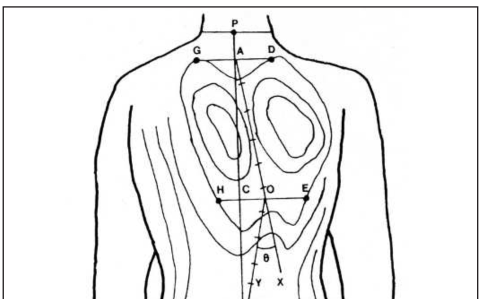

Figure 2. Algorithm for defining Cobb-angle[24]

On the basis of the *Figure 2,* angle is valid, that:

$$\Theta = \angle CAO + \angle CBO = Y1 + Y2 \quad (1)$$

To determine it, the line through the P and Q must be drawed, through the center of the neck and the waist. Then the moire curve on the scapulae, which shows the largest asymmetry must be found, and must be sectioned with a line perpendicular to PQ to get the H, C and E points. To the moire curve on which the H and E points lie tangent must be drawed from the top, resulting the G, A and D points. On the basis of the Figure 6 the I, B and F can be determined, and d1 , d2 and d3 values can be calculated.

$$d1 = 1/2(CH + CE) \quad (2)$$
$$d2 = 1/2(AD + AG) \quad (3)$$
$$d3 = 1/2(BF + BI) \quad (4)$$
$$\tan Y1 = |d1 - d2|/CA \quad (5)$$
$$\tan Y2 = |d1 - d3|/BC \quad (6)$$

eq. 5 and *eq. 6* must be substituted in *eq. 1,* then Cobb-angle can be calculated.

B) The conduction of the experiments

Two series of measurements were carried out, with the same person. The first series included seven recordings, and the body center of the subject stood with an average 400 mm in front of the reference surface. Between the recordings of each measurement, the subject took a short break, then went back to the measurement location. In between recording about one minute has passed. When the recordings was taken the subject was in a natural position, only held back the breath in the usual way, in the length of the exposure. The second series included seven recordings too, although the center line of the subject's body was located in the reference plane. The conditions otherwise were identical to the first series.

These two series of measurements was used to answer the following questions:

1. Cobb-angle, calculated by moire patterns of the same person, with the same independent circumstances (in a freely and loosely assumed position) add up fluctuation, which show the sensitiveness of the method to the subject's set.

2. From the values of Cobb-angles – calculated by pictures, which were taken in two different positions – the impact of the tested surface's position compared to reference surface was examined.

3. It can be seen from the descriptive algorithm of Cobb-angle that the set of E and H points contains a lot of subjective factors, and thus uncertainty, and therefore it was investigated, that within the same picture chosen the E and H points in different ways, how much uncertainty is caused with respect of the rate of Cobb-angle.

6. The measured data

Number	First series	Second series
	Cobb-angle [°]	Cobb-angle [°]
1	3.81	3.52
2	9.05	5.16
3	13.70	14.71
4	2.77	8.23
5	13.71	13.31
6	3.47	3.07
7	2.67	9.98
Average	7.02	8.00
Deviation	5.06	4.64

Table 1. The calculated values of Cobb-angle from the first and second recordings

As a first step the values on the basis of both series was submitted normality analysis with Kolmogorov–Smirnov's goodness to fit test[26]. The sample's empirical distribution's and a theoretical distribution function's fitting to each other was examined. The null hypothesis was, that the test sample and the theoretical distribution function does not differ in the significance level.

From the results, on the basis of the first and second series, the maximum value of test indexes *(Tables 2 and 3)* in both cases are less than the threshold (0.9D = 0.436), so there is no reason to reject null hypothesis, the data series of both samples can be considered as normal distribution on the confidence level (90%).

x_i	f_i	f_{ic}	$F_n(x_i)$	u_i	$F(u_i)$	D_i
2.00	2	2	0.29	–0.89	0.1841	0.1016
3.00	2	4	0.57	–0.70	0.2420	0.3294
4.00	0	4	0.57	–0.50	0.3085	0.2629
5.00	0	4	0.57	–0.30	0.3821	0.1893
6.00	0	4	0.57	–0.10	0.4602	0.1112
7.00	0	4	0.57	0.09	0.5398	0.0316
8.00	0	4	0.57	0.29	0.6179	–0.0465
9.00	1	5	0.71	0.49	0.6915	0.0228
10.00	0	5	0.71	0.69	0.7580	–0.0437
11.00	0	5	0.71	0.89	0.8159	–0.1016
12.00	0	5	0.71	1.08	0.8643	–0.1500
13.00	2	7	1	1.28	0.9032	0.0968

Table 2. The results of the normality analysis on the basis of first and second series (x_i – data, f_i – frequency, f_{ic} – sum of relative frequency, F – value of distribution function, d – value of test index)

x_i	f_i	f_{ic}	$F_n(x_i)$	u_i	$F(u_i)$	Di
3	2	2	0.285714	–0.86207	0.1841	0.1016
5	1	3	0.428571	–0.43103	0.3446	0.0840
7	1	4	0.571429	0	0.5000	0.0714
9	1	5	0.714286	0.431034	0.6664	0.0479
11	0	5	0.714286	0.862069	0.8051	–0.0908
13	2	7	1	1.293103	0.9015	0.1

Table 3. The results of the normality analysis on the basis of first and second series (x_i – data, f_i – frequency, f_{ic} – sum of relative frequency, F – value of distribution function, d – value of test index)

After the data series of both sample was considered as normal distribution on the confidence level, an answer was sought, whether the two samples in point of deviation and average can be considered part of the same population. In other words, the measured surface's and reference surface's distance from each other – in case of the tested dimensions – has no significant effect on the outcome. The comparison of the variances were performed with the Fischer–Snedecor's F test[27]. According to the null hypothesis, the two models – on the confidence level – are representative samples of normal distributions, which have same variance. In the course of the comparison of the two samples's variances, the test index was Femp = 1.1892, which is less than the critical.

So here was also no reason to throw away the null hypothesis, the two sample by variance on 90% significance level, can be considered as part of the same population.

To compare the averages, since the two samples is different – this case can be considered as a test with control group – two-sample t-test[28] were applied. By the null hypothesis, that two samples, on the confidence level, are the representative samples of normal distributions, which have same expected value. The two-sample t-test's empirical test index value is temp = 0.3776 which is smaller in this case too, than the critical value; t0.9crit = 1.782. So, according to the comparison of averages, there was also no reason to throw away the null hypothesis, that, the two samples, on 90% significance level, in point of averages can be considered part of the same population. It can be allocated, that on the significance level – the values of Cobb-angles calculated on basis of the recordings, which were made in the above mentioned circumstances – the subject's distance from the reference surface has no effect on the results, the system is not sensitive to this parameter.

To find out how the E and H point's settings impact the results, within the same record – which was made, when the examined surface was on the place of the reference surface – the E and H points were set in various places, as the algorithm described. From the resulting values of Cobb-angles, the average and deviation values can be calculated and conclusions can be drawn.

On the basis of *table 4.* it was found, that within one picture several times and independently intaked H and E points effected the deviation of the resultant Cobb-angle with lesser extent *(Table 4.)* than the total sample, but it had a significant effect, so the settings in the evaluation must be held carefully.

Number	Cobb-angle [°]
1	3.68
2	2.68
3	3.94
4	4.86
5	4.44
6	3.68
7	3.54
8	3.20
Average	3.751
Deviation	0.680

Table 4. The effect of the settings of E and H points on the uncertainty of Cobb-angles

7. Conclusions

According to the tests with the equipment, and control measurements the following statements can be made:

1. statement: The distance between the reference surface and the center of the subject's body – about 400 mm in the surroundings before the reference surface – has no significant effect to the rate of the Cobb-angle. Which was specified with the known algorithm and calculated from the moire patterns, which was made with the precalibrated, electronic moire equipment.

2. statement: The deviation – calculated from the Cobb-angle, which was specified from the moire patterns, was made with the moire equipment, from the subject, standing in the same position, without any particular body-setting algorithm – can be kept within five degrees.

3. statement: The deviation – calculated from the Cobb-angle, which was specified from the moire patterns, was made with the moire equipment – due to uncertainty of the settings of E and H points can be kept within 1 degree.

8. Comments and further research opportunities

In connection with the measurements, as well the further research, the following remarks can be made.

1. It would be worth to repeat the experiments with larger number of sample.

2. It would be worth to carry out the experiments with a person, whose scoliosis is diagnosed and more significant, medical history is known and who is not familiar with the system.

3. On the basis of the recordings, it would be worth to carrie out a complex examination, that the uncertainty of identification of certain points how much impact the resultant uncertainty, when determinate the Cobb-angle.

4. It would be worth that moire stripes – within moire patterns – will be subjected to a thinning image processing algorithm, to reduce the uncertainty of reading out datas.

REFERENCES

1. *Theocaris PS.* Moire Fringe in Strain Analysis. Pergamon Press, 1969.
2. *Patorski K, Kujawinska M.* Handbook of the Moire Fringe Technique. Elsevier, Amsterdam, 1993.
3. *Durelli AJ, Parks VJ.* Moire Analysis of Strain. Prentice-Hall, Englewood Cliffs, New Jersey, 1970.
4. *Parks VJ.* Geometric Moire, SEM Handbook of Experimental Mechanics, Prentice-Hall, Englewood Cliffs, New Jersey, 1987.
5. *Parks VJ.* Strain measurement using grids. Optical Engineering, 1982, Vol. 21: pp. 633–639.
6. *Orosz M.* Az idiopathiás scoliosis konzervatív kezelése. Gyermekgyógyászat 2005;56(6): pp. 651–657.
7. *Adir IV, Wijk MC, Armstong WD.* Moire topography in scoliosis screening. Clin. Orthop., 1977;129: pp. 165–171.
8. http://www.scolinea.hu/gerincferdules
9. *Cheneau J.* Ein Weg zur richtigen Skoliosebehandlung. Orth. Tech. 1990;4:222.
10. *Cheneau J.* Das original Cheneau-Skoliosen-Korsett. Orth. Tech. Dortmund, 1997.
11. *Cobb JR.* Outline for study of scoliosis. Am. Acad. Orthop. Surg. 1948;5:261–266.
12. *Orosz M.* Az idiopathiás scoliosisról. Mozgásterápia. 2000;1: pp. 3–8.
13. *Orosz M, Marlok F.* A Cheneau korzett. Rehabilitáció, 1997;1: pp. 10–11.
14. *Orosz M.* Hibásan készített és alkalmazott Cheneau korzettek kudarca a strukturális scoliosis kezelésében. Magyar Traumat. 2000;2: pp. 83–90.
15. http://www.e-radiography.net
16. *Batouche M, Benlamri R and Kholladi MK.* A computer vision system for diagnosing scoliosis using moire images. Computers in Biology and Medicine, July 1996; Volume 26, Issue 4: pp. 339–353.
17. *Ruggerone M, Austin JHM.* Moire Topography in Scoliosis, Correlations with Vertebral Lateral Curvature as Determined by Radiography. Physical Therapy, 1986; Vol. 66, No. 7: pp. 1072–1077.
18. *Laulund T, Sjbjerg JO, Hrlyck E.* Moire Topography in School Screening for Structural Scoliosis. Acta orthopedica, 1982; Vol. 53, No. 5: pp. 765–768.
19. *Windischbauer G.* Survey on application of moire-techniques in medicine and biology. In Optics in Biomedical Sciences, Proceedings of the International Conference. Springer-Verlag Berlin, 1981; pp. 244–249.
20. *Takasaki H.* Moire Topgraphy. Applied Optics, June 1970; Vol. 9, No. 6: pp. 1467–1472.
21. *Takasaki H.* Moire Topgraphy. Applied Optics, June 1973; Vol. 12, No. 4: pp. 845–850.
22. *Laulund T, Sjbjerg JO and Hrlyck E.* Moire Topography in School Screening for Structural Scoliosis. Acta orthopedica, 1982; Vol. 53, No. 5: pp. 765–768.
23. *Wenzel K, Antal Á, Molnár J, Tóth B, Tamás P.* New Optical Equipment in 3D Surface Measuring. Journal of Automation Mobile Robotics & Intelligent Systems, 2009;(4)3: pp. 29–32.
24. *Kamal SA.* Determination of degree of correction of spinal deformity by moire topographs. In. Moire Fringe Topography and Spinal Deformity, Proceedings of the 2nd International Symposium, Gustav Fischer Verlag, Stuttgart, 1983; pp. 117–126.
25. *Neugebauer H.* The different methods of measuring the curvature of scoliotic spine. In. Moire Fringe Topography and Spinal Deformity, Pro-

ceedings of the 2nd International Symposium, Gustav Fischer Verlag, Stuttgart, 1983; pp. 17–26.

26. *Vincze I.* Matematikai statisztika ipari alkalmazásokkal. Műszaki Kiadó, Budapest, 1968.

27. *Varga L.* Bevezetés a didaktikai kutatások módszereibe. Tankönyvkiadó, Budapest, 1986.

28. *Kemény S, Deák A.* Kísérletek tervezése és értékelése. Műszaki Könyvkiadó, Bp., 2000.

29. *Moreland MS, Pope MH, Armstrong GWD.* Moire fringe topography and spinal deformity. International Symposium on Moire Contourography and Spine Deformity, Basin Harbor, Pergamon Press – New York, 1980.

30. *Tanoue T, Nakano S, Hyoungseop K, Joo kooi T, Ishikawa S, Otsuka Y, Shimizu H, Shinomiya T.* An automatic detection method of spinal deformity from moire topographic images employing asymmetric degree of shoulder and waistline. International IEEE Conference on Automation and systems ICCAS07, Seoul, 2007; pp. 1282–1285.

31. *Hyoung SK, Kazufumi I, Seiji I, Yoshinori O, Hisashi S.* Discriminating spinal deformity employing centroids difference on the moire images. Systems and Computers in Japan, Vol. 32, Issue 7: pp. 20–28.

32. *Frontino G, Negri V, Rinaldi E.* Photographic moire method for preliminary diagnosis of spine deformity. Ateneo Parmense Acta Biomed. 1980;51(1): pp. 33–8.

33. *Dovica M.* Komponenty a moduly mini- a mikromechanizmov. Monografia. Edıcia vedeckej a odbornej literatury SjF TU v Koiciach, Typo Press, Koice, 2002; p. 150.

34. *Dovica M, Gmiterko A, Henriczyova T.* Basic Study of the Mobile Minimechanism for Moving Inside the Tubes with Small Diameter. 16. Internationales Kolloqium Feinwerktechnik 1–3. October 1997.

35. *Kauch P, Dovica M, Henriczyova T.* Walking mini-robots with compliant body. Proceedings of the sixth conference on mechanical engineering, May 29–30, 2008. Budapest, I7, ISBN 963 420 947 8

The authors would like to thank NKTH (Research and Technology Office of Hungarian Government) for the support since this study has been carried out as part of the project TECH 08-A1/2-2008-0121 (NKTH).

The research was also supported by HUNOROB project (HU- 0045), a grant from Iceland, Liechtenstein and Norway through the EEA Financial Mechanism and the Hungarian National Development Agency.

Zselyke Gaal
Budapest University of Technology and Economics
H–1111 Budapest, Műegyetem rkp. 3.